Immunoprophylaxis of Influenza using AAV Vector Delivery of Cross-Subtype Neutralizing Single Domain Antibodies

JOANNE MARIE M. DEL ROSARIO

Thesis submitted for the degree of

Doctor of Philosophy

Infection and Immunity

University College London

2020

To Chris, as fate would have it.

To Teki, thank you for everything.

DECLARATION

I, Joanne Marie M. Del Rosario, confirm that the work presented in this thesis is my own. Where information has been derived from other sources, I confirm that this has been indicated in the thesis.

_____

ABSTRACT

Cross-subtype neutralizing single domain antibodies against influenza present new opportunities for immunoprophylaxis and pandemic preparedness. Their simple modular structure and single open reading frame format are highly amenable to gene therapy-mediated delivery. R1a-B6, an alpaca-derived single domain antibody (nanobody), that is capable of potent cross-subtype neutralization *in vitro* of H1N1, H5N1, H2N2, and H9N2 influenza viruses, through binding to a highly conserved epitope in the influenza hemagglutinin stem region, was previously described. To evaluate the potential of R1a-B6 for immunoprophylaxis via adeno-associated viral (AAV) vector delivery, it was reformatted as Fc fusions of mouse IgG1 (ADCC-) and IgG2a (ADCC+) isotypes. This is also to extend R1a-B6's half-life and to assess the requirement for ADCC for efficacy of R1a-B6 *in vitro* and *in vivo*. It was found that reformatted R1a-B6 of either mouse IgG isotype retained its potent binding and neutralization activity against different Group I influenza A subtypes *in vitro.* The findings in this study also demonstrate that a single intramuscular injection in mice of AAV encoding R1a-B6-Fc was able to drive sustained high-level expression (0.5–1.1 mg/mL) of the nanobody-Fc in sera with no evidence of reduction for up to 6 months. R1a-B6-Fc fusions of both isotypes gave complete protection against lethal challenge with both pandemic A/California/07/2009 (H1N1)pdm09 and mouse-adapted avian influenza A/Vietnam/1194/2004 (H5N1). These data suggest that R1a-B6-Fc delivered via AAV is capable of cross-subtype protection and ADCC was not essential for protection. These findings reveal that AAV delivery of cross-subtype neutralizing nanobodies may be an effective strategy to prevent influenza infection and provide long-term protection independent of a host induced immune response.

IMPACT STATEMENT

Although vaccines are the main countermeasure against pandemic influenza, their timely implementation and ineffectiveness in vulnerable patient groups present challenges. We need a pro-active and pre-emptive approach in tackling influenza especially in the case of a pandemic emergency. Novel interventions using broadly neutralizing monoclonal antibodies (mAbs) are under clinical development, however their structural complexity, expensive production and requirement for repeated injections are limitations to widespread use. Adeno associated virus (AAV) vectors were used to deliver a much simpler broadly neutralizing single domain antibody (nanobody R1a-B6) specific for a highly conserved epitope in the influenza hemagglutinin stem region. A one-time intramuscular delivery route aiming for longer expression and stricter dosing control in preference to intranasal delivery that may be obstructed due to congestion and a reflex sniffing response of the recipient leading to reduced efficacy of delivery was evaluated. Findings demonstrate high level, long-term expression *in vivo*, which protected mice from lethal challenge by both pandemic H1N1 and highly pathogenic avian influenza H5N1. Surprisingly, Fc-mediated antibody dependent cellular cytotoxicity (ADCC) was not essential for R1a-B6 efficacy when expressed at high levels *in vivo* which contrasts with that described previously for similar stem binding human mAbs when injected as purified protein. These findings have implications in developing the optimum antibody format and delivery option to provide safe, long-term protection, independent of the patient's immune response and prior exposure to influenza, that can be utilized in the instance of a pandemic.

ACKNOWLEDGEMENTS

I would like to extend my gratitude to the following people who have made this PhD a unique and positive learning experience. The support of these amazing people has been vital in the most challenging and humbling of times.

My supervisors, Dr. Yasuhiro Takeuchi and Dr. Simon Hufton, for really taking on the job and teaching, correcting, and guiding me every step of the way. I finish this PhD, hopefully a better scientist, and definitely a better person, than I was before, because of your training, encouragement, patience, kindness and friendship. I have been very blessed to have you as my advisers.

The DPSM faculty and team, and the Chemistry unit of the University of the Philippines Manila for their unwavering support from start to finish of my PhD. None of this would have been possible without you.

Professor Mary Collins for helpful insight and advice. I would not have been here if you and Yasu did not take a chance on me.

Professor Paul Digard and Dr. Laura McCoy, whose extensive examination have helped make this piece of work better. I have learned so much in those 4 hours.

Dr. Matthew Smith for all the exciting influenza work that you taught me. It has been a pleasure sharing the bench with such an awesome scientist like you.

Christina Ball, Paul Risley, Dr. Kam Zaki and Dr. Ilaria Nisoli for sharing your expertise and time with me.

Dr. Othmar Engelhardt and Dr. Nigel Temperton for being supportive and critical collaborators, who have enriched this body of work.

Rose, Alan, Shaun, Christine, Vicky and all the wonderful people in the Biological Services Division at NIBSC for going over and beyond to help me with the animal work.

Our colleagues at the Biotherapeutics Division and the Influenza Resource Center at NIBSC for help and advice with this project.

My former students, for always cheering me on. Your belief in me has made me become more of what I already am.

The friends that I have made here in London especially Bea, Jasmine and Pedro, and Chris's family who have made being in another country an incredibly fun, uplifting and a most rewarding experience. And all my friends back in the Philippines and scattered all around the world who have always cheered me on and believed in me even at times when I doubt myself.

Gabby, Ciara, Andrea (x2) and Diana, for listening to all my ranting, and for always calming me down when things don't go as planned.

Jules, Kevin, Dem, Jireh and Hermie, eternal friends, rambunctious supporters, together we are untouchable.

Arlou, it is finally done! And I share this victory with you, one of many in our bright future.

Tom, Ryan and Martin, NIBSC became home because you were there. Work did not feel like work, and we fostered a happy, productive, supportive environment, that I would always cherish.

Teki, for being my rock. I have borrowed from your strength so much and you have kept me standing through the best and worst of it.

My family and my Bicho for your unconditional love and faith in me. Being away from you has not been easy but I thank you for sharing my dreams and helping me in making them happen, and always, always, praying for me. This is the product of all our sacrifices.

Chris, my clever boy, for all the late nights, stimulating discussions and inspiring banter. For suffering and rejoicing with me and holding my hand through our inflatable bed journey. Everything will be worth it in the end. Smart ka talaga for sharing this incredible adventure with me.

And finally, infinite thanks to HIM, the Giver of all good things.

TABLE OF CONTENTS

LIST OF FIGURES

LIST OF TABLES

ABBREVIATIONS

Aap	AAV Assembly Protein
AAV	Adeno-associated virus
AAVR	AAV Receptor
ACIP	Advisory Committee on Immunization Practices
Ad	Adenovirus
ADCC	Antibody dependent cell cytotoxicity
ADCP	Antibody-dependent cell-mediated phagocytosis
ADIN	Antibody-dependent intracellular neutralization
AID	Activation-induced cytidine deaminase
ALT	Alanine aminotransferase
Amp^R	Ampicillin resistance gene
ANOVA	Analysis of variance
ARP-1	Anti-rotavirus protein 1
aTTP	Acquired Thrombotic Thrombocytopenic Purpura
bGH polyA	Bovine growth hormone polyadenylation signal
bnAb	Broadly neutralizing antibody
BSA	Bovine serum albumin
BSL	Biosafety level
Cap	Capsid (protein)
CD	Cluster of differentiation
CDC	Complement dependent cytotoxicity
CDR	Complementarity determining region
CHO	Chinese hamster ovary
CMV	Cytomegalovirus
cRNA	Complementary RNA
Ct	Threshold Cycle
CTL	Cytotoxic T lymphocyte
CV	column volumes
DC	Dendritic cell
DMEM	Dulbecco's Modified Essential Medium
dpi	days post infection
EC_{50}	Half maximal effective concentration
ELISA	Enzyme-Linked Immunosorbent Assay
ER	Endoplasmic reticulum
F	forward

Fab	Antigen binding fragment
Fc	Fragment crystallizable
FCS	Fetal calf serum
FcγR	Fc gamma Receptor
FcRn	Neonatal Fc Receptor
FDA	(US) Food and Drug Administration
FGFR	Fibroblast growth factor receptor
FIX	coagulation factor IX
FMD	Foot and Mouth Disease
FR	Framework region
FVIII	coagulation factor VIII
GPCR	G-protein coupled receptor
HA	Hemagglutinin
HAI	Hemagglutination inhibition assay
HAU	Hemagglutination units
HCAb	Heavy chain only antibody
H&E	Hematoxylin and Eosin
HEK	Human embryonic kidney
HPAI	Highly pathogenic avian influenza
HRP	Horseradish Peroxidase
HSV-2	Herpes Simplex Virus-2
IAV	Influenza A virus
IBV	Influenza B virus
IC_{50}	half-maximal inhibitory concentration
IFN	Interferon
Ig	Immunoglobulin
IIV	Inactivated influenza vaccine
IL	Interleukin
ILZ	Isoleucine zipper domain
IM	Intramuscular
IN	Intranasal
ITR	Inverted terminal repeat
IV	Intravenous
LAIV	Live Attenuated Influenza Vaccine
LB	Luria-Bertani
LCA	Leber congenital amaurosis
LPAI	Low pathogenicity avian influenza

LPL	Lipoprotein lipase
LV	Lentivirus
M	Matrix
mAb	Monoclonal antibody
MCS	Multiple cloning site
MDAb	Multidomain antibody
MDCK	Madin-Darby canine kidney
MEM	Minimum Essential Medium
MERS-COV	Middle East Respiratory Syndrome Coronavirus
MHC	Major histocompatibility complex
MLD_{50}	Mouse 50% Lethal Dose
MLV	Moloney murine leukaemia virus
MN	Microneutralization Assay
MPER	Membrane proximal external region
mRNA	Messenger RNA
MW	Molecular Weight
MWCO	Molecular Weight Cut-Off
NA	Neuraminidase
nAb	Neutralizing antibody
NAI	Neuraminidase Inhibitor
Nb	Nanobody
NC	Nitrocellulose
NEP	Nuclear export protein
NFAT-RE	Nuclear Factor of Activated T cells-Response Element
NK	Natural Killer cells
NP	Nucleoprotein
NS2	Non-structural protein 2
OAS	Original Antigenic Sin
PA	Acidic Polymerase
PAMP	Pathogen associated molecular pattern
PB	Basic Polymerase
PBS	Phosphate Buffered Saline
PBS-T	Phosphate Buffered Saline-Tween20
PDGF-R	Platelet-derived growth factor receptor (PDGF-R)
PEG	Polyethylene Glycol
PEI	Polyethylene Imine
PFA	Paraformaldehyde

PRR	Pathogen recognition receptor
qPCR	quantitative real-time polymerase chain reaction
R	Reverse
rAAV	Recombinant Adeno-Associated virus
RDE	Receptor Destroying Enzyme
RdRp	RNA-dependent RNA polymerase
Rep	Replication (protein)
RIV	Recombinant Influenza vaccine
RLU	Relative Luminescence Unit
RPE65	Retinal pigment epithelium-specific 65-kDa
RPMI	Roswell Park Memorial Institute
RSV	Respiratory Syncytial Virus (RSV)
rt-PCR	Reverse transcription polymerase chain reaction
SCID	Severe combined immunodeficient
$sddH_2O$	Sterile double distilled water
SDS-PAGE	Sodium Dodecyl Sulfate Polyacylamide Gel Electrophoresis
SERCA2a	sarcoplasmatic calcium ATPase
sIgA	Secretory IgA
SHM	Somatic hypermutation
shRNA	small hairpin RNA
SMA	Spinal muscular atrophy
SMN	Survival of motor neuron protein
TAE	Tris-Acetate-EDTA
$TCID_{50}$	Tissue Culture Infectious Dose 50%
TF	Triple flask
TKpA	Thymidine kinase polyadenylation
TLR	Toll-like receptor
TNF	Tumor necrosis factor
TPCK	Tosyl phenylalanyl chloromethyl ketone
t-RBC	Turkey red blood cells
TRIM21	Tripartite-motif containing protein 21
UTR	Untranslated region
VLP	Virus-Like particle
vRNA	Viral RNA
vRNP	Viral ribonucleoprotein complexes
WHO	World Health Organization
WPRE	Woodchuck posttranscriptional regulatory element

CHAPTER 1

INTRODUCTION

1.1 Thesis Overview

This thesis will have the following content:

Chapter 1 presents a review of literature of influenza and strategies for its prevention and treatment using immunotherapy, with an emphasis on nanobodies and gene therapy using Adeno-associated Virus (AAV) vector delivery.

Chapter 2 describes in detail the materials and methods employed in this study.

Chapter 3 demonstrates the production, characterization, ability to activate antibody dependent cell cytotoxicity (ADCC), cross-subtype binding and neutralizing activity of the nanobody R1a-B6 in different formats against various Group I influenza A subtypes *in vitro* as a preliminary step to *in vivo* studies.

Chapter 4 shows the production, purification and characterization of high titer AAV viruses expressing R1a-B6 transgenes and negative control nanobody for use in *in vivo* influenza mouse challenge experiments.

Chapter 5 provides evidence of broadly protective humoral immunity against influenza generated by AAV delivery of R1a-B6-Fc independent of ADCC activity through *in vivo* challenge studies in mice.

Chapter 6 offers concluding remarks and ideas for future work.

1.2 Influenza

1.2.1 Influenza A Virus (IAV) Biology

Influenza viruses are segmented, negative sense, single-stranded, enveloped RNA viruses belonging to the Orthomyxoviridae family [1, 2] Within this family, there are three influenza types that circulate in humans, influenza A, B, and C [3, 4]. They are further classified into subtypes based on the host range and the combination of their surface protein components or antigens. Of great significance to humans are

influenza A (IAV) and B (IBV) viruses, which rapidly spread around the world in seasonal epidemics; imposing considerable economic burden in terms of lost productivity in affected individuals and in some cases causing death [4, 5].

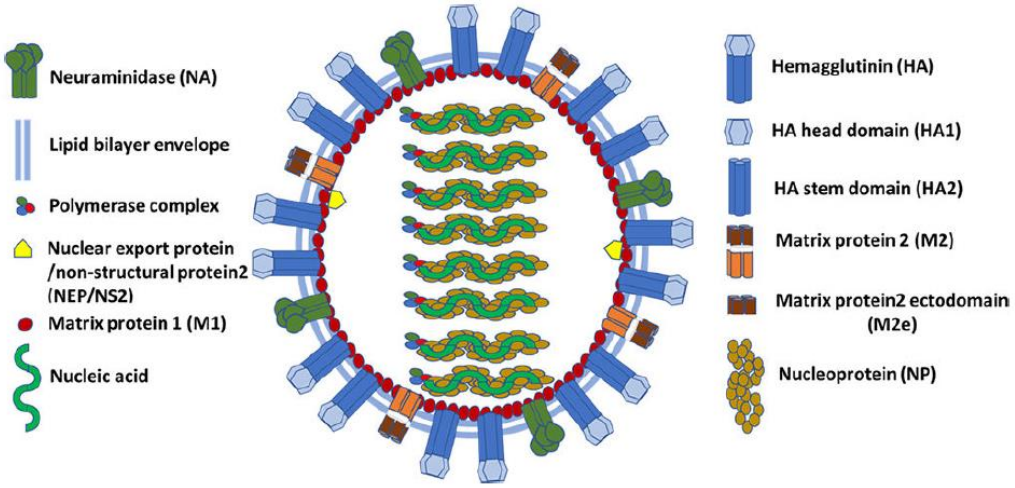

Figure Error! No text of specified style in document. Schematic representation of influenza A virus (IAV) and its components. Adapted from [6].

Influenza contains a lipid membrane studded with the two major membrane glycoproteins, hemagglutinin (HA) and neuraminidase (NA) [1, 2, 7] (**Figure 1.1**). The surface glycoprotein HA is responsible for viral cell attachment and entry into host cells via sialic acid receptors [7-9]. NA, the other major glycoprotein, is a glycosidase [10] that cleaves sialic acids during the later stages of infection allowing efficient release of virion progeny [11]. The matrix (M2) ion channels traverse the lipid envelope [7], and together with the two other integral membrane proteins, HA and NA, they overlay a matrix of M1 protein, which encloses the virion core [1]. The influenza A virus genome is made up of eight negative-sense, single-stranded viral RNA (vRNA) segments encoding structural and functional proteins [2]. These vRNAs are found as individual viral ribonucleoprotein complexes (RNP) which are made up of the nucleoprotein (NP) and the heterotrimeric RNA-dependent RNA polymerase, composed of two basic polymerases (PB1 and PB2) and one acidic polymerase (PA) subunit [2, 6, 12-14].

Together with the RNPs, the nuclear export protein (NEP) also called the non-structural protein 2 (NS2), are found inside M1 [2] (**Figure 1.1**).

The surface influenza glycoproteins HA and NA are recognized by the immune system and can trigger an immune response. As a result, influenza is subject to continuous immune-driven selection especially in the exposed globular HA head domain with distinct epitopes undergoing constant antigenic drift [15-20]. Antigenic drift is the gradual accumulation of nucleotide mutations and amino acid substitutions in influenza HA, resulting in the emergence of new antigenic variants or strains [9]. The changes associated with antigenic drift happen continually and randomly over time as the virus replicates [21]. A segmented genome enables antigenic shift, wherein an influenza A virus strain acquires an HA or sometimes an NA segment from another IAV of a different subtype in a zoonotic reservoir [9, 22]. This reassortment may give rise to a completely novel virus to which the human population has no pre-existing immunity, with the potential to become pandemic influenza. The most recent example is the pandemic A(H1N1)2009 strain, a quadruple-reassortant virus, containing genes from Asian and European swine influenza, North American avian influenza and human influenza virus [23].

Influenza A viruses (IAV) infect the widest host range – human, other mammals including pigs, horses, cats, ferrets, rodents, seals and bats, and most commonly, avian species, inflicting the most severe morbidity among influenza A-C [24-26]. According to the diversity of the influenza HA and NA genes, IAVs have been classified into 18 antigenic HA subtypes (H1-H18) and 11 antigenic NA subtypes (N1-N11) [4, 27, 28]. Based on phylogenetic analysis, HA subtypes are divided into two groups: Group 1 - H1, H2, H5, H6, H8, H9, H11, H12, H13, H16, H17 and H18 subtypes, and Group 2 - H3, H4, H7, H10, H14 and H15 [29]. Furthermore, the influenza A virus is divided into different serotypes, combinations of HA and NA, based on serological reactivity against hyperimmune anti-HA and anti-NA sera to these viruses [27, 30].

From its reservoir of wild birds, IAVs are able to transmit from domestic poultry, which is the gateway to infection of mammals, most notably, swine and humans [22]. These zoonotic viruses are not easily transmitted between humans; however, some viruses acquire the capacity to spread to humans through adaptation or acquisition of new genes from human influenza viruses leading to the emergence of a novel virus that can start a pandemic [4]. IAV serotypes H1N1, H1N2, H2N2, H3N2, H5N1, H7N2, H7N3, H7N9, H10N7 have been confirmed in humans in the past [25, 30-34]. While there are many genetically distinct subtypes from recombination of HA and NA in IAV, only three HA (H1, H2, and H3) and two NA (N1 and N2) subtypes have caused human pandemics that have been recorded in history [2, 31, 35].

1.2.2 Replication Cycle

The influenza virus life cycle can be divided into the following stages: i) viral attachment and entry into host cells, ii) entry of viral ribonucleoproteins (vRNP) into the nucleus facilitating synthesis of viral RNA and proteins, iii) RNA packaging and virion assembly, and lastly, iv) virus budding and release [31, 36].

Viral attachment and entry into host cells is facilitated by the influenza virus' hemagglutinin (HA). Studies of the crystal structure of the HA molecule reveals it as a trimer with two structurally distinct regions: a globular head, an antiparallel β-sheet containing the receptor-binding site, and a stem region comprised of a triple-stranded coiled-coil of α-helices [7, 37]. It initially exists as a HA precursor, HA0, made up of two subunits: HA1, which contains the receptor binding domain, and HA2, which contains the fusion peptide. These subunits are linked by disulfide bonds [7, 37]. Influenza viruses recognize sialic acid on the host cell surface such as N-acetylneuraminic acid in humans [9, 22, 37]. Two major linkages between sialic acid and the penultimate galactose residues of carbohydrate side chains are found in nature, Neu5Ac α(2,3)-Gal and Neu5Ac α(2,6)-Gal [7]. HA on the surface of the influenza virus recognizes these sialic acid residues and depending on the type of

influenza, will have preferential specificity for either α(2,6) linkages on ciliated epithelial cells of the upper respiratory tract for human IAV or α(2,3) linkages on epithelial cells of duck intestines for avian IAV [2, 38, 39]. These differences in HA receptor specificity define IAV host range [39]. However, expression of either sialic acid receptor is also possible in humans, avian and swine [40] facilitating bidirectional transmission and generation of novel influenza viruses [1].

Following attachment to host cell receptors, IAV is taken up by the cell mainly through clathrin-coated receptor-mediated endocytosis or by macropinocytosis [41]. The metastable HA is first cleaved by host proteases into the fragments HA1 and HA2, making it susceptible to an irreversible conformational change that promotes fusion of the viral and cellular membranes [42, 43]. Cleavage is required to enable exposure of the hydrophobic domain on the N-terminus of HA2 or the “fusion peptide”. Fusion of the viral envelope with the endosomal membrane is then triggered by the low pH environment of the endosome (pH 5-6) [42]. The M2 ion channel is then opened, allowing proton influx from the endosome that acidifies the interior of the virus particles and disrupting internal protein-protein interactions [44]. This allows packaged viral ribonucleoprotein (vRNP) complexes to dissociate from M1 into the cellular cytoplasm [44].

The vRNPs enter the nucleus, site of influenza virus RNA synthesis, through the nuclear pores via an active mechanism mediated by nuclear localization signals from NP and using an array of host nuclear factors [12, 22, 36, 44, 45]. In the nucleus, the RNA-dependent RNA polymerase (RdRp) of influenza virus, made up of PA, PB1 and PB2, creates messenger RNA (mRNA) templates for viral protein synthesis, and complementary RNA (cRNA) intermediates, exact copies of viral RNA (vRNA), to be used as templates for further transcription of genomic vRNA [46, 47].

Both vRNA and mRNA are transported to the cytoplasm, where viral proteins are generated in the ribosome and in endoplasmic reticulum (ER)-associated ribosomes for the membrane proteins HA, NA, and M2 [12, 31]. RNPs are then formed

in the nucleus and are later transported to the cell membrane. IAVs are able to target the complete set of vRNPs to appropriate sites in the plasma membrane where they are localized and aggregate to produce infectious viral particles [12, 36].

Budding occurs at the cell membrane, initiated by HA and NA which can alter membrane curvature [48]. HA and NA cytoplasmic tails then recruit M1 via tail binding, facilitating the formation of filamentous virions [48, 49]. M2 is then recruited to the budding site causing membrane scission and the final release of the budding assembled virion [48]. NA then liberates the virions by enzymatically cleaving sialic acids from cell surface receptors and from carbohydrate side chains on nascent virions, thereby preventing HA aggregation and viral clumping at the cell surface [10, 11, 50, 51].

1.2.3 Pathogenesis

Pathogenesis is the consequence brought about by a virus essentially hijacking its host, using its biosynthetic machinery to replicate [52]. Influenza virus replication is subject to the defence mechanisms developed by the host against the infection, and disease severity is the result of this interplay [53]. In infections caused by the 1918 H1N1 or the H5N1 influenza virus, excessive inflammatory reactions known as “cytokine storm” with markedly higher levels of pro-inflammatory cytokines such as interferons (IFNs), tumor necrosis factors (TNFs), interleukins (ILs), and chemokines, have been detected [54-58]. These results indicate that chemokine levels correlate strongly with disease severity. Host specificity and pathogenicity are therefore the result of the interaction of numerous host factors with all viral proteins [59-61].

It is generally accepted that wild aquatic birds are the major reservoir for influenza A viruses. In avians, low pathogenicity avian influenza (LPAI) is an infection of the gastro-intestinal tract and is usually asymptomatic [1, 39, 62, 63]. Transmission is predominantly though feces [1, 63]. Moreover, the presence of avian influenza in water supplies aids its transmission to shore birds and aquatic mammals such as seals

and whales [53, 64]. Migratory transmission via feces results in the spread of influenza to domestic poultry over a wide area [32].

Occasionally, highly pathogenic strains of the virus (HPAI), H5 and H7, cause disease and high fatality rates in birds [65]. These pathogenic types of influenza not only infect gastrointestinal epithelial cells but also have the capacity to replicate in internal organs via systemic infection and are shed in feces in high concentrations [65]. LPAI and HPAI are differentiated by their cleavage sequence, the sequence of a few amino acids where the HA0 is cleaved into HA1 and HA2 during viral membrane fusion [43, 59, 66, 67]. In HPAI, there are several basic amino acids at this cleavage sequence, allowing HA cleavage by ubiquitous host cellular proteases [59, 68]. This polybasic cleavage sequence allows activation of the HA in virtually all cell types, resulting in high pathogenicity in birds [59, 68].

On the other hand, LPAIs contain a single arginine residue at the cleavage site of HA, which is cleaved only by trypsin-like proteases and only produce localized infection of the respiratory and/or intestinal tracts, causing asymptomatic or mild infection with restricted pathogenicity [65, 67, 69]. However, it has been shown that LPAIs are often able to acquire multiple nucleotide mutations to create codons for basic amino acids at the HA cleavage site, thereby rendering the virus capable of causing systemic infection with fatal outcomes in birds and poultry [70-73].

Viruses containing polybasic cleavage sites can be highly pathogenic in humans, however a panoply of other factors are probably involved as well [65]. Pandemic viruses from 1918, 1957, and 1968, had a protein in their repertoire, PB1-F2, that is associated with increased virulence in humans [74]. The degree of identity between the new strain and those of other circulating human viruses is also a factor. If viruses are antigenically distinct, exposure and subsequent immunity to one does not mean immunity to the other strains, giving rise to morbidity.

HA stability, as measured by IAV's ability to cause membrane fusion, also appears to be essential for adapting emerging influenza viruses to humans [22]. In H5

HPAI, it was found that mutations in the viral HA receptor-binding domain conferred binding to human type receptors over the preferred avian type receptors but reduced HA stability that was reverted by compensatory mutations [75]. Other studies have also shown that ferret-adapted respiratory droplet-transmissible H5N1 viruses exhibited a shift to human-type specificity via mutations in the HA head [76, 77]. HA mutations in H7N9 have also indicated H7 HA receptor preference to a predominantly human binding specificity, however the H7 IAV still remains a weak binder to human glycan receptor analogs due to loss of HA stability [72]. These findings suggest that the acquisition of human-type receptor-binding specificity results in an unfavorable change in HA stability that requires compensatory mutations to offset the reduction in virus fitness. As such, the viral hemagglutinin protein, which dictates tissue tropism and thereby systemic spread, serves as one of the major determinants for IAV pathogenicity by limiting interspecies transmission and the establishment of virus lineages in new hosts [22, 24, 25, 61, 78, 79].

Although there is evidence for the direct transmission of influenza from avian to other animals [32, 71, 80-82], adaptation of the virus is essential for onward transmission in a new host species [53, 60, 61]. This can occur through direct interspecies transmission of avian viruses to humans, either after time in an intermediate host, or after a reassortment event with one or more different viruses that gives rise to a virus capable of replicating and subsequently spreading in humans.

Influenza also affects other mammals aside from humans. Pigs have been hypothesized to be “mixing vessels” for human and avian influenza viruses [83] as their respiratory epithelium contain receptors for either influenza type, with Neu5Ac α(2,3)-Gal and Neu5Ac α(2,6)-Gal extensively detected in the major porcine organs [84]. It was also shown that there is high similarity of sialic acid expression patterns in the respiratory tract between pig and human, making reassortment of multiple viruses of human and swine origin possible in either species. Pigs infected with IAV show symptoms such as acute respiratory disease characterized by fever, inactivity,

decreased food intake and malaise, within the disease incubation period of 1 and 3 days with rapid recovery beginning 4–7 days after onset [1]. Equine influenza also shares the same symptoms as that described for pigs and humans [1, 62, 85].

1.2.4 Burden and Epidemiology

In 2020, the currently circulating IAV strains ("seasonal") in humans are subtypes A(H1N1) and A(H3N2) influenza viruses [5]. Despite a certain level of immunity conferred by past infections and vaccination, influenza still causes significant morbidity and mortality in humans. The World Health Organization (WHO) estimates that seasonal influenza is responsible for 1 billion cases of flu, 3–5 million cases of severe illness, and 300,000 to 645,000 deaths worldwide annually [5, 86]. In the US, the burden of influenza is currently estimated to be 25–50 million cases per year, leading to about 250,000 hospitalizations and 37,000 deaths [87]. The estimated average annual total economic burden of seasonal influenza to the healthcare system and society was $11.2 billion ($6.3–$25.3 billion) in 2018 [87].

In developed countries, annual seasonal influenza epidemics infect about 10–20% of the population each season, causing febrile illness that ranges in severity from mild to debilitating and can lead in some instances to hospitalization and even cause death [5]. Hospitalization and death occur mainly in high risk groups, people aged 65 or over, pregnant women, children under 5 years of age, individuals with chronic medical conditions, immunocompromised patients, and to some extent, health care workers who are at high risk of acquiring infection due to increased exposure to the virus [5, 54, 86, 88]. The highest mortality rates are in sub-Saharan Africa, southeast Asia, and among people aged 75 years or older [86].

However, the greatest risk to human life and livelihood is the occurrence of an influenza pandemic [35, 89, 90]. Influenza pandemics occur when a novel influenza virus, often of zoonotic origin, emerges and infects a naive human population giving rise to sustained human to human transmission [3, 4, 22]. Their quick global spread

comes with an abrupt upsurge in illness, leaving response capacity insufficient. The last century saw pandemic influenza viruses belonging to only three subtypes, H1, H2 and H3 [35, 89], and will be discussed herein.

The “Spanish influenza” pandemic of 1918 still stands as one of the most fatal events in human history, killing an estimated 50 million people globally [91]. The causative agent was an avian-like H1N1 subtype and is thought to be the common ancestor of circulating human H1N1 and swine H1N1 influenza [74]. What was unique about this pandemic was that it mostly affected people from the 25–34 age group with mortality brought about by co-morbidity with bacterial pneumonia particularly devastating [65, 74].

In 1957, an influenza virus acquired three novel avian gene segments, H2, N2, and PB1, giving rise to the “Asian influenza” pandemic [65]. This pandemic resulted in an estimated 1-4 million deaths globally from 1957-1959, with the brunt of the impact of the pandemic delayed to the last two years in 44% of the countries it affected [92]. The “Hong Kong influenza” pandemic arrived 11 years later, and affected people from 1968-1969 [65]. Part of the population born in 1968 or later did not have any protective immunity to the circulating H2N2 from the previous pandemic. The 1968 pandemic virus replaced the previous H2N2 subtype, as the H2 and PB1 gene segments were replaced by reassortment with an avian-like H3 HA and PB1, with its’ neuraminidase remaining the same [65]. Its’ sporadic nature and milder impact in terms of morbidity and mortality (1 million deaths worldwide from 1968-1970 [93]) compared to its ancestors in different regions of the world is hypothesized to be mediated by N2 immunity from the previous pandemic in all age groups and to the HA antigen in the elderly [93]. This H3N2 virus has now circulated globally for 52 years as seasonal influenza [5].

The most recent global pandemic in 2009 was caused by an IAV H1N1 strain, now called A(H1N1)pdm09 or “swine flu” [4]. This virus possesses NA (N1) and M genes of Eurasian avian-like swine virus origin, HA (H1), NP, and NS genes of classical

swine virus origin (1918), PB2 and PA of avian origin from a swine triple reassortant lineage, and a PB1 of human H3N2 virus origin [94]. What is interesting is that in the case of A(H1N1)pdm09, many of the molecular markers associated with high pathogenicity or pandemic potential are not present such as the polybasic cleavage site found in HPAI [94, 95], nonetheless, it was still able to create much havoc.

In recent years, swine flu has spread from continent to continent, killing livestock and causing many human deaths [5]. In the United States alone, it is estimated that there were approximately 60.8 million cases (range: 43.3–89.3 million), 274,304 hospitalizations (195 086–402 719), and 12,469 deaths (8868–18 306) due to pandemic A(H1N1) in 2009 [96]. There was higher mortality among children and young adults, with only 10% of deaths reported for those over 65 years of age [97]. The virus continues to co-circulate globally today, along with H3N2 influenza A viruses descended from the 1968 pandemic [5].

1.2.5 Pandemic threats

Over the past 30 years the continuous spread of H5 and H7 HPAI viruses in poultry and wild bird populations in several continents has led to devastating effects in poultry, and in the case of sporadic human infection, death [35, 63, 65, 79, 98-101]. Viruses that are categorized as HPAI are currently restricted to the H5 and H7 subtypes as they are known to acquire the requisite polybasic insertional mutation at the HA cleavage site that makes them highly pathogenic in poultry [35, 80]. Although H5 and H7 avian viruses were shown to cause death in humans, none of these strains was easily transmitted from person to person [33, 70, 72, 80, 81, 99, 102-105] and their acquisition of genes from circulating human influenza viruses does not seem to be prevalent [90]. The danger is when these HPAI viruses evolve rapidly, mutating over an unpredictable period, into a highly lethal version that can sustain human to human transmission [65]. Studies have revealed that both H5 and H7 have the ability

to become transmissible among mammals, however these viruses require further adaptation in order to adapt fully to humans [89, 106].

Low pathogenic avian influenza (LPAI) viruses such as H9 or H10 have also been reported, but their effects are not as pronounced or widespread as HPAI [35, 74]. However, current H9N2 viruses, some with the ability to bind to human receptors, and already capable of causing human disease, are another potential source of a future pandemic [35, 79].

It is difficult to predict where and when the next pandemic will occur, and the ease of global travel means the risk from pandemic influenza can only increase. However, it is prudent to think of influenza circulating in both human and animal reservoirs as requiring vigilant surveillance [82]. The 2009 H1N1 pandemic became a public health emergency that exposed vulnerabilities in preparedness responses on a local and global scale. The WHO, the only global agency that can lead a pandemic response, is hampered by structural impediments [107]. It relies on funding from member states, each of which have vested interests that may limit a coherent and coordinated response during a global health emergency. At the time, the WHO's biggest failure was being unable to distribute enough influenza vaccine to all affected countries in a timely manner [107].

Today, questions remain regarding implementation of essential policies to limit damages to life and livelihood in a pandemic. As outlined by the WHO, pandemic preparedness involves strategies to reduce human exposure, intensifying capacity for rapid containment, stockpiling of antiviral drugs for prophylaxis, strengthening early warning systems, rapid investigation of cases and clusters, and building general capacity for healthcare [108]. Most importantly, we have to fill in the gaps of our scientific understanding of the influenza virus, inter-species transmission, host response and immunity, and environmental factors [89, 107]. This will enable us to predict novel influenza pandemics and develop more effective influenza vaccines and therapies that can protect against antigenically diverse influenza viruses.

Modern developments in DNA and protein biotechnologies have facilitated the discovery and engineering of cross-neutralizing/broadly neutralizing antibodies (bnAb) in different formats against influenza. During a pandemic, wherein vaccines are still unavailable, bnAb therapy could be useful in lowering morbidity and mortality. An alternative means of generating broadly protective humoral immunity against influenza is the employment of gene therapy vectors to express bnAbs. This strategy does not require the individual to mount an immune response against influenza akin to vaccination but protects via production of bnAbs without involving the immune system and may be a plausible approach to protect vulnerable patients against pandemic influenza.

1.2.6 Prevention and Treatment

Influenza prevention is still centered on vaccination [5, 109-112]. The nature of influenza viruses, constantly undergoing minor genetic changes in their globular hemagglutinin (HA) head region, requires annual reformulation of influenza vaccines to match the circulating strains [113, 114]. The current strategy for vaccine strain selection is to choose a virus that is antigenically representative of circulating viruses as determined by hemagglutination inhibition assay (HAI) and then subsequent testing against a panel of ferret antisera that was raised by infection with only a single virus. The WHO Global Influenza Surveillance and Response System (GISRS) recommends seasonal influenza vaccine compositions to be developed biannually for the Northern and Southern hemispheres that can protect the population against influenza viruses that are predicted to circulate during the upcoming season [5]. Influenza vaccination zones are decided by grouping countries with a similar onset period of their main influenza season where the circulating influenza viruses are closely related to the recommended vaccine viruses [115]. These zones are also in place to observe seasonal patterns and virus antigenic characteristics to decide which of the Northern or Southern hemisphere vaccines should be given to countries in the tropics and

subtropics. Currently, there are 8 geographical influenza zones, with Kenya and Malaysia categorized as an additional zone having year-round influenza activity without any distinct peaks [115].

Seasonal influenza vaccines must protect against and restrict virus transmission of H1N1, H3N2 and Influenza B viral strains currently circulating in humans globally [109]. The US Centers for Disease Control and Prevention's (CDC) Advisory Committee on Immunization Practices (ACIP) recommend the use of recombinant influenza vaccines (RIV), inactivated influenza vaccines (IIV) and live attenuated influenza vaccines (LAIV) for target groups to protect against influenza [109, 116]. The recommendations for influenza vaccination generally include people under 65 years of age who are at high risk of complications from influenza, individuals over the age of 65, pregnant women, health care workers with high exposure to the disease and high-risk cases such as those with chronic cardiac, respiratory metabolic, neurological conditions and morbidly obese people [117].

Recombinant flu vaccines (RIV) are created synthetically by combining HA DNA with baculovirus and growing this in a host cell line to produce large quantities of viral HA in a shorter time [109]. An advantage of RIVs is that they do not require the presence of a candidate vaccine virus or embryonated chicken eggs for production. The more popular choices are the Inactivated Influenza Vaccine (IIV) and the Live Attenuated Influenza Vaccine (LAIV). The Inactivated Influenza Vaccine (IIV), administered intramuscularly, is the most common type of vaccine given and is prepared from purified inactivated influenza viruses [118]. IIVs are recommended for adults aged 18 to 64 [119]. Live Attenuated Influenza vaccines (LAIV), on the other hand, contain influenza virus strains that are adapted to grow at a lower temperature [6] and are administered intranasally to mimic the natural route of virus infection. LAIVs are recommended for children aged 2 to 17 and is given as a nasal spray [119].

The most established correlate of protection from vaccination remains to be the Hemagglutination Inhibition (HAI) titer that measures IgG antibody titers pre- and post-

vaccination [120]. Vaccine response is then measured by determining seroconversion—the percentage of subjects with a 4-fold increase in antibody titres, and seroprotection—the percentage of subjects with HAI antibody titres ≥ 1:40 post-vaccination [121]. IIV has been shown to elicit protective humoral immunity by producing neutralizing antibodies that target epitopes on influenza HA [110, 122, 123]. LAIV on the other hand gives rise to more rapid and efficient innate and adaptive immune responses [123, 124].

In a study of young children 6 to 36 months of age, it was shown that HAI antibody responses were similar for both IIV and LAIV, however, only LAIV induced significant increases in T cell responses [125]. In adult subjects, 18 to 49 years of age, it was found that LAIV induced only minimal increases in serum HAI responses which were significantly lower than the responses induced by IIV, and both LAIV and IIV induced minimal and transient T cell responses to replication-competent whole virus [126]. In another study with adult subjects, it was also found that there was a 50% reduction in laboratory-confirmed influenza among subjects who received IIV compared with those given LAIV [123]. In a study comparing antibody responses of the elderly versus young adults after IIV vaccination, it was found that the adjusted odds-ratio (OR) of responses from 0.24 to 0.59 in terms of seroconversion and seroprotection in the elderly to vaccination with H1, H3 and Influenza B, corresponding to a clinical efficacy of 17–53% compared to 70-90% in young adults [121]. These results show that LAIV is more protective in children probably because they have not been previously exposed to either influenza virus or had no history of influenza vaccination enabling an increased vaccine-induced T cell response. In adults with pre-existing influenza immunity, LAIV immunogenicity may be limited resulting in a less impressive immune response [126]. It is also known that the elderly do not respond well to vaccination largely due to their less adaptable antibody responses to influenza, immune senescence and previous exposure that affects the cross-reactivity of

vaccine-induced antibodies. [88, 127, 128]. These findings imply that the elderly may need a more immunogenic vaccine than the ones available.

Although vaccines have been shown to be efficient for protection against seasonal influenza, several pitfalls are still associated with vaccination [112, 123, 124, 129-131]. There is no influenza vaccine that directly protects infants <6 months of age [116], or optimally protects the elderly population [88, 127]. Seasonal vaccination will also not be able to protect in the instance of a pandemic as it is designed to target circulating not emerging strains. Analyses from 2009 have shown that previous seasonal vaccination may either decrease or increase the risk of pandemic A(H1N1) pdm09 infection depending on the existing cross-subtype immunity in the community [132]. It was further shown that IIV vaccination in children prior to the 2009 pandemic, resulted in lower rates of serologically confirmed seasonal A/H1N1 and A/H3N2 infection but higher rates of pandemic A/H1N1 infection compared to the placebo group [133]. These findings bear implications for the use of seasonal vaccines during a pandemic and still warrant further investigation.

In more practical terms, the entire vaccination process is a complex global collaboration between regulators and manufacturers that puts huge pressure on the system to get it right within such a demanding time frame [110, 112, 131]. In a pandemic, it is estimated that a delay of 6 months is to be expected until the vaccine for the matching pandemic strain is rolled out to the public [132, 134]. In year 2000, about 85% of the world's supply of influenza vaccine was produced by only 9 vaccine companies located in 9 countries [134]. Also, this tedious process does not always guarantee a perfect match between the circulating influenza strain and the manufactured vaccine. As an example, during the 2016-2017 vaccination season, there was a single mutation in the egg-grown A(H3N2) vaccine's HA region leading to a mismatch with the circulating A(H3N2) strain, resulting in the vaccine's limited efficacy [135].

There are also additional factors that determine vaccine efficacy aside from circulating strain and vaccine mismatch. The theory of “original antigenic sin” (OAS) hypothesizes that the antigens on influenza strains encountered in childhood permanently shape the antibody response, boosting immune response upon exposure to related strains at the expense of responding to novel antigens [129, 136]. Moreover, variation in vaccine immunogenicity, individual suitability and response, clinical history, and instigating herd immunity are critical factors in the success of vaccination in any given season [109, 123, 129, 130].

Although vaccination is the main method to control the spread of influenza in humans, the use of antiviral drugs for treatment or chemoprophylaxis of influenza is also recommended [137, 138]. Antivirals offer an additional countermeasure against new rapidly spreading and/or potentially pandemic influenza viruses. Early treatment with antivirals reduces the duration of symptoms and risk of some complications (bronchitis, otitis media, and pneumonia) and hospitalization, and may decrease mortality among high-risk populations [138]. Prophylaxis with antivirals is also possible but depends on several factors including individual patient differences [109]. Patients that are not from high risk groups are managed via symptomatic treatment while those with severe or progressive clinical illness associated with or diagnosed as influenza are prescribed with antiviral drugs as soon as possible [109, 138].

In most countries, antivirals to control influenza infection are currently limited neuraminidase inhibitors that target the sialidase active site of neuraminidase [137, 139, 140]. These drugs are known to reduce the duration of viral replication and improve prospects of survival [109, 141]. Neuraminidase inhibitors, zanamivir, oseltamivir, and peramivir, block the release of newly formed virus particles, preventing viral spread [137, 139, 140]. They have all been proven to be highly potent inhibitors of influenza neuraminidase and can be delivered via different routes, inhalation (zanamivir), oral (oseltamivir) and intravenous (peramivir) [138].

However, as in the case of antibiotic resistance, antiviral drug resistance to influenza is now a major concern. All currently circulating influenza viruses are resistant to adamantane antiviral drugs, M2 ion channel inhibitors, due to mutations in the viral genome rendering these antivirals ineffective and obsolete as treatment options [141-143]. As for the NAI inhibitors, prior to the 2009 H1N1 pandemic, almost 100% of the globally circulating H1N1 subtypes were resistant to oseltamivir, the most commonly used NAI [141, 142]. This has changed following the 2009 IAV H1N1 pandemic, with this subtype which is oseltamivir-sensitive, becoming one of the dominant seasonal influenza virus strains [142]. As such, NAIs are now being given as first-line therapy because of historically low resistance rates, relatively infrequent side effects, and versatility as to different routes of administration and dosage formulations [138-140]. This, however, comes with caveats, as cases of resistance against H5N1 [144] and significant neuropsychiatric events in children of varying ages in Japan [140] have been reported. In 2018, a new class of antiviral drug for influenza, baloxavir marboxil (Xofluza), has been approved in Japan and the US [145]. Baloxavir marboxil targets the endonuclease function of the influenza viral PA polymerase subunit preventing the transcription of viral mRNA [145]. It is now recommended for the treatment of both IAV and IBV for patients aged 12 and above [138].

With the antivirals approved and available for dissemination, we now have prospects for combination therapy employing antivirals with different mechanisms of action [145]. The search for and development of new antivirals must also be prioritized and strengthened to ensure protection against seasonal influenza and as an emergency response in the case of a pandemic [139].

Currently, our options to prevent and treat influenza are rather limited when it comes to dealing with a pandemic threat. Vaccination provides little protection against highly diverged influenza strains since the precise antigenic properties of a new pandemic strain cannot be predicted, so stockpiled vaccines for seasonal influenza

may be poorly antigenically matched to the pandemic virus. Practical considerations for pandemic influenza vaccine development include isolation and characterization of the pandemic strain, manufacturing capacity, the ability of candidate vaccine strains to grow well in eggs, and biological safety containment of parent strains for vaccine development [5, 63]. The use of antiviral drugs is a more reactive rather than proactive solution to influenza; one that is a step behind an ever-changing virus. Given these difficulties, alternative approaches and various treatment options that can elicit effective broad-strain immunity regardless of influenza antigenic variation especially in high-risk groups is a welcome and most sought-after possibility.

1.3 Innate Immune Response to Influenza

The innate immune system is the first line of defense after a virus has overcome the external physical protective barriers of the body such as skin and mucus membranes. In IAV, the host's airway epithelial cells are first targeted. During IAV entry, viral conserved components called pathogen associated molecular patterns (PAMP) are recognized by host pathogen recognition receptors (PRR) and toll-like receptors (TLR) in innate immune effector cells [55]. This gives rise to an acute inflammatory response that is marked by activation of pro-inflammatory cytokines or chemokines that rapidly recruit innate effector cells such as natural killer cells (NK), monocytes, macrophages, dendritic cells and neutrophils [56].

Some of these cytokines have proven immunoregulatory and antiviral properties. Tumor necrosis factor (TNF) such as TNF-α [146] and Interleukins (IL) such as IL-1 [56] and IL-6 [147] were found necessary to lessen severity of illness due to H1N1 infection, with downregulation or loss of these pro-inflammatory cytokines leading to pronounced lung damage and, ultimately, death in mice. IL-22 on the other hand, although not playing a direct role in survival against H3N2 infection in mice, protects against pulmonary damages associated with subsequent bacterial superinfections [148].

However, cytokines can also contribute to the symptoms and pathology associated with the infection as in the case of cytokine storms which are associated with disease severity [56]. Severe cytokine storm, with markedly higher levels of IFN, TNF-α, IL-6, and chemokines, has been detected in patients hospitalized with severe influenza infections [149]. It was found that infection with highly pathological avian influenza H5N1 gave rise to production of IFN-α, IL-1β and TNF-α, to name a few, and IFN-β, IL-1β, and IL-6 are specific to infections with H9N2 [150]. These results show that chemokines and cytokines play a role in inflammation and histopathological changes, that are also dependent on the serotype of infecting IAV.

Dendritic cells (DC) and macrophages are also known to bridge the innate and adaptive immune response by recognizing foreign antigens at the site of infection and displaying them on their cell surface for recognition of B and T cell lymphocytes [55, 151]. The adaptive immune response then commences when T lymphocytes recognize viral antigens presented by DCs. Cytotoxic T Lymphocytes (CTL) produce cytokines and chemokines and effectively eliminate infected respiratory epithelial cells by granule exocytosis and engagement of TNF [151, 152]. CD4+ (Cluster of differentiation 4) T cells or Helper T cells (T_H) exert their effects on IAV indirectly mainly through cytokine production and B cell stimulation for antibody production [153, 154].

1.4 Antibody Immune Response to IAV

The humoral immune system, via its mucosal and systemic arms, is mainly responsible for lasting immunity against influenza [118, 155, 156]. It is at the helm of inducing virus-specific antibody responses against various influenza antigens, especially against the two surface glycoproteins HA and NA [118], with the presence of these antibodies correlating with protective immunity. As such, different immunoglobulin (Ig) isotypes play different roles in protection and influenza pathogenesis [157, 158].

Influenza infection, like that of most pathogens, activates an acute humoral response, stimulating secretion of antibodies by membrane-anchored immunoglobulin on the B-cell surface [159]. Antigen-specific IgM is widely accepted as the primary humoral response, appearing as early as 2 days after symptom onset [160], and diminishes quickly when long-lived IgG-secreting plasma cells and influenza-specific B memory cells are produced [158, 161, 162]. IgM is also co-expressed with IgD on the surface of mature B cells prior to antigenic stimulation [163], but the function of IgD still remains unclear to this day [164]. IgD appears to be evolutionary conserved within species but is suggested to be involved in microbial sensing and immune activation [164]. IgM antibodies are usually of lower affinity than IgGs but their pentameric nature compensates for this by enabling simultaneous binding to multivalent antigens, conferring high overall avidity [165]. IgM is mainly thought to contribute to virus control by activating the complement cascade and complement-mediated opsonization and increasing IgG responses [161, 162, 165]. IgM, however, may only play a minor role in viral clearance during influenza infection [162].

Differentiation into plasma cells usually occurs in germinal centers of lymph nodes, the spleen, or mucosa-associated lymphoid tissue driven by antigenic recognition and T-cell cytokines [166]. During differentiation, isotype switching involving deletion of intervening DNA sequences between specific recombination sites occurs, allowing antibodies to switch from IgM and IgD to another isotype such as IgA and IgG [166]. This isotype/class switch is thought to change the effector function of the antibody and improve its ability to eliminate the pathogen that induced the response [167].

The mucosal tissues are the main entry point of influenza and provides the first line of defence against infection together with the innate immune system. Mucosal or secretory IgA (SIgA) antibodies are produced locally by plasma cells in the lymphoid tissue at the site of infection and travel along the respiratory tract to airway epithelial cells [55, 156]. Nasal secretions contain neutralizing antibodies primarily of the IgA

isotype target influenza HA and NA [155]. SIgA prevents influenza virions from adhering to susceptible cells, thus inhibiting host invasion by the virus [55]. The antibody response in the upper respiratory tract is governed by IgA, and it is assumed that the mucosal IgA response targets approximately the same antigens as the IgG response that comes much later [160, 168, 169]. The local IgA response stimulated by natural infection lasts for at least 3–5 months, and is influenza-specific [155].

Additionally, during influenza infection, serum antibodies of the IgG subtype can be found in the mucosal respiratory tract and afford long-lived protection [55, 118, 159, 170]. IgG accounts for about 10–20% of plasma protein in human serum, of which there are four subtypes, IgG1, IgG2, IgG3 and IgG4 [171]. In humans, the majority of IgG antibodies targeting influenza virus are of the IgG1 subtype [158, 160, 162, 168], which is thought to interact strongly with Fcγ receptors (FcγRs) [172], making this IgG subtype effective at virus neutralization and activation of FcγR-mediated effector functions [168]. In mice, inactivated influenza (IIV) vaccination induces high IgG2a, low IgG1 and IgG2b, and very low IgG3 levels of antibody in serum [173, 174]. Mouse IgG2a is the murine equivalent of human IgG1 [172].

Typically, it is assumed that majority of antibodies induced by natural infection or vaccination will target influenza HA, with lower-level responses to NA, M2 and internal proteins also being induced [20, 55, 118, 168]. This preference for HA is due to them being present in larger numbers on the surface of the virus relative to other virus proteins, and as such, are easily accessible to antibodies and B cell receptors [17, 20, 175, 176]. Because of their ability to block virus attachment and entry into host cells, neutralizing antibodies directed against the trimeric globular head of the HA molecule are thought to mediate resistance to influenza infection [160]. Immune response induced by natural infection protects against reinfection with the same virus or an antigenically similar viral strain and may lead to long-lasting immunity to the infecting virus [118, 168, 177].

Serum anti-HA antibodies are the most commonly measured correlate of protection against influenza [117, 156, 178], as measured by the hemagglutination inhibition (HAI) assay [179]. A protective serum antibody HAI titer ≥ 40 is the universally accepted seroprotective titer, which corresponds to 50% protection from influenza as demonstrated in numerous studies, with higher serum HAI titers associated with higher rates of protection [120, 180-182]. This threshold was first established in 1972 [120], and is still yet to be replaced to this day, even with findings that correlates of protection may differ depending on the infecting virus strain, age and health status of recipient and history of exposure to nature influenza infection and/or vaccination to name a few [88, 121, 160, 182].

In mice, it was found that both vaccination and infection produced influenza subtype specific IgG antibodies that persisted up to 18 months even without re-exposure [165]. These antibodies which persisted in circulation still protected mice 20 months later after a lethal challenge with the same virus subtype [165]. In the case of natural infection or vaccination, neutralizing titers against the infecting or vaccine strain were high enough to meet the protective threshold [165, 183].

The isotype-specific antibody response has also been documented in human subjects undergoing either primary or secondary infection with IAV. Studies have shown serum antibody increase in IgM (~86%), IgG (~100%), and IgA (~96%) during primary infection in healthy adults [158, 184]. Secondary infection of the same IAV gave rise to a serum antibody titer increase in only IgG (68%) and IgA (74%), but this was less than was observed during primary infection [184]. An increase in IgG and IgA antibodies with increasing age of the serum donor was also observed, with serum titers for both isotypes showing correlation [158, 160, 185]. These findings are interesting in the context of vaccination, as there is evidence that location of infection influences the correlate of protection being observed, with systemic immunization inducing protective IgG whilst intranasal immunization induces protective IgA, however

it is suggested that both IgG and IgA work together to prevent infection [125, 126, 169, 182, 185].

Post-vaccination or infection, a strong correlation between the levels of isotype-switched IgG detected in the blood and the serological response showing antibody responsiveness demonstrate seroconversion [186]. However, these antibody titers can decline in time as was observed in adults and especially the elderly post pandemic 2009, giving rise to possible re-infection and recurrent epidemics by the same strain [187].

1.5 Passive Immunotherapy against Influenza

Antibody-based protection underlies passive transfer, whereby the administration of sera or purified antibodies into naïve patients transiently confers immunity [188]. Passive immunotherapy has long been employed for prophylaxis, intervention, and treatment of diseases caused by various microorganisms such as bacteria, fungus, parasites and viruses [189-191]. Antibodies have been administered in different forms, such as plasma or serum, pooled human immunoglobulin for intravenous (IV) or intramuscular (IM) use from immunized or convalescent donors, and as monoclonal antibodies that provide immediate immunity and protection from infection to at-risk individuals [26, 189-194].

Passive transfer of serum from convalescing influenza patients is one option which has been deployed with some success [195, 196]. Even with advances in vaccine development [110, 113, 197] and small molecule antiviral therapeutics [198-200], there is still no established way of conferring complete protection against a pandemic threat or dealing with severe influenza especially in high risk groups. Passive immunotherapy using antibodies with potent neutralizing capacity may be an ideal rapid treatment strategy for influenza infection [194]. This strategy provides the opportunity to protect at-risk segments of the population, most importantly, first responders to a novel strain, as well as those who respond poorly to vaccination [193,

201]. However, this comes with practical caveats. Convalescent plasma collection is highly dependent on the availability and eligibility of donors, and the time constraints from collection to fractionation and production, make it a rather tedious process with inherent safety issues such as adventitious contamination [202]. The scalability of this process during a global pandemic is also a limitation.

Nonetheless, other antibody-based therapies aside from convalescent plasma are available. Because antibodies are naturally produced by the immune system in response to infection, they are known to have low toxicities [189]. Antibodies are also versatile in that they could bind to a single epitope using their fragment antigen binding region (Fab) and perform a variety of functions such as toxin and virus neutralization, complement activation, engage in antibody-dependent cellular cytotoxicity and opsonization in conjunction with other cellular and host mediators via their fragment crystallizable (Fc) region [26, 193, 203, 204].

However, the use of antibodies especially against infectious is beset with safety issues in the form of immunogenicity, hypersensitivity, treatment-related infusion and anaphylactic reactions, high specificity leading to a probable exaggeration of the intended pharmacology, generation of anti-drug antibodies and other adverse effects due to clearance and efficacy [205]. The clinical consequences of these reactions range from local to life-threatening [206]. One of the most infamous examples of failed antibody therapy was that of anti-CD28 antibody TGN1412 [207]. In the first human clinical trial, TGN1412 triggered a cytokine storm that caused near fatal systemic inflammations due to massive production of pro-inflammatory cytokines resulting in pulmonary infiltrates, lung and renal failure and disseminated intravascular coagulation in 6 patients [207]. Therapy employing antibodies with immunomodulatory properties like B-cell depleting anti-CD20 Rituximab and epidermal growth factor receptor inhibitors Cetuximab and Bevacizumab, has also led to adverse infusion reactions in most/all lymphoma patients, usually within hours of starting the first infusion, thereby requiring hospitalization [206]. This highlights the need for conducting longer term

chronic toxicity studies depending on the intended duration of treatment. Another issue is a mismatch of tolerability parameters when an antibody intended for human use is tested for safety in an animal model. This makes findings in animal toxicology studies not entirely predictive of potential immunogenicity in humans.

In the case of influenza, neutralizing antibodies against the major surface glycoproteins of IAV, HA, NA, and M2 have been shown to be effective in protection from disease in mice and ferrets [192, 208-210]. Moreover, immunotherapy with antibodies for influenza was not shown to interfere with the development of antiviral adaptive immunity, allowing the formation of memory responses to influenza viruses in future [192, 194].

Much of antibody efficacy depends on which part of the virus the antibody binds to [175, 192, 211, 212]. Antibodies usually bind to the HA head domain to block viral attachment to host cells or the HA stem to inhibit virus fusion after endocytosis [26, 175, 212]. Antibodies generated by vaccination generally induce a narrow, strain-specific response against the highly variable head domain of HA and thus will have little or no efficacy against drifted or shifted strains [88, 116, 158, 160, 168, 213, 214]. Conversely, the hemagglutinin stalk domain has been identified to harbor neutralizing epitopes that are conserved among influenza A virus subtypes [215]. These epitopes, that have been found to be cross-reactive [208, 215-219] evolve at a significantly slower rate than the HA head domain, with evolution not directed at evading neutralizing antibody responses [16]. Targeting these sites will improve antibody efficacy against rapidly evolving influenza viruses [9, 22, 210, 215, 216, 220, 221].

Given the overall promise and current limitations of passive immunization in influenza, it is highly desirable to identify and/or engineer antibodies that bind with high affinity and are cross-subtype neutralizing against many or all influenza strains that are capable of infecting humans [193].

1.5.1 Broadly neutralizing antibodies (bnAb)

The hemagglutinin glycoprotein (HA) is subject to continuous mutation driven by the selective pressure of the antibody response, which is primarily directed against the globular HA head [16, 198, 222-228]. Most antibodies that bind to the HA head recognize antigenically similar strains within a single HA subtype and are prone to selecting escape mutants [208, 223, 225]. In contrast, heterosubtypic antibodies should be capable of neutralizing multiple subtypes of influenza A, making them attractive options for future development.

Mammalian species' IgGs are heterodimeric four-chain antibodies composed of two identical heavy chains and two identical light chains. The heavy chain, the larger of the two chains, is a single polypeptide that contains four Ig domains, consisting of V_H and C_H1 which form part of the variable antigen binding region (Fab) domain and two constant Fc domains (C_H2 and C_H3). The light chain is composed of two Ig domains, V_L and C_L. The heavy and light chains are linked such that the V_H – C_H1 domains are paired with the V_L – C_L domains to make up the variable region (Fab), which is responsible for antigen recognition. The N-terminal regions of V_H and V_L are characterized by extensive variability in their amino acid sequence [229, 230]. Disulfide bonds at a flexible hinge region separates the Fab and Fc domains [171]. The fragment crystallizable/constant region (Fc) is the part of the antibody that interacts with effector molecules by binding to Fcγ receptors on their surface [171]. The Fc region, in contrast to the Fab region, is less variable and differs only between distinct immunoglobulin classes and subclasses [171]. Because they are structurally built in this manner, antibodies are at the crossroads of the human immune response against infection as they can also link up with the effector arm of the immune system. This includes activation of the complement system, phagocytosis, degranulation and cell cytotoxicity [55, 159, 168].

Each antibody variable region heavy and light chain is organized into four framework regions (FR1-FR4) that are relatively invariant and three complementarity determining regions (CDR1-CDR3) that are hypervariable and participate in antigen

binding [166]. The CDRs of both the heavy and light chain participate in the formation of the antigen-binding pocket [166], with the CDR3 regions of V_H and V_L localized at the center of the antigen- binding site [229]. During affinity maturation, genes encoding for the V regions of the antibody heavy and light chain undergo mutations after antigen stimulation, to produce antibodies with higher affinity for the antigen [166, 231]. Because the CDR3 regions are localized at the centre of the antigen- binding site, incorporation of mutations in CDR3 during affinity maturation is thought to be predominantly responsible for improved antibody specificity [229].

The diversity of antibody repertoires is generated by genetic recombination and somatic mutation of the immunoglobulin genes [166, 229]. The immunoglobulin loci contain gene fragments coding for the variable domains of the antibody heavy and light chain. The light chain loci have only variable (V) and joining (J) gene segments, whereby the heavy chain locus additionally has a diversity (D) gene segment [166, 232]. These gene segments randomly recombine in the “joining” process generating diverse loci combinations [232]. V-D-J recombination in the variable heavy chain potentially results in greater diversity compared to V-J recombination of the variable light chain. Additionally, the antibody repertoire is further diversified in germinal centers by introduction of mutations in the variable domains of the heavy and light chain by activation-induced cytidine deaminase (AID) in a process called somatic hypermutation (SHM) [232]. This involves stabilizing mutations in FRs and CDRs, enabling them to evolve in real time to defend against infection [229, 233-236].

The isolation of broadly neutralizing antibodies against influenza A viruses has been a long sought-after goal for influenza therapy [6, 193, 197]. Antibody libraries can be constructed by cloning genes directly from lymphocytes of immunized animals and expressing them as a single-domain library of antibody heavy- or light-chain variable regions or as a combinatorial library of antigen-binding (Fab) fragments in bacteria [210, 235, 237, 238]. Using phage or yeast display technology, broadly

neutralizing antibodies can be isolated by a series of steps involving antigen selection and repeated rounds of binding, washing, elution and amplification [239, 240].

Libraries such as these were constructed to isolate monoclonal antibodies (mAb) with broad heterosubtypic neutralizing activity against influenza [34, 210, 238]. These studies have yielded several broadly reactive neutralizing antibodies from various sources: non-immune [210] and immune [209] human antibody phage display libraries, human IgM+ memory B cells of seasonal influenza vaccines [238] and H5N1 outbreak survivors [34], that could be used for passive immunization. Findings from these studies reveal that all broadly neutralizing antibodies that were isolated use the same germ-line encoded CDR's (V_H1-69) and interact with influenza virus in similar fashion [34, 209, 210, 217, 234, 238].

Rather than functioning by steric hindrance by blocking viral access to cellular receptors as in HA head-binding neutralizing antibodies, these antibodies inhibit viral fusion by inserting themselves into a hydrophobic site on the helical stem of the HA trimer thereby preventing the conformational change that initiates the fusion process [34, 217, 238]. A plethora of broadly neutralizing human monoclonal antibodies (mAb) against the HA stalk domain have been isolated ever since [208-210, 218, 241-245]. As opposed to anti-HA head mAbs, stalk-reactive antibodies do not show hemagglutination inhibition activity but are still able to neutralize virus [110, 209, 222, 227].

Aside from neutralization, antibody-dependent cell-mediated cytotoxicity (ADCC) by employing Fc-mediated effector functions and complement-dependent cytotoxicity are thought to contribute to protection conferred by these antibodies against influenza *in vivo* [111, 208, 209, 227, 246, 247]. Strong evidence of the need for Fc effector engagement was demonstrated in a study by DiLillo et al. [246], with results showing that all neutralizing and non-neutralizing anti-HA and anti-NA Abs that are heterosubtypic that were tested required Fc-γ-receptor (FcγR) interaction when given at low doses for protection of mice *in vivo*, while strain-specific mAbs did not.

Additionally, mice that were *Fcer1g*$^{-/-}$ (lacking the FcR-γ chain and do not express activating FcγRs, were not protected from influenza challenge even with administration of a broadly-neutralizing mAb that was shown to protect in wild type mice [246]. Furthermore, it has been shown that Fc-mediated effector functions contribute to *in vivo* prophylactic efficacy of anti-HA stem antibodies at low antibody doses, while at high antibody doses protection is primarily mediated by virus neutralization [208, 247], leading us to speculate that FcγR engagement may compensate for low concentrations of these mAbs in the serum. Other studies have shown that M2e-specific mAbs that could activate human NK cells *in vitro* were able to provide protection from lethal influenza challenge in mice via an Fc-receptor dependent mechanism [248].

Isolation of these cross-neutralizing monoclonal antibodies has led to the exploration of their therapeutic use aimed at generating long-term humoral activity *in vivo* especially in immunocompromised populations [141]. What is unusual is that in the case of CR6261 [209], and F10 [210], broadly-neutralizing human mAbs against influenza, antibody binding is mediated only by their heavy-chain domains, with no contact with the antigen being made by the light chains. This has prompted our interest in naturally occurring "heavy-chain only" antibodies such as those that can be isolated from camelid species as possible immunotherapeutics against influenza.

1.5.2 Nanobodies (Nb)

Camelid species (*Camelus dromedarius, Camelus bactrianus, Lama glama, Lama guanoco, Lama alpaca* and *Lama vicugna*), in addition to conventional IgG (of the IgG1 isotype) (**Figure 1.2**), also have naturally-occurring heavy-chain-only antibodies (HCAb), that lack the light chain V_L-C_L (camelid IgG2 and IgG3) [249]. The heavy chain of the HCAb is composed of three instead of four globular domains with the C_H1 domain of classical antibodies missing **(Figure 1.2)** [249, 250]. Light chains do not associate with the C_H1-free heavy chains; however, the heavy chains still pair

up through their constant domains. A single variable domain in the HCAb serves as the smallest part of the antibody that can recognize antigens and is referred to as V_HH (~15 kDa) [251] also known as nanobodies (Nbs) or single domain antibodies (sdAb) [250] **(Figure 1.2)**. This single N-terminal domain (V_HH) binds antigen without requiring domain pairing [252]. These heavy-chain dimers are devoid of light chains, but nevertheless have an extensive antigen-binding repertoire [249, 253].

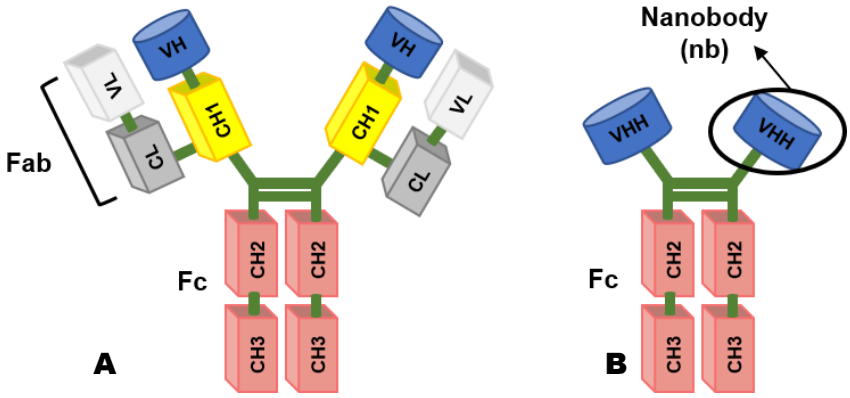

Figure 1.2. Schematic representation of naturally occurring antibodies in sera of camelids. (**A**) Conventional heterotetrameric antibody found in mammalian species containing two light chains (L) and two heavy chains (H). (**B**) Homodimeric heavy-chain antibody (HCAbs), which comprise only H chains with a deleted C_H1 region that can be found in camelid species. Indicated by an arrow is the V_HH, the smallest antigen-binding fragment of an HCAb, also called Nanobody (Nb). Fab, antigen binding fragment (variable domain); Fc, crystallizable fragment.

Similar to conventional V_H domains, V_HH contain four framework regions (FRs) that form their core structure and three complementarity-determining regions (CDRs) that are involved in antigen binding [254]. Camelid heavy-chain IgGs compensate for their lack of a V_L domain by somatic hypermutation in their complementarity determining regions (CDR) [250, 251]. This leads to an extended hypervariable loop region that enables their CDRs to increase diversity and adopt novel conformations that increase binding surface and allow access to occluded epitopes [250, 251, 255]. Moreover, in comparison with the V_H of conventional antibodies that have conserved hydrophobic framework-2 (FR-2) residues, HCAbs have these hallmark amino acids in FR-2 frequently mutated into more hydrophilic amino acids, enabling them to avoid

association with the variable light chain domain [250, 256]. In some cases, their longer CDR3 folds back on the V_HH framework, burying amino acids which are primarily involved in association with antibody light chains [252, 256, 257]. Because of this, they are usually not hampered by solubility and aggregation problems typical of single V_H domains from conventional antibodies [258].

V_HH display full antigen-binding specificity and can be isolated and produced separately as nanobodies (Nb) [250, 259]. Nanobodies have several advantages over conventional IgGs making them attractive options for immunotherapy. A nanobody's small size and their elongated and protruding CDR3 loops allow them to recognize hidden and hard to reach epitopes and cavities [250, 251, 259, 260]. Because it is in single domain format, it also leaves a smaller footprint on the antigen compared to classical antibodies [219, 253, 261]. They also have the advantage of high physicochemical stability and high solubility making them easier to manipulate [254, 256, 259, 262, 263]. Due to these useful physical properties, nanobodies can be formulated as long shelf-life, ready-to-use solutions. Additionally, as they can survive harsh conditions of temperature and pH and remain biologically active [260], they can be used for oral delivery and topical applications.

The ease by which genes coding for these nanobodies can be cloned and expressed in bacterial systems combined with the recent advances in mammalian protein production have encouraged engineering of these single-domain antibodies for use as research tools in biotechnology and medicine [253, 260, 264]. The flexibility provided by employing different expression strategies is critical because the fusion moieties might require specific conditions for correct folding or post-translational modifications that can only be achieved in eukaryotic systems and not in prokaryotic cells. The conventional procedure of obtaining mAbs requires cloning of two antibody gene fragments, generation of a combinatorial library and expression requiring glycosylation in appropriate host systems [252, 253]. The use of V_HH is more

straightforward as only one domain has to be cloned and expressed to generate an intact antigen-binding fragment [251].

Nowadays, nanobodies can be easily cloned and selected for antigen specificity using immune libraries [254]. Immune libraries are based on peripheral blood lymphocytes isolated from a camelid that has been immunized with antigen of interest to generate high affinity V_HH [265]. Natural somatic antibody maturation then creates an enormous diversity of affinity-matured nanobodies. Antigen-specific V_HH are then isolated by phage, yeast or ribosome display [266].

As an example, immune single-domain libraries from camelids can be generated by immunization of the camelid by repeated subcutaneous injections in presence of adjuvant. After some time, peripheral blood lymphocytes are recovered from collected blood samples. An rt-PCR step is performed to obtain cDNA by amplifying the V_HH gene segments from lymphocyte RNA. The V_HH repertoire generated is then cloned in a phage display vector and transformed in a bacterial host. The V_HHs are expressed at the tip of the phage particles and after 2–3 rounds of panning, individual clones producing antigen-specific V_HH can be obtained [267, 268]. Recently, Golden Gate Cloning has been employed for the cloning step; yielding greater than 10^8 transformants with near 100% of the clones containing a phage display vector with the correct insert length of a V_HH, an improvement from the classic procedure [269].

Naïve and synthetic libraries can also be used to generate V_HH [254]. The advantage of using these libraries is that no experimental animal handling is involved as they are built based on a well characterized V_HH and in synthetic libraries, CDR alterations are due to saturating site-specific mutagenesis, making the process more controlled [251, 254]. However, naïve and synthetic libraries often recognize the antigen with low affinity, hence the preference for immune libraries [253].

However, one of the disadvantages of using V_HH is that due to their small size, they rapidly pass the renal filter, which has a cutoff of about 60 kDa, resulting in their

faster blood clearance [254]. This shorter serum half-life compared to conventional antibodies limits the efficacy of V_HH in many parenteral applications. Therefore, the success of nanobodies in therapy will come down to the specific applications or targets as some treatments would require improved blood levels over a prolonged time whilst others may only require transient or localized nanobody expression [260]. Another consideration is that nanobodies may have to be "humanized" to reduce possible immunogenicity for further therapeutic applications. This requires mutation of camelid-specific amino acid sequences, mostly in the FR-2 region, to their human heavy chain variable domain equivalent without compromising on their expression level, affinity, solubility, and stability [270]. Depending on the intended downstream application, nanobodies may require reformatting and further improvement to be employed as effective therapeutics.

1.5.2.1 Nanobody Re-Formatting to increase Half-Life

Human IgGs have an elimination half-life ($t_{1/2}$) of 10-21 days, and murine IgGs have a $t_{1/2}$ ~5 days [271, 272]. In contrast, employing mouse models, it was found that nanobodies are cleared rapidly from the blood, with a $t_{1/2}$ of 1.5 hours [273]. The highest initial levels of V_HH were found in kidneys (15 minutes post-intravenous injection), which is characteristic of a renal excreted protein [273]. This rapid clearance can hamper the nanobody's efficiency, as maintaining its levels in circulation is necessary to optimally achieve its functions. V_HH can be administered by repeated dosing or injection, but this is restrictive and not cost-efficient. Nonetheless, it is possible to manipulate the nanobody's intrinsic affinity properties, increase its valency, or add an antibody Fc domain to prolong half-life and maintain therapeutic threshold concentrations for a longer period [266]. The circulating half-life of IgGs is dependent on its association with the neonatal Fc receptor (FcRn) [274]. FcRn which binds all IgG isotypes in mice and humans, plays a central role in regulating the catabolism and thus the half-life of IgG as well as its functions in the immune system [204].

Oligomerization of nanobodies commonly via flexible glycine–serine linkers, can easily be employed without the mispairing and solubility issues inherent to single-chain variable fragment-based dimers and multimers [258]. Two similar or different HCAbs can also be tethered to the structural upper hinge of a natural antibody to generate bivalent or bispecific constructs, respectively [275]. V_HH can be displayed or anchored on the surface of stable proteins such as ferritin, which is widely produced in bacteria and mammals, to make a low molecular-weight polymer called “fenobodies” [276]. Chemical modification of nanobodies with polyethylene glycol (PEG), a water-soluble polymer to increase their molecular weight but maintain therapeutic efficiency can also be explored. In a study that aimed to determine distribution of different molecular weight PEG molecules after IV administration in mice, it was found that PEG samples of higher molecular weight were retained in the blood circulation for a longer period than those of lower molecular weight [277]. Low MW PEG however, showed a larger volume of distribution [277]. This was shown to decrease blood clearance of V_HH delivered via passive immunization in guinea pigs [278].

A successful strategy to improve the pharmacokinetic profile of V_HH is by coupling it to serum albumin. Albumin, with a molecular weight of 66.5 kDA, is the most abundant human plasma protein (35–50 g/L serum) [279]. It has an average half-life of 19 days, making it an attractive conjugate for therapeutic molecules with shorter half-lives [279]. Albumin has an extended $t_{1/2}$ due to its binding to FcRn in a pH-dependent manner, similar to IgG [280]. Studies were done to test clearance rates in monkeys and mice of nanobodies fused to serum albumin when given intravenously, and results were very similar between the two species. In mice and monkeys, nanobodies linked to albumin resulted in a 167 and 376-fold decrease in clearance compared to the monovalent counterpart and a terminal half-life of 0.82 and 4.9 days, respectively, close to the actual $t_{1/2}$ of albumin in the species [281].

The strategy to extend half-life by binding to serum albumin was tested for anti-rabies nanobodies in a mouse challenge model [282]. Half-life of the nanobody

constructs was increased through linkage with a third V_HH targeted against albumin [282]. This intervention was found to significantly prolong survival or even completely rescue mice from rabies with the therapeutic effect depending on the dose, affinity and brain and plasma half-life of the V_HH construct [282].

To treat rheumatoid arthritis by inhibiting cytokine interleukin-6 (IL-6)-induced inflammation, ALX-0061, composed of an affinity-matured interleukin-6 receptor (IL-6R)-targeting V_HH domain fused to another V_HH albumin-binding domain, was tested *in vitro* and *in vivo* [283]. It was shown to have high affinity for IL-6R; a dose-dependent and complete inhibition of IL-6-induced inflammatory parameters, and a plasma half-life of 6.6 days after a single intravenous administration in cynomolgus monkeys [283]. These studies show that albumin binding as a half-life extension technology resulted in expected pharmacokinetics that increased the duration of nanobodies in circulation.

All nanobodies mentioned previously came from immune libraries and displayed high affinity towards the antigen, however, this may not always be the case. Nanobodies exhibiting low-affinity interactions may acquire enhanced breadth and/or potency through an avidity effect by joining two or more V_HH into multivalent constructs using flexible linkers [228, 275]. In a broad study to determine effects of V_HH avidity on virus neutralization by Hultberg et. al [284], llama-derived nanobodies were tested against envelope proteins of Respiratory Syncytial Virus (RSV), Rabies virus and H5N1 Influenza. They found that making the V_HH bivalent, trivalent or biparatopic significantly improved neutralization potencies by about 4,000-fold for RSV, 1,500-fold for Rabies virus and 75-fold for influenza H5N1, compared to monovalent V_HH [284]. IC_{50} values obtained via reformatted V_HH were also lower than attained by marketed mAb Synagis (Palivizumab) against RSV [284].

In the same vein, Palomo et. al [285] improved on monovalent nanobody Nb017 that binds to the human respiratory syncytial virus (hRSV) fusion (F) glycoprotein, by making it the trivalent nanobody ALX-0171. Following results from Hultberg et. al, ALX-0171 is about 6,000 to 10,000 times more potent than Nb017 in

neutralization tests with strains of hRSV antigenic groups A and B, even outperforming palivizumab, a monoclonal humanized IgG1 antibody directed against the same epitope of the RSV F protein and currently used as a prophylactic anti-RSV treatment [285].

Available bnAbs against HIV-1 target the membrane proximal external region (MPER) of the HIV-1 glycoprotein gp41, however these MPER-specific neutralizing antibodies are not induced upon immunization [286]. Lutje Hulsik et. al aimed to produce MPER-specific V_HH by immunizing llamas with proteoliposomes containing trimeric gp41 consisting of the HIV-1 Env transmembrane region and MPER [286]. They selected a V_HH, 2H10 and made it bivalent, observing an approximate 20-fold increase in affinity in neutralization of various sensitive and resistant HIV-1 strains compared to its monovalent counterpart [286].

The same approach was employed by Matz et. al [287] to generate a panel of broadly neutralizing single domain antibodies (sdAb) that bind to either the CD4 or the coreceptor binding site of HIV-1. They found that there was no significant improvement in neutralizing activity as measured by IC_{50} values when sdAbs were made multivalent compared to monovalent [287]. However, several multivalent sdAbs could neutralize a broader spectrum of pseudoviruses including HIV-1 subtypes A, B, C, and G, while monovalent sdAbs could only neutralize the HIV-1 envelope used for initial llama immunization and further selection [287].

Another approach to extend nanobody half-life for downstream immunotherapy is “piggy-backing” onto an IgG molecule that is known to have a longer half-life [266]. To treat Foot and Mouth Disease (FMD), Harmsen et. al [288] developed “V_HH2”, a structure involving two V_HH domains separated by a small flexible linker, with one V_HH that is FMD virus-neutralizing, and the other V_HH binding to porcine IgG. They showed that V_HH2 can bind bifunctionally to both targets with the molecule having an elimination half-life of 280±53 hours, a 100-fold increase from the projected $t_{1/2}$ of the FMDV-neutralizing V_HH on its own [288].

Stalin Raj et. al. [289] isolated nanobodies from dromedaries immunized and subsequently challenged with Middle East respiratory syndrome coronavirus (MERS-Cov). These V_HH from immune libraries demonstrated highly potent neutralizing activity against the virus by binding to the receptor binding domain of the viral spike protein *in vitro* [289]. These V_HH were then linked to a human Fc domain lacking the C_H1 exon, forming an HCAb. Intraperitoneal injection of V_HH and HCAb 6 hours before lethal MERS-Cov challenge in mice, resulted in death of all mice given the monovalent V_HH around 7 days post infection and survival of all mice that received the HCAb [289]. Serum half-life of the HCAb was found to be approximately 4.5 days [289].

CXCR4-specific nanobodies, that are involved in G protein-coupled receptor (GPCR) signalling associated with survival and recurrence of certain types of blood cancers were made bivalent and fused with the Fc domain of human IgG1 [290]. These nanobody-Fc molecules were found to exhibit better antagonistic properties in tumor-mediated signalling and anti-HIV activity through binding to the HIV-co-receptor CXCR4 than their monovalent counterparts and the clinically approved antagonist already in the market [290]. These findings are in line with what was described previously with bivalent nanobodies and with incorporation of an Fc domain further enhancing their therapeutic potency.

All approaches presented were designed to improve binding affinity and extend the half-life *in vivo* of very potent highly specific nanobodies. Further optimization could potentially lead to more pronounced therapies against cancers, tumors, viruses and other infectious diseases.

1.5.2.2 Nanobodies with Effector Functions

Aside from increasing plasma half-life of nanobodies to prolong their therapeutic activity, attachment of an Fc domain also enables molecules to interact with Fcγ-receptors (FcγR) found on immune cells [203]. Attachment to cellular receptors by the appended antibody Fc region leads to recruitment of innate immune

effector cells via antibody-dependent cell-mediated cytotoxicity (ADCC), antibody-dependent cell-mediated phagocytosis (ADCP) and complement-dependent cytotoxicity (CDC) [171, 172, 291]. Fc function therefore links the adaptive immune system to the potent effector functions provided by the innate immune system [203].

IgG subclasses differ in their ability to bind to FcR, which in turn dictate how they mediate effector functions [171, 291]. Activating Fcγ Receptors in mice are FcγRI, FcγRIII and FcγRIV which favorably interact with mouse IgG2a, and in humans, FcγRI, FcγRIIA and FcγRIIIA, which interact with human IgG1 and IgG3; with FcγRIIB inhibitory in both mice and humans [172, 291]. Furthermore, activating FcγRIV in mice is closely related to FcγRIIIA in humans [292].

In the study by Bobkov et. al [290], nanobody-Fc (fused to human IgG1) that inhibited tumor signalling and HIV entry induced ADCC and CDC-mediated cell death. Binding of the Fc region of the nanobody to FcγRIII of effector cells such as natural killer (NK) cells resulted in their degranulation [290]. As such, these constructs were able to combine the excellent tumor and viral inhibiting properties of llama-derived single-domain antibodies with Fc-mediated effector functions of conventional antibodies.

A V_HH anti-rotavirus protein 1 (ARP1) was shown to confer protection against rotavirus induced-diarrhea in a neonatal mouse model by binding to the most abundant and highly conserved rotavirus inner capsid protein VP6 [293]. However, the mechanism of ARP1 neutralization is not yet understood. Gunaydin et. al [294] fused ARP1 to mouse IgG1 Fc, and was given at a suboptimal dose known to be non-protective in the mouse model to evaluate the role of Fc-mediated effector functions and avidity in *in vivo* rotavirus infection. When given in equimolar amounts, among monovalent ARP1, bivalent ARP1 and Fc-ARP1, only Fc-ARP1 reduced the prevalence, duration and severity of diarrhea, suggesting that protection is due to Fc-mediated neutralization of rotavirus [294].

Another lesser known Fc receptor that is found in all cells, the tripartite-motif containing protein 21 (TRIM21), is also involved in “antibody-dependent intracellular neutralization” (ADIN) [295]. TRIM21 binds virus-antibody complexes in the cytoplasm and targets virions for degradation by proteasomes [295]. In the same study by Gunaydin [294], they also investigated the role of FcRn and TRIM21 mediated recognition of (Fc-ARP1)-rotavirus immune complex, by inserting an amino acid mutation in Fc-ARP1, at a position that was previously shown to be crucial for TRIM21 and FcRn activity [295]. They found that this mutation completely prevented the binding of Fc-ARP1 to FcRn leading to reduced protection conferred by the Fc-ARP1 mutant against rotavirus in mice. Neutralization of rotavirus by the mutant Fc-ARP1, however, was not completely inhibited suggesting different mechanisms of neutralization aside from ADCC or ADIN [294].

Equipping V_HH with effector functions that do not rely on the host’s response has also been investigated [266]. In the case of Herpes Simplex Virus-2 (HSV-2), V_HH R33 that binds to HSV-2 glycoprotein D, was identified from an immune llama derived-library, but was found to not have any neutralizing activity *in vitro* [296]. However, when expressed with the cytotoxic domain of *Pseudomonas aeruginosa* exotoxin A, making it an immunotoxin, R33 then went on to potently kill HSV-2-infected cells, with an IC_{50} in the nanomolar range [296]. V_HH have also been used in dual function liposomes for the prophylaxis of HIV/AIDS [297]. Liposomes were coated with anti-gp120 nanobodies conjugated via either non-covalent metal chelation or a covalent linkage and were also used to encapsulate the hydrophobic antiviral drug dapivirine; both strategies resulted in reduction of HIV-1 replication *in vitro* [297].

The many advantages that single-domain antibodies confer due to their robustness and the ease by which they can be reformatted into better versions to improve their therapeutic efficacy is something that we can exploit going forward in our quest to develop highly versatile and effective treatments against disease.

1.5.2.3 Nanobodies against Influenza

It is fitting that single domain antibodies have become attractive therapeutic molecules against infectious diseases, most notably influenza. Influenza poses several targets for nanobody therapy such as the HA head, HA stem, NA and M2 proteins. With reformatting and delivery, these nanobodies may be implemented as prophylaxis or therapy that can be used in cases of an influenza pandemic, to mitigate health and economic impacts.

A study by Wei et. al [298] generated V_HH from synthetic camel libraries specifically targeting native M2 ion channel (ectodomain of M2, M2e), thought to be conserved in human IAV. The isolated V_HH, M2-7A, showed neutralization against both amantadine-sensitive and resistant IAV *in vitro*, with a modicum of protection observed for mice treated with 200 µg 24 hours after lethal viral challenge followed by an additional treatment at 48 hours [298]. Since the V_HH did not have an Fc fragment, activity against influenza is mainly attributed to blockage of M2 ion channel on the virion. This shows us that repeated dosing of an effective V_HH is a viable treatment option against influenza infection.

Ibanez et. al [299] showed that intranasal administration of a nanobody specific for the receptor binding site of H5N1-HA suppresses replication of H5N1 virus *in vivo*, with bivalency making the V_HH 60-fold more effective *in vivo* and a thousand-fold *in vitro,* than its monovalent counterpart. Prophylactic or therapeutic administration of the bivalent V_HH with as little as 25 µg/kg was also able to protect mice from H5N1 challenge, despite mice losing weight initially but later recovering [299]. However, a K189E substitution in HA1 was found to abolish the neutralizing effect of H5-V_HH, indicating that the conserved positively charged lysine residue is essential for H5-V_HH binding [299].

Tillib et. al [300] employed the same approach by immunizing a two-hump camel (*C. bactrianus*) with a mouse-adapted H5N2 strain, obtaining a panel of V_HH with modest neutralizing activity. Neutralizing activity was later increased by addition

of a camel hinge-originated spacer sequence and an isoleucine zipper domain (ILZ) to the nanobody. *In vivo,* the formatted nanobodies demonstrated complete protection in mice, when given 100 µg intraperitoneally or intranasally, 2 hours before of 24 hours after lethal challenge [300].

Cardoso et. al [301] isolated and characterized 13 H5N1 neuraminidase-binding nanobodies generated by a V_HH phage display library from an alpaca immunized with N1. Of these 13, 11 showed binding to NA, and 4 had neutralization activity *in vitro* [301]. They reformatted the most promising candidates into bivalent V_HH (N1-V_HHb) and/or fused them to a mouse IgG2a Fc domain (N1-V_HH-Fc), with the bivalent constructs demonstrating a 2- to 3-log-fold further increase in viral inhibitory potential compared to their monovalent counterparts [301]. Intranasal administration of a high dose of N1-V_HHb 24 hours before an H5N1 challenge protected mice against death, but significant body weight was still lost [301]. They also observed that the N1-V_HH-Fc formats were able to provide greater protection than the N1-V_HHb formats with a single dose resulting in 100% survival, even if the administered molar amount of the N1-V_HH-Fc was 10 to 50 times less than the bivalent constructs. However, the best N1-V_HH did not have any antiviral activity against the oseltamivir-resistant H5N1 H274Y virus *in vitro*, but one N1-V_HH-Fc was able to protect mice against a challenge with the same H5N1 mutant virus [301]. This indicates that protection by NA-based antibodies is not strictly reliant on neuraminidase inhibition (NAI) activity, provided that an Fc domain is present to contribute Fc receptor-dependent effector functions.

Hufton et. al. isolated nanobodies capable of neutralizing different influenza strains by immunizing alpacas with recombinant HA of A/California/07/2009(H1N1)pdm09 and using phage antibody library technology [268]. Following immunization, V_HH genes were cloned into a phage display vector for *E. coli* expression and library production [240]. Antigen-specific V_HH were then selected via phage display against A(H1N1)pdm09. From these V_HH antibodies, R1a-B6 was found to have broad cross-subtype neutralizing activity *in vitro* against pandemic H1N1,

highly pathogenic H5N1, H9N2, and when made bivalent, against H2N2. It was further shown to bind to a highly conserved epitope in the hemagglutinin stem region overlapping with the fusion peptide (**Figure 1.3**) suggesting its mechanism of action takes place post-attachment via inhibition of viral membrane fusion. This is demonstrated by the lack of hemagglutination inhibition activity, loss of binding to HA at acidic pH and absence of binding to the HA head domain [219, 268]. Furthermore, R1a-B6 has its epitope overlapping [219] with that of CR6261 [238] and F10 [210], human monoclonal antibodies that have been proven to have broad cross-subtype protection against influenza, suggesting that R1a-B6 may have similar potential as an immunotherapeutic.

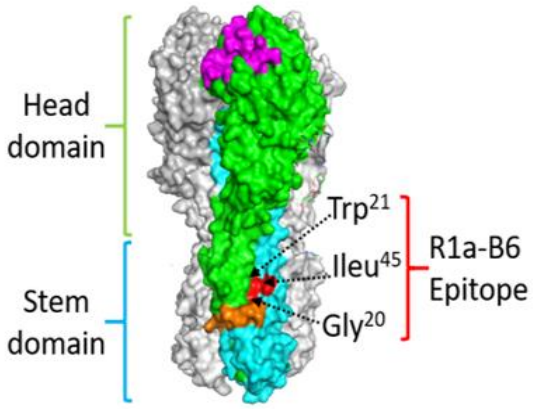

Figure 1.3. Surface structure model of hemagglutinin (HA) showing R1a-B6 epitope residues. HA trimer of A(H1N1)pdm09 (PDB structure 3AL4) showing the key epitope residues of R1a-B6, Gly20, Trp21, and Ile45 (shown in red) located in the HA stem region (cyan). The receptor binding site (magenta), fusion peptide (orange), and head domain (green) are also illustrated [302].

Although the use of nanobodies against influenza is an attractive approach, several drawbacks must also be considered. Nanobodies are a less-validated format compared to human or humanized mouse antibodies that are in clinical development. Twenty-five years after the discovery of nanobodies, Caplacizumab™, a bivalent nanobody targeting von Willebrand factor to treat acquired Thrombotic Thrombocytopenic Purpura (aTTP) [303] was approved in Europe in 2018, and later

by the US FDA in 2019. Currently licensed mAbs have a typical half-life ranging from two days to one month *in vivo*, requiring frequent or repeated dosing and/or delivery at high concentrations [272]. The nanobody must be reformatted in such a way that it will be retained in the peripheral circulation long enough to neutralize virus and have a clinical effect. Camelid nanobodies also have to be humanized as stated previously for them to proceed further as human therapies. To this effect, the recent availability of numerous expression systems for mAb production, half-life extension technologies, and alternative delivery mechanisms using DNA, RNA or virus vectors are paving the way for more effective and long-lasting immunotherapy with broadly neutralizing antibodies and nanobodies [222].

1.6 Gene Therapy and Viral Vectors

Gene therapy is a process that involves modification, addition, silencing or replacement of faulty genes with non-defective ones with the goal of curing or preventing disease or medical conditions brought about by defective genes. The earliest gene therapy approaches were aimed at correction of hereditary single gene disorders [304]. Today, gene therapy has come a long way, and is employed to correct complex multigenic and multifactorial diseases, to restore metabolic functions, for targeted drug or small molecule delivery and to treat infectious diseases [305, 306]. The general aim has not changed through the years, it remains to be direct, targeted and safe *in vivo* gene delivery.

In order to insert new genes directly into cells, vehicles called “vectors” which are genetically engineered to deliver genes are employed [307, 308]. Viruses have been exploited as vectors for many years owing to their highly evolved mechanisms for efficient delivery of genetic material to host cells [308]. The success of gene therapy is still built on understanding the molecular basis of how viruses when engineered as viral vectors interact with the host [309]. For gene therapy to work, vectors must be reproducibly and stably propagated and purified to high titers, attach

and enter target cells, deliver transgenes specifically to the tissue or organ of interest and mediate gene delivery and transgene expression for a prolonged period with no or very minimal toxicity [308-310].

Engineered viral vectors should ideally harness the viral infection pathway but avoid the subsequent expression of viral genes that leads to replication and/or toxicity. To accomplish this, viral particles encapsulate a modified genome carrying a therapeutic gene cassette in place of the coding regions of the viral genome [310]. Only sequences that are required in cis for functions such as packaging the vector genome into the virus capsid are left intact. The deleted genes encoding proteins that are involved in replication or capsid/envelope proteins are included in a separate packaging construct to provide helper functions in trans [310]. This separation between cis and trans coding elements prevents recombination into productive viral particles but instead leads to the production of replication-defective particles able to specifically transduce new genetic information into target cells [309].

There are numerous viral vectors that are under development for gene therapy with some of them able to integrate into the host genome and others persisting extrachromosomally as episomes [308]. In choosing the most suitable vector system for therapeutic applications, vector tropism, transgene size, duration of transgene expression and vector immunogenicity are the most important factors to consider [307].

Gammaretroviruses were the earliest vectors for gene therapy, with the first viral vector based on Moloney murine leukaemia virus (MLV) [309]. Retroviruses tend to establish persistent gene infection only in dividing cells; this is usually well tolerated by the host but may also cause latent diseases such as malignancy and immunodeficiency [308]. Lentiviruses (LV) such as human immunodeficiency virus type 1 (HIV-1) are also members of the retrovirus family [308]. A breakthrough in 1996 showed lentiviral vectors as capable of transduction of both mitotic and nondividing cells and mediate stable *in vivo* gene transfer into terminally differentiated neurons [311, 312].

Adenoviruses (Ad) have been classified into six species (A–F) that infect humans with over 50 serotypes able to cause infection [313]. Of these, human adenovirus serotypes 2 (Ad2) and 5 (Ad5) of species C are the most widely used for gene delivery [313]. Ads offer many advantages as gene therapy vectors as they are known to infect both dividing and non-dividing cells, are stable, can accommodate large transgenes and can be produced at high titers [308, 309, 313, 314]. However, the use of recombinant Ad2 and Ad5-based vectors have been found to be non-targeted, resulting in humoral and cellular immune response from high vector doses [307]. This has been partially rectified by the advent of first, second and third generation Ads with almost all viral genes contributing to immunogenicity deleted [308, 313].

Currently, lentiviral vectors (LV) and adenovirus vectors (Ad) are popular viral vector choices for the treatment of several diseases [315]. LVs integrate transgenes into the host genome, enabling long term gene expression in a wide variety of both dividing and non-dividing cells [308], whereas Ads exhibit transient, but rapid gene expression which may be ideal for responding to infectious disease outbreaks [188, 308]. LVs encoding a mixture of broadly neutralizing HIV antibodies have been proven to be efficacious in the treatment of HIV infection in humanized mice [316]. Genetic delivery of an anti-RSV antibody to protect against pulmonary infection with RSV [317] and immunotherapy with a recombinant adenovirus expressing an HA (H5)-specific single-domain antibody that protected mice from lethal influenza infection [318] were both made possible using adenoviral vectors. At the time of writing, there have been 546 registered clinical trials employing Adenovirus, with 19 in Phase III and 2 in Phase IV involving gene therapy in advanced malignant tumors [315]. For lentiviruses, there are 302 listed clinical trials, with 13 of them in Phase III trials to treat β-thalassemia, multiple myeloma and B-cell non-Hodgkin lymphoma [315].

1.6.1 Recombinant Adeno-Associated Virus (rAAV)

Alongside the viruses mentioned previously, recombinant Adeno-associated virus is one of the most popular vectors for gene therapy [319, 320]. First discovered as a contaminant of Adenovirus stocks, wild type adeno-associated viruses (AAVs) are members of the *Dependovirus* genus of the parvovirus family which rely on co-infection with other viruses, mainly adenoviruses (Ad) or herpes simplex virus (HSV), to replicate [321-324].

AAV has a single-stranded DNA genome of approximately 4.8 kilobases (kb) coding for three genes, *rep* (Replication), *cap* (Capsid), and *aap* (Assembly) [308, 325]. The *rep* gene encodes four proteins (Rep78, Rep68, Rep52, and Rep40), which are required for viral genome replication and packaging, while *cap* expression gives rise to the viral capsid proteins (VP1, VP2 and VP3) [319, 320, 324-326]. It is estimated that the viral coat is comprised of 60 proteins arranged into an icosahedral structure with the capsid proteins in a molar ratio of 1:1:10 (VP1:VP2:VP3) [325, 326]. Of these three capsid proteins, VP3 (61-kDa) constitutes majority of the capsid's protein content [326], making it the choice protein to assess vector quantity [327]. The *aap* gene encodes the assembly activating protein (AAP) that is thought to provide a framework for capsid assembly [325]. These coding sequences are flanked by inverted terminal repeats (ITRs); T-shaped, base-paired hairpin structures that are required for genome replication and packaging [100, 321, 324, 325].

The AAV life cycle begins by binding to host cell surface receptors/coreceptors such as heparan sulfate, fibroblast growth factor receptor 1 (FGFR1), sialic acid, platelet-derived growth factor receptor (PDGF-R) [321], and the recently discovered AAV Receptor (AAVR), universal receptor involved in AAV infection of all serotypes [328]. The virus is then endocytosed and transferred through the endosomal compartment; from there it is trafficked intracellularly to the nucleus where the virus uncoats [319, 323]. In the presence of helper virus (adenovirus or herpesvirus), the lytic stage ensues [321] where the genome is replicated, and virions are produced. DNA replication is thought to involve a self-priming single-strand displacement

mechanism that is initiated by DNA polymerization via host polymerases at the 3' hairpin primer of the single-stranded genome to produce duplex monomers. These structures are nicked on the parental strand opposite the original 3' end position to generate free 3' hydroxyl groups to provide a primer for the next round of replication [323]. Without a helper virus, AAV establishes latency by undergoing specific integration into a genome site, termed as the adeno-associated virus integration site 1 (AAVS1), a 4kb region on chromosome 19 (q13.4) [319].

There are different AAV serotypes isolated from various species offering diverse antigenicity and a broad range of tissue tropism, receptor usage, host specificity [319, 324, 325] and immunogenicity of the vector *in vivo* [329]. Much of the diversity amongst different AAV isolates can be traced to the major capsid protein (VP3) [326]. It is this variation in VP3 surface topologies that determines the differences in cell surface attachment and receptor usage, intracellular trafficking pathways, gene transfer efficiencies and antigenicity between closely related serotypes [326, 329].

Although widespread in the human population, wild type AAV has not been associated with any human disease, which makes it more convenient and safer to work with [319, 323, 324, 330]. rAAV vectors, derived from wild type AAV, have been modified to improve safety and are suitable vectors for clinical gene therapy [307, 308, 324]. In rAAV, the *rep* and *cap* genes have been deleted, leaving only the 145 bp 5' and 3' inverted terminal repeats (ITRs) [319, 320, 331]. This then allows the insertion of a transgene with transcriptional control elements in between the ITRs as replacement for the deleted *rep* and *cap* genes [188]. This important deletion greatly reduces AAV integration into the host genome because the sequences coding for the native AAV proteins needed for integration are not present, further improving its safety profile. Wild-type AAV is also known to integrate into a specific locus on chromosome 19, AAVS1, but this natural occurrence is eliminated in rAAV, with the virus forming circular concatemers that persist as episomes in the nucleus of transduced cells

instead [114, 188, 319, 320]. *rep* and *cap* genes are then supplied in trans and can be of a different serotype to that of the ITRs, essentially creating a “pseudotyped” virus.

Most, if not all, rAAVs contain AAV2 ITRs as it is the most characterized, and the capsid can be the same or a different serotype (AAV2/x) [320, 332]. The differences in transduction efficiency and immune responses among rAAV serotypes has been well-documented in various animal models [333, 334]. Zincarelli et al did a comparative study on luciferase transgene expression of AAV2 pseudotyped with serotypes 1–9 after systemic delivery by tail vein injection in mice [329]. They found that expression can be detected at 7 days post injection (dpi) for AAV serotypes 1, 6, 7, 8, and 9, 14 dpi for AAV4 and AAV5, and 29 dpi for AAV2 and AAV3. Liver was the most transduced organ for all serotypes, with AAV8 having uniform expression throughout the hindlimb, abdominal, and thoracic regions, and AAV9 showing the highest expression in heart. It was also shown that AAV8 and AAV9 transduce tissues more ubiquitously than the other serotypes do, with AAV9 having the most robust tissue expression, although this comes with several safety issues [329].

A limitation to the effective use of AAV as a gene therapy vector is the prevalence of pre-existing neutralizing antibodies (nAbs) to AAV capsids in humans [335, 336]. A worldwide epidemiology study by Calcedo et. al revealed that neutralizing antibodies to AAV2 were the most prevalent in all regions tested followed by AAV1, with seroprevalence of nAbs significantly lower for AAV7 and AAV8 [337]. It was found that this pre-existing AAV vector immunity hinders gene expression of secreted proteins in mouse liver diminishing therapeutic capacity [338]. It was hypothesized that preformed capsid that was able to enter hepatocytes at the time of transduction, but was not being actively synthesized by the cell, can gain access to major histocompatibility complex class I (MHC I) presentation pathways [336]. This resulted in expansion of a pre-existing pool of capsid-specific $CD8^+$ memory T cells, generated via prior exposure to wild-type AAV [336]. The impact of these nAbs could potentially be minimized by using less prevalent AAV serotypes, such as AAV5 or

AAV8 over AAV2, intramuscular (IM) vector administration as opposed to intravenous (IV), and the prudent choice of promoters that will preferentially direct transgene expression in muscle rather than liver [336, 338, 339].

1.6.2 rAAV in clinical trials

Alongside LVs and Ads, AAV is also widely used in gene therapy clinical trials; with about 244 studies listed at the time of writing [315]. Of these, there have been 24 registered Phase III clinical trials using different AAV serotypes to treat various diseases such as Leber Hereditary Optic Neuropathy, Leber Congenital Amaurosis, advanced metastatic prostate cancer, X-linked Chloroideremia, enzymatic deficiencies, spinal muscular atrophy, and hemophilia A and B [315].

One of the most prominent studies involving AAV is for the treatment of human lipoprotein lipase (LPL) deficiency that causes elevated levels of serum triglycerides leading to recurrent and life-threatening pancreatitis [340]. Successful AAV2/1 intramuscular delivery of alipogene tiparvovec, Glybera, to replace the defective lipoprotein lipase in patients, has led to its approval in Europe as the first ever gene therapy product for humans in 2012 [341]. However, it was pulled out of the market in 2017 due to low demand and its hefty price tag. Nonetheless the story of Glybera has highlighted the challenges of gene therapy, that of balancing efficacy, safety, and economy, to produce the next generation of gene therapy products for future use.

Many rAAV clinical trials have been focused on the treatment of monogenic inherited disorders. The disease known as Leber congenital amaurosis (LCA) develops due to mutations in the RPE65 (retinal pigment epithelium-specific 65-kDa) gene, causing a severe form of inherited retinal blindness in infants and children [342]. Voretigene neparvovec-rzyl is composed of human RPE65 incorporated into AAV2/2 and is injected into the subretinal space, facilitating expression of RPE65 in retinal pigment epithelial cells [342]. It was found to be safe and to improve functional vision

in previously medically untreatable cases, leading to its approval as Luxturna™ by the US Food and Drug Administration (FDA) in December 2017 [342].

Spinal muscular atrophy (SMA) is a rare genetic disease resulting in progressive muscle wasting and loss of motor neuron function caused by a mutation in the survival motor neuron 1 (SMN1) gene [343]. A study in 2018 by Hinderer et al [344] revealed that high dose intravenous ($2x10^{14}$ vg/kg) gene therapy of human survival motor neuron protein (SMN) via AAV2/9 in monkeys and piglets led to instances of severe life-threatening toxicity via hepatocellular injury and intravascular coagulation within five days of vector administration. These findings are particularly worrying as the same AAV2/9 vector had been successfully used by AveXis to treat infants with SMA Type 1 in clinical trials of AVXS-101 (Zolgensma) [345]. However, caution must be used in interpreting results of these animal studies and their relevance to human clinical trials [344]. Nonetheless, in May 2019, the US FDA approved onasemnogene abeparvovec, Zolgensma, a one-time AAV-delivered therapy for SMA treatment [343]. The treatment price is $2.125 million, making it one of the costliest drugs ever made. This treatment is a potential lifeline for newborns and infants but at the same time this also highlights how expensive this kind of therapy is. This drives our efforts to improve gene therapy solutions and their associated costs.

The most common clinical trials based on AAV therapy in recent years have been in Hemophilia A and B, rare X-linked blood clotting disorders caused by mutations in the genes encoding coagulation factor VIII (FVIII) for Hemophilia A and factor IX (FIX) for Hemophilia B leading to deficiency [346]. Disease severity is classified according to the plasma level of FVIII or FIX activity, with the only treatment available being lifelong intravenous infusion of these coagulation factors [346]. Clinical trials employing intramuscular injection of rAAV2-hFIX indicated that muscle tissue transduction was successful; however, circulating plasma FIX levels in all patients were less than the required level for a therapeutic effect [347]. An improvement to this was the use of AAV2/8-hFIX vector which became the first liver-directed AAV gene

therapy trial to show sustained therapeutic FIX levels and improved clinical outcomes in patients with hemophilia B [348]. However, in patients who received the highest dose of vector, T cell-mediated clearance of AAV-transduced hepatocytes was observed, with associated elevation of liver enzyme levels. This response has been overcome by a short course of glucocorticoids, without the loss of hFIX expression [348].

In a follow-up study, improvements were made to the vector to evaluate the long-term safety and efficacy of AAV2/8-hFIX therapy in the same cohort of hemophilia B patients. They found that a single intravenous injection of vector resulted in an increase in plasma FIX activity from less than 1% to a sustained level of up to 6% of the normal value in all 10 patients, and this remained stable for up to a period of 4 years [349]. Substantial clinical improvements were achieved in all patients; however this was also coupled with a dose-dependent, increase in anti-AAV capsid neutralizing antibody levels which did not have direct clinical consequences [349]. These findings will prevent subsequent gene transfer with vector of the same serotype in future. A rise in serum alanine aminotransferase (ALT) which is associated with a decline in FIX levels, suggesting a loss of transduced hepatocytes, was also observed [349]. It occurred consistently at 7 to 10 weeks post gene delivery but was also resolved after intervention with steroids.

Unlike inherited disorders, the magnitude of transgene expression required for therapeutic intervention in non-inherited disease may be substantially higher. Nevertheless, AAV vector-derived cardiac gene therapy of cardiac specific isoform of the sarcoplasmatic calcium ATPase (SERCA2a) has emerged as a new platform to treat cardiac disorders by improving calcium handling by cardiomyocytes [350]. AAV can also effectively transduce cancer cells *in vitro* and has been employed to deliver transgenes such as anti-angiogenesis genes, cytotoxic or suicide genes, cytokines for stimulating the immune system, tumor suppression and anti-tumor genes, DNA

encoding small hairpin RNAs (shRNA), antigens to stimulate antigen-presenting cells, and antibodies that block signalling in cancer cells and various tumor models [351].

With the concept already proven, rAAV technology should expand into broader indications with a larger patient base. Given their clinical efficacy and favorable expression profile, the use of rAAV vectors is a promising platform for delivering therapeutics and/or prophylaxis against infectious diseases such as influenza *in vivo*.

1.6.3 rAAV and influenza

Following the 2009 H1N1 influenza virus pandemic, the first study utilizing a recombinant trivalent AAV vaccine to protect against influenza was carried out [352]. Codon-optimized genes for HA, NP and M1 of A/Mexico/4603/2009 (pH1N1) of pandemic swine origin influenza virus were expressed via an AAV2/9 vector to demonstrate the induction of virus-specific T and B-cell responses in mice and protection from divergent influenza strains [352]. They found that mice immunized with trivalent AAV vaccine produced high titer neutralizing antibodies to the A/Hamburg/08/2009(H1N1v), a homologous H1N1 strain to vaccinating influenza virus, but could not cross-neutralize the heterologous A/Puerto Rico/8/34(H1N1) (PR8) strain *in vitro* [352]. Additionally, only 40% of mice that were vaccinated were protected from a lethal PR8 challenge *in vivo*, suggesting that the immune response to NP, not the humoral response to H1 played a more pivotal role in partial protection against PR8 [352]. Based on their data, the authors argued that although this vaccine candidate did not induce sterilizing immunity it may mitigate the clinical symptoms, diminish the transmission rate, and, thus, generate a “basic level” of immunity before the strain-specific vaccines have been made available.

Borrowing from a successful study involving HIV treatment using immunotherapy [353], a remarkable study in 2013 utilized AAV to systemically produce antibodies against influenza even without exposure to the virus, in a process vastly different from vaccination in which the body's own immune system generates

antibodies against the disease. Aptly called “vectored immunoprophylaxis”, this strategy aimed to generate broadly protective humoral immunity against diverse influenza strains in mice [354]. Using this approach, broadly neutralizing anti-influenza antibodies, F10 [210] and CR6261 [238], were cloned in an AAV2/8 vector and given intramuscularly to mice resulting in antibody expression (150-200 µg/mL) for more than a year. This led to neutralization of different influenza subtypes *in vitro* and protection against challenge with different H1N1 strains (A/California/07/2009, A/Solomon Islands/3/2006, A/Puerto Rico/8/1934) *in vivo* in Balb/C and severe combined immunodeficient (SCID) mice [354].

Limberis et. al [355], evaluated the potential of intranasal delivery via AAV2/9 in mice, ferrets and macaques of FI6 [208], a broadly neutralizing antibody, in protecting against various strains of influenza. They estimated 0.5 µg/ml in the nose, 2.0 µg/ml in the lung, and about 120 ng/mL of FI6, 14 days post-AAV administration in mice. In macaques, onset of expression was 14 days post administration, with levels peaking around day 60 and declining thereafter until ~ 100 days. Lethal challenge with PR8 in mice given 10^{11} vg AAV resulted in complete protection. Ferrets given 10^{12} vg AAV that were challenged with A/Vietnam/1203/2004 (H5N1) showed minor weight loss but fully recovered, while in those infected with A/Mexico/InDRE4487/2009 (H1N1), a highly virulent strain in ferrets, 50% survived [355].

As a follow-up to address the need for an alternative strategy against influenza in high risk groups, the same group as above conducted passive immunization of FI6 using AAV9 administered intranasally to young, old, and severe combined immunodeficient (SCID) mice. Mice were protected and exhibited no signs of disease following A/Puerto Rico/8/1934 (H1N1) (PR8) challenge [356].

In a landmark study in 2018, a consortium harnessed broadly neutralizing llama single domain antibodies for passive immunotherapy and delivery via gene therapy against influenza A and B [357]. They isolated two influenza A (SD36 and SD38) and two influenza B (SD83 and SD84) sdAbs that were able to neutralize a panel of

influenza viruses *in vitro.* They found that linking all 4 V_HH together and appending human IgG1-Fc to create multi-domain antibody (MDAb) MD3606 generated more potent and broader cross-reactivity than the individual sdAbs [357]. Prophylactic treatment of mice via intravenous administration of various doses of MD3606 a day before challenge protected them from lethal infection with diverse influenza A and B viruses. Antibody-dependent cellular cytotoxicity (ADCC) also contributed to *in vivo* efficacy, as MDAbs with ADCC activating Fc regions protected all mice from a lethal influenza challenge when given a high (5 mg/kg) or low dose (1 mg/kg) of MDAb, while mice given 1 mg/kg MDAb with a non-ADCC activating Fc region were not protected [357]. This highlights the contribution of Fc effector functions for protection via passive immunotherapy *in vivo*. They also inserted MD3606 in an AAV9 vector which was administered to mice intranasally 7 days before challenge with 5 LD_{50} A/Puerto Rico/8/34-MA (H1N1), 5 LD_{50} A/Hong Kong/1/68-MA (H3N2), or 5 LD_{50} B/Lee/40-MA. Results showed that intranasal delivery of AAV9 MD3606 provided full protection in mice at doses as low as 5 x 10^8 vg [357]. These results are promising and may prove useful if translated for human use or as an alternative strategy to annual influenza vaccination and for pandemic preparedness plans.

These studies suggest that the ability of rAAV vectors to provide long term stable transgene expression in different animal cells, their low immunogenicity, and overall versatility, make them attractive gene therapy tools for vaccine delivery and immunoprophylaxis vectors against influenza.

1.7 Universal Influenza Vaccine

The World Health Organization, in its global influenza strategy for 2019-2030 has set up lofty goals that come under the mantra of “Prevent, Control and Prepare” [108]. This involves reducing the burden of seasonal influenza, minimizing the risk of zoonotic influenza, and mitigating the impact of pandemic influenza. Strategic objectives include promotion of research and innovation, strengthening of global

influenza surveillance, expansion of seasonal influenza prevention and control policies, and strengthening pandemic preparedness and response [108].

As such, development of a universal influenza vaccine is now, more than ever, a top priority. At a workshop spearheaded by Anthony Fauci, David Baltimore and Peter Palese at the US National Institutes of Health in 2017, influenza experts from around the world tried to identify knowledge gaps in influenza research and develop strategies to fill them [358]. They have agreed on the minimum requirements for a universal influenza vaccine: ‘‘Thus, a reasonable target for a universal influenza vaccine would be: A vaccine with ~75% protection against symptomatic disease caused by group 1 and group 2 influenza A viruses lasting at least 12 months in all populations.’’ [358]. It was surmised that protection against influenza A was paramount, as it causes significant seasonal morbidity and mortality and all major pandemics have derived from influenza A strains, but influenza B will also be a component of the vaccine. Protection for at least 12 months was considered essential, to provide protection for a full season. However, a target of 5 to 10 years, common with many vaccines, would be preferable. The vaccine should ideally be effective in all age groups, although different vaccines might be needed to provide optimal protection in certain populations and would depend on the characteristics of pre-existing immunity and epidemiology in the area [358].

Approaches targeting novel antigens in influenza, usually conserved epitopes of the HA stem and head, NA, M2, and NP, should be prioritized, as well as finding a better correlate of protection than the classic HAI titer [359, 360]. The integral part of these strategies involve skewing of the antibody response towards these conserved regions to generate a more broadly-neutralizing response that would potentially protect against all circulating influenza strains and emerging subtypes [215, 361, 362]. The use of virus-like particles (VLP) that mimic aspects of native influenza, synthetic viruses, nucleic-acid based platforms, and viral vectors, as new paradigms for vaccination have been put forward [6, 110, 197].

Although targeted research to improve current vaccine antigens, platforms, and manufacturing will most likely lead to enhanced effectiveness of influenza vaccination, the ultimate objective of a universal influenza vaccine still requires development of a completely transformative approach involving design, strategy and implementation [360]. Until then, evidence from studies and literature presented in this chapter present a strong argument for an alternative, faster strategy that can be used against seasonal influenza and emerging novel pandemic viruses. Delivery of broadly neutralizing nanobodies against influenza via specially engineered recombinant AAV would enable production of these powerful molecules in our bodies to generate systemic immunity independent of natural or induced immune response to influenza or vaccination respectively.

1.8 Thesis Objectives

The work presented in this thesis aimed to test whether R1a-B6, re-formatted with a mouse Fc region, when given prophylactically as a single intramuscular injection via AAV-mediated delivery, would be able to generate broadly protective humoral immunity against different Influenza A viral subtypes in mice. The relative importance of the Fc region and its ability to activate effector functions with the objective of mitigating some of the safety concerns associated with ADCC was also investigated. Findings are discussed in the context of designing the optimum transgene for AAV vector delivery of R1a-B6 to accomplish long term, safe, broad protection from pandemic influenza in vulnerable patient groups. Specifically, the main points of investigation are as follows:

i) Assessment of cross-subtype binding and neutralizing activity of nanobody-Fc fusion proteins against influenza *in vitro.*

ii) Production of highly purified and well-characterized recombinant AAV vectors to be utilized as carriers of cross subtype neutralizing single domain antibodies for *in vivo* studies.

iii) Demonstration of protection of mice from lethal A/California/07/2009 (H1N1)pdm09 and A/Vietnam/1194/2004 (H5N1) NIBRG-14ma via AVV-mediated delivery of nanobody-Fc.

iv) Exploration of the necessity of the Fc domain for half-life extension and effector function in vectored immunoprophylaxis against influenza.

CHAPTER 2

MATERIALS AND METHODS

2.1 General

2.1.1 Propagation and maintenance of cell cultures

2.1.1.1 ExpiCHO-S™ cells

Originating from the Chinese hamster ovary (CHO) cell line, ExpiCHO-S™ (Thermo Fisher Scientific A21933) cells were utilized to transiently produce nanobody-Fc proteins. Cells were maintained in ExpiCHO™ expression medium (Thermo Fisher Scientific A21933) at 37°C and 8% CO_2 with shaking at 125 rpm and passaged upon reaching a density of $4x10^6$ – $6 x10^6$ viable cells/mL.

2.1.1.2 Human embryonic kidney (HEK) 293T cells

HEK293T cells, kind gifts from Dr. Els Henckaerts (King's College London), were utilized for AAV virus production, generation, and neutralization of influenza pseudotypes. They were maintained in complete medium, Dulbecco's Modified Essential Medium (DMEM) (Sigma D6546) supplemented with 10% (v/v) heat-inactivated Fetal Calf Serum (FCS) (Sigma 14A138), 1% (v/v) L-glutamine (Sigma G7513), and 1% (v/v) Penicillin-Streptomycin (PenStrep) (Sigma P0781). Cells were incubated at 37°C and 5% CO_2.

2.1.1.3 Madin-Darby canine kidney (MDCK) cells

MDCK cells were utilized in influenza $TCID_{50}$ and microneutralization assays. They were maintained in complete medium supplemented with 1% (v/v) Amphotericine B (Sigma A2942). Cells were incubated at 37°C and 5% CO_2.

2.1.2 Restriction Digestion

Restriction digest of plasmids was done using *EcoRI-HF* (New England Biolabs) and *BamHI-HF* (New England Biolabs) unless otherwise stated. For every restriction digest, the restriction cocktail consisting of 5 µL 10X CutSmart Buffer (New

England Biolabs), 10 U each of the restriction enzyme, 1 µg of plasmid DNA to be digested, and the appropriate volume of nuclease-free water, to make a 50 µL volume final solution was prepared. Restriction cocktails were incubated at 37°C for 1 hour and aliquots were run on a 1% (w/v) agarose gel in 1X Tris-Acetate-EDTA (TAE) running buffer (1 mM Na_2EDTA (Sigma), 40 mM Tris base (Sigma), 20 mM glacial acetic acid). Bands corresponding to the empty vector and released insert were visualized via staining with SYBR™ Safe DNA Gel Stain (Invitrogen S33102).

2.1.3 Sodium Dodecyl Sulfate Polyacylamide Gel Electrophoresis (SDS-PAGE)

A discontinuous Laemmli SDS-PAGE setup was carried out using a 4% (w/v) polyacrylamide-bis-acrylamide stacking gel and a 12% (w/v) polyacrylamide-bis-acrylamide separating gel (1.5 mm plates). Gels were loaded with up to a total of 30 uL consisting of sample and 6X Reducing SDS Page Loading Buffer (40% (v/v) 10% SDS, 25% (v/v) 1.5 M Tris, pH 6.8, 20% (v/v) glycerol, 0.02 % (w/v) bromophenol blue, 6% (v/v) β-mercaptoethanol) (BioRad) for reducing gels or 5X Non-Reducing SDS PAGE Loading Buffer (40% (v/v) 10% SDS, 25% (v/v) 1.5 M Tris, pH 6.8, 20% (v/v) glycerol, 0.02 % (w/v) bromophenol blue) for non-reducing gels.

Precision Plus Protein™ Dual Color Standards (BioRad 1610374) was employed as protein marker. All samples were heated for 5 minutes at 95°C prior to loading. The gels were initially run in 1X Running Buffer (25 mM Tris, 192 mM Glycine, 0.1% SDS, pH 8.3) at 80 V and increased to 150 V after the loading dye reached the separating gel. The gel was then run until the loading dye reached the bottom of the gel.

The gel was then taken out of the glass cassette and fixed in 100 mL of fixing solution (50% (v/v) methanol, 7% (v/v) acetic acid) for 30 minutes. Fixing solution was discarded and a fresh 100 mL of fixing solution was added followed by incubation for 30 minutes. For routine SDS PAGE gels, gels were stained with 0.1 % (w/v) Coomassie® R-250 (Thermo Fisher Scientific) in 40% (v/v) ethanol and 10% (v/v)

glacial acetic acid, overnight. The next day gels were then destained (10% (v/v) methanol, 7% (v/v) glacial acetic acid) until bands were clearly seen and background staining was minimal.

2.1.4 Western Blotting

SDS-PAGE gels were rinsed with Phosphate Buffered Saline (PBS) (Sigma D8662), pH 7.0 to remove any trace of SDS. Each gel was then sandwiched with filter papers and put on top of a piece of Amersham™Protran™ Premium 0.45 µm nitrocellulose (NC) membrane (GE Healthcare 10600008). The sandwich was soaked in cold Transfer Buffer (20% (v/v) methanol, 25 mM Tris, 192 mM glycine, pH 8.3) and put in a cassette in a Mini-PROTEAN Tetra Vertical Electrophoresis Cell (BioRad). The immunoblot was run at 350 mA for 2 hours at 4°C. NC membrane was extracted from the sandwich and washed with PBS-T (0.1% (v/v) Tween20 in PBS). It was then blocked with 5% (w/v) skimmed milk in PBS-T for 1 hour with constant shaking at room temperature. Membrane was then incubated with a 1:5000 dilution of Anti-mouse IgG (Fc Specific)-Peroxidase (Sigma A0168) in 5% (v/v) skimmed milk in PBS-T overnight at 4°C. The next day, membrane was washed five times with PBS-T for 5 minutes each time. Membrane was then stained with SigmaFast™ 3,3'-diaminobenzidine (Sigma D4293).

2.1.5 Enzyme-Linked Immunosorbent Assay (ELISA)

A 96-well clear flat-bottom plate (Nunc 269620) was coated overnight at 4°C with 50 µL/well of 5 µg/mL influenza virus antigen standard diluted in PBS. The next day, plates were washed three times with wash buffer (0.1% (v/v) Tween in PBS). Plates were then blocked with 50 µL blocking buffer (0.2 M Tris, 1% (w/v) BSA, 0.02% (w/v) Kathon pH 7.5) and incubated for 1 hour at 37°C. One hundred µL of serial two-fold dilutions in blocking buffer ranging from 4 µg/mL to 1 ng/mL of purified R1a-B6-mIgG1, R1a-B6-mIgG2a, R1a-B6, and cAb1-mIgG2a were tested in duplicate. Plates were then incubated for 2 hours with shaking at 225 rpm at 37°C. Plates were again

washed three times. Secondary antibody, anti-mouse IgG (Fc Specific)-Peroxidase (Sigma A0168) at a 1:2000 dilution was used to detect R1a-Bg-mIgG1, R1a-B6-mIgG2a and cAb1-mIgG2a; while monoclonal anti-polyHistidine-Peroxidase clone HIS-1 (Sigma A7058) at a 1:1000 dilution was used to detect R1a-B6. One hundred µL of the secondary antibody was added and plates were incubated for 1 hour. Plates were again washed three times. One hundred µL per well of TMB substrate (Thermo Scientific 34029) was added to the plate and the reaction was stopped with 0.5 M HCl or 0.5 M H_2SO_4. Plates were read on a SpectraMax M5 ELISA plate reader using SoftMax Pro software. Absorbance at 450 nm was taken.

2.1.6 Statistical analysis

All analyses were performed with GraphPad Prism 8.12 for Windows (GraphPad Software). The Student's t test was used to determine differences between the means of two groups. To determine whether differences exist among the means of three or more groups, analysis of variance (ANOVA) was carried out. If differences were found, the post-hoc Tukey multiple comparison test was performed to identify if there is a significant difference between pairs of experimental groups.

2.2 Production and purification of nanobody-Fc fusion proteins

2.2.1 Cloning nanobody-Fc in mammalian expression vector

Gene sequences for R1a-B6-mIgG1 and R1a-B6-mIgG2a, designed by Dr. Simon Hufton and Dr. Tiziano Gaiotto, and cAb1-mIgG2a [252], were released from pIRESneo (Clontech) vector by restriction digestion (**Section 2.1.2**). Released inserts were then excised and extracted using QIAquick Gel Extraction Kit (Qiagen 28704) as per manufacturer's instructions. Destination vector, pcDNA™ 3.4-TOPO® (Invitrogen A14697) with a multiple cloning site (MCS) inserted, was also digested with *EcoRI-HF* (New England Biolabs) and *BamHI-HF* (New England Biolabs) to accommodate inserts. Digested pcDNA™ 3.4-TOPO® (Invitrogen) was purified using a QIAquick PCR Purification kit (Qiagen 28104) and eluted in nuclease-free H_2O.

Samples were again viewed via gel electrophoresis and DNA concentration of inserts and destination vector were determined by measuring Absorbance at 260 nm (A_{260}) via NanoDrop™ (Thermo Fisher Scientific). Digested pcDNA™ 3.4-TOPO® (Invitrogen) plasmids were then dephosphorylated by incubation for 30 minutes at 37°C with Antarctic Phosphatase (New England Biolabs M0289S). Phosphatase was then heat-inactivated at 65°C for 5 minutes. Dephosphorylated pcDNA™ 3.4-TOPO® (Invitrogen) plasmids and R1a-B6-mIgG1, R1a-B6-mIgG2a, and cAb1-mIgG2a inserts were ligated overnight at room temperature in a 1:3 vector to insert molar ratio (50 ng vector:20 ng nanobody-Fc) with T4 DNA Ligase (New England Biolabs M0202S). Afterwards, samples were run on a MinElute Reaction Cleanup Kit (Qiagen 28204). Vectors now containing inserts were then electroporated into TG1 electroporation competent cells (Agilent Technologies 200123) in a 1 mm cuvette using Gene Pulser Xcell™ (BioRad) with the following conditions: 1.8 kV, 25 µF, 200 Ω. One hundred microliters of competent cell transformants were then plated on Luria Bertani (LB)-carbenicillin plates and left to grow overnight. The following day, a single colony was cultured in 3 mL of LB broth-carbenicillin. For plasmid DNA mini preparations, 2 mL of the overnight cultures were transferred to microcentrifuge tubes and centrifuged at >12,000*xg* for 2 minutes. Supernatant was decanted before proceeding to plasmid DNA extraction using the Plasmid Mini Kit (Qiagen 12125). For DNA midi-preparations, 100 mL of Lb-broth-carbenicillin was inoculated with 100 µL of the cultures from the DNA mini preparation. Large-scale preparation of endotoxin-free plasmid DNA using NucleoBond® Xtra Midi EF Kit (Macherey Nagel 740420.10) was also carried out the next day. Extracted DNA from both mini and midi preparations then underwent restriction digestion (**Section 2.1.2**). Inserts were then sequenced via the Sanger method by GATC Biotech.

2.2.2 Transfection in ExpiCHO-S™ cells

Cells were transiently transfected using the Max Titer protocol as described in the ExpiCHO™ Expression system (Thermo Fisher Scientific A21933) user guide. Briefly, cells of a density of $6x10^6$ cells/mL were transfected with 1 µg total plasmid DNA per mL of culture medium and incubated at 32°C, 5% CO_2 for 14 days. On the day of harvest, suspension cultures (125 mL – 1 L) were centrifuged at 3000*xg* for 5 minutes. The crude supernatant was transferred to appropriate tubes and kept at 4°C.

2.2.3 Protein A Affinity Chromatography

Cell supernatants were purified using a 1 mL HiTrap™ Protein A HP (GE Healthcare 17040203) chromatography column. For R1a-B6-mIgG1, a high salt binding buffer (1.5 M glycine, 3 M sodium chloride, pH 8.9) and an elution buffer made up of 0.1 M sodium citrate, pH 3.5 were used. For R1a-B6-mIgG2a and cAb1-mIgG2a, the Ab Buffer Kit (GE Healthcare 28-9030-59) consisting of Binding Buffer (0.2 M sodium phosphate, pH 7.0) and Elution Buffer (1 M glycine-Cl, pH 2.7) was utilized. Briefly, the column was first washed with 10 column volumes (CV) of binding buffer before application of around 30 mL of sample. Column was again washed with 5 CV of binding buffer before eluting with 5 CV of elution buffer. Samples were then neutralized with 1 M Tris-Cl, pH 9.

Eluted 1 mL fractions were checked for presence of protein by measuring absorbance at 280 nm (A_{280}) factoring in a correction for absorbance at 340 nm via NanoDrop™. Presence of protein was confirmed using SDS-PAGE (**Section 2.1.3**).

2.2.4 Dialysis

Eluted fractions with high A_{280} readings that showed bands of appropriate size in SDS-PAGE gels were pooled and injected into 20,000 Molecular Weight Cut-Off (MWCO) Slide-A-Lyzer® Dialysis Cassettes (Thermo Fisher Scientific 66003) for removal of low molecular weight contaminants, buffer exchange, and desalting via dialysis in a 10 L solution of 1X PBS overnight at 4ºC. Purified and dialyzed nanobody-Fc fusion proteins were again analyzed by SDS-PAGE (**Section 2.1.3**) in both reducing

and non-reducing conditions and Western Blotting (**Section 2.1.4**). A_{280} readings were again taken to determine protein concentration.

2.3 *In vitro* assays for nanobody-Fc specificity and neutralization activity

2.3.1 Influenza ELISA Panel

The nanobody-Fc constructs were tested for binding to influenza antigen standards from the National Institute for Biological Standards and Control (NIBSC) as listed in Table 2.1 via ELISA (**Section 2.1.5**).

Table 2.1. List of influenza antigen standards from NIBSC used in this study.

Influenza Antigen Standard	NIBSC code	Abbreviation
A/Brazil/11/78(H1N1)	79/560	BL/78(H1N1)
A/Johannesburg/82/96(H1N1) NIB-39	97/518	JHB/96(H1N1)
A/Beijing/262/95(H1N1) NYMC X-127	97/760	BX/95(H1N1)
A/New Caledonia/20/99(H1N1) IVR-116	06/170	NC/99(H1N1)
A/Solomon Islands/3/2006(H1N1) IVR-145	07/102	SI/06(H1N1)
A/Brisbane/59/2007(H1N1) IVR-148	08/100	BR/07(H1N1)
A/California/07/2009(H1N1)pdm09 NYMC X-179A	09/174	CA/09(H1N1)
A/Michigan/45/2015(H1N1) NYMC X-275	17/182	MI/15(H1N1)
A/Brisbane/02/2018(H1N1) IVR-190	18/238	BR/18(H1N1)
A/Singapore/1/57(H2N2)	99/714	SG/57(H2N2)
A/Uruguay/716/2007(H3N2) NYMC X-175C	08/278	UY/07(H3N2)
A/Texas/50/2012(H3N2) NYMC X-223A	13/116	TX/12(H3N2)
A/Vietnam/1194/2004(H5N1) NIBRG-14	09/184	VN/04(H5N1)
A/Anhui/01/2005(H5N1) BCD-RG6	07/290	AH/05(H5N1)
A/turkey/ Turkey/01/2005(H5N1)	07/112	turkey/TR/05(H5N1)
A/duck/Singapore/Q/F119-3/1997(H5N3) NIB-40	00/552	duck/SG/Q/F119-3/97(H5N3)
A/chick/Hong Kong/G9/97(H9N2) NIBRG-91	08/228	chick/HK/G9/97(H9N2)
A/Hong Kong/1073/99(H9N2)	08/208	HK/99(H9N2)
A/Brisbane/10/2010(H1N1) cell derived antigen	11/134	BR/10(H1N1)
A/Christchurch/16/2010(H1N1) NIB-74	10/258	CX/10(H1N1)
B/Brisbane/60/2008	13/234	B/BR/08

2.3.2 Antibody Dependent Cell Cytotoxicity (ADCC) reporter assay

White opaque 96-well Nunclon™ plates (Thermo Fisher Scientific 136101) were coated overnight at 4ºC with 5 µg/mL A/California/07/2009(H1N1) (NIBSC 09/174). R1a-B6-mIgG1, R1a-B6-mIgG2a, and cAb1-mIgG2a serial dilutions ranging from 10 µg/mL to 0.25 ng/mL were made in assay diluent (Roswell Park Memorial Institute (RPMI) medium 1640 supplemented with 4% low-IgG serum) provided in the mFcγRIV ADCC Reporter Bioassay Kit (Promega M1201). Twenty-five µL of the nanobody-Fc (protein) and/or mouse serum dilutions were added to the coated plates. A vial of mFcγRIV Effector cells (Promega M1201) kept in liquid N_2 was thawed in a 37°C water bath with gentle agitation. Cell suspension was then mixed by pipetting gently 3 times. Six hundred twenty-five µL of the cell suspension was then transferred to 3.6 mL of prewarmed (37°C) assay diluent to a 15ml conical tube. Twenty-five µL of the cell suspension was then transferred to each wells of the 96-well plate coated with HA antigen and nanobody-Fc (protein) and/or mouse serum dilutions. Assay plates were covered and incubated at 37°C, 5% CO_2 for 6 hours. The assay plate was then removed from the incubator and equilibriated to ambient temperature. Seventy-five µL of Bio-Glo™ Reagent (Promega M1201) was then added to each well. Plate was then incubated at room temperature for 30 minutes. Plate was read using the GloMax® Navigator (ProMega). Activation of mouse FcγRIV by proteins or mouse sera was then reported as Relative Luminescence Units/mL (RLU/mL).

2.3.3 Growth of Challenge Virus A/California/07/2009(H1N1)pdm09 (CA/09)

A dozen embryonated chicken eggs (9-11 days old) were placed in a tray with the blunt end up and examined for any damage prior to inoculation via candling. For each egg, a line was drawn to separate the air sac and to identify the least venous part on its side for inoculation. The blunt end of the egg was then cleaned by wiping with 70% (v/v) ethanol and two small holes were punched using a sterile 22-gauge needle, one on top to release pressure and another on the side of the egg. Using PBS as a

diluent, stock A/California/07/2009/(H1N1)pdm09 (10^7 $TCID_{50}$/mL) was diluted tenfold five times to make a 10^{-5} working solution. One hundred microliters (100 µL) of the virus dilution was inoculated by inserting the needle about half an inch in the hole on the egg's side via a short stabbing motion and piercing the amniotic membrane to reach the allantoic cavity. Holes on top of the egg and the side were then sealed with melted wax. Eggs were incubated for 48 hours at 35°C. The night before harvest, eggs were chilled at 4°C. The next day, the blunt ends of the eggs were cracked open using an egg topper. The broken shell was removed using sterile forceps. Using a sterile spatula, the allantoic membrane was pushed aside and the allantoic viral fluid aspirated and transferred to a 15 mL falcon tube. The collected allantoic fluid from all eggs was then centrifuged at 1500*xg* for 20 minutes to remove excess blood and tissues that might be present. Viral RNA was extracted using Trizol LS (Invitrogen 10296010) and segments of hemagglutinin (H1) and neuraminidase (N1) were amplified by reverse transcription PCR (rtPCR) using an in-house protocol at the Influenza Resource Center (IRC) at NIBSC. Standard rtPCR reactions were performed using the Biometra TRIO Combi Multi Block Thermal Cycler (Analytik Jena). For both the HA and the NA genes, a final volume of 20 µL containing 0.25 µM each of Forward (F) and Reverse (R) primers, 12.5 µL 2X Reaction Mix SuperScript™ III One-Step RT-PCR System with Platinum™ Taq High Fidelity DNA Polymerase (Invitrogen 12574030), 0.5 µL SuperScript™ III One-Step RT-PCR System with Platinum™ Taq High Fidelity DNA Polymerase (Invitrogen 12574030) and 5 µL of RNA template was prepared. Reverse transcription was carried out for at 42°C for 60 minutes followed by reverse transcriptase deactivation at 94°C for 2 minutes. The PCR was carried out with 30 cycles of denaturation at 94°C for 30 seconds, annealing at 50°C for 30 seconds and extension at 68°C for 3 minutes. A final extension at 68°C for 5 minutes was also included. PCR amplicons for HA and NA were sequenced by GATC Biotech via the Sanger method.

2.3.4 Hemagglutination Assay

A hemagglutination assay was performed to ascertain which harvested virus aliquots should be pooled to get the highest viral titer. A row of a 96-well U-bottom plate was dedicated to a single sample. One hundred microliters of each viral sample was aliquoted onto column 1. Samples were then diluted two-fold across the plate until column 11 by transferring 50 µL of the virus sample and mixing with 50 µL PBS. Column 12 was left as a negative control containing PBS only. Fifty microliters of 0.7% (v/v) turkey red blood cells in PBS (t-RBCs) were added to each well of the plate followed by incubation for 30 minutes at room temperature. The hemagglutination titration endpoint is defined as the highest dilution of virus that still causes complete hemagglutination. The hemagglutination titre in hemagglutination units (HAU) is the reciprocal of this dilution. Viruses with the highest HAUs were pooled together in a 50 mL tube and centrifuged at 1500*xg* for 20 minutes at 4°C. They were then aliquoted in 1.5 mL pre-labelled tubes and stored at -80°C.

2.3.5 Hemagglutination Inhibition Assay (HAI)

All sera were treated with Receptor Destroying Enzyme (RDE) (Seiken) in a 1:4 dilution and incubated overnight at 37°C. The next day, sera were again incubated at 56°C for another 30 minutes to deactivate complement. Twenty-five microliters of mouse sera was aliquoted into duplicate wells of a V-bottom 96-well plate and serially diluted two-fold in PBS across one row before the addition of 4 HAU A/California/07/2009(H1N1)pdm09 or A/Vietnam/1194/2004(H5N1) NIBRG-14ma to all wells. After 90 minutes incubation at room temperature, 50 µL 0.5% (v/v) t-RBCs was added to each well and HAI titer was determined as described previously (**Section 2.3.4**).

2.3.6 Determination of Viral Tissue Culture Infectious Dose 50% ($TCID_{50}$)

All $TCID_{50}$ assays were carried out in duplicate plates per virus. Virus diluent consisting of complete DMEM supplemented by 1% (v/v) Amphotericin B (v/v) (Sigma

A2942) was prepared. For every assay, a fresh ampule of virus kept at -80°C was thawed. A 10^{-4} dilution of virus was made and 150 µL of this was plated on row A of columns 1 to 10 of a 96-well U-bottom plate. One-hundred eighty microliters of virus diluent was then distributed to all the remaining wells of the plate. Twenty microliters of the starting 10^{-4} dilution from columns 1 to 10 of row A were transferred serially to the next row (A1 to B1, A2 to B2, etc. up until A10 to B10), making dilutions of 10^{-4}, 10^{-5}, 10^{-6}, and so on until 10^{-11}. Pipette tips were changed after each dilution. Column 11 contained virus diluent only and column 12, MDCK cells only. Plates were incubated for 30 minutes at room temperature.

MDCK cells seeded the night before at about 70-90% confluency in 96-well plates were washed three times with PBS to remove any trace of FCS. One hundred microliters of the virus dilutions prepared previously were then transferred to the plate containing the MDCK cells (A1 to A1, B1 to B1 and so forth). The plate was then incubated for 1 hour at room temperature. Afterwards, the viral dilutions were discarded and replaced with 100 µL of freshly-prepared Infection Medium (10% (v/v) 10X Minimum Essential Medium (MEM) (Sigma M0275), 0.7% (v/v) Bovine Serum Albumin fraction V solution 7.5% (Sigma 10735078001), 2% (w/v) $NaHCO_3$ (Sigma S8761), 1% (v/v) HEPES (Sigma H0887), 0.5% (w/v) DEAE dextran (Sigma 93556), 1% (v/v) Pen-Strep (Sigma P0781), 1% (v/v) L-glutamine (Sigma G7513), 1% (v/v) Amphotericine B (Sigma A2942), 0.7% (v/v) Tosyl phenylalanyl chloromethyl ketone (TPCK)-treated trypsin (Sigma T4376)). Plates were then incubated for 72 hours at 37°C and 5% CO_2.

Supernatants were then transferred to round-bottom 96-well plates and 50 µL of 0.7% (v/v) turkey red blood cells (t-RBCs) in PBS were added (**Section 2.3.4**) and the highest dilution with complete hemagglutination in 10 wells in a single row was recorded. The number of hemagglutination positive wells after this row was also recorded and $TCID_{50}$ was calculated using the Reed-Muench method [363].

2.3.7 Influenza Microneutralization (MN) Assay

Terminal mouse sera were heat inactivated for 30 minutes at 56°C to deactivate complement. Assay diluent was prepared as in the $TCID_{50}$ assay (**Section 2.3.6**). One hundred µL of either nanobody-Fc (serially diluted two-fold from 256 nM to 128 pM) or heat-inactivated sera from mice treated with AAV encoding transgenes (diluted 1:25 to 1:3200) was added to 100 µL of 10^3 $TCID_{50}$/mL A/California/07/2009/(H1N1)pdm09. A positive control of ferret antiserum against A/California/07/2009/(H1N1)pdm09 was included. The assay was carried out and neutralization titer was obtained using HA readout (**Section 2.3.4**). The MN titre was defined as the last well showing complete inhibition of hemagglutination.

2.3.8 Lentiviral Pseudotype Neutralization Assay

The plasmid containing A/Vietnam/1194/2004(H5N1) HA pseudotype with luciferase reporter [364] was obtained from Dr. Nigel Temperton at the Medway School of Pharmacy. For the H5 pseudotype, three-plasmid co-transfection was carried out as described previously [312]. Briefly, $3x10^6$ HEK 293T cells in complete DMEM were seeded in 10 cm^2 plates and incubated at 37°C, 5% CO_2 overnight. The next day they were transfected using Opti-MEM™ (Thermo Fisher Scientific 31985062) and Polyethylene Imine (PEI) with the following plasmids: pI.18 HA plasmid (A/Vietnam//1194/2004(H5)) [364], luciferase reporter plasmid pCSFLW [364], and p8.91 gag-pol (Gag-Pol expression plasmid [312]). Plates were incubated at 37°C, 5% CO_2. At least 8 hours post-transfection, medium was replaced and 3 U of exogenous Neuraminidase (Sigma N2876) was added. Forty-eight hours post-transfection, supernatant was collected, passed through a 0.45 µm filter and stored at −80°C.

The following pseudotypes with luciferase reporters [364], A/Korea/426/68(H2N2) (KR/68) and A/Hong Kong/1073/99(H9N2) (HK/99) were also

provided by Dr. Nigel Temperton. All three pseudotypes (H2, H5 and H9) were used for the pseudotype neutralization assays.

Pseudotypes were first titrated on HEK293T cells by making a two-fold serial dilution of 100 µL of the viral pseudotype across a 96-well plate in duplicate. One hundred µL of $1x10^4$ HEK 293T cells was added to each well and plates were incubated at 37ºC, 5% CO_2 for 48 hours. Supernatant was harvested and transferred to white opaque Nunc 96-well plates (Thermo Scientific 165306) and read using the GloMax® Navigator (ProMega) using the Promega GloMax® Luminiscence Quick-Read protocol. Viral pseudotype titer was then determined in Relative Luminescence Units/mL (RLU/mL).

For viral pseudotype neutralization assays, serial two-fold dilutions of nanobody-Fc were made ranging from 32 nM to 1 pM on a 96-well tissue culture plate. Influenza pseudotypes at a concentration of $1.0x10^6$ RLU/well were then added to the nanobody-Fc dilutions and this mixture was incubated for 1 hour at 37ºC. Afterwards, $1.0x10^4$ 293T cells were added to each well. Pseudotype virus only controls (no neutralization) and cell only controls with no virus (which served as the 100% neutralization control) were included in the test plate. Plates were incubated for 48 hours at 37ºC and 5% CO_2. Supernatant was then harvested and virus titered as above. Half-maximal inhibitory concentration (IC_{50}) values were calculated using GraphPad Prism 8.

2.4 AAV production and characterization

2.4.1 Plasmid transformation and DNA preparation

Four plasmid constructs, AAV-R1a-B6-mIgG1, AAV-R1a-B6-mIgG2a, AAV-R1a-B6 and AAV-cAb1-mIgG2a, were generated by Dr. Kam Zaki by cloning the nanobody transgenes (**Figure 3.1**) into the AAV2 inverted terminal repeat (ITR)-containing plasmid pTRUF11 (**Figure 4.**1) via restriction digest with *EcoRI* and *BamHI* (**Section 2.1.2**).

The rAAV plasmids were transformed in XL-1 Blue (Stratagene 200249) competent cells via heat shock and plated on Luria Bertani (LB) agar plates with 50 µg/mL ampicillin (Amp) (Sigma A5354) (LB-Amp). After overnight incubation at 37°C, five colonies from each plate were picked and transferred to separate 15 mL falcon tubes with 3 mL LB-Amp broth. Cultures were incubated overnight at 37°C with shaking at 225 rpm.

For plasmid DNA mini-preps, 2 mL of the overnight cultures were transferred to microcentrifuge tubes and centrifuged at 15,000*xg* for 2 minutes. Supernatant was decanted before proceeding to plasmid DNA extraction using the Plasmid Mini Kit (Qiagen 12125). Extracted DNA was digested (**Section 2.1.2**) with *NcoI* (Promega) to check for integrity.

For plasmid DNA midi-preps, 100 mL of LB-Amp broth was inoculated with 100 µL of the cultures from the mini-preps. These cultures were incubated overnight at 37°C with shaking at 225 rpm. The next day cultures were centrifuged at 2000*xg* for 30 minutes and the supernatant was decanted before proceeding to extraction of endotoxin-free plasmid DNA using the NucleoBond® Xtra Midi EF Kit (Macherey Nagel 740420.10). Extracted DNA was again digested (**Section 2.1.2**) with *NcoI* (Promega) to check for integrity.

To check for ITR integrity, which is necessary for AAV replication, all plasmid DNA obtained from both DNA mini and midi-preps were digested with *SmaI* (Promega) (**Section 2.1.2**). All DNA extracts were quantified using NanoDrop™ (Thermo Scientific) and transgenes were sequenced by GATC Biotech via the Sanger method.

2.4.2 Transient Transfection of 293T cells for cell factory production

Twelve triple flasks (TF) were used per AAV construct to make a cell factory. HEK293T cells were grown to a density of 4.0×10^7 293T cells in a final volume of 100 mL per triple flask of complete DMEM. Cells were incubated at 37°C, 5% CO_2 overnight. Transfection was carried out at approximately 80% cell confluency (around

24 hours post-seeding). Recombinant AAV vectors pseudotyped with serotype 8 capsid containing AAV2 ITRs (AAV2/8) were generated by transient transfection of 293T cells. For each triple flask, a plasmid DNA mix (**Table 2.2**) composed of pHelper, pAAV construct (**Figure 4.1**), and pAAV2/8/Rep-Cap (pLT2-AAV8) was first made. A polyethyleneimine (PEI)-OptiMem mixture (**Table 2.2**) was also made and combined with the plasmid DNA mix. For every µg of plasmid in the previously prepared plasmid DNA mix, 3.5 µL of PEIMax (1 mg/mL) (PolySciences 24765-1) was added to OptiMem™ (Thermo Fisher Scientific 31985062). The plasmid DNA mix and the PEI-OptiMem mixtures were combined and incubated for 20 minutes at room temperature with constant mixing. Culture medium in the triple flasks from the day of seeding was discarded. The plasmid DNA Mix and PEI-Optimem mix were combined with 100 mL complete DMEM and added to each triple flask. Flasks were incubated at 37°C, 5% CO_2 for 72 hours.

Table 2.2. Amounts of individual AAV transfection components.

Solutions	*Amount in µg or µL*	*OptiMem™ (mL)*
Plasmid DNA Mix		
pHelper	41.5 µg	5.1
pAAV	13.8 µg	
pAAV2/8/Rep-Cap	13.8 µg	
PEI-OptiMem Mix		
PEIMax	241.85 µL	4.9

2.4.3 Viral Harvest

After 72 hours, media was poured out of each triple flask and into a 2 L collection vessel. Cells in triple flasks were washed with 20 mL PBS, and this wash was also added to the 2 L collection vessel. The volume of supernatant collected including the wash liquid was measured. For every 100 mL of supernatant, 31.3 g $(NH_4)_2SO_4$ (Sigma) was added and dissolved in sterile double distilled water (sddH_2O)

via a magnetic stirrer on a mixing plate for 10-15 minutes to ensure complete solubilization of $(NH_4)_2SO_4$. The mixture was then transferred to 1 L conical tubes and incubated for 30 minutes on ice. Afterwards, the tubes were centrifuged (Beckman Coulter Avanti J-26S XP) at 8300*xg* for 30 minutes. Supernatant was discarded and the pellet from all 12 TFs was resuspended in 20 mL AAV Lysis Buffer (150 mM NaCl, 50 mM Tris pH 8.5) and marked as "supernatant".

To cells in the triple flask, 15 mL of 0.25% Trypsin-EDTA (1X) (Sigma T4049) was added. TFs were incubated for 5 minutes at 37°C with frequent vigorous tapping until complete cell detachment was observed. Twenty mL complete DMEM was added to each TF to deactivate the trypsin. Contents of all 12 triple flasks were collected in 50 mL conical tubes and centrifuged at 1800*xg* for 15 minutes. Supernatant was discarded. All pellets were combined and resuspended in 20 mL AAV Lysis Buffer. This mixture was marked as the "crude lysate".

Cells were lysed by subjecting the "supernatant" and "crude lysate" to three freeze/thaw cycles (alternating -80°C for 30 minutes and 37°C water bath for 15 minutes). Supernatant and crude lysate were stored at -80°C after the last freeze-thaw cycle.

2.4.4 AAV Purification

2.4.4.1 Benzonase treatment

$MgCl_2$ (Sigma) was added separately to crude lysate and supernatant to make a final concentration of 1 mM $MgCl_2$. For a cell factory (12 TFs), 10,000 U Benzonase® (Novagen 70746-4) was added (split between supernatant and crude lysate). The tubes were mixed by inversion several times and incubated on a 37°C water bath for 1 hour. Tubes were then centrifuged at 1800*xg* for 20 minutes to clarify the lysate by pelleting the cell debris.

2.4.4.2 Iodixanol gradient

Different solutions with varying amounts of iodixanol (OptiPrep™ Sigma D1556) were prepared to make a gradient for AAV purification (**Table 2.3**). The solutions were pipetted in the following order in SV141Ti ultraclear centrifuge tubes (Beckman Coulter); (i) 1.55 mL 60% iodixanol, (ii) 1.55 mL 40% iodixanol, (iii) 1.88 mL 25% iodixanol, and (iv) 2.8 mL 15% iodixanol. Solutions were pipetted very slowly and gently to ensure that layers were well-formed with clear and distinct boundaries. Afterwards, the gradient was topped up with 3 mL of the virus fluid (crude lysate and/or supernatant) per tube.

The tubes were then centrifuged at 273,620*xg* for 3 hours at 18°C in a Beckmann Coulter Optima L-90K Ultracentrifuge using the SW41 rotor. After centrifugation, the clear band that can be seen between the 60% and 40% iodixanol layers was extracted via aspiration using a needle connected to a plunger. Typically, around 5-10 mL of virus fluid was obtained from this procedure.

Table 2.3. Components of solutions making up the Iodixanol Gradient [365].

Percentage (v/v)	*OptiPrep™ (Sigma) (mL)*	*5M NaCl (mL)*	*5x TD* (mL)*	*ddH_2O (mL)*	*Phenol Red (Sigma) (µL)*	*Total volume (mL)*
15%	7.5	6.0	6.0	10.5	-	30.0
25%	8.3	-	4.0	7.7	50.0	20.0
40%	10.2	-	3.0	1.8	-	15.0
60%	15.0	-	-	-	37.5	15.0

* 5X TD buffer is made up of 1 M $MgCl_2$ and 2.5 M KCl. (-) indicates no amount.

2.4.4.3 Virus concentration

Virus bands extracted from the iodixanol gradient were concentrated using VivaSpin20 MWCO 100 kDa (Sartorius VS20S1). Briefly, 5 mL of PBS was added to the VivaSpin20 column to clean and wet the membranes. This was aspirated, after which 10 mL of PBS was added and the column was centrifuged at 500*xg* for 2

minutes. Flowthrough was discarded and the remaining PBS was aspirated. Six mL of virus fluid was added to the column and topped up with PBS to 20 mL. The tube was centrifuged at 500*xg* for 5 minutes. The remaining virus fluid was added, and the solution topped up again with PBS to 20 mL. In between centrifugation steps, the solution was completely homogenized by pipetting up and down several times. The tube was again centrifuged at 500*xg* for 5 minutes until only 5 mL of liquid was left. The flowthrough was collected in a 50 mL falcon tube and labelled “flowthrough #1”. The tube (with the remaining 5 mL virus) was again topped up with PBS to 20 mL. The tube was again centrifuged at 500*xg* for 5 minutes until only 5 mL of liquid was left. The flowthrough was collected in another 50 mL falcon tube and labelled “flowthrough #2”. The tube (with the remaining 5 mL virus) was again topped up with PBS to 20 mL and centrifuged at 500*xg* for 5 minutes until only 1 mL of liquid was left. The flowthrough was collected in another 50 mL falcon tube and labelled “flowthrough #3”. The remaining 1 mL of virus fluid inside the chamber was collected and sterilized using a 0.45 µm filter in the hood. Virus was stored at 4°C.

2.4.5 AAV Characterization and Titration

2.4.5.1 Quantification of Capsid particles via SDS-PAGE

A discontinuous Laemmli SDS-PAGE setup was carried out as described previously (**Section 2.1.3**). Standards of Bovine Serum Albumin (BSA) (Pierce Biotechnology/Thermo Scientific 23209) were made starting from 2000 ng and serially diluted two-fold down to 62.5 ng. Standards loaded on gels ware made up of 10 µL BSA, 5 µL sddH_2O, and 3 µL 6X Loading Buffer.

Instead of Coomassie staining, the gel was stained overnight with Sypro® Ruby Protein Gel Stain (Supelco S4942) on a container wrapped with aluminum foil to protect from light with gentle agitation. After destaining (**Section 2.1.3**) and prior to imaging, the gel was rinsed twice in ultrapure water for 5 minutes.

The gel was viewed using “GeneSnap from Syngene” and analyzed using the “GeneTools from Syngene” program. In brief, rectangular boxes were drawn enclosing the region of the bands to be quantified which included all BSA standards and the VP3 band from each sample. All values were reported as integrated intensity values. A standard curve was generated by plotting the amount of BSA versus the integrated fluorescence intensity. Capsid titers were quantified via linear regression in GraphPad Prism 8.12.

2.4.5.2 Determination of Viral Genome Size and Integrity via Alkaline Gel Electrophoresis

A 1X alkaline electrophoresis buffer was prepared from a stock of 50X (2.5 M NaOH, 50 mM EDTA). The 1X buffer was cooled down to 4°C. A 0.8% (w/v) agarose gel was made and while cooling down, enough 50X alkaline electrophoresis buffer to make it 2% (v/v) was added. Twelve microliters of AAV virus was combined with 4 µL of 4X Alkaline Sample Loading Buffer (20% (v/v) glycerol (Sigma), 4X alkaline electrophoresis buffer, 1.2% (w/v) SDS (Sigma), ~2 mg xylene cyanol (Sigma)) and loaded into wells. Five µL of HyperLadder™ 1 kb (Bioline 33053) was added as Molecular Weight marker for DNA quantitation. The gel was run at 20 V overnight at 4°C. The next day, the gel was incubated in 3 gel volumes of 0.1 M Tris (Sigma), pH 8.0 for 1 hour with gentle agitation. The Tris buffer was then discarded and replaced with 1 gel volume of GelRed™ Nucleic Acid Gel Stain, 3X in Water (Biotium 41001) in 0.1 M NaCl (Sigma) and incubated for 2 hours with gentle rocking in the dark. Afterwards, the gel was rinsed briefly in ultrapure water twice.

The agarose gel was viewed using “GeneSnap from Syngene” and analyzed using the “GeneTools from Syngene” program. For the standards, the first 8 bands of HyperLadder™ 1 kb were quantitated with the 10 kb band corresponding to 100 ng, 8 kb band to 80 ng, 6 kb band to 60 ng, 5 kb band to 50 ng, 4 kb band to 40 ng, 3 kb to 30ng, 2.5 kb to 25ng, and 2 kb to 20ng. Values were reported as integrated intensity

values. A standard curve was generated by plotting the mass of the different HyperLadder™ 1 kb bands versus the integrated fluorescence intensity. Viral genome titers were quantified via linear regression in GraphPad Prism 8.12.

2.4.5.3 Measurement of Vector Genomes via Quantitative Real Time PCR (qPCR)

Vector genome titers were quantified by amplifying rAAV genome sequences corresponding to a 129 bp fragment of the Cytomegalovirus (CMV) promoter upstream of the transgene. AAV samples were diluted 1:10, 1:100, 1:1000 and 1:10000 in sddH_2O. For the standard curves, plasmids obtained from the previous midi preps were digested for 3 hours with *EcoRI* (Promega) to linearize them (**Section 2.1.2**). Linearized plasmids were then purified using a QiaQuick PCR Purification Kit (Qiagen 28104) and the concentrations determined using NanoDrop™. The mass of one copy of each plasmid was calculated by multiplying the number of bases with 1.096×10^{-21} g (the average mass of one nucleotide). Plasmid dilutions of 10^9 copies to 10^1 copies were made for the standard curve.

Table 2.4. qPCR primer and probe sequences for CMV.

Target	*Amplicon size (bp)*	*ID*	*Sequence 5'→3'*	*T_M (°C)*
CMV [366]	129	CMV-F	TTC CTA CTT GGC AGT ACA TCT ACG	70
		CMV-R	GTC AAT GGG GAG ACT TGG	66
		Probe	FAM – TGA GTC AAA CCG CTA TCC ACG CCC A - TAMRA	78

qPCR was performed using the Mx3005P™ (Stratagene). For the CMV reaction, a final volume of 20 µL containing 20 µM each of Forward (F) and Reverse (R) primers, 10 µM of CMV probe (**Table 2.4**), 10 µL 2X Quantitect (Qiagen 204443) and 1 µL of DNA template was prepared. The PCR was carried out with initial denaturation at 95°C for 15 minutes followed by 40 cycles of denaturation at 94°C for

15 seconds and annealing/extension at 60°C for 30 seconds. All samples and standards were tested in duplicate.

2.5 Mouse experiments

All mouse experiments and husbandry were conducted by the Biological Services Division (BSD) of the National Institute for Biological Standards and Control (NIBSC). I assisted in the culling of mice at the end of each *in vivo* study conducted at Biosafety Level 2 (BSL2) (tolerability and A(H1N1) challenges) and processed all biological samples obtained. Lung homogenization, $TCID_{50}$ determination and hemagglutination inhibition assay for mice challenged with A(H5N1) were conducted by colleagues at the Influenza Resource Center (IRC) at NIBSC.

2.5.1 Mouse 50% Lethal Dose (MLD_{50}) determination of CA/09 by *in vivo* titration

Twenty (20) female BALB/c mice, 6-8 weeks old were obtained from Charles River Laboratories and housed at the Biological Services Division (BSD) at NIBSC. The following virus dilutions of A/California/07/2009/(H1N1)pdm09 (CA/09) in PBS were prepared, 10^5 $TCID_{50}$/mL, 10^4 $TCID_{50}$/mL, 10^3 $TCID_{50}$/mL, and 10^2 $TCID_{50}$/mL.

Mice were divided into five groups of four for each dilution series of virus. One group was given the negative control, PBS. Mice were then individually identified, and weights were recorded daily for three days prior to virus inoculation. On the day of viral challenge, mice were sedated and inoculated with 50 µL of specified virus dilution or PBS per group by the intranasal (IN) route. Remaining inoculum was stored on ice and back titrated on the day for confirmation of viral activity. Weights and clinical observations were carried out twice daily from day 1 of infection to day 14.

Animals at severity limit for the study (20% weight loss) and/or showing physical and behavioral symptoms or distress were euthanized. At day 14 post-infection, all remaining mice were culled and lungs were harvested. Collected blood was left to clot for 1 hour at room temperature. Serum was separated via centrifugation

at 2,000*xg* for 10 minutes at 4°C and stored at -20°C. A lung from each mouse was snap-frozen. The other lung was washed in PBS and fixed in 4% (v/v) paraformaldehyde (PFA) for histology.

2.5.2 Mouse tolerability studies

Twenty-eight (28) female BALB/c mice, 6-8 weeks old were obtained from Charles River Laboratories and housed at BSD, NIBSC. Mice were divided into four groups of six for each of the AAV constructs. For every group, the following AAV doses in vector genomes (vg) were prepared via dilution with PBS (Sigma D8662) to a 50 µL volume: (i) 1.0×10^{11}, (ii) 3.3×10^{10}, and (iii) 1.0×10^{10}. Each dose was given to 2 mice via intramuscular (IM) injection. A control group consisting of 4 mice was given 50 µL PBS. Mice were weighed daily and monitored for any signs of disease or distress. Animals that exhibited behavioral and physical signs of distress or lost 20% of their initial body weight were culled. Mice were bled (~50 µL) at 0, 2, 4, 6, 8, 10, 12, 16, 20, and 24 weeks post-AAV administration. Collected blood was left to clot for 1 hour at room temperature and serum was separated via centrifugation at 2,000*xg* for 10 minutes at 4°C and stored at -20°C. At the end of 24 weeks, all mice were culled, terminal bleeds (~500 µL) collected, and lungs harvested.

2.5.3 Mouse protection studies

For each of the challenge experiments, 40 female BALB/c 6-8 week old mice were obtained from Charles River Laboratories and housed at BSD, NIBSC. Mice were divided into five groups of eight. All groups were weighed and observed for 2 days before being pre-bled on day -2. On day 0, mice from groups 1-4 were injected intramuscularly (IM) with a 50 µL volume of 1×10^{11} vg AAV-R1a-B6-mIgG1, AAV-R1a-B6-mIgG2a, AAV-R1a-B6, and AAV-cAb1-mIgG2a respectively. Mice from group 5 were given 50 µL PBS. Thirty-nine (39) days later, mice were bled to determine serum antibody titers. Six weeks after the start of the study, mice were challenged intranasally (IN) with 21 MLD_{50} A/California/07/2009/(H1N1)pdm09 (CA/09) or 10

MLD_{50} A/Vietnam/1194/2004(H5N1) NIBRG-14ma (VN/04). Weights and clinical observations were made twice daily for 14 days or until the endpoint of loss of 20% of initial body weight was observed and/or clinical symptoms of poor health such as abnormal behavior and appearance, difficulty in breathing, sunken abdomen, pinched waist, and ocular symptoms were deemed too severe for mice to remain in the study. Lungs were harvested, immediately snap-frozen, and stored at -80°C. Terminal bleeds were also collected. For the H5N1 challenge experiment, an additional 3 mice per group, were added and culled 3-days post-challenge, to quantify influenza titers in the lungs and for histological analysis.

2.5.4 Lung Homogenization

Bijoux were pre-weighed prior to transfer of snap-frozen lungs. Lungs and bijoux were then weighed together, and mass of the lungs determined by difference. To each bijoux, 2 mL of virus diluent (**Section 2.3.6**) was added and lungs were homogenized using a blender. The mixture was centrifuged at 18,000*xg* for 2 minutes and the supernatant was used to quantify residual virus in lung tissue via $TCID_{50}$ determination (**Section 2.3.6**).

2.5.5 Histology

Mouse lungs were washed in PBS and fixed with 4% paraformaldehyde (PFA). Following fixation, tissues underwent standard paraffin embedding and processing. Four-micron-thick sections were then cut using the Leica RM2125 RTS Microtome. Slides were prepared and stained with hematoxylin and eosin (H&E) (Vector Laboratories Inc. H-3502). High definition scans were taken using Pannoramic Digital Slide Scanner (3D HISTECH) and analyzed using CaseViewer 2.3 (3D HISTECH). Inflammation was scored in blinded fashion as follows: 0 = no to minimal inflammation, 1 = occasional infiltration in bronchioles, 2 = infiltration of bronchioles and slight thickening of perivascular walls; 3 = mass infiltration of bronchioles, thickening of perivascular walls, and lung rupture.

2.5.6 Ethics

AAV mouse tolerability studies were peformed under United Kingdom Home Office project license # PPL70/8091 under the “Vector Immunogenicity” protocol. Influenza challenge studies using A/California/07/2009(H1N1)pdm09 were performed under United Kingdom Home Office project license # P856F6831 under the protocol for “Protection from Infection with Influenza virus”. Influenza challenge studies using A/Vietnam/1194/2004(H5N1) NIBRG-14ma were performed under United Kingdom Home Office project license # P30D4C513 under the protocol for “Protection from Infection with Influenza virus or virulent influenza virus”.

CHAPTER 3

PRODUCTION, PURIFICATION, AND CHARACTERIZATION OF NANOBODY-FC FUSIONS AGAINST INFLUENZA

3.1 Overview

In addition to vaccination and antiviral drugs, the use of recombinant monoclonal antibodies (mAbs) that are broadly neutralizing against influenza is a promising strategy to counter annual epidemics and pandemic threats. These mAbs, several of which are already in clinical development, bind to functionally conserved epitopes such as those in the influenza hemagglutinin (HA) stem, thereby providing strain independent protection [192, 201, 209, 210, 238].

Structural analysis of several of the earliest human mAbs against the influenza HA stem revealed that they employ only their heavy chains for antigen recognition [209, 210]. This implies that the light chains were not required for binding to these difficult to access epitopes. In a single domain antibody, the target-binding module is composed of a single V_HH domain as opposed to non-covalently associated variable domains, V_H and V_L in a conventional antibody. The longer CDR3 loop in a V_HH enlarges the potential interaction surface with the target antigen contributing to the diversity and specificity of the paratope [260]. In addition, some of the most potent cross-neutralizing human mAbs described reveals somatic hypermutation constrained to particular germline genes [34, 209, 210, 236, 238]. This prompted our interest in naturally occurring “heavy-chain only” antibodies from camelids and our isolation of high affinity broadly neutralizing single domain antibodies (sdAb) or nanobodies against influenza A and B [268, 367].

R1a-B6, a potent alpaca derived nanobody capable of cross subtype neutralization of pandemic A(H1N1)2009, highly pathogenic avian influenza H5N1, H2N2 and H9N2 [219, 268] has been previously described. R1a-B6 neutralizes influenza through binding to a highly conserved epitope in the HA stem and blocking

the low pH induced conformational change required for viral membrane fusion. As a single domain antibody fragment of approximately 15 kDa, R1a-B6 would be rapidly cleared from circulation in a matter of hours, which would prohibit any activity *in vivo* [281, 283]. To achieve maximum protective levels in the systemic circulation, additional strategies to enhance its pharmacokinetics are required [294]. In this study, R1a-B6 was fused to both a mouse IgG1 (ADCC-) and IgG2a (ADCC+) Fc domain to both extend half-life and to evaluate to what extent ADCC might be required for efficacy of R1a-B6 *in vitro* and *in vivo*. The Fc domain is largely responsible for the extended serum persistence of mAbs by pH dependent interaction with FcRn and recycling through the kidneys [368]. In addition, the Fc domain mediates interactions with the effector arm of the immune system and recent reports have suggested ADCC is required for efficacy of human mAbs specific for the influenza HA stem [246, 247].

The work presented in this chapter was aimed towards demonstrating the protective efficacy of the reformatted nanobody R1a-B6 against different Group I influenza A subtypes *in vitro.* Additionally, it was aimed to show that fusion of the nanobody to a mouse Fc region would enable it to recruit effector functions, which may be essential for its protective effect *in vivo,* by performing surrogate ADCC assays. The overall goal is to design and evaluate an optimal nanobody format that can be employed for immunotherapy which can then be an alternative option in the prevention and treatment of influenza.

In this chapter, the following objectives were accomplished:

(i) production and purification of nanobody-Fc fusions,

(ii) demonstrated cross-subtype binding against influenza A Group I strains *in vitro* of nanobody-Fc fusions,

(iii) binding and activation of mouse FcγRIV effector cells by nanobody-Fc fusions,

(iv) production and $TCID_{50}$ determination of A/California/07/2009 (H1N1)pdm09,

(v) production and titration of representative lentiviral vector-based influenza A Group I pseudotypes, and

(vi) neutralization of live A/California/07/2009(H1N1)pdm09 and representative influenza A Group I pseudotypes *in vitro* by nanobody-Fc fusions.

3.2 Results

3.2.1 Production and purification of nanobody-Fc proteins

For this study, plasmid constructs encoding nanobodies that were previously designed and synthesized by Simon Hufton and Tiziano Gaiotto. The nanobody sequences were reformatted as Fc fusions separated by a mouse hinge region. The mouse C_H1 domain was removed and the C-terminal end of the nanobody was directly fused to the N-terminus of the mouse hinge region followed by the C_H2-C_H3 domains of either mouse IgG2a or mouse IgG1. In total, four constructs, (i) R1a-B6 mouse Fc IgG1, (ii) R1a-B6 mouse Fc IgG2a, (iii) monovalent R1a-B6 [268] and (iv) negative control mouse Fc IgG2a fusion carrying a nanobody cAb1 specific for chicken egg white lysozyme [252], were cloned into a mammalian expression vector.

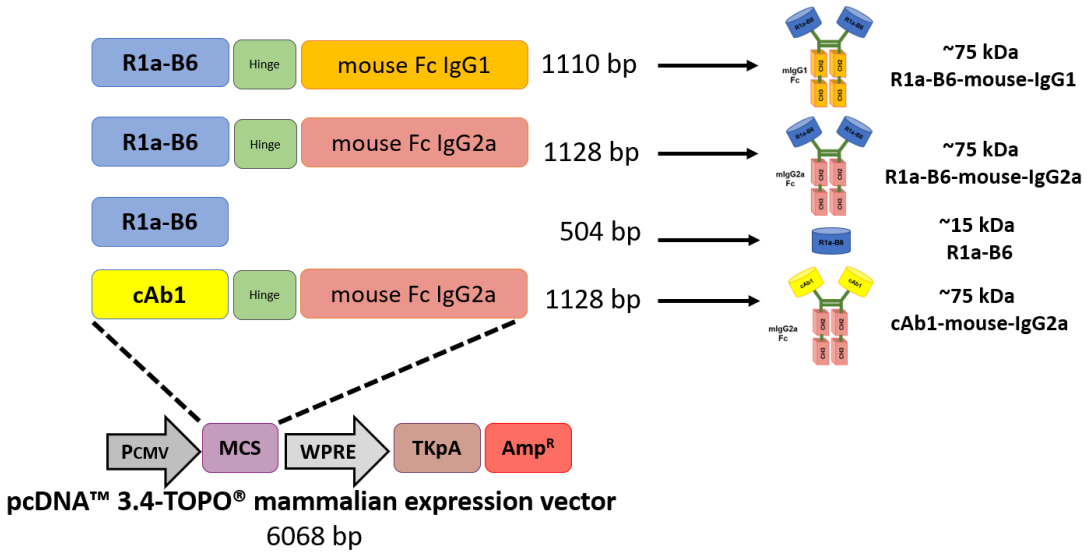

Figure 3.1. Graphical representation of R1a-B6 reformatted for *in vivo* gene delivery. Constructs were cloned into the multiple cloning site (MCS) of pcDNA™3.4-TOPO® (Thermo Fisher Scientific) and produced *in vitro* in ExpiCHO™ (Thermo Fisher Scientific) cells. These constructs were also cloned into an AAV expression system for protein expression *in vivo* (Chapter 5).

The pcDNA™3.4-TOPO® (Thermo Fisher Scientific) vector contains the Woodchuck posttranscriptional regulatory element (WPRE) to enhance transcript expression under the full-length human cytomegalovirus (CMV) immediate-early promoter/enhancer (**Figure 3.1**). It also contains the Herpes Simplex Virus thymidine kinase polyadenylation (TKpA) signal for proper termination and processing of the recombinant transcript and an Ampicillin resistance (Amp^R) gene for selection in *E. coli* (**Figure 3.1**). These different versions of R1a-B6 (**Figure 3.1**) were designed to test antigen-antibody binding, virus neutralization, requirement for half-life extension, and the possible contribution of ADCC on the antiviral effect of the nanobody Fc *in vitro* and *in vivo*.

Production of R1a-B6-mIgG1, R1a-B6-mIgG2a, and cAb1-mIgG2a plasmid DNA that is pure, high-yield, and endotoxin-free for protein production was first accomplished. R1a-B6 plasmid DNA and proteins were already produced previously [268]. Plasmid DNA containing nanobody-Fc was extracted from bacterial cultures after several rounds of scale-up production and endotoxin-free DNA midi preparations. DNA concentrations for all plasmid constructs were determined and were on average around 5-10 µg/µL. This is sufficient for large-scale transfection in ExpiCHO™ cells.

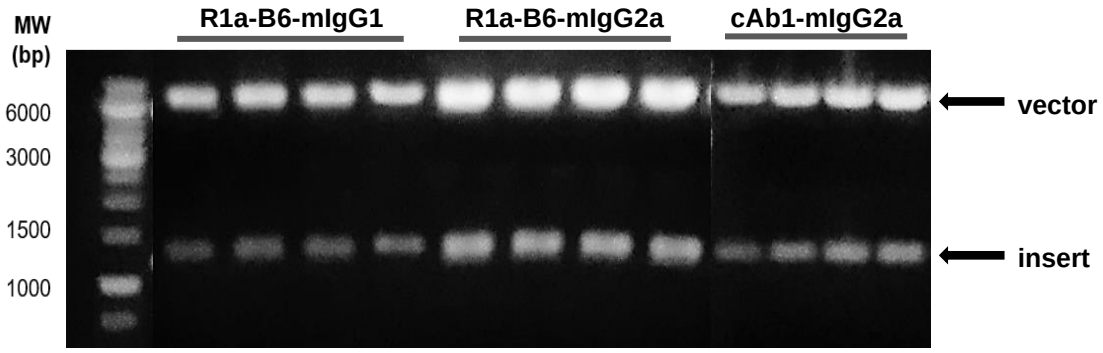

Figure 3.2. RE digestion using *EcoRI* and *BamHI* of pcDNA™3.4-TOPO® (vector) containing nanobody-Fc (insert) from DNA plasmid midi preparations. For all constructs, bands at ~6000 bp showing the vector and another band at ~1200 bp showing the released insert were observed. Promega 1 kb DNA Molecular Weight (MW) ladder was used as reference.

Upon digestion with *BamHI* and *EcoRI* (**Figure 3.2**), the restriction enzymes used to clone the nanobody-Fc inserts, the carrier plasmid (6068 bp) and the released inserts (~1100 bp) appear as bands on the gel consistent with theoretical fragment sizes after restriction enzyme digestion. Nanobody-Fc inserts were sequence verified against original nanobody sequences designed and produced previously (unpublished data from Hufton lab) and results adhered to expected sequence profiles.

The extracted DNA was then utilized for transfection in the ExpiCHO™ expression system (Thermo Fisher Scientific) which employs suspension-adapted Chinese hamster ovary (CHO) cells for high yield transient protein production. Since the nanobody-Fc fusions were being expressed for the first time, a pilot time course study, utilizing 30 mL ExpiCHO™ suspension cultures per construct was performed first. Cells and/or media were harvested at several time points post-transfection to identify the optimal duration of the expression run (**Figure 3.3**). For the ExpiCHO™ "Max" expression protocol, the manufacturer recommended harvesting proteins 12 to 14 days post-transfection, with the protocol supporting protein expression for a maximum of 14 days.

Protein expression can be observed in the crude supernatant as early as day 3 for all nanobody-Fc constructs and increases thereafter for R1a-B6-mIgG2a and cAb1-mIgG2a, with the highest absorbance seen in supernatant collected on day 14 (**Figure 3.3**). For R1a-B6-mIgG2a, absorbance against CA/09 picked up as the expression run went on, increasing from day 3 to day 14 (**Figure 3.3**). Absorbance was uniform throughout for R1a-B6-mIgG1 which was unusual (**Figure 3.3**). It can be attributed to being unable to dilute the supernatant further to show a more complete titration. However, expression and functionality of R1a-B6-mIgG1 seems to be unaffected by this as observed and presented later in the chapter. From this, it can be gathered that protein expression was successful, with nanobody-Fc fusions generated from transient transfection correctly folded and functional. This is evidenced by proteins being able to bind to influenza HA (CA/09) for R1a-B6-mIgG of both subtypes

and lysozyme for cAb1-mIgG2a. The highest yield of nanobody-Fc can be obtained by harvesting on day 14 post-transfection (**Figure 3.3**).

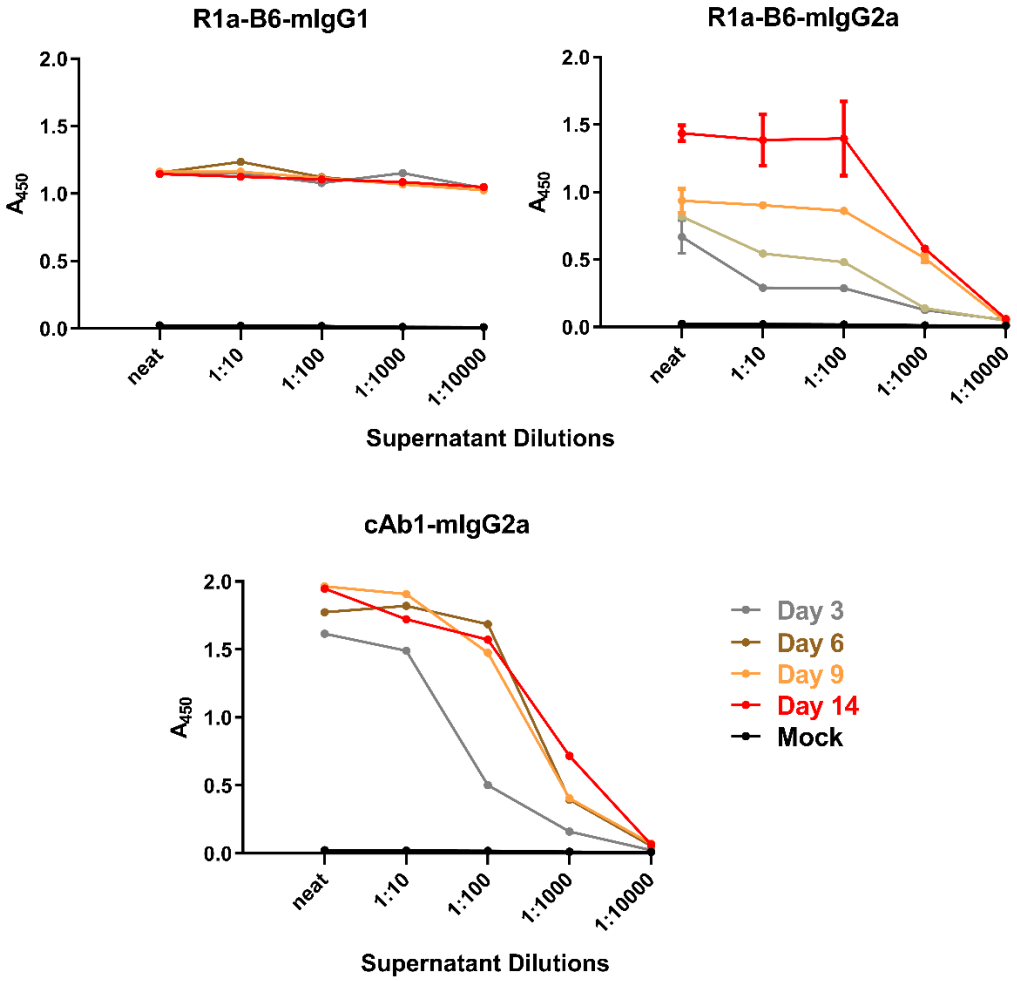

Figure 3.3. Activity *in vitro* of nanobody-Fc as tested via ELISA after specified harvest points. Supernatant from ExpiCHO™ cultures transfected with R1a-B6-mIgG1, R1a-B6-mIgG2a, and cAb1-mIgG2a were harvested at days indicated and activity was tested against reference standard A/California/07/2009(H1N1)pdm09 for R1a-B6-mIgG and chicken egg white lysozyme for cAb1-mIgG2a. Mock indicates supernatant from transfection with no DNA and serves as the negative control in this experiment. Points are shown as the mean and standard error of two replicates.

From 30 mL pilot studies, a scale-up transfection of 500 mL for each nanobody-Fc was carried out. Supernatant was harvested on day 14 and purified in batches by running it through a Protein A affinity column. Protein absorbance at 280 nm was taken via nanodrop and eluates with the highest readings were run on SDS-PAGE gels to confirm presence of protein. Eluates containing proteins of the right size

were pooled together and dialyzed overnight in PBS. They were then analyzed on 12% polyacrylamide gels in reducing and non-reducing conditions and transferred to nitrocellulose membranes and detected with anti-mouse-Fc IgG HRP (GE Healthcare) (**Figure 3.4**).

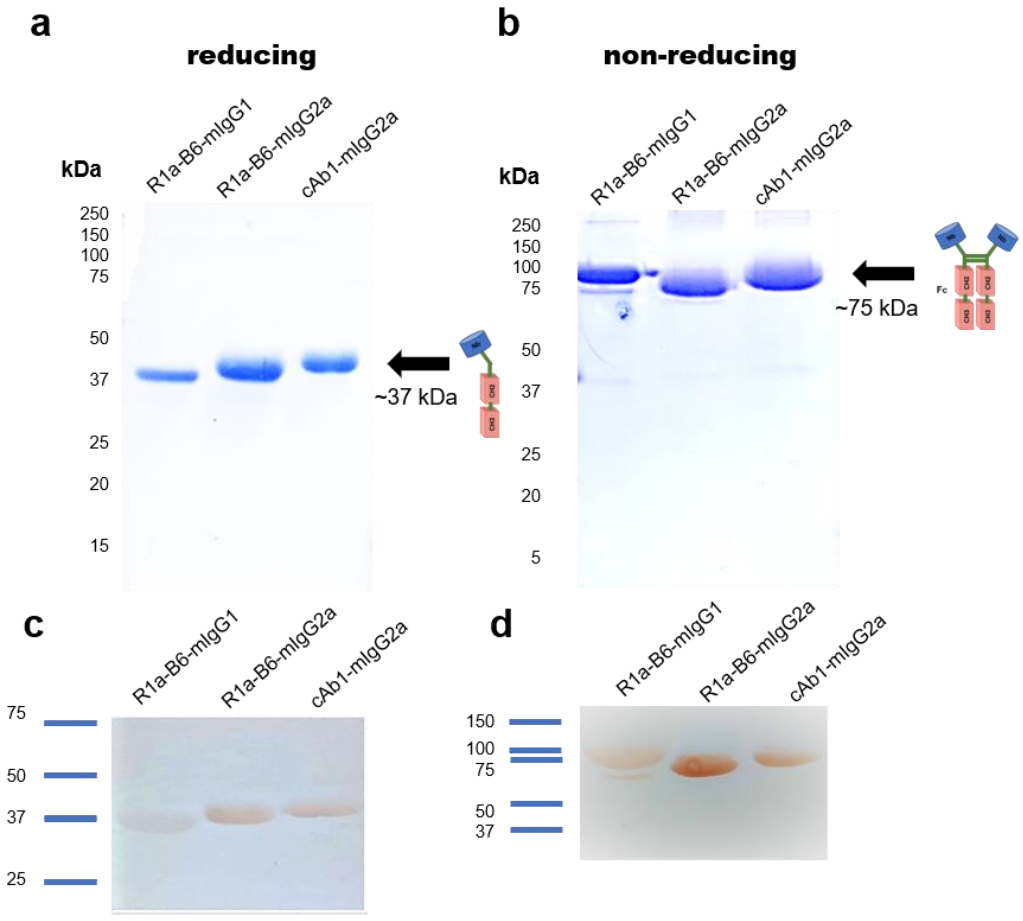

Figure 3.4. Detection of nanobody-Fc fusion proteins in SDS-PAGE and Western blot analysis. Detection of proteins in reducing (**a,c**) and non-reducing (**b,d**) conditions in Coomassie blue-stained SDS-PAGE gels (**top,a,b**) and by an anti-mouse-IgG-Fc-HRP in Western blots (**bottom,c,d**). Theoretical molecular weights (MW) for R1a-B6-mIgG1, R1a-B6-mIgG2a, and cAb1-mIgG2a are ~37 kDa under denaturing (reducing) conditions, and ~75 kDa under non-reducing conditions.

After purification, a product of approximately 75 kDa was seen under non-reducing conditions demonstrating the formation of a dimeric Fc fusion protein (**Figure 3.4**). As only single domain variable fragments were produced, nanobodies fused to the Fc region of a mouse IgG with a deleted C_H1 domain, the proteins produced (~75 kDa) are approximately half the size of ordinary mouse IgGs which are around 150

kDa. The nanobody-Fc fusions are encoded by single gene fragments and translated from one open reading frame, and this is a distinct advantage over two-chain monoclonal antibodies. No other bands were seen aside from the expected nanobody-Fc proteins in all gels and blots showing the purity of the preparation (**Figure 3.4**).

3.2.2 Binding of R1a-B6-Fc against a broad range of Group I influenza A subtypes

Influenza viruses infect humans mainly because of their ability to undergo antigenic variation via antigenic shift and drift of the globular hemagglutinin (HA) head domain [110, 112]. Within each influenza subtype, there is a continuous antigenic drift [369]. Seasonal vaccination generates subtype-specific antibodies that will have little or no efficacy against drifted strains [110]. It is desired to have antibodies that will elicit a broad, cross-subtype specific response in order to address a pandemic threat.

Hufton, et.al previously reported the cross-reactivity of R1a-B6 against A(H1N1) and A(H5N1), and when present in a bivalent format, also against A(H2N2), and A(H9N2) [268]. In this study, bivalent R1a-B6 with an appended Fc region (**Figure 3.1**), in addition to monovalent R1a-B6 were employed to investigate the breadth of reactivity of the nanobody-Fc fusions via binding in an ELISA against a panel of influenza A reference standards (**Table 2.1**). The influenza antigen reference reagents used in this study were made at the Influenza Resource Centre (IRC) at the National Institute for Biological Standards and Control (NIBSC), one of the four WHO Essential Regulatory Laboratories (ERLs) that manufacture these preparations of inactivated whole virus. Reference antigens are freeze-dried, calibrated and assigned a potency value via rigorous methods that have been globally standardized [370]. These influenza reference reagents are then used for vaccine manufacture and standardization worldwide.

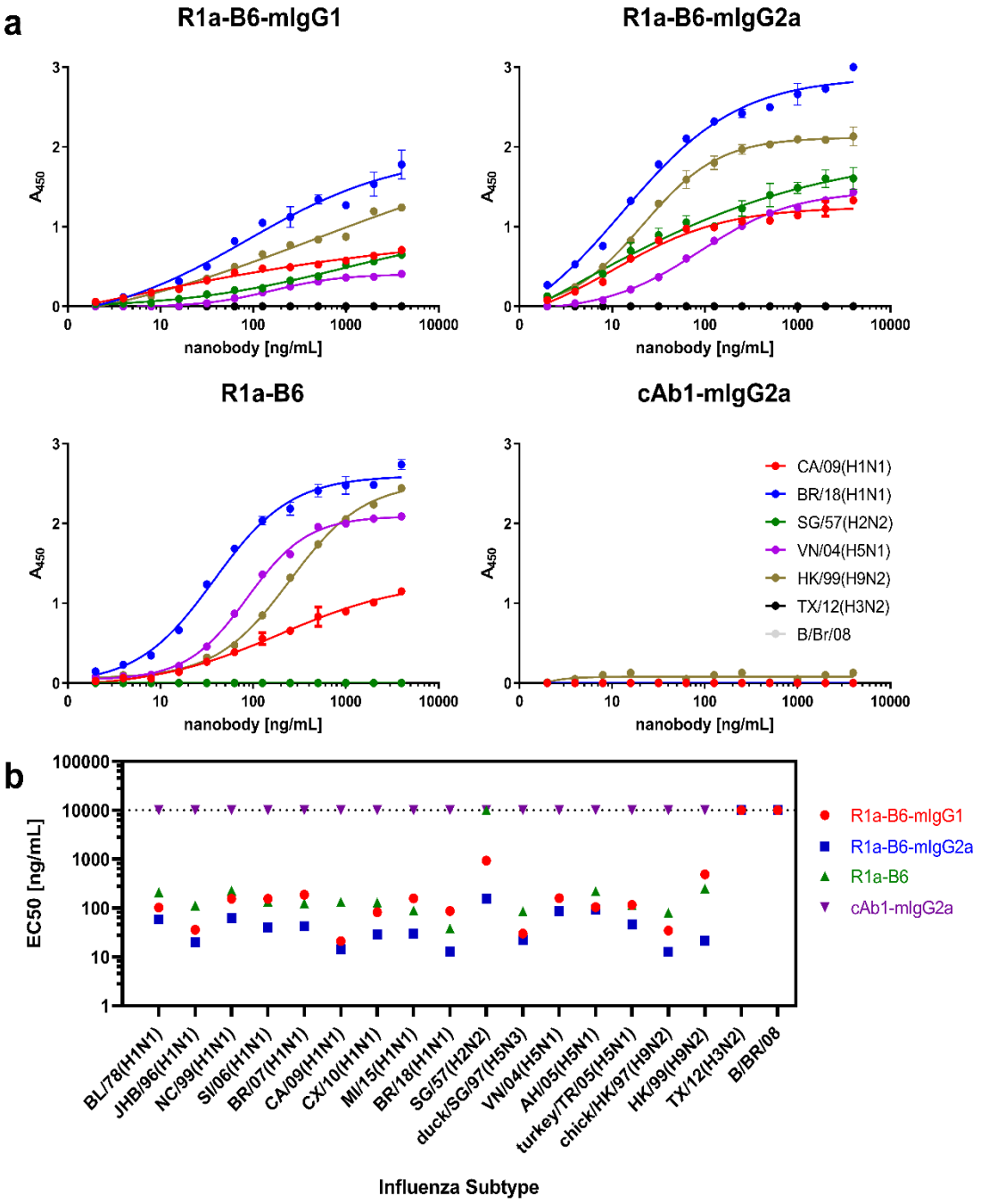

Figure 3.5. Binding of different R1a-B6 formats against a broad range of influenza A subtypes as tested by ELISA. (**a**) Standard curves showing binding of nanobody constructs from concentrations of 4 µg/mL to 2 ng/mL against representative Influenza A Group I, Group II and influenza B reference reagents. Binding was measured in duplicate and average absorbance was plotted against purified nanobody Fc dilutions. (**b**) Binding as shown by half maximal effective concentration (EC_{50}) of nanobody-Fc was measured in duplicate. All values above the dotted line indicate no binding activity.

To test for binding, a panel of influenza reference reagents composed of representative A(H1N1) strains that were present in a 40 year time span from A/Brazil/11/78(H1N1) to A/Brisbane/02/2018(H1N1), H2N2, H5N1, and the more distant H9N2 strain, all from group I influenza A, was employed. H3N2 from group II influenza A and an influenza B virus served as negative controls.

R1a-B6 appended with a mouse Fc region of either IgG1 or IgG2a isotype retained the binding activity of monovalent R1a-B6 as shown previously [268]. Binding was strongest against BR/18(H1N1) for both R1a-B6-Fc and R1a-B6 (**Figure 3.5a**). R1a-B6-mIgG2a seems to show better binding to all strains tested compared to R1a-B6-mIgG1, but this may be just down to preferential binding of the secondary antibody used in the ELISA to mouse IgG2a over mouse IgG1. R1a-B6-mIgG showed strong binding to all A(H1N1) and A(H5N1) strains regardless of year of circulation (**Figure 3.5a**).

The EC_{50} values against H1-HA and H5-HA were in the same range, around ~20-160 ng/mL for R1a-B6-mIgG1, and ~12-90 ng/mL for R1a-B6-mIgG2a. Binding to the more divergent subtype, H2, was generally lower for R1a-B6-mIgG as compared to that for H1 and H5, with EC_{50} values of 930 ng/mL for R1a-B6-mIgG1 and 155 ng/mL for R1a-B6-mIgG2a, but still better than monovalent R1a-B6 which showed no binding (**Figure 3.5b**). R1a-B6-mIgG and monovalent R1a-B6 strongly bound to H9N2 (chick/HK/97 and HK/99) (**Figure 3.5b**), with EC_{50} values of ~30-450 ng/mL for R1a-B6-mIgG1, ~12-20 ng/mL for R1a-B6-mIgG2a, and ~80-250 ng/mL for R1a-B6, better than previously reported [268]. The negative control nanobody construct, cAb1-mIgG2a did not bind to any of the influenza HA reference standards as expected. There was also no binding observed against the H3N2 strain which belongs to influenza A group II and also the influenza B virus (**Figure 3.5b**).

3.2.3 Binding and activation of mouse FcγRIV effector cells by nanobody-Fc fusions

It was previously believed that neutralizing antibodies against influenza, both HA head and stem-binding, provide protection exclusively through engagement of their variable region but this has been challenged in recent years with the contributions of mechanisms conferred by the Fc domain of the antibody proving vital to survival against lethal influenza infection in mice *in vivo* [208, 246, 247]. To test the requirement for half-life extension and to address the need for effector activation in the case of antibody dependent cell cytotoxicity (ADCC) in the prophylactic efficacy of R1a-B6, three single gene encoding proteins (**Figure 3.1**) were fused to a mouse Fc fragment of either an IgG1 or IgG2a isotype. Mouse IgG isotypes differentially interact with Fc gamma receptors (FcγR) on effector cells, with mouse IgG2a being the most potent having high affinity for activating FcγR, whereas mouse IgG1 is the least potent, preferentially interacting with inhibitor FcγR [292].

Available ADCC assays today usually measure antibody-mediated killing of target cells by activated NK effector cells [128, 248]. This requires the use of peripheral blood mononuclear cells and purified NK cells from donors, which may be hard to obtain. Surrogate assays that do not directly measure killing but instead rely on the NK cell degranulation [371-373] and the release of perforins, granzymes, cytokines and chemokines from effector cells as measured by modern fluorometric techniques to indirectly calculate cytotoxicity [373] have also been employed.

Here a mouse FcγRIV ADCC Reporter Bioassay (Promega) to test whether the nanobody-Fc fusion proteins are functionally capable of inducing ADCC was employed. This ADCC reporter bioassay allows our nanobodies equipped with a mouse Fc region to be tested with their respective FcγRs, in this case FcγRIV, the predominant receptor involved in ADCC in mouse [172, 291]. However, whether the nanobody-Fc proteins actually induce ADCC or not *in vitro* or *in vivo* to protect against influenza can not be answered by this approach.

Briefly, 5 µg/mL of CA/09 antigen per well was plated on a 96-well plate and incubated this overnight at 4°C. This is a departure from the Promega protocol that

uses adherent target cells, either a Jurkat T cell line or Raji cells, that are transfected with and express the target antigen. Nanobody-Fc dilutions were then made and were incubated with the HA antigen for 2 hours, similar to an ELISA. The supplied mFcγRIV Effector cells are then incubated for 6 hours with the nanobody-Fc dilutions and the HA antigen coated on the plate. These effector cells then bind to the Fc domain of ADCC activating nanobodies resulting in mFcgRIV signalling and Nuclear Factor of Activated T cells-Response Element (NFAT-RE) mediated luciferase activity. This bioluminescent signal is then detected and quantified using Bio-Glo™ Luciferase Assay System (Promega).

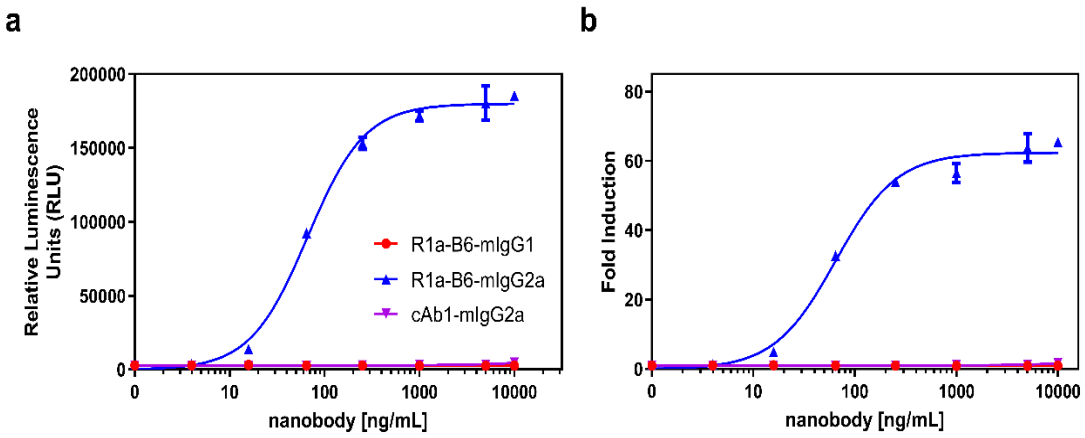

Figure 3.6. *In vitro* ADCC activation of nanobody-Fc fusion proteins. Activation of luciferase reporter gene is shown in (**a**) relative luminescence units (RLU) and (**b**) fold induction of luminescence. Both (**a**) and (**b**) are measured as a function of nanobody-Fc concentration against A/California/07/2009(H1N1)pdm09 reference standard. Points are shown as the mean and standard deviation of three replicates.

Nanobody-Fc fusions in a range of concentrations from 10 µg/mL to 4 ng/mL as determined by A_{280} protein readings were then tested for ADCC activity. As expected, only R1a-B6-mIgG2a which is specific against the H1N1 antigen and with an activating mouse Fc region, showed substantial ADCC activity, about 200,000 RLU (**Figure 3.6a**). R1a-B6-mIgG2a also demonstrated ~70-fold induction in luminescence activity compared to R1a-B6-mIgG1 and cAb1-mIg2a (**Figure 3.6b**). There was no induction of luciferase activity by R1a-B6-mIgG1(**Figure 3.6**), as this mouse IgG

isotype does not bind to mFcγRIV [172, 291]. Likewise, there was no luciferase signal for cAb1-mIgG2a, as it is unable to bind to the target antigen CA/09 HA (**Figure 3.5**).

The RLU values reported here are relatively less than that reported elsewhere ($1x10^6$ RLU) [357] and the manufacturer's technical manual ($8x10^5$ RLU) (Promega). However, the difference between the fold induction of luminescence, about ~60-70-fold increase, between the mouse-Fc IgG2a (ADCC+) and mouse-Fc-IgG1 (ADCC-) antibodies is reflected in our findings (**Figure 3.6b**). Transient expression of HA by target cells results in higher assay sensitivity [374], which can explain the difference between absolute RLU values that were observed and that of previous studies. As a cell line expressing HA was not employed, there was no need to optimize parameters such as the effector:target cell ratio, number of target cells per well or cell density, and incubation time with the effector cells, all of which may have given a stronger RLU signal. These parameters are dependent on and will change with the target system employed. Nonetheless, these results show very little background noise as observed with the ADCC negative constructs R1a-B6-mIgG1 and cAb1-mIgG2a having RLU values <2000 (**Figure 3.6a**), and with the fold induction the same as that reported by the manufacturer using control antibodies and their own target cell line (Promega). These results demonstrate that the nanobody-Fc fusion induces reporter gene expression only when target antigen and mFcγRIV are cross-linked, as in the case of R1a-B6-mIgG2a, and that clearly, R1a-B6-mIgG1 and cAb1-mIgG2a are unable to activate FcγR.

3.2.4 Production of challenge virus and viral pseudotypes for *in vitro* neutralization assays

3.2.4.1 Validation and $TCID_{50}$ Determination of A/California/07/2009(H1N1)pdm09 (CA/09)

For validation, PCR amplification of the full length H1 (1700 bp) and N1 (1400 bp) genes of the live A/California/07/2009/H1N1(pdm09) grown in eggs was carried

out. Sequences of the HA and NA genes produced were then verified to establish that there were no mutations in these genes that could possibly affect the virus's immunogenic or antigenic profile. DNA sequence of CA/09 HA gene was compared against Influenza A virus (A/California/07/2009(H1N1)) segment 4 hemagglutinin (HA) gene, with NCBI Reference Sequence: NC_026433, and CA/09 NA gene was compared to Influenza A virus (A/California/07/2009(H1N1)) segment 6 neuraminidase (NA) gene, with NCBI Reference Sequence: NC_026434. Verification showed no mutations in the HA and NA genes of live virus we produced.

A hemagglutination assay was then carried out to determine which viral fluid from the 24 individual eggs that were inoculated could be combine for use in *in vitro* and *in vivo* assays. Samples that scored 256 Hemagglutinin Units (HAU) or higher were pooled and a $TCID_{50}$ assay on this stock was carried out to determine working concentrations and challenge dose. Via an HA readout (**Figure 3.7**) and the Reed-Muench method [363], the $TCID_{50}$ of the A/California/07/2009/H1N1(pdm09) stock produced was found to be $10^{7.95}$ $TCID_{50}$/mL (average of 6 independent trials).

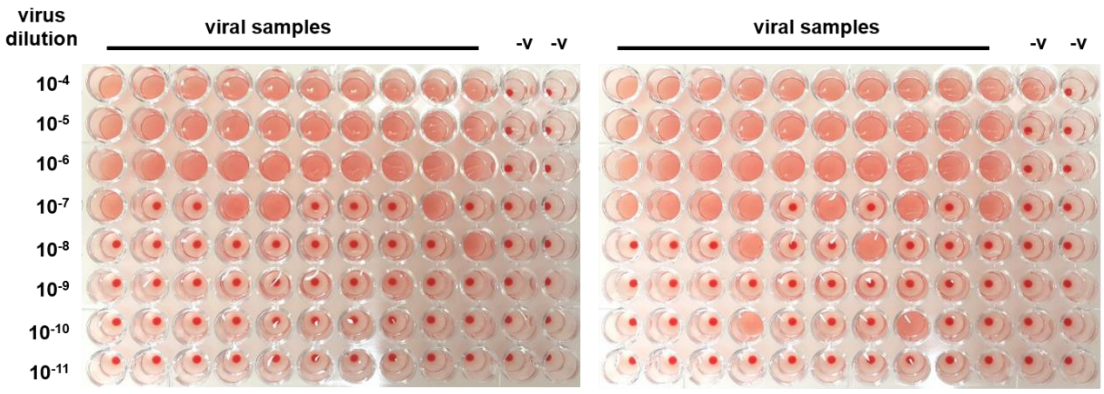

Figure 3.7. Representative plates for $TCID_{50}$ determination of A/California/09/2009 (H1N1)pdm09 stock using an HA readout. Wells with sunken t-RBCs at the bottom are negative for virus, while wells that have hemagglutinated t-RBCs are positive for virus. The highest dilution with complete hemagglutination in 10 wells in a single row was recorded as well as the number of hemagglutination positive wells after this row for $TCID_{50}$ determination. -v indicates cell only (MDCK) controls

We then used this stock of A/California/07/2009(H1N1)pdm09 (CA/09) for our *in vitro* microneutralization assay (**3.2.5**) and our *in vivo* mouse challenge experiment (Chapter 5).

3.2.4.2 Production and titration of influenza A pseudotypes

To correlate with binding activity data (**Figure 3.5**), nanobody-Fc functionality via *in vitro* neutralization assays against selected Group I influenza A strains was tested. Aside from CA/09, a pandemic H1N1 strain, A/Vietnam/1194/2004 (H5N1) (VN/04), a highly pathogenic avian influenza H5N1 virus, A/Korea/426/1968 (H2N2) (KR/68), an H2N2 virus that genetically diverged from the human H2N2 virus that caused the 1957 Asian pandemic, and A/Hong Kong/1073/1999 (H9N2) (HK/99), an H9N2 human influenza virus of avian origin, were also tested. While it is logistically easy to deal with low pathogenic strains of influenza, studies on strains that are uncommon and not widespread in the population such as VN/04, KR/68 and HK/99, are considerably hampered by availability of BSL facilities and highly trained and qualified people required for handling and processing these viruses.

The use of pseudotyped viruses presents a good alternative to live viruses for research. Viral pseudotypes or chimeric viral particles, are generated via the incorporation of surface glycoproteins from one virus (in this case, influenza) onto the core of another virus either by coinfection or cotransfection of specific genes inserted into plasmids [364]. Pseudotyping has been employed to great effect as a substitute for live viruses in influenza serological and neutralization assays [68, 364, 375, 376]. Perhaps the greatest advantage of using these viral pseudotypes is that they are safer than wild type and/or reassortant viruses as they undergo abortive replication and do not give rise to replication-competent progeny [311, 312].

As live influenza viruses KR/68, VN/04 and HK/99 were unavailable for use in *in vitro* neutralization assays due to BSL3/4 restrictions, lentiviral-based influenza virus pseudotyupes, consisting of a surrogate virus core, in this case HIV, that can integrate

into cells [312] were instead produced. We used the p8.91 gag-pol plasmid, a second generation vector derived from pCMVΔR9 [312], as the packaging construct, which contains the human cytomegalovirus (hCMV) immediate early promoter, which drives the expression of all viral proteins required in trans. This plasmid is defective for production of its own viral envelope and the accessory protein Vpu. The virus core is then surrounded by a lipid envelope with the hemagglutinin (HA), the major influenza glycoprotein on its surface. The HA envelope (sourced from Nigel Temperton of the Viral Pseudotype Unit, Medway School of Pharmacy) was supplied as a separate plasmid in trans. A plasmid encoding a firefly luciferase reporter gene was also supplied. The decrease in expression of luciferase in response to the presence of our nanobody-Fc constructs is then measured in influenza neutralization assays [364].

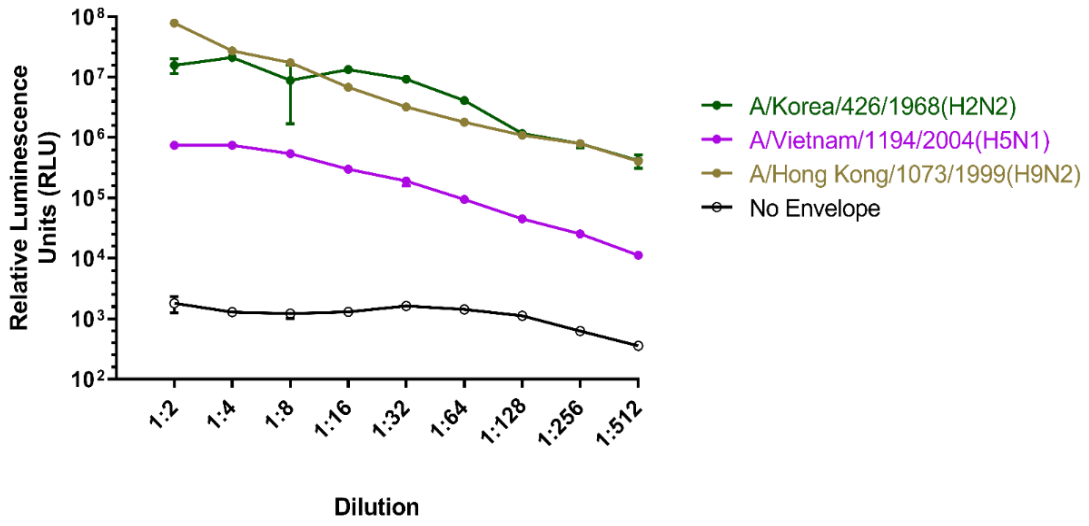

Figure 3.8. Titration of influenza virus pseudotypes. Pseudotyped lentiviral particles with HA envelopes of A(H2N2), A(H5N1), and A(H9N2), and firefly luciferase reporter genes, were titrated in HEK293T cells. Each point represents the mean and standard error of four replicates per dilution. Readout is expressed in relative luminescence units (RLU).

Plasmid DNA of p8.91, pHA (envelope) and pCSFLW (reporter) and co-transfected DNA from these three plasmids to 293T cells were first produced. Supernatant containing virus was harvested after 48 hours. Pseudotype titers were then obtained via subsequent infection of HEK293Tcells. After 48 hours of incubation,

to permit cell transduction and expression of firefly luciferase, cells were lysed in the presence of a luciferase substrate prior to assessing luciferase activity.

A dilution-dependent luciferase signal was observed for all pseudotypes that were produced and titrated, with the no envelope control showing very low background noise (**Figure 3.8**). The titers obtained (**Figure 3.8**) were comparable to those of Temperton, et. al for H5N1 pseudotypes with an HIV core [68], and are suitable for use in pseudotype neutralization assays employing nanobody-Fc as prescribed [68, 284]. The final titers obtained for the viral pseudotypes as expressed in RLU/mL were as follows: (i) 2.27 x 10^9 RLU/mL A/Korea/426/1968(H2N2) (KR/68), (ii) 8.49 x 10^7 RLU/mL A/Vietnam/1194/2004(H5N1) (VN/04), and (iii) 5.28 x 10^9 RLU/mL A/Hong Kong/1073/1999(H9N2) (HK/99).

3.2.5 Neutralization of representative influenza A subtypes by R1a-B6

The influenza microneutralization (MN) assay is highly sensitive and specific for detecting virus-specific neutralizing antibodies against influenza viruses [179]. Moreover, it is also an excellent test of antibody functionality *in vitro.* We performed the MN assay using a hemagglutination readout for live virus A/California/07/2009(H1N1)pdm09 (CA/09). It was attempted to produce a CA/09 pseudotype, but the viruses obtained had very low titers (data not shown) that would be insufficient for use in an MN assay. The pseudotype neutralization assay with luciferase readout was employed for the pseudotyped A/Korea/426/1968(H2N2) (KR/68), A/Vietnam/1194/2004(H5N1) (VN/04), and A/Hong Kong/1073/1999(H9N2) (HK/99) influenza strains.

Different ranges of nanobody concentrations that were serially diluted two-fold for neutralization against each influenza subtype were prepared. Against the live virus CA/09(H1N1), the starting dilution was 5 µM, and for the pseudotypes, 32 nM for KR/68(H2N2), 128 nM for VN/04(H5N1), and 4 nM for HK/99(H9N2). This variation is due to the differences in neutralization activity of the nanobodies against the specific

influenza subtype. As such, it was necessary to titrate out the nanobodies to see the definitive endpoints of complete (100%) and no (0%) neutralization activity.

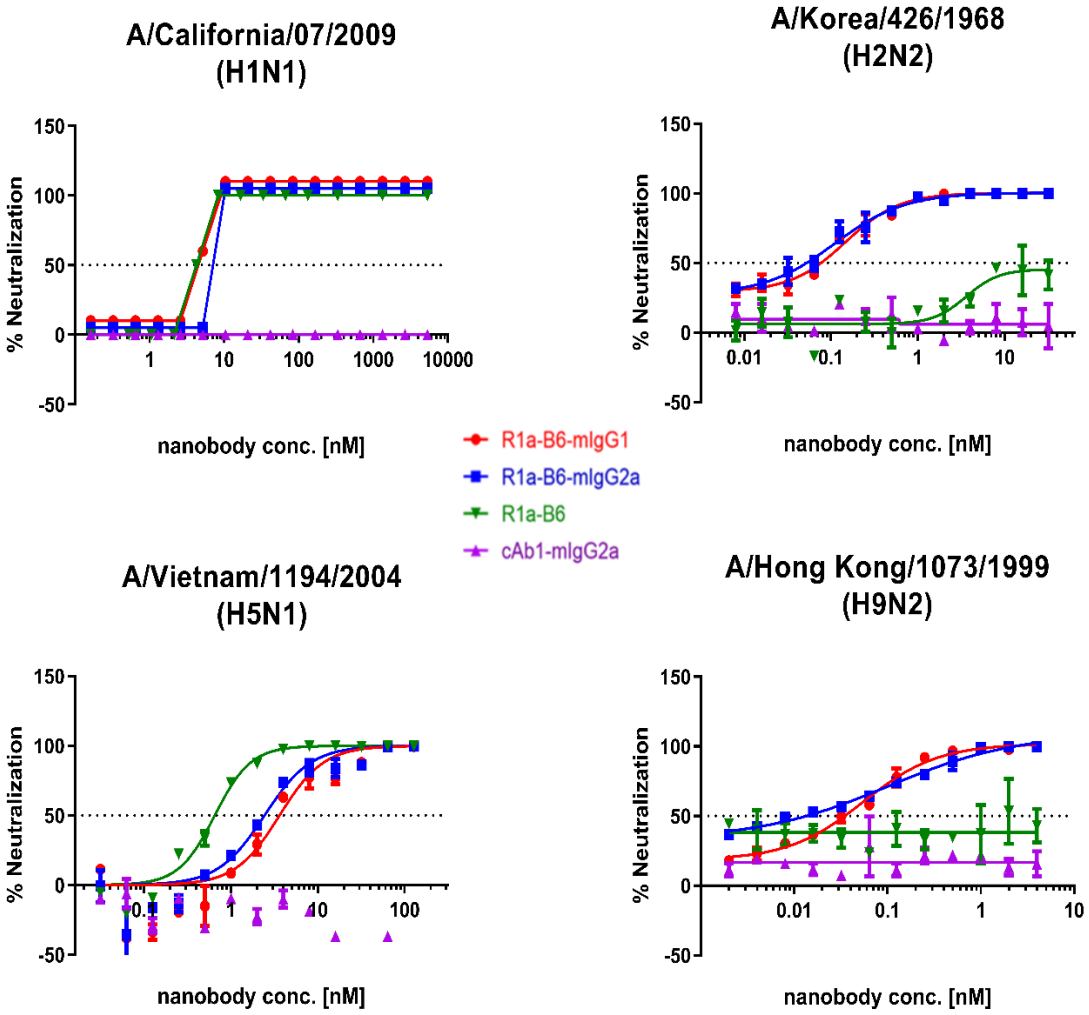

Figure 3.9. Neutralization of different influenza A strains *in vitro* by R1a-B6. Neutralization of live virus CA/09(H1N1) (10^3 $TCID_{50}$/mL) was measured via an influenza microneutralization assay HA readout. Neutralization of pseudotypes KR/68(H2N2), VN/04(H5N1) and HK/99(H9N2) A/Korea was measured by a luciferase reporter assay**.** Proteins are serially diluted two-fold from a starting concentration ranging from 128 nM to 1 pM for all pseudotypes. $1.0x10^6$ RLU of influenza pseudotype was then added to each well. For all plots, each point represents the mean and standard error of two replicates per dilution.

R1a-B6-mIgG was able to neutralize key Group I Influenza A subtypes, A(H1N1), A(H2N2), A(H5N1) and A(H9N2) *in vitro* while cAb1-mIgG2a showed no neutralization activity against any of the influenza A strains (**Figure 3.9**). Both R1a-B6-mIgG1 and R1a-B6-mIgG2a showed similar trends in neutralization of all influenza

subtypes. Monovalent R1a-B6 was able to neutralize H1N1 and H5N1 but was unable to neutralize H2N2 and H9N2 effectively (**Figure 3.9**), similar to previous reports [268]. Some neutralization activity can be seen for R1a-B6 against KR/68(H2N2) at very high concentrations (~10 nM); increasing the concentration further seems to have no effect on neutralization. There was an anomalous trend observed for R1a-B6 against HK/99(H9N2), with neutralization in the figure constant at around ~30-40% regardless of nanobody concentration (**Figure 3.9**). This experiment has been repeated several times with the same result. Experiments involving further dilution of R1a-B6 to get a baseline value against HK/99(H9N2) is recommended. As such neutralization against this subtype by R1a-B6 remains inconclusive.

Half-maximal inhibitory concentration (IC_{50}) of each nanobody construct against the viral strains tested via GraphPad Prism 8.1.2 was determined. Standard curves (**Figure 3.9**) were obtained by normalizing the RLU values against that of the pseudotype only controls corresponding to no neutralization and cell-only (no virus) controls corresponding to 100% neutralization. A non-linear regression (curve fit) analysis on the normalized data using a log [inhibitor] versus normalized response variable slope equation to compute for the IC_{50} values was then carried out.

Table 3.1. IC_{50} values of nanobody constructs against different influenza subtypes *in vitro*.

Influenza Virus Subtype	**IC_{50} (nM)**			
	R1a-B6-mIgG1	**R1a-B6-mIgG2a**	**R1a-B6**	**cAb1-mIgG2a**
*A/CA/09(H1N1)**	5.20 ± 0.01	7.99 ± 0.01	4.27 ± 0.01	-
A/KR/68(H2N2)	0.146 ± 0.040	0.110 ± 0.006	-	-
A/VN/04(H5N1)	3.621 ± 0.030	2.431 ± 0.014	0.650 ± 0.002	-
A/HK/99(H9N2)	0.027 ± 0.002	0.082 ± 0.001	-	-

* A/CA/09(H1N1) neutralization assay was carried out using a standard cell-based assay with hemagglutination readout and using live virus. All other assays were carried out using a Luciferase reporter assay and influenza pseudotype viruses (*n=3*). IC_{50} is half maximal inhibitory concentration. (-) indicates no neutralization activity.

IC_{50} values obtained for the nanobody-Fc fusions that were neutralizing in the luciferase pseudotype assay were in the picomolar range for KR/68(H2N2) and HK/99(H9N2) compared to the IC_{50} values obtained using the hemagglutination readout and live virus which was in the nanomolar range in the case of CA/09(H1N1) (**Table 3.1**). The IC_{50} values obtained for VN/04(H5N1) was in the same range as that of CA/09(H1N1). It is hypothesized that in a pseudotype virus, the HA glycoprotein is more readily available and present at lower densities on the viral surface as compared to the wild type virus, and that the neutralizing epitopes more accessible to the neutralizing nanobody-Fc due to the absence of the other major surface glycoprotein, NA [377, 378]. In comparison, the whole virus containing all its subunits, may present a more challenging route for attachment of neutralizing nanobodies. However, this may vary depending on the virus subtype and the mode of action of the neutralizing antibody. At present, this theory is still under investigation, but findings in this thesis adhere to the presented hypothesis.

Previously, it was demonstrated that bivalency increased the breadth of neutralizing activity of R1a-B6 enabling it to neutralize H2N2 (NIBRG-147) and increasing its potency against the more divergent strain H9N2 (NIBRG-91) [268]. Our findings here corroborate that evidence of monovalent R1a-B6 showing little to no neutralizing activity against A(H2N2) and A(H9N2). R1a-B6 exhibited strong neutralization activity against A(H1N1) and A(H5N1) (**Figure 3.9, Table 3.1**). Bivalent R1a-B6-mIgG1 and R1a-B6-mIgG2a showed comparable potency with each other and monovalent R1a-B6 against A(H1N1) and A(H5N1), and very good potency against A(H2N2) and A(H9N2), better than R1a-B6, for which IC_{50} values were unable to be obtained (**Table 3.1**). The nanobodies, being bivalent are also able to functionally interact with HA more easily, leading to robust neutralization activities against all representative Influenza A viruses tested here. On this basis, we can deduce that making R1a-B6 bivalent and appending an Fc region to it, have improved its neutralizing activity against A(H2N2) and the drifted A(H9N2) (**Figure 3.9, Table 3.1**).

The strong neutralizing activity observed for R1a-B6, in its' revised Fc format and original monovalent form demonstrates its functionality and utility against different subtypes of influenza *in vitro.*

3.3 Discussion

This chapter aimed at showing the therapeutic potential of R1a-B6 mouse Fc fusion nanobodies against influenza *in vitro* as a preliminary step before *in vivo* testing. R1a-B6 was improved by making it bivalent [268], increasing its half-life and introducing possible antibody-dependent effector functions by fusing the second and third constant domains (C_H2-C_H3) of a mouse IgG1 or IgG2a heavy chain to it. This resulted in a bivalent nanobody-Fc dimer that consisted of two 37.5 kDa subunits, as compared to the 15 kDa size of a monovalent nanobody (**Figures 3.1** and **3.4**). Because of their size, nanobodies delivered via passive transfer are rapidly cleared from circulation by free glomerular filtration in the kidney (molecular weight cut-off 66 kDa) [281]. Prolonging the nanobody's half-life will not only maintain the therapeutic threshold for a longer time but will also reduce the frequency of drug administration which will significantly benefit the patient [266, 281]. Expression of nanobody-Fc constructs in ExpiCHO™ cells, followed by Protein A chromatography and dialysis yielded relatively pure proteins with the anticipated molecular weights (**Figure 3.4**) that are still able to bind to CA/09 (**Figure 3.3**).

Purified R1a-B6-Fc fusion proteins were then shown to bind to a broad panel of whole influenza virus reference reagents (**Figure 3.5**) and neutralize key Group I Influenza A subtypes, A(H1N1), A(H2N2), A(H5N1) and A(H9N2) (**Figure 3.9** and **Table 3.1**). As reported previously [268], converting R1a-B6 into a bivalent format was shown to increase the breadth of neutralizing activity to include the more divergent influenza subtype A(H2N2) rather than increasing maximum levels of potency on A(H1N1) and A(H5N1). It was previously speculated that this is related to the mechanism of action of R1a-B6 which mediates its effect after the virus has already

attached to the cell surface and been internalized, as opposed to HA-head binding antibodies that usually inhibit viral attachment and entry [268]. It was suggested that internalization of the virus nanobody complex may be a rate limiting step in the potency of stem binding antibodies, so conversion to a bivalent format does not increase potency above a certain maximum threshold. As such, converting R1a-B6 from a monovalent to bivalent Fc fusion is seen to enhance potency for more divergent subtypes (i.e. A(H2N2) and A(H9N2)) with a lower affinity interaction, thereby extending the breadth of binding and neutralization of the nanobody [228]. Whereas for higher affinity interactions against A(H1N1) and A(H5N1), no further enhancement is seen as a maximum level of potency has already been reached.

Neutralization assays employing viral pseudotypes were carried out at BSL2 level and allowed a rapid, reliable, safe and easy assessment of the cross-neutralizing response of our nanobody-Fc fusions against influenza subtypes which are difficult to obtain and handle. Results were generated as digital readouts that are sensitive to picomolar quantities (**Figure 3.9** and **Table 3.1**). It was previously reported that neutralizing antibody titers against H5N1 determined by the pseudotype assay, strongly correlated with titers obtained via traditional HAI assays using horse erythrocytes and the MN for human, ferret and avian sera [68]. It was also found to be significantly more sensitive than the turkey erythrocyte HAI, the traditional method [179], for the detection of antibodies to H5 HA [68]. Comparing R1a-B6 IC_{50} values obtained against reverse genetics reassortants [268], results here show that neutralizing activity was ten-fold higher for H5N1, while there was no IC_{50} generated for H9N2 using the viral pseudotype. Hufton et. al used the reverse genetics reassortant of A/chicken/Hong Kong/G9/1997 (H9N2) (chick/HK/97(H9N2)) strain for their neutralization assay [268] whereas the human A/Hong Kong/1073/1999 (H9N2) (HK/99) pseudotype was employed here. Looking at the generated ELISA data, we can see that binding activity as shown by EC_{50} values was lower for chick/HK/97(H9N2) compared to that for HK/99(H9N2) for R1a-B6 (**Figure 3.5**), suggesting that

neutralization activity will probably be similar, with lower IC_{50} values being observed against chick/HK/97(H9N2) over HK/99(H9N2).

In humans, it was found that HA-specific ADCC mediating antibodies are induced by vaccination and/or infection with influenza virus [128, 372, 379]. It is also generally accepted that monoclonal anti-stem antibodies given via passive immunotherapy can induce ADCC *in vitro* and further require FcγR interaction for optimal *in vivo* protection suggesting ADCC activity may assist in protective immunity to influenza [246, 247, 380, 381]. In this study, R1a-B6 fused to mouse IgG1 which is ADCC negative, and to mouse IgG2a which is ADCC positive (**Figure 3.6**) were employed to test for FcγR interaction. An engineered effector cell line with luciferase reporter activity (FcγRIV ADCC Reporter Bioassay Promega) created for single assay thaw and use format to further reduce variability was utilized to test whether the nanobody-Fc fusion proteins are functionally capable of activating FcγR resulting in intracellular luciferase production. R1a-B6-mIgG2a was shown to be capable of activating ADCC. It was also revealed that there is no difference in the *in vitro* binding activity (**Figure 3.5**) and neutralizing activity (**Figure 3.9**) of R1a-B6-mIgG1 and R1a-B6-mIgG2a to various influenza A subtypes regardless of their Fc region (**Figure 3.5**). How these findings affect the *in vivo* prophylactic efficacy of R1a-B6 is presented in Chapter 5.

The ADCC assay employed here was used for convenience and economy and simply answers the question of whether the nanobody-Fc can engage effector functions. It must be pointed out that this assay does not directly measure antibody-mediated killing of influenza-infected target cells, as do all surrogate assays and results must be interpreted with caution [382]. If the nanobody-Fc fusions can actually engage effector cells *in vitro* and *in vivo* to protect against influenza can not be satisfactorily answered by this assay. However, it is a starting point for ADCC studies that may improve the potency and efficiency of the final therapeutic product.

The efficient production and characterization of reformatted R1a-B6 fused to a mouse Fc region was shown here. R1a-B6 appended with a mouse IgG2a Fc was capable of activating ADCC *in vitro*, in contrast to R1a-B6-mIgG1 and cAb1-mIgG2a. Most importantly, R1a-B6-Fc retains and improves on monovalent R1a-B6's binding and cross-subtype neutralizing activity against different influenza A group I subtypes *in vitro*. The findings in this chapter show that the potent *in vitro* characteristics of R1a-B6 make it a promising candidate for immunotherapy against influenza *in vivo.*

CHAPTER 4

PRODUCTION, PURIFICATION, AND TITRATION OF AAV ENCODING NANOBODY-FC FUSIONS AGAINST INFLUENZA

4.1 Overview

Passive immunotherapy using monoclonal antibodies (mAbs) with broad cross-subtype neutralizing activity against influenza has stimulated much interest in recent years with several mAbs currently in clinical development [192, 201, 209, 210, 238]. Broadly neutralizing antibodies (bnAb) are very rare in infected humans as stem reactive memory B cells normally exist at very low frequencies and are only boosted in the context of exposure to a very different HA protein, and immune response to vaccines is almost always strain specific [168]. Nonetheless bnAbs have been isolated from humans infected with influenza [210, 245] as well as from influenza vaccinees [122, 208, 241, 242, 383] in the past. It was also found that under certain conditions, they can make up a major part of the immune response, as exemplified by the response after being vaccinated/infected by A(H1N1)pdm09 [241, 245].

People who have a more diverse history of influenza infection have higher titers of broadly neutralizing antibodies, suggesting that prior encounters with diverse influenza virus strains greatly impact the kind of antibodies that can be generated [384]. These rare antibodies usually bind to conserved epitopes such as those in the hemagglutinin (HA) stem, thereby providing strain independent protection. However, for passive immunotherapy to provide sufficient long-term protection, frequent repeated injections are required which would be prohibitively expensive in low resource areas with no public health infrastructure. A more practical and cost-effective strategy would be to use antibody gene therapy. With a single administration, gene immunotherapy may potentially provide long term sustainable protection through antibody production in situ, within the patient.

Viruses are highly evolved natural gene vectors that have emerged as efficient delivery vehicles for therapeutic genes in clinical gene therapy [307]. Recombinant Adeno-Associated virus (rAAV) vectors have been modified to improve safety and are able to provide long term stable transgene expression in different animal cells [319, 320, 334, 385]. AAV-mediated delivery of broadly neutralizing human monoclonal antibodies against the HA stem has already been proposed as a possible approach to protect from influenza [354, 355, 357]. Despite these findings, significant challenges remain for the successful development of vectored immunoprophylaxis for influenza. The use of AAV is still hampered by limitations to the size and complexity of antibody transgenes that it can express [386]. This is a challenge for antibody gene therapy given that mAbs are large complex glycoproteins comprising four separate chains. As such, smaller, simpler binding molecules expressed from a single open reading frame would be a significant advantage [320, 323].

In this study, single domain antibodies as an alternative to conventional mAbs for gene therapy delivery via AAV against influenza were employed. This is distinct to previous studies that have tried the same approach in that intramuscular delivery of an alpaca-derived cross-neutralizing nanobody instead of AAV9 intranasal delivery [355, 357, 387] was utilized. Direct intramuscular injection of AAV8 allows for a simple method for crossing the blood vessel barrier to attain systemic gene transfer in muscle tissue [388, 389]. Muscle then becomes a biofactory for expressing antibodies against influenza. This strategy has previously been shown to be effective in mice against HIV [353] and influenza [354].

Additionally, immune response following AAV administration poses a significant barrier to gene transfer in humans [336, 390]. Neutralizing antibodies to AAV2 are prevalent worldwide [337] and this is problematic because AAV2 is the most widely characterized and used rAAV vector [365, 391, 392]. This limitation can be overcome by using different serotypes such as AAV8 or AAV9. However, in the case of AAV9, low levels of protein expression and genome copy numbers of AAV2/9 has

been detected in the brain and testes after systemic injection in mice [329]. This is an important safety issue for future clinical investigation of this serotype as it could possibly alter germline genes [329]. As such, it was decided to instead use AAV8 capsid in this study. The use of AAV8 for efficient gene therapy in muscle, heart and liver has been well documented [334, 389, 393]. And here, the choice of muscle specific delivery and AAV2/8 as vector serotype is expected to provide higher level, more sustainable transgene expression over a longer period of time, in comparison to AAV2/9 mediated intranasal delivery which has been shown to decrease in macaques after 3-4 months [336, 338, 355].

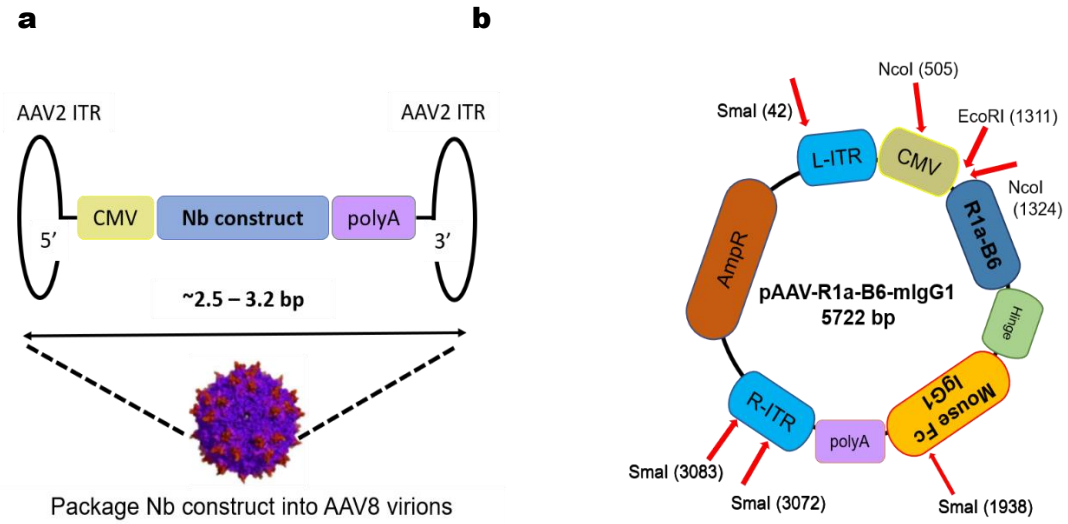

Figure 4.1. AAV construct design to test protective effect of recombinant anti-flu neutralizing nanobody R1a-B6 against influenza by AAV vector delivery. (**a**) Nanobody constructs were cloned into an AAV expression system with AAV2 inverted terminal repeats (ITR) under a CMV promoter and a polyA region for protein expression. Transgenes are then packaged into AAV virions with an AAV8 capsid. (**b**) Representative map of AAV plasmid containing important elements, the left (L) and right (R) ITRs, CMV promoter, transgene (R1a-B6-hinge-mouse Fc IgG), and restriction sites for *NcoI, EcoRI* and *SmaI* used for diagnostic digestion. Plasmid map not drawn to scale.

The nanobody constructs (**Figure 3.1**) (i) R1a-B6 mouse Fc IgG1, (ii) R1a-B6 mouse Fc IgG2a, (iii) R1a-B6 and (iv) cAb1-mouse IgG2a were previously cloned by Dr. Kam Zaki into an AAV2-based transfer vector plasmid containing two 145 bp inverted terminal repeats (ITR) (pAAV) (**Figure 4.1**). Expression of transgenes is

under the control of a CMV promoter with a β-globin intron and leader sequence preceding the coding sequence and a bovine growth hormone polyadenylation signal (bGH polyA) following it (**Figure 4.1**).

These constructs were then used to produce recombinant AAV viruses for influenza immunoprophylaxis via the triple transfection method [365] (**Figure 4.2**). In this method, three plasmids are utilized for transfection: an AAV helper plasmid, the ITR transgene cassette (pITR), and the plasmid containing *rep* and *cap* that lack ITRs to circumvent packaging of the wild type genome. AAV containing the transgenes are then packaged into pre-formed empty capsids within the nucleus of producer cells (**Figure 4.2**).

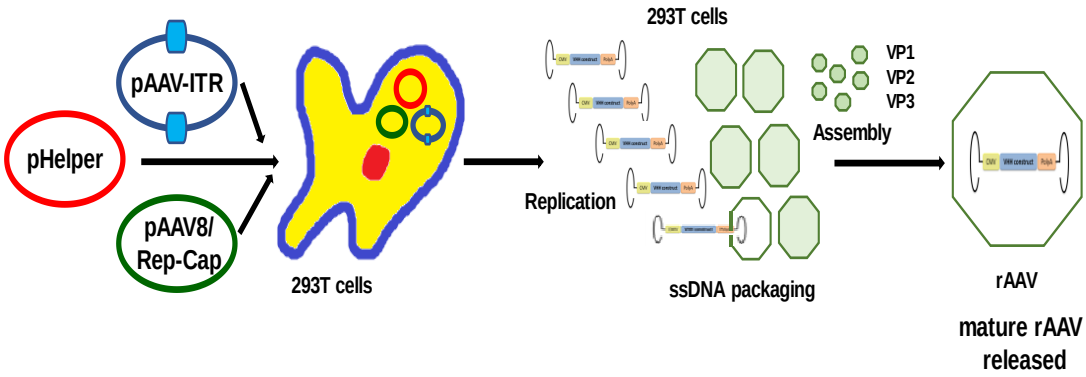

Figure 4.2. Schematic diagram of the triple transfection method to produce rAAV. rAAV is produced by transfection of three plasmids: transgene plasmid (pITR) containing the nanobody Fc fusion construct, the pHelper plasmid (adenoviral proteins E2a and E4orf6 [394]) and pAAV2/8/Rep-Cap (pLT2-AAV8 codes for serotype 2 Rep78 and serotype 8 VP1, VP2 and VP3 capsid proteins) in adherent 293T cells. Newly synthesized DNA in ssDNA format is incorporated into pre-formed capsids and the infectious AAV particles are released from producer cells.

Crucially, after high yield production, AAV vectors must be purified to support downstream therapeutic and/or clinical applications. Popular methods of purification include gradient centrifugation using iodixanol or cesium chloride [365], ion exchange chromatography, receptor-specific affinity purification, traditional affinity chromatography, and gel filtration [325]. Following purification, AAVs containing the desired transgenes were then characterized for genome titer and integrity, before *in*

vivo studies were conducted. AAV vectors can be characterized as follows: a) physical presence of genomes in viral particles via dot-blot assay and quantitative real-time polymerase chain reaction (qPCR), b) infectivity of the viral particles using an infectious center assay, c) ability to transduce an infected cell via a transduction assay, c) physical observation of the viral particles as a population using electron microscopy, d) physical characterization of the size and integrity of genomes using alkaline gel electrophoresis, and e) physical characterization of amount of viral capsids using ELISA or SDS-PAGE [332, 365, 395]. A combination of two or more characterization methods is enough for accurate assessment of AAV titer prior to further studies.

In this chapter, the following objectives were accomplished:

(i) production and purification of high titer AAV viruses expressing R1a-B6-mouse-Fc fusion transgenes and negative control nanobody for *in vivo* gene therapy

(ii) characterization of AAV in terms of number of capsid particles, genome size, and gene copy numbers.

4.2 Results

4.2.1 Production of AAV of high titer and purity

AAV vector plasmid DNA containing the gene of interest that is pure, high-yield, and endotoxin-free was first produced as these will be used in downstream applications involving mice. Nanobody constructs (**Figure 3.1**) with the following sizes: (i) R1a-B6-mIgG1, 1110 bp, (ii) R1a-B6-mIgG2a, 1128 bp, (iii) R1a-B6, 504 bp, and (iv) cAb1-mIgG2a, 1170 bp, were previously cloned into an AAV vector (**Figure 4.1**). All AAV vector plasmids containing nanobody transgenes are approximately 5.8 kb in size, with the AAV-R1a-B6 plasmid being slightly smaller at 5.1 kb as the transgene does not include a mouse Fc region.

After scale-up production in *E. coli* (500 mL - 1 L cultures), plasmid DNA was extracted via an endotoxin-free preparation. DNA concentrations obtained were in the

range of 2-5 µg/µL for all AAV constructs. Diagnostic digestion was performed using *NcoI* that cuts within the CMV promoter and the multiple cloning site preceding the transgene for all constructs (**Figure 4.1**). Results showed that the digested DNA bands had sizes consistent with theoretical fragment sizes (**Figure 4.3**). DNA extracts were sequence-verified against R1a-B6 sequences by Hufton et. al (unpublished), and all samples adhered to expected sequence profiles.

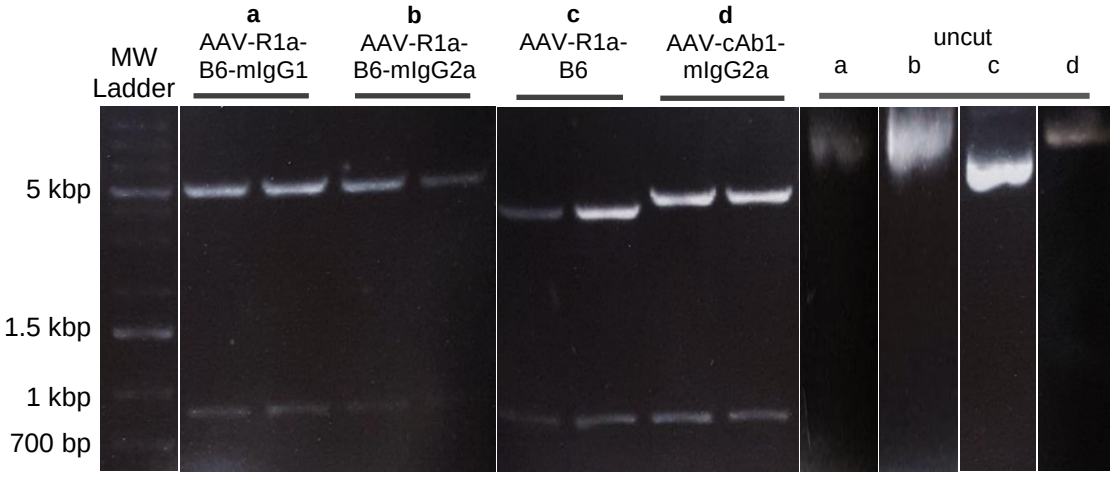

Figure 4.3. Restriction enzyme (RE) digestion using *NcoI* of AAV constructs from DNA plasmid preparations. For all constructs digested with *NcoI*, bands at ~819 bp and another band at ~4900 bp for AAV-R1a-B6-mIgG1, AAV-R1a-B6-mIgG2a, and AAV-cAb1-mIgG2a, and ~4300 bp for AAV-R1a-B6 were observed.

After sizes of AAV plasmid DNA were confirmed, AAV plasmid DNA integrity was then checked. AAV vectors are designed to consist of an appropriately sized expression cassette flanked by ITRs, the origin of replication and primer for second-strand synthesis by DNA polymerase [319, 325]. During bacterial transformation in *E. coli*, these ITRs become unstable and are prone to deletion [325]. Before transfection into host cells it is necessary to check for ITR integrity with an enzyme such as *SmaI* which cuts within unstable portions of the ITR. The sizes of the resulting fragments are then determined via gel electrophoresis.

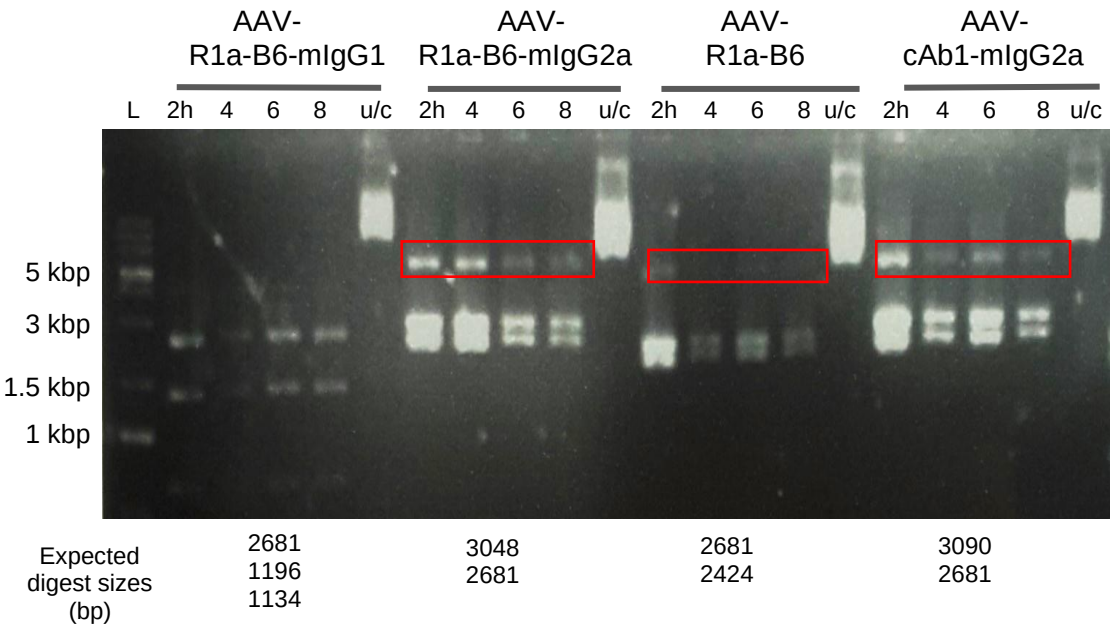

Figure 4.4. *SmaI* digest of AAV plasmid constructs. Aliquots were taken after 2, 4, 6 and 8 hours (h) to monitor progress of digestion. Bands in red boxes indicate unexpected bands from the RE digest. U/C stands for uncut plasmids, L for the molecular weight ladder.

Expected band sizes after *SmaI* digestion were observed for all AAV constructs (**Figure 4.4**). However, bands corresponding to about 5000 bp (indicated by red boxes) can also be seen for all constructs except for AAV-R1a-B6-mIgG1. These bands most probably represent a population that contains small deletions in the ITR region in this plasmid preparation. It has been reported that this is a frequent occurrence and even the best plasmid preparations contain about 5–15% of DNA containing small deletions in the ITR [325]. The problems that this will pose for further downstream applications are not deemed to be significant [325]. Results of the *SmaI* digest suggest that majority of the population for each plasmid preparation have intact ITRs (**Figure 4.4**).

AAV was then produced via triple transfection in adherent HEK293T cells. Harvesting the virus involves lysing cells via three freeze/thaw cycles to fully release AAV. Digestion with benzonase was then carried out to degrade all nucleic acid impurities, both DNA and RNA that have not been packaged into virions. Purification

was then carried out using a discontinuous iodixanol gradient. Affinity chromatography can also be done, and is a popular choice [314]. However, a major disadvantage of affinity chromatography is the indiscriminate purification of both empty and vector-containing AAV particles in the virus preparation [332]. The presence of empty particles contributes to the antigenicity of the viral prep and is deemed problematic for gene therapy applications. The iodixanol gradient can separate out contaminants from an impure AAV preparation owing to differences in apparent density of macromolecules in iodixanol solutions. An iodixanol gradient consisting of 15% (v/v), 25% (v/v), 40% (v/v) and 60% (v/v) iodixanol solutions and phenol red to distinguish each gradient were prepared for this purpose. The 15% (v/v) iodixanol band contains 1M NaCl to destabilize ionic interactions between macromolecules [365]. The 25% (v/v) and 40% (v/v) bands are used to separate contaminants with lower densities, including empty capsids, from full capsids. Around 80% of the AAV can be recovered between the 40% (v/v) and 60% (v/v) fractions [392]. And as such, the 60% (v/v) band served as a cushion for genome-containing virions. Typically, 5-8 mL of AAV fluid was recovered per cell factory.

The recovered AAV viruses underwent buffer exchange using Vivaspin20®, which employs a semi-permeable vertical membrane that separates the virus from low molecular-weight compounds and salts that might have contaminated the preparation after iodixanol gradient purification. Unlike dialysis, which relies on passive diffusion, this diafiltration step forces substances and water through the membrane by centrifugation, purifying and concentrating the AAV virus in one step. From the ~8 mL fluid post-iodixanol gradient purification, the volume of the AAV virus is reduced to around 1 mL. Purified AAV virus containing the transgenes were then characterized and titered prior to *in vivo* use.

4.2.2 Visualization of AAV capsid protein content for absolute quantification of viral particles

The presence of intact and abundant capsids is required for AAV containing the gene of interest to proliferate in host cells. A highly-purified virus preparation should result in an SDS PAGE gel with only VP1, VP2, and VP3 capsid proteins visible, with VP3, the most abundant capsid protein, quantified to determine capsid titers [327].

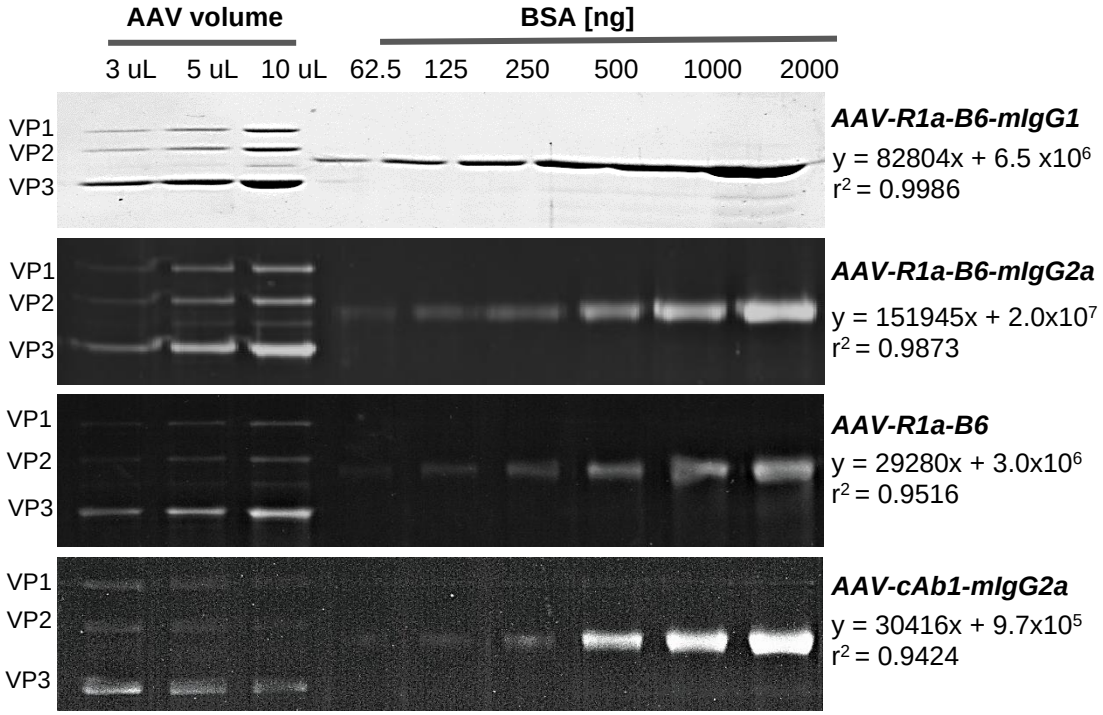

Figure 4.5. **Visualization of capsid proteins and quantification of viral particle titers in Sypro® Ruby Protein Gel-stained SDS PAGE gels.** The indicated volume of AAV particles was separated on a 12 % (v/v) reducing SDS–polyacrylamide gel. Positions of the viral capsid proteins, VP1 (87 kDa), VP2 (72 kDa), and VP3 (61 kDa) and BSA standards (66 kDa) are indicated. The linear equation of the BSA standard curve for each gel is shown on the right. Regression analysis demonstrated the linearity of the band intensities over the entire range of BSA masses.

Bovine serum albumin (BSA) was employed as reference material in the standard curve analysis for absolute AAV particle titer determination. To obtain the amount of VP3 present in each AAV sample, a standard curve was generated by plotting the amount of BSA in nanograms (ng) against the background-corrected luminescence intensity of the BSA band. Regression analyses yielded an equation of the line that allowed the calculation of the mass of VP3 for each AAV construct. Assuming that there is an estimated 50 VP3 molecules per capsid [327], Kohlbrenner et. al calculated that each viral particle contains 4.987×10^{-9} ng of VP3 for AAV2 [396].

AAV8 shares ~84% amino acid sequence homology to AAV2 [397, 398], and thus the same mass for our approximations was employed. To estimate the number of viral particles present in the gel, the mass of VP3 (in ng) generated from the standard curve was divided by the mass in ng of VP3 per viral particle (4.987×10^{-9} ng). Finally, to calculate the viral titer in particles per mL, the viral particle number was divided by the volume of virus loaded onto the gel.

No other prominent bands for all viruses tested aside from the three main capsid proteins, VP1, VP2, and VP3 (**Figure 4.5**) was observed in the gel. VP1, VP2, and VP3 also appeared in the expected 1:1:10 ratio as per band intensity analyses. Based on the BSA standard curves generated, the viral titer for each AAV construct is as follows: (i) 1.50×10^{13} AAV-R1a-B6-mIgG1 particles/mL; (ii) 8.85×10^{12} AAV-R1a-B6-mIgG2a particles/mL; (iii) 6.65×10^{12} AAV-R1a-B6 particles/mL, and (iv) 2.42×10^{12} AAV-cAb1-mIgG2a particles/mL.

4.2.3 Physical characterization of the size and integrity of genomes

Viral genomes were extracted from virions and analyzed using alkaline gel electrophoresis under denaturing conditions to determine if genomes were intact and pure [365]. The assay which is carried out in alkaline conditions (~pH 12.7) enables denaturation of double-stranded DNA. As a result, DNA is maintained in a conformation where secondary structures are disrupted. Hence, migration through the alkaline gel is solely based on size.

Bands of the following sizes were obtained: (i) ~3.1 kb AAV-R1a-B6-mIgG1; (ii) ~3.1 kb AAV-R1a-B6-mIgG2a; (iii) ~2.5 kb AAV-R1a-B6, and (iv) ~3.2 kb AAV-cAb1-mIgG2a (**Figure 4.6**). These bands represent the transgene cassette flanked by left and right ITRs (**Figure 4.1a**) and are the expected full sizes of the packaged genomes if they were intact. Unexpected bands that are approximately 5 kb in size also appear for all virus samples (**Figure 4.6**). As these stocks were digested extensively with benzonase, these bands represent encapsidated genomes that are bigger than the

full-sized product. Single-stranded AAV with genomes smaller than 4.7 kb, which is the case here (~3.1 – 2.5 kp), can load more DNA into the capsid until it is no longer energetically favorable for Rep to do so [323]. It has also been observed that in some cases a dimer-sized vector genome band can be present when the vector genome size is less than half the size of wild-type AAV (<2.5 kb) [399]. Nevertheless, bands of the correct size were present at much higher densities than the unexpected bands.

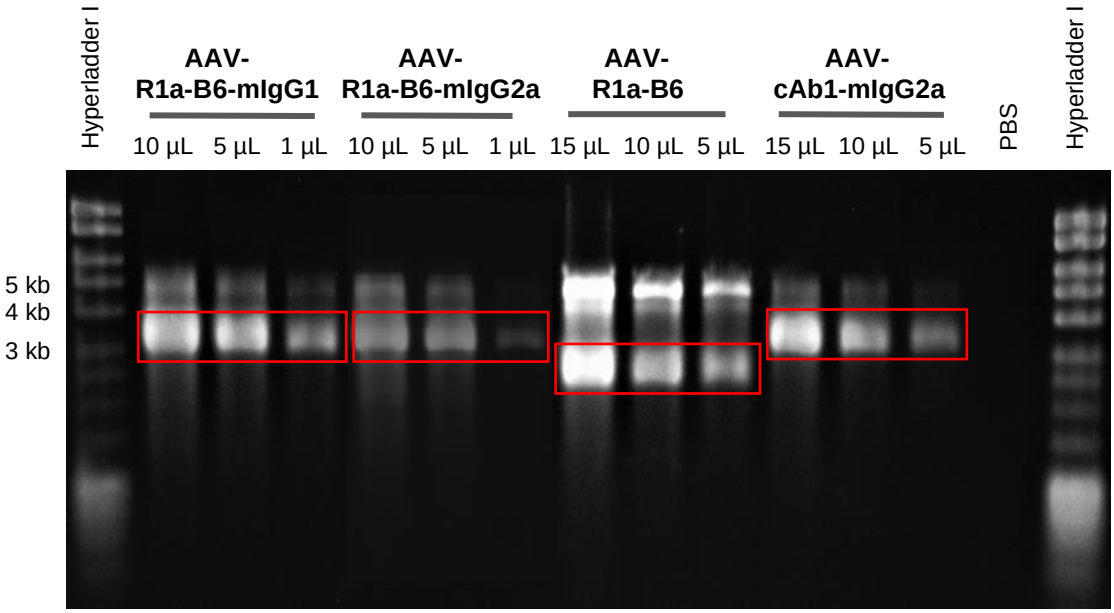

Figure 4.6. Characterization of genome size and viral integrity by alkaline gel electrophoresis. The indicated volume of AAV samples was separated on a 0.8% (w/v) alkaline agarose gel. The first 8 bands of the Hyperladder I (Bioline) was used for standard curve quantitation with the 10 kb band corresponding to 100 ng, 8 kb band to 80 ng, 6 kb band to 60 ng, 5 kb band to 50 ng, 4 kb band to 40 ng, 3 kb to 30ng, 2.5 kb to 25ng, and 2 kb to 20ng. PBS was used as a negative control. Bands enclosed in red boxes indicate full-size viral genomes.

Viral titers obtained via alkaline gel electrophoresis were expressed in terms of viral genomes per mL (vg/mL). To obtain viral genomes per mL present in each AAV sample, a standard curve was generated by plotting the amount of DNA present in the Hyperladder I bands in nanograms (ng) against the background-corrected net pixel density of the band. Regression analyses yielded an equation of the line that allowed the calculation of the mass of DNA present for each AAV construct. This mass was then divided by the theoretical weight of the AAV construct and the volume of AAV

sample used to determine the titer based on viral genomes per mL. The viral titer for each AAV construct is as follows: (i) 1.24 x 10^{13} AAV-R1a-B6-mIgG1 vg/mL; (ii) 3.89 x 10^{12} AAV-R1a-B6-mIgG2a vg/mL; (iii) 6.96 x 10^{12} AAV-R1a-B6 vg/mL, and (iv) 5.78 x 10^{12} AAV-cAb1-mIgG2a vg/mL.

4.2.4 AAV Vector Genome Quantification via qPCR

A general qPCR protocol was employed that allows the genome titer determination of vectors independent of transgene by using primers that anneal within the cytomegalovirus (CMV) promoter [366, 400, 401]. A 129 bp fragment of the CMV promoter was amplified to obtain viral titers expressed in terms of copies or viral genomes per mL (vg/mL). The quantitative PCR assay was validated by generating standard calibration curves for CMV PCR products (**Figure 4.7**). Standard curves were prepared for each construct by first linearizing the AAV plasmid with *EcoRI*. The mass of 1 copy of the AAV plasmid was then calculated by multiplying the size of the plasmid (in bp) to the mass of one DNA base pair (1.09 x 10^{-21} g). This amount was then multiplied with 10^9, to obtain the mass of DNA that should be present in 1 µL of 10^9 copies of plasmid. This amount is the final concentration of our 10^9 copies standard solution. This amount was then divided with the initial concentration of the linearized plasmid, with the resulting amount multiplied by 100 to obtain the volume of linearized plasmid needed to prepare 100 µL of the standard at 10^9 copies. A ten-fold serial dilution was then made from 10^9 to 10^3 copies to generate a set of standards for quantification.

All AAV samples were diluted 1:10, 1:100, 1:1000, and 1:10000 in nuclease-free water. Linear regression analysis was then performed using CMV copies of standards versus Ct. From the equation of the line generated (**Figure 4.7**), copy number of samples based on their Ct was estimated. qPCR analysis of CMV amplification of AAV standards revealed a linearity correlation coefficient (R^2) of ~0.99 for all samples (**Figure 4.7**). Difference in Ct values within duplicates was <0.5 Ct for

both standards and samples. For all AAV samples, initial CMV copies of 1.00 x 10^9 were detected at around cycle 10 (**Figure 4.7**). The negative control, PBS, had Ct values > 32 Ct showing very low background amplification. Regression analysis demonstrated linearity over the entire range of copies for CMV for all AAV-nanobody constructs.

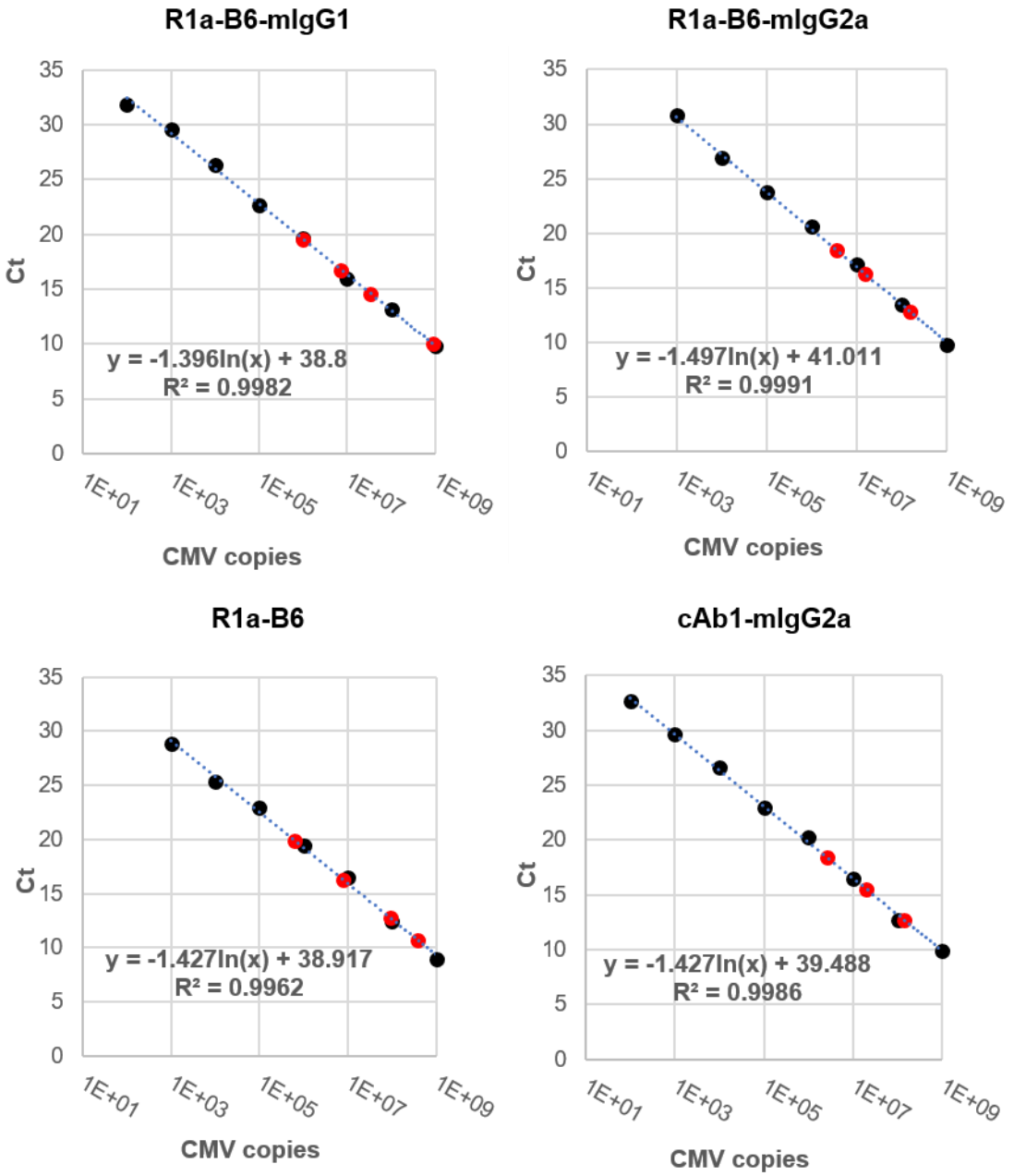

Figure 4.7. Determination of AAV genome copy number via CMV standard curve qPCR linear regression analysis. CMV copies were plotted against the Threshold Cycle (Ct). Black dots represent standards (linearized AAV plasmid DNA) and red dots represent AAV-nanobody viruses at different dilutions. Equation of the line and R^2 values are also indicated. All qPCR measurements were done in triplicate.

Based on CMV amplification via qPCR, the viral titer for each AAV construct is as follows: (i) 8.69 x 10^{12} AAV-R1a-B6-mIgG1 vg/mL; (ii) 1.45 x 10^{13} AAV-R1a-B6-mIgG2a vg/mL; (iii) 6.87 x 10^{12} AAV-R1a-B6 vg/mL, and (iv) 1.66 x 10^{13} AAV-cAb1-mIgG2a vg/mL.

4.2.5 Summary of AAV vector titers

AAV vector titers obtained using three different methods per construct were tabulated and statistical tests were employed to assess differences among quantification methods. At a significance level (α) of 0.05, a value of $p \leq \alpha$ indicates a significant difference. Based on two-way analysis of variance (ANOVA) ($\alpha = 0.05$), it can be concluded that the titers obtained employing different methods are significantly different per construct *(p=0.0258).* This finding is expected as titers will vary based on the construct and not on the methods used to quantify them. This is further corroborated by findings via 2-way ANOVA that there is no significant difference in the means of the titers regardless of method used to obtain them *(p=0.0854).* Given this, what can be looked at is how titers vary per quantification method within the constructs. To accomplish this, a post hoc multiple comparison Tukey test at 95% Confidence Interval (α=0.05) was performed.

Results showed that there was no significant difference in the titers obtained using all three methods for AAV-R1a-B6-mIgG1 and AAV-R1a-B6 (**Figure 4.8**). For AAV-R1a-B6-mIgG2a, there is a significant difference between the genome titers (vg/mL) obtained from alkaline gel electrophoresis and qPCR of the CMV gene fragment (**p = 0.0054*) (**Figure 4.8**). For AAV-cAb1-mIgG2a, there is a significant difference between the capsid particles and vector genomes based on CMV analysis *(**p=0.0375),* and genome titers (vg/mL) obtained from alkaline gel electrophoresis and qPCR of the CMV gene fragment (****p = 0.0405*) (**Figure 4.8**). For all constructs, there was no significant difference between titers obtained via quantification of capsid particles and alkaline gel electrophoresis. The titers we produced show high

correlation with each other and appear to be sufficient for *in vivo* experiments (**Figure 4.8**) based on previous studies using the same AAV serotype [353, 354].

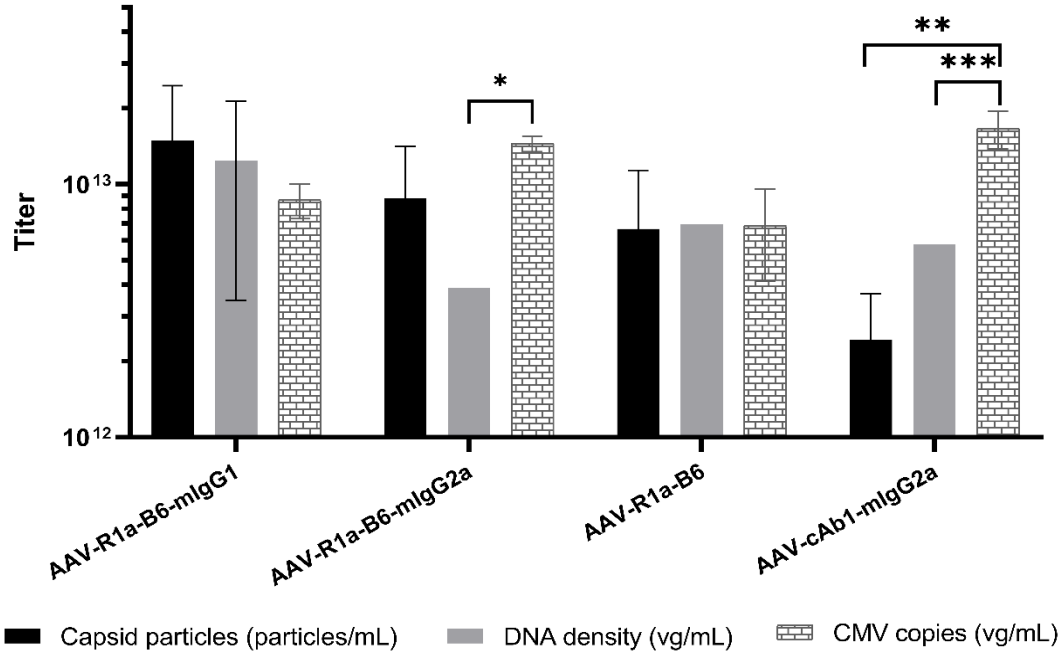

Figure 4.8. Summary of vector titers obtained via different AAV vector characterization techniques. Capsid particles were obtained via SDS-PAGE and genome titers via alkaline gel electrophoresis and qPCR. Significant differences between titers obtained for each group via Tukey test are shown via brackets *(*p=0.0054, **p=0.0375, ***p=0.0405).* Error bars show mean and standard error of three replicates.

4.3 Discussion

The strategy presented here to protect mice against influenza using cross-neutralizing nanobody-Fc fusions requires a vector that would provide robust long-term transgene expression in systemic circulation without substantial toxicity. Of all currently available viral vectors, AAV is unique because of its safety profile and broad tissue tropism. Unlike recombinant adenoviral vectors which yield high initial gene expression that diminishes rapidly due to immune clearance, AAV vector-based gene expression is persistent [393].

Muscle has been targeted in gene therapy not only for correction of muscle diseases, but also as a biofactory to produce and secrete therapeutic proteins into the

bloodstream for treatment of diseases in trans in distant organs [388, 393]. This is true in the case of Glybera, the first approved AAV gene therapy treatment designed to reverse lipoprotein lipase deficiency [340]. For this purpose, an AAV2 ITR plasmid pseudotyped with an AAV8 capsid was chosen to be delivered intramuscularly. It has been shown that AAV8 can efficiently cross the blood vessel barrier to attain systemic gene transfer in a variety of organs including muscle [388, 389], and can transduce tissues more ubiquitously compared to other AAV serotypes [329, 393]. The low turnover rate of muscle cells should, in principle, mean that the AAV transgenes can be maintained for much longer [388, 389]. This delivery method is also simpler to implement in resource poor settings alongside other immunizations. The choice of localized muscle delivery and AAV8 as vector serotype is expected to provide higher level, more sustainable transgene expression over a longer time.

In this chapter, AAV of high titer, around 10^{13} vector genomes per milliliter, was produced using the triple transfection method. Purification is via iodixanol gradient followed by diafiltration involving buffer exchange, concentration and desalting. Iodixanol gradients allow a fast, simple, non-toxic, and reproducible rAAV purification protocol that yielded AAV virus stocks of high titer and purity. It can be estimated that our AAV preparations with a titer of ~$1x10^{13}$ vg/mL per construct are sufficient for intramuscular delivery of 50 µL of $1x10^{11}$ vg AAV into 100 mice for *in vivo* experiments.

Establishing viral titers is crucial for *in vivo* use. With the time and resources available, it was decided to characterize the virus according to its physical properties. Results show a high purity virus preparation with only VP1, VP2, and VP3 capsid proteins visible in an SDS gel (**Figure 4.5**). Encapsidated particles were also in the range of 10^{13}-10^{12} particles/mL for all four constructs, indicating similar packaging efficiency. The genome size of AAV vector stocks analyzed by alkaline gel electrophoresis gives a number of how much vector genomes are encapsidated. It is desirable that purified viruses have virions containing the full-size genome, however, irregular-sized genomes can sometimes contaminate viral preparation as was

observed (**Figure 4.6**). However, it is argued that densities of the bands containing the correct packaged vector genomes are much higher than those of the packaged irregular-sized genomes. It is unlikely that this will have a substantial effect on titers obtained using this method.

Viral titers by determining genome copies of encapsidated genome products via qPCR were also obtained. This is the most widely accepted method for determining dosage of AAV products for *in vivo* testing [325, 365, 395]. This is also particularly useful when rAAV vectors have difficulty in infecting cell lines *in vitro,* leading to an inexact infectious titer [324, 365]. In this case, the vector genome titer and the infectious titer ratio can be extremely high, as there are a lot of vectors detected but infection is low, giving an unclear picture of AAV yield from manufacturing.

All in all, viruses were successfully produced with satisfactory titers (**Figure 4.8**). For each AAV construct, number of capsid particles per mL and vector genomes per mL were in the range of 10^{12} to 10^{13}. Titers obtained via qPCR were slightly higher than that obtained using capsid quantification and alkaline gel electrophoresis. This may be attributed to the sensitivity of the method used, as qPCR relies on real-time gene quantification, while the other two methods use pixel densitometry and manual assignment of areas on the gel to be quantified. Nonetheless, a combination of the above characterization and titration procedures with their own advantages and disadvantages have given us confidence in our estimation of AAV viral titers for *in vivo* use. For future experiments, we will employ the titers obtained from qPCR of the CMV gene fragment.

In summary, the adaptable production, purification, and characterization methods described here can be used for production of high-purity and high-titer AAV vectors suitable for preclinical testing in an animal model of disease.

CHAPTER 5

PROTECTION OF MICE AGAINST INFLUENZA BY AAV-MEDIATED DELIVERY OF R1a-B6

5.1 Overview

The work presented in this chapter was aimed towards generation of broadly protective humoral immunity independent of the natural or vaccine induced immune response against influenza in mice. This was achieved via a single intramuscular injection of AAV encoding R1a-B6-Fc, a cross-neutralizing, HA stem-binding nanobody fused to a mouse Fc region of either IgG1 or IgG2a isotype. This approach may be adapted as a treatment strategy for high-risk or immunocompromised groups that do not respond well to vaccination. Moreover, it can be a proactive measure against pandemics, wherein pre-existing immunity and immunity generated via seasonal vaccination may be unable to protect against emerging divergent HA subtypes.

R1a-B6 was previously described as an alpaca derived nanobody capable of cross subtype neutralization of pandemic A(H1N1)2009, highly pathogenic avian influenza H5N1, and divergent strains H2N2, and H9N2 [219, 268]. In this chapter, it was evaluated if R1a-B6's potent *in vitro* neutralizing activity (**Chapter 3**) can translate into *in vivo* efficacy. In addition, by delivering R1a-B6 in different formats via AAV, the importance of the Fc domain for half-life extension and effector function to R1a-B6's prophylactic efficacy *in vivo* was explored. Previous findings suggest that anti-influenza antibodies, both hemagglutinin head and stalk-binding, necessitate interactions with FcγRs on effector cell populations to mediate *in vivo* protection [246]. It was already observed that R1a-B6-mIgG2a produced *in vitro* is able to activate ADCC (**Figure 3.6**). Thus, whether ADCC as mediated by the nanobody's Fc region is necessary for protection of mice in an influenza challenge is investigated.

Evaluation of promising anti-influenza prophylactic therapies utilizes multiple steps before proceeding to clinical studies. This includes testing in *in vitro* assays to check for functionality, and importantly, employment in *in vivo* assays using appropriate animal models. Popular laboratory animal models used for study of potential influenza virus inhibitors include the ferret and the mouse, with a variety of parameters used to indicate the severity of infection and its inhibition by therapy [85, 402, 403]. The administered treatment should be safe, tolerable and not adversely affect the test animal's health before any further studies pertaining to efficacy can be carried out.

The ferret has been a preferred animal model for influenza researchers mainly because they exhibit many of the typical signs of human influenza infection, most notably, fever [85, 402, 403]. However, ferrets are expensive, and require special housing requirements, limiting sample size in experiments where large animal-to-animal variability may hamper significant trends of efficacy among treatment groups [402]. It has also been shown that data obtained in ferrets may not always be predictive of clinical antiviral efficacy due to differences in dosing, pharmacokinetics, bioavailability, and systemic toxicity [404-407]. Route of administration for both influenza virus or therapeutic has also been shown to be a major consideration in the ferret model, with procedures other than intranasal delivery unable to result in any observable effect [354, 405].

Due to these considerations and the initial aims of the study, influenza mouse models were utilized, allowing the use of a larger number of subjects to obtain statistically robust data. Their small size, reduced cost, highly characterized and well-studied immune system, and the wide availability of commercial kits for measurement of immune factors, make mice useful for influenza research [62, 85, 408]. The success of mouse models for initial *in vivo* safety and efficacy studies for antiviral drugs approved for use against influenza viruses have been reviewed by Bouvier et. al [408], cementing their value in *in vivo* work.

Another factor to consider is the route of administration and the immune response that will be generated both against the AAV vector and the nanobody transgene. Seroprevalence of pre-existing neutralizing antibodies to AAV vector capsids remains a problem [336, 337, 390] that may prevent a percentage of the population from receiving gene therapy in a clinical setting. The choice of AAV8 for intramuscular (IM) administration has been shown to circumvent this issue [338]. It was found that the presence of naturally occurring pre-existing neutralizing antibodies against AAV8 had no effect on transgene expression in the muscle, only interfering in gene expression in the liver in mice [338]. They also discovered that IM re-administration of the same AAV8 vector in mice and rhesus macaques had no effect on transgene expression. This makes the choice of IM AAV8 delivery of therapeutic transgenes against influenza a preferable option. As for nanobody immunogenicity, several studies in mice have shown that there is an absence of circulating immunoglobulins directed against camelid nanobodies after intravenous injection, even after repeated doses [251, 273]. Additionally, there was no T-cell response generated against the nanobodies in treated mice [251, 273]. A mouse Fc region instead of a human Fc has also been appended to the nanobody to lessen immunogenicity in murine challenge models. A mouse Fc is also compatible with mouse FcγR, allowing the assessment of the probable role of Fc effector activation in protection of mice from an influenza challenge.

In this chapter, the following objectives were accomplished:

(i) MLD_{50} determination of challenge virus A/California/07/2009(H1N1)pdm09,

(ii) demonstration of nanobody-Fc expression *in vivo* after intramuscular delivery via AAV,

(iii) neutralization of A/California/07/2009(H1N1)pdm09 *in vitro* by sera from AAV-treated mice

(iv) exploration of cross-subtype binding and neutralization activity of sera from AAV-treated mice against Influenza A Group I strains *in vitro*,

(v) demonstration of binding and activation of FcγRIV effector cells in mice given nanobody-Fc fusions delivered by AAV,

(vi) established protection of mice from lethal influenza pandemic H1N1 challenge via AAV-mediated delivery of nanobody-Fc, and

(vii) shown cross-subtype influenza protection via AAV-mediated delivery of nanobody-Fc in an H5N1-mouse adapted challenge model.

Findings are discussed herein in the context of designing the optimum transgene for AAV vector delivery of R1a-B6 to accomplish long term, safe, broad protection from pandemic influenza in vulnerable patient groups.

5.2 Results

5.2.1 Determination of Mouse Lethal Challenge Dose (MLD) of A/California/07/2009(H1N1)pdm09 (CA/09)

To determine the mouse lethal challenge dose of CA/09 that was successfully produced and titrated (**Figure 3.7**), dilutions of 10^2, 10^3, 10^4 and 10^5 $TCID_{50}$/mL (50 µL) of the live virus were given intranasally to 4 groups consisting of 4 mice each. A control group was given PBS. The mandated endpoint of the study was loss of 20% or more of initial body weight and/or severe symptoms of influenza infection such as difficulty in breathing, sunken abdomen, and pinched waist.

All mice that were given 10^5 $TCID_{50}$/mL and 10^4 $TCID_{50}$/mL of CA/09 rapidly lost weight by day 2 and were all culled by day 6 (**Figure 5.1-5.2**). Mice that were given 10^2 $TCID_{50}$/mL of virus all lost weight by day 5 post-challenge but recovered around day 9 and regained their initial weight by day 14 (**Figure 5.2**). Similar to mice given the higher viral doses, mice given 10^3 $TCID_{50}$/mL of CA/09 rapidly lost weight around day 5, with three out of four mice culled by day 8 (**Figure 5.1**). However, one mouse from the 10^3 $TCID_{50}$/mL group followed the trend of mice given 10^2 $TCID_{50}$/mL CA/09 and survived until day 14 (**Figure 5.2**).

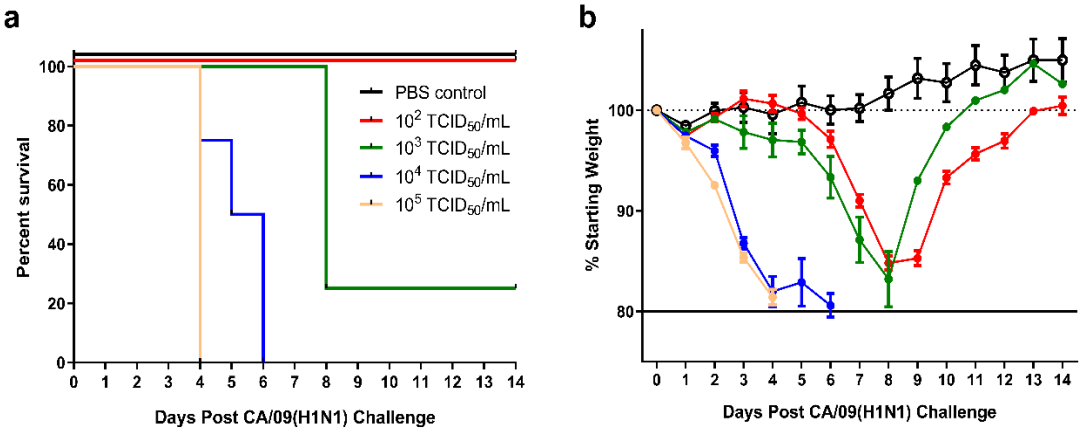

Figure 5.1. Survival of BALB/c mice after infection with different doses of CA/09. BALB/c mice were infected intranasally with 50 µL of CA/09 at the indicated doses and were monitored for survival (**a**) and weight loss (**b**) for 14 days. For (**b**), the plots show mean and standard error of four recipient mice per viral dose. Blue (days 4-6) and green (days 8-14) series represent weights from surviving mice only on days indicated.

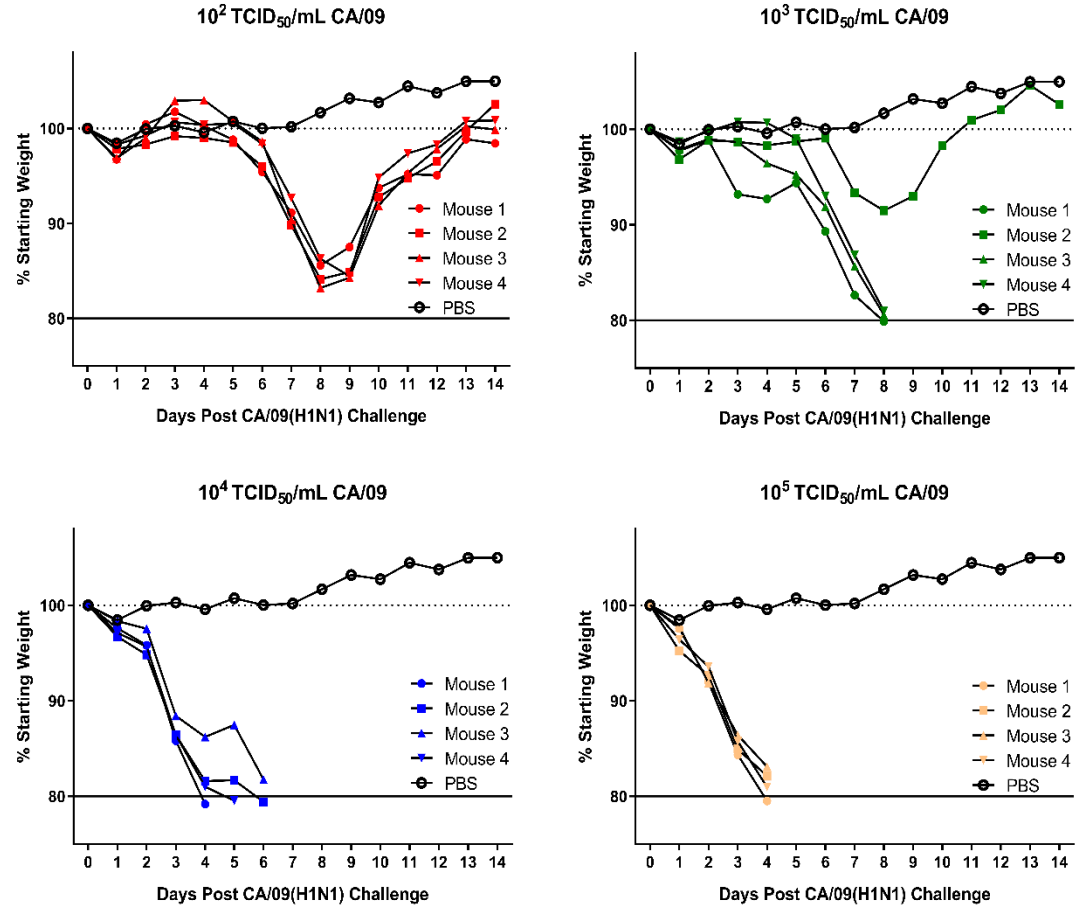

Figure 5.2. Weight monitoring in individual mice post-challenge with different doses of CA/09. The plots show weights of four recipient mice per viral dose. The mean weights of four mice given PBS were included in each plot as healthy controls. Mice were monitored for 14 days.

From this data, it was concluded that 50 µL of 10^4 $TCID_{50}$/mL of virus would be a sufficient lethal challenge dose for our *in vivo* experiment to test the ability of AAV-nanobody-Fc to protect mice against influenza. Using the Reed-Muench method [179, 363], $10^{2.67}$ $TCID_{50}$/mL was calculated to be the mouse lethal dose 50% (MLD_{50}) of this batch of A/California/07/2009(H1N1)pdm09, and 21 MLD_{50} CA/09 to be equivalent to 50 µL of 10^4 $TCID_{50}$/mL, the identified mouse lethal challenge dose.

Lungs were harvested from all mice as they were culled and a $TCID_{50}$ assay was performed on the homogenized lung samples to determine the amount of virus present. This would give an idea of the viral load in mice that were untreated, and a comparative value for future challenge studies can be obtained. No virus was detected in all mice that were given 10^2 $TCID_{50}$/mL and in 2 mice that were given 10^3 $TCID_{50}$/mL of CA/09 (**Figure 5.3a**). For mice infected with 10^4 $TCID_{50}$/mL and 10^5 $TCID_{50}$/mL CA/09, all of which were culled by day 6, the average $TCID_{50}$ was $10^{5.3}$ $TCID_{50}$ CA/09 /g tissue. These findings correlate viral load and survival, with all mice with no viral load surviving until the end of the study.

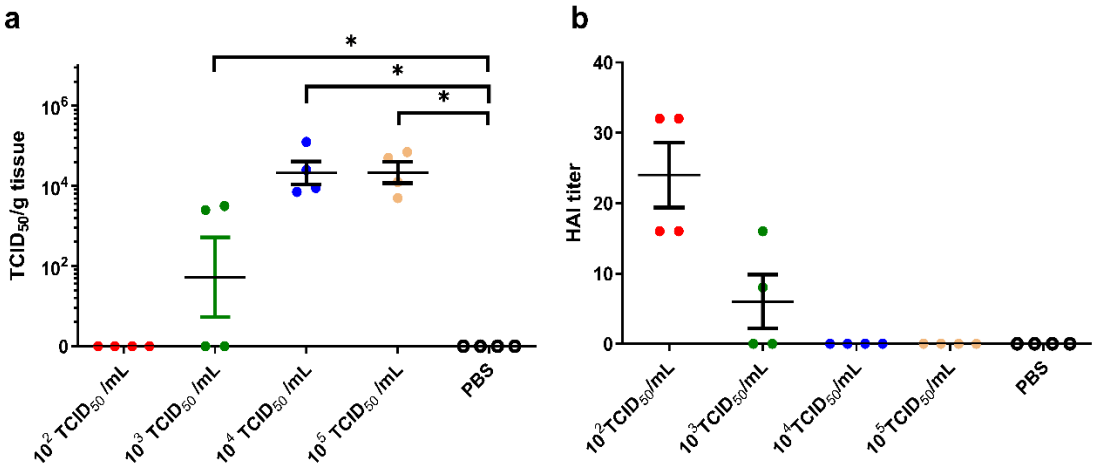

Figure 5.3. Recovered viral titers as indicated by $TCID_{50}$ per gram lung tissue and HAI titers obtained from harvested terminal mouse lung samples. (**a**) Viral titers were determined for homogenized lung samples after challenge with different doses of CA/09. Significant differences in residual virus titers in lung tissue are shown in brackets *(*p < 0.05)*. (**b**) Antibodies inhibiting HA hemagglutination were detected via HAI. HAI titers are expressed as the highest dilution of serum that inhibited hemagglutination. For both plots, each dot represents an individual mouse.

Neutralizing antibodies directed against the globular HA head block virus attachment to host cells by disrupting the binding of the virus to host receptors. The hemagglutination inhibition assay (HAI) is a surrogate assay for the presence of neutralizing antibodies which bind to the HA head domain and block the receptor binding site [120]. This assay is based on the tendency of influenza HA to bind to red blood cells (RBCs) causing them to agglutinate [179]. In the presence of antibodies specific to influenza HA, potential binding of HA to RBCs is blocked, inhibiting hemagglutination. From the 1970s up to this day, an HAI titer ≥40 is considered the primary immune correlate of protection, with higher serum HAI titers associated with higher rates of protection [120, 181]. The HAI assay was conducted to ascertain if mice produced specific anti-hemagglutunin head antibodies post-challenge.

Mice that survived influenza challenge, all four from the 10^2 $TCID_{50}$/mL and a single mouse from the 10^3 $TCID_{50}$/mL groups, cleared the virus (**Figure 5.3a**) and showed HAI titers of 8-32 (**Figure 5.3b**). No HAI titers were detected for groups given 10^4 and 10^5 $TCID_{50}$/mL CA/09, as mice from these groups were culled by day 6, and this might not be enough time to generate antibodies (**Figure 5.3b**). Our results show a direct relationship between HAI titer and survival in this challenge model.

Colleagues at the Influenza Resource Center (IRC) at the National Institute for Biological Standards and Control (NIBSC) have previously determined the mouse lethal dose 50% (MLD_{50}) for our other challenge virus, the mouse-adapted A/Vietnam/1194/2004 (H5N1) NIBRG-14ma (VN/04). They found this to be $10^{5.8}$ $TCID_{50}$/mL, and the challenge dose to be 20 µL or 10 MLD_{50} of this virus stock with a titer of $10^{7.5}$ $TCID_{50}$/mL (unpublished data).

5.2.2 *In vivo* expression of nanobodies following intramuscular (IM) AAV delivery

To test the ability of AAV-mediated delivery to express the nanobody constructs and to determine the optimum AAV dose for mouse challenge models, a dose ranging

study of a single IM injection of 1.0 x 10^{10} vg (vector genomes), 3.3 x 10^{10} vg and 1.0 x 10^{11} vg of each AAV vector was given to BALB/c mice. Expression levels in mouse sera was tested for a duration of 24 weeks while observing for any symptoms of stress or discomfort to assess tolerability and long-term safety.

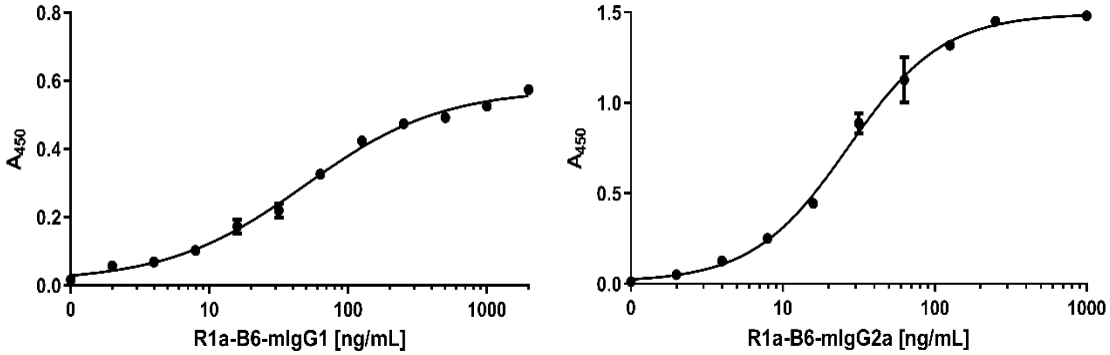

Figure 5.4. Representative recombinant nanobody standard curves for detection of nanobodies in mouse sera. Absorbance at 450 nm of nanobody protein standards against CA/09 reference standard or lysozyme was plotted and fitted to non-linear dose response curves. For all plots, each point represents mean and standard error of two replicates.

Binding of R1a-B6-(Fc) to CA/09 and cAb1-mIgG2a to lysozyme was detected via ELISA. For each construct, a set of nanobody constructs that was previously produced and characterized (**Chapter 3**) of known concentrations (range of 1 ng/mL to 1000 ng/mL) was transferred to a plate coated with CA/09 or lysozyme. This served as the set of standards. The log concentration of these standards was then plotted as X values and their absorbance signal as Y values and these data were fit to a dose-response variable slope model: Y=Bottom + (Top-Bottom)/(1+10^((LogEC_{50}-X)*HillSlope)), where the "Top" is the maximal response and the "Bottom" is the basal response (**Figure 5.4**). Concentration of recombinant nanobody produced *in vivo* that bound to reference antigen (CA/09 or lysozyme) was then estimated by non-linear regression.

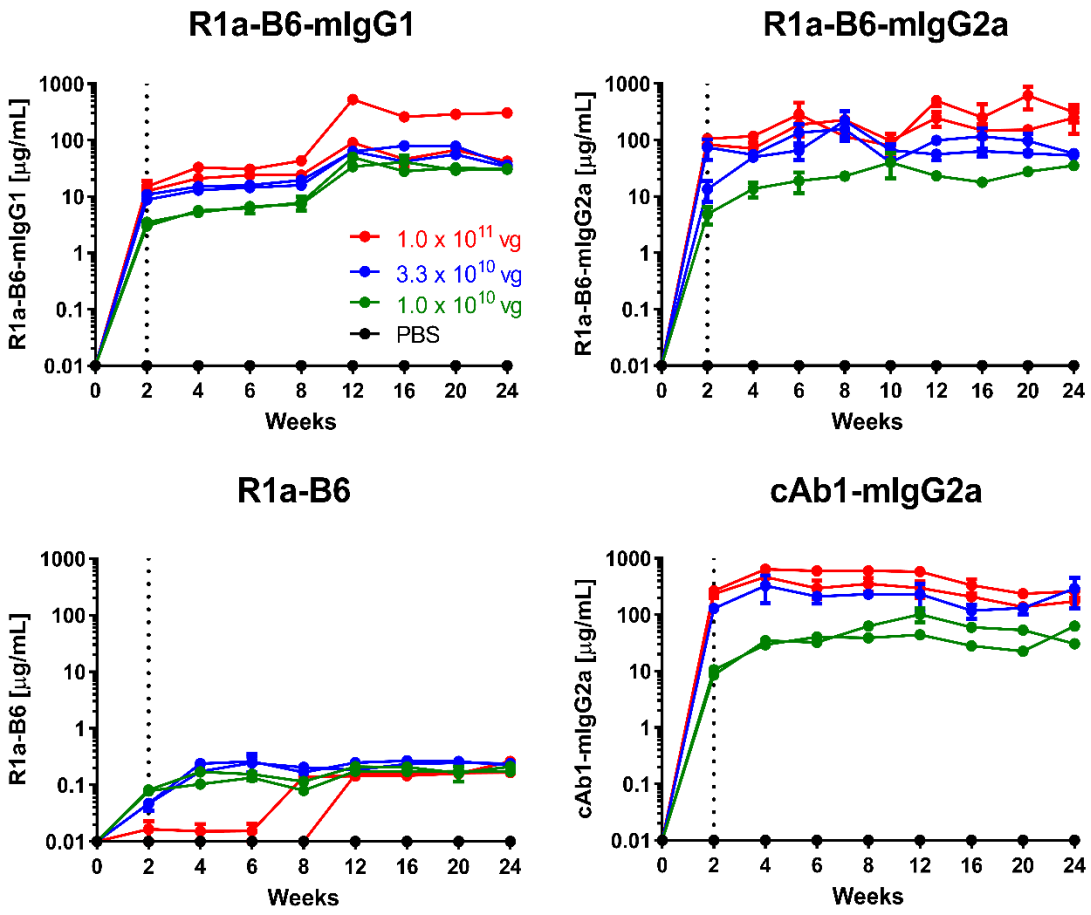

Figure 5.5. AAV dose ranging study of nanobody constructs in mice. Different R1a-B6 constructs and the control nanobody, cAb1, were given via AAV in vector genome (vg) doses of 1.0 x 10^{10} vg (green series), 3.3 x 10^{10} vg (blue series), and 1.0 x 10^{11} vg (red series). Mice that were given PBS are indicated by the black series. Nanobodies in serum of BALB/c mice were measured from week 0 to 24. Each individual series corresponds to a single mouse. The dotted line represents the point (2 weeks) at which nanobody expression levels were first measured. A mouse given 1.0 x 10^{10} vg of R1a-B6-mIgG2a was culled before the end of the study on welfare grounds. Post-mortem examination did not reveal anything study or procedure related and concluded that this was an unfortunate and unrelated event. For all plots, each point represents mean and standard error of two replicates.

Detectable levels of nanobody-Fc fusion were seen for all vector doses in mouse sera within 2 weeks of injection (**Figure 5.5**). Beyond 2 weeks, nanobody-Fc levels increased, reaching a plateau during weeks 6-12, with concentrations being maintained at high stable levels with no reduction for the duration of the 24-week study. Peak concentrations of ~560 µg/mL for R1a-B6-mIgG1, ~1100 µg/mL for R1a-B6-mIgG2a, and ~600 µg/mL for cAb1-mIgG2a, were detected (**Figure 5.5**). These

results are comparable to the IgG concentration in mouse sera of around 50-200 µg/mL after 64 weeks of human mAbs CR6261 and F10 delivered intramuscularly via AAV [354]. Monovalent R1a-B6 showed very low levels in serum compared to the Fc fusions, reaching a peak concentration of around 0.36 µg/mL by week 6 which remained for the duration of the study (**Figure 5.5**). In all cases, mice did not show any symptoms of distress or ill health that could be attributed to AAV or transgene expression for the full 24 weeks.

Appending a mouse Fc region to these nanobodies and expression via AAV allowed the nanobody-Fc constructs to persist in circulation at the levels observed for up to 24 weeks (**Figure 5.5**). This is apparent when comparing the serum concentration of constructs with an Fc region to that of monovalent R1a-B6. It was stated previously that due to their small size, nanobodies rapidly pass the renal filter, resulting in their faster blood clearance [254], which is evident here. Detectable levels of R1a-B6 even after 24 weeks, albeit ~2000 times less relative to the nanobody-Fc constructs, is solely due to its' continuous expression via AAV.

Mice given the highest vector dose of 1.0×10^{11} vg produced the highest nanobody titers (**Figure 5.5**, red series). The difference is substantial compared to that of the lowest dose, 1.0×10^{10} vg (**Figure 5.5**, green series), with mice given this dose having nanobody-Fc concentrations unable to breach the 100 µg/mL level. As there are appreciable nanobody-Fc levels detected in serum at 6 weeks post-AAV administration (**Figure 5.5**), we decided to challenge mice with influenza (CA/09 and VN/04) at this time point, with weeks 6-8 as the study window.

In healthy adults, the normal range of IgG at any one time is accepted to be 700–1600 mg/dL [409]. The observed levels of nanobody-Fc in serum in this study is on average around 10% of the acceptable range, and so the findings here have implications for actual clinical treatment in future. Immunoglubulin is one of the safest biological products available, however adverse side effects although rare, ranging from mild to severe, have still been documented [410]. Majority of adverse effects are

associated with high doses of immunoglobulin [410]. Thus, determining a dose that will guarantee the efficacy of therapy and will minimize adverse effects is an urgent focus prior to clinical therapy.

5.2.3 *In vitro* neutralization of CA/09 by sera from mice receiving AAV transgenes

To determine if mice that received AAV were expressing functional R1a-B6, *in vitro* neutralization assays against pandemic A/California/07/2009(H1N1) (CA/09) were performed. It should be noted that these mice were naïve and have not been exposed to influenza, hence it is assumed that neutralization of CA/09 will be due to nanobody-Fc and not a natural immune response to infection.

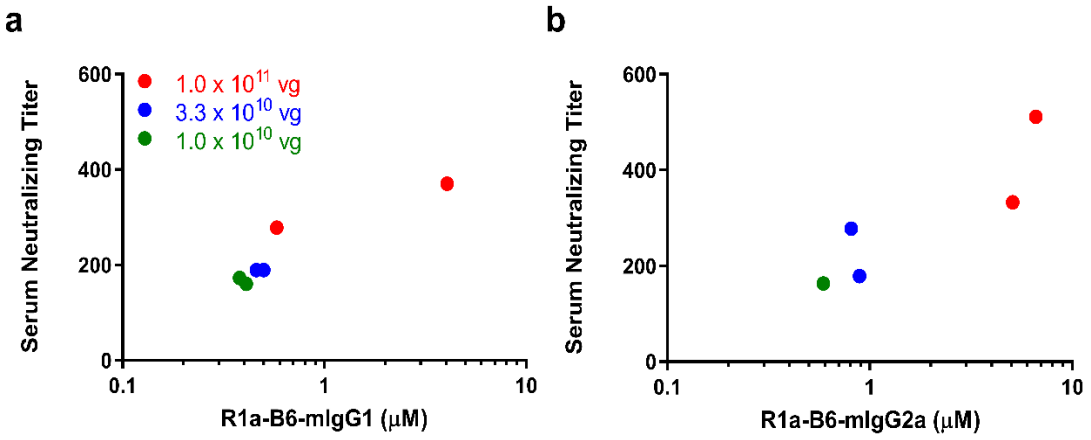

Figure 5.6. CA/09 neutralizing activity of mouse sera. Serum was taken from mice 24 weeks after they were injected with different doses of AAV encoding (**a**) R1a-B6-mIgG1 and (**b**) R1a-B6-mIgG2a and neutralizing activity was tested against 10^3 $TCID_{50}$/mL of CA/09. The serum *neutralizing titer* is expressed as the reciprocal of the highest dilution at which influenza infection is completely blocked. For all plots, each point represents an individual mouse serum sample.

Terminal sera (24 weeks) from mice expressing R1a-B6-mIgG1 and R1a-B6-mIgG2a were able to neutralize CA/09 (**Figure 5.6**). The level of neutralization directly correlated with serum concentration as detected by ELISA which in turn correlated with AAV vector genome dose (**Figure 5.6**). In contrast, mice expressing the control nanobody against lysozyme, cAb1, did not show any neutralization of CA/09, as

expected (data not shown). Similarly, no neutralization of CA/09 was seen with monovalent R1a-B6, which correlated with serum levels being approximately 1000-fold less in molar equivalence than the levels attained by the Fc fusions (data not shown). The AAV vector dose of 1.0 x 10^{11} vg gave the highest nanobody serum concentrations (**Figure 5.5**) and serum neutralizing titer (~300-400) against CA/09 (**Figure 5.6**) and was chosen for protection studies.

5.2.4 Cross-subtype binding and neutralization activity against Influenza A Group 1 strains of R1a-B6 produced via AAV-mediated delivery

Mouse sera 6-weeks post AAV IM administration of 1.0 x 10^{11} vg of each nanobody construct (**Figure 3.1**) (*n=8*/group) was obtained and tested for cross-influenza subtype binding activity. These mice were naïve and had not been exposed to influenza so binding to heterologous strains can be attributed solely to R1a-B6 expressed *in vivo* and not to naturally produced antibodies that are usually induced via vaccination or exposure to virus. Binding activity in serum to different reference standards was detected via ELISA. For each reference reagent, a set of protein standards was prepared and run on the same ELISA plate as the serum samples. Binding is indicated by the concentration of recombinant proteins estimated from standard curves of the corresponding activity (**Section 5.2.2**).

Sera from mice expressing R1a-B6-mIgG1 (**Figure 5.7a**) and R1a-B6-mIgG2a (**Figure 5.7b**) had binding activity against all Group I Influenza A subtypes tested. For both R1a-B6-Fc constructs, binding was similar against all H1N1, H2N2, H5N1, and H9N2 subtypes. Mice expressing monovalent R1a-B6 showed lower binding against the panel of whole influenza virus antigen standards (**Figure 5.7c**), and this is most probably due to very low serum levels of monovalent R1a-B6 compared to mice receiving the R1a-B6 Fc fusions. Serum from mice expressing cAb1-mIgG2a and those given PBS for binding to different influenza HA did not show any binding activity against all influenza subtypes tested (data not shown).

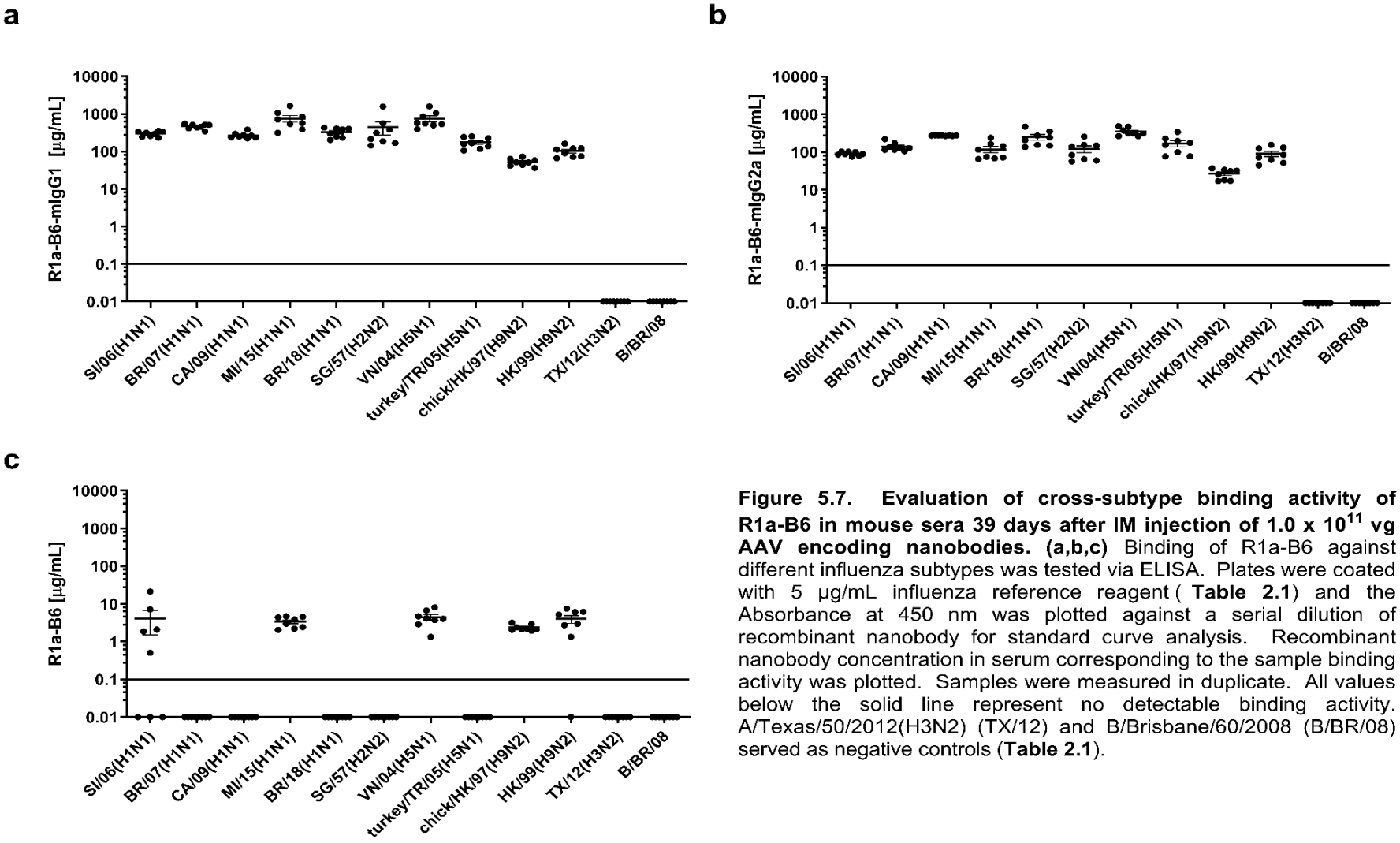

Figure 5.7. Evaluation of cross-subtype binding activity of R1a-B6 in mouse sera 39 days after IM injection of 1.0 x 10^{11} vg AAV encoding nanobodies. (a,b,c) Binding of R1a-B6 against different influenza subtypes was tested via ELISA. Plates were coated with 5 µg/mL influenza reference reagent (**Table 2.1**) and the Absorbance at 450 nm was plotted against a serial dilution of recombinant nanobody for standard curve analysis. Recombinant nanobody concentration in serum corresponding to the sample binding activity was plotted. Samples were measured in duplicate. All values below the solid line represent no detectable binding activity. A/Texas/50/2012(H3N2) (TX/12) and B/Brisbane/60/2008 (B/BR/08) served as negative controls (**Table 2.1**).

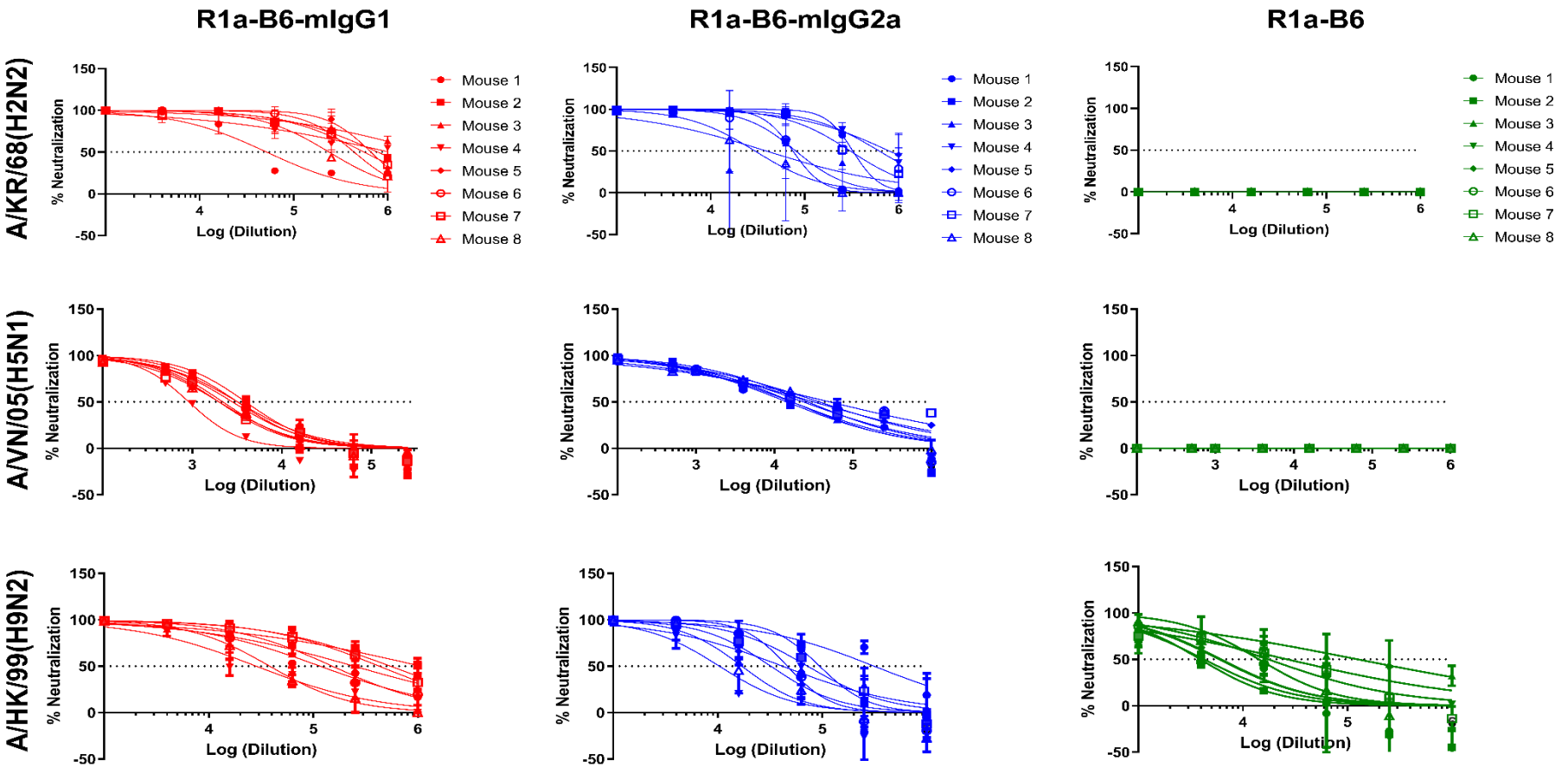

Figure 5.8. ***In vitro*** **neutralization of influenza pseudotypes by nanobodies from mouse sera.** Neutralization was carried out via a Luciferase-reporter assay. Mouse sera was diluted to obtain neutralization dose response curves. For all plots, each point represents the mean and standard error of two replicates per dilution. Each series corresponds to a single mouse. *n*=8 mice/group.

In addition to cross-subtype binding, R1a-B6-Fc in mouse sera also demonstrated potent cross-neutralizing activity against Group I Influenza A pseudotypes H2, H5, and H9 (**Figure 5.8**). Similar to previous findings [268], serum from mice that received AAV-R1a-B6 was not able to neutralize the H2N2 pseudotype but was able to potently neutralize H9N2 (**Figure 5.8**). The same serum samples did not show any neutralization against H5N1, a departure from recombinant R1a-B6's potent *in vitro* neutralizing activity as shown previously (**Figure 3.9** and **Table 3.1**). However, this is probably due to R1a-B6's limited serum concentration (**Figure 5.5**) and not because of lack of potency. Sera from mice that received cAb1-mIgG2a were also tested, and all samples showed no neutralization at any cAb1-mIgG2a concentration (data not shown). These results demonstrate that R1a-B6-Fc has retained its *in vitro* cross-subtype binding and neutralizing activity when produced *in vivo*.

5.2.5 Protection of mice from lethal influenza challenge via AAV-mediated delivery of nanobodies

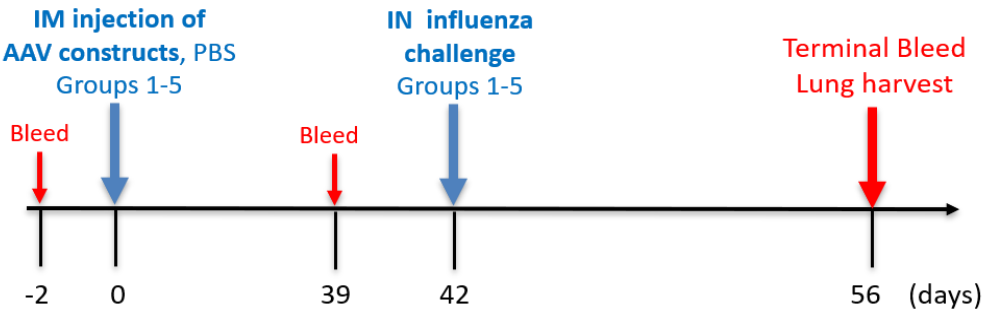

Figure 5.9. Study schedule of influenza challenge. Groups 1-5 indicate mice given AAV-R1a-B6-mIgG1, AAV-R1a-B6-mIgG2a, AAV-R1a-B6, AAV-cAb1-mIgG2a, and PBS, respectively in this order, intramuscularly. Mice were challenged on day 42 with either A/California/07/2009(H1N1)pdm09 (CA/09) or A/Vietnam/1194/2004(H5N1) NIBRG-14ma (VN/04).

Following successful tolerability studies which lasted 6 months, survival of mice undergoing prophylactic administration of R1a-B6 using AAV delivery before challenge with CA/09 and VN/04 was evaluated. For both challenges (**Figure 5.9**), 1.0 x 10^{11} vg

AAV encoding R1a-B6-mIgG1, R1a-B6-mIgG2a, R1a-B6, cAb1-mIgG2a, and PBS (negative control), was injected intramuscularly into different groups of BALB/c mice (*n=8*/group). Thirty-nine days post-AAV injection, nanobody expression was quantified prior to lethal challenge with influenza. Mice were challenged with either 21 MLD_{50} CA/09 or 10 MLD_{50} VN/04 and observed for 14 days.

5.2.5.1 A/California/07/2009(H1N1)pdm09 (CA/09) challenge

Prior to the challenge, 300-500 µg/mL of nanobody Fc fusions via CA/09 H1N1 ELISA for R1a-B6-Fc and against lysozyme for cAb1-mIgG2a (**Figure 5.10a**) was detected, whereas for monovalent R1a-B6, we were unable to detect any substantial levels in the sera tested on day 39 (**Figure 5.10a**). This range is still consistent with previous findings (**Figure 5.5**) and differences may be due to mouse to mouse variability. After confirmation of transgene expression in mouse sera, we proceeded with CA/09 challenge via intranasal delivery. Weight loss and clinical symptoms of influenza were observed during the 14-day study window or until mice were culled.

There was no weight loss or symptoms of influenza infection observed in mice given R1a-B6-mIgG1 and R1a-B6-mIgG2a (*n=16*) for the duration of the study demonstrating complete protection from influenza (**Figure 5.10b-e**). In contrast, animals expressing the control anti-lysozyme specific nanobody cAb1-mIgG2a and those given PBS showed symptoms of influenza including difficulty in breathing, pinched waists and sunken abdomen 3 days post-challenge. These mice lost 20% of their initial body weight and were all culled by day 6 of the study (**Figure 5.10b-c,g**).

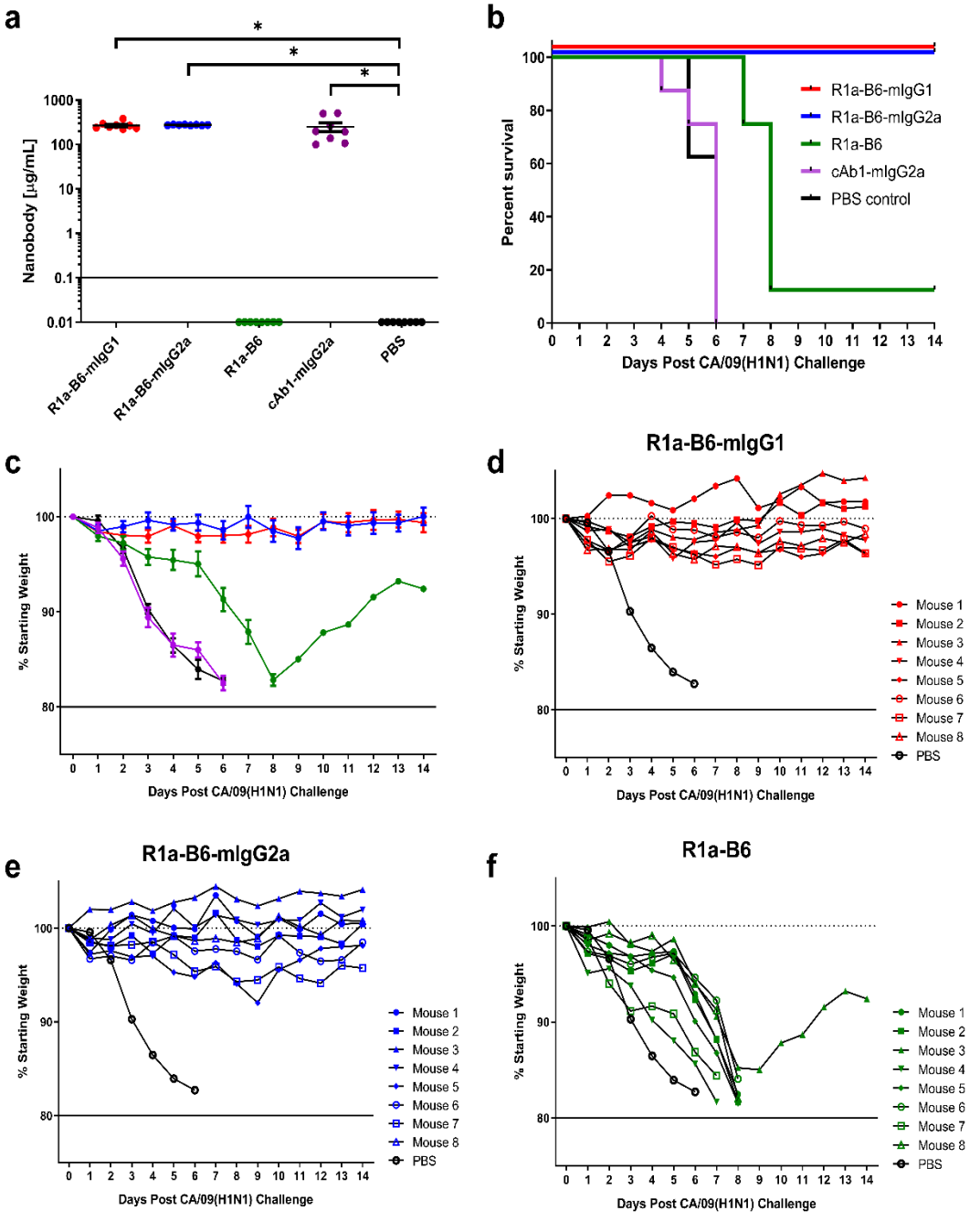

Figure 5.10. Prophylactic efficacy of AAV expressed nanobodies in a mouse challenge model of pandemic H1N1 CA/09. (**a**) Total nanobody-Fc in serum was measured by ELISA in samples taken 39 days after IM injection of AAV vectors. Comparisons are shown in brackets ($p<0.05$). BALB/c mice were then infected intranasally with 21 MLD_{50} CA/09 42 days post-AAV IM injection. Mice were monitored for survival (**b**), weight loss summarized (**c**), and individually (**d-g**) for 14 days. For (**a,d-g**), each point represents an individual mouse. The plots show mean and standard error of eight recipient mice per nanobody construct. PBS series is plotted as the mean weight of 8 mice.

In addition, there was no observable difference in the prophylactic efficacy of mice receiving R1a-B6-mIgG2a compared to R1a-B6-mIgG1 (**Figure 5.10d-e**). Mice given monovalent R1a-B6 without a mouse Fc, showed symptoms of influenza infection 6 days post-challenge, which was a delay of 3 days compared to control groups given cAb1-mIgG2a and PBS (**Figure 5.10b-c,f**). Seven mice (*n=7*) from the monovalent R1a-B6 group eventually succumbed to infection and were culled on days 7-8 due to rapid weight loss. However, a single mouse (Mouse 3) from this group started gaining weight around day 9 and survived until the end of the study (**Figure 5.10f, Table 5.1)**. It was also noted that this mouse was of a higher than average starting weight, which may have contributed to it surviving the challenge.

Terminal mouse lung samples were processed, and viral titers in the lung at the time of sacrifice was determined and differences in the mean determined by Student's t-test. Mice expressing R1a-B6-mIgG1, R1a-B6-mIgG2a, and R1a-B6 had significantly lower $TCID_{50}$/g CA/09 than mice given cAb1-mIgG2a and PBS *(*p < 0.05).* All mice that were given cAb1-mIgG2a and PBS, with lungs harvested on days 4-6, had high viral loads with titers in the range of 10^3-10^6 $TCID_{50}$/g lung tissue (**Figure 5.11a**). For mice given AAV encoding R1a-B6-mIgG1 and R1a-B6-mIgG2a, with lungs harvested on day 14, the end of the study, no virus was detected in lung homogenates except for one mouse in the R1a-B6-mIgG2a group that had ~10^3 $TCID_{50}$/g CA/09 (**Figure 5.11a, Table 5.1**). Mice given AAV-R1a-B6 (7 mice culled on days 7-8, 1 mouse culled on day 14) had significantly lower viral titers than mice given PBS *(*p<0.05)* (**Figure 5.11a**). The single surviving mouse, Mouse 3 (lung harvest on day 14), and Mouse 8 (lung harvest at day 8), from the group expressing R1a-B6 did not appear to have any virus present in the lungs (**Figure 5.11a, Table 5.1**). This implies that R1a-B6 mediated clearance of virus occurs in the lungs via mechanisms different from IgG transcytosis which is governed by FcRn interaction [411].

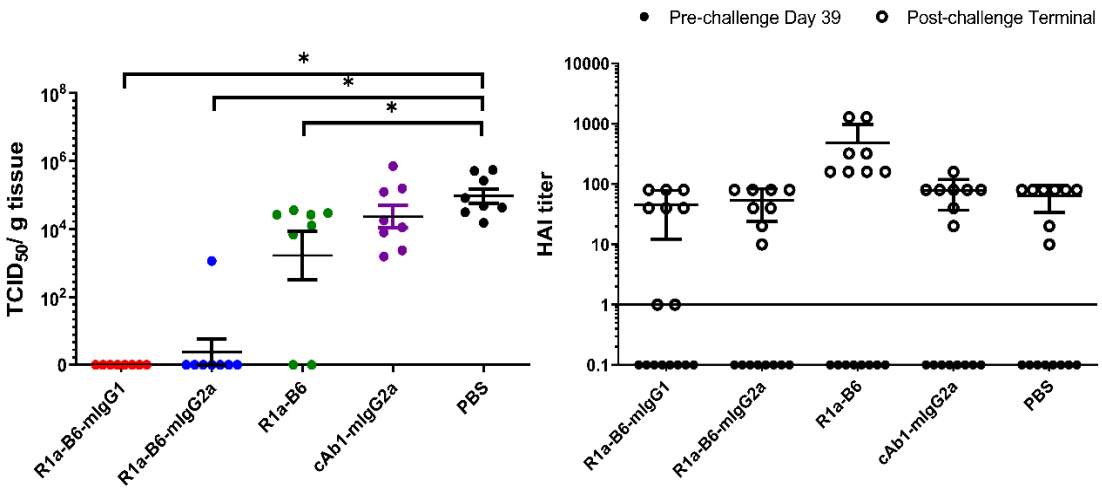

Figure 5.11. Recovered viral titers as indicated by $TCID_{50}$ per gram lung tissue and HAI titers obtained from harvested mouse lung samples at the end of the CA/09 challenge experiment. Lungs were harvested and terminal bleeds were obtained at 14 days for all mice given AAV-R1a-B6-mIgG1 and AAV-R1a-B6-mIgG2a, and for Mouse 3 in the AAV-R1a-B6 group, at days 7-8 for the rest of the mice in this group, and at days 4-6 in mice given AAV-cAb1-mIgG2a and PBS. (**a**) Viral load was determined as indicated by $TCID_{50}$ per gram of tissue from lung homogenates as mice were culled during the 14-day challenge window. Comparisons are shown via brackets (*$p<0.05$) as determined by Student's t-test. (**b**) Naturally induced immune response in mice pre- and post-CA/09 challenge was assessed via Hemagglutination Inhibition (HAI) titers 39 days post-AAV administration and 3 days pre-challenge (•), and from post-challenge terminals bleeds ($_o$). HAI titers are expressed as the highest dilution of serum that inhibited hemagglutination completely. Points below the solid line represent no HAI activity. For (**a-b**), each point represents an individual mouse. Mean and standard error of eight recipient mice per treatment is shown in (**a**).

To compare anti-influenza immune response pre- and post-CA/09 challenge, we employed a hemagglutination inhibition (HAI) assay on terminal mouse serum samples (**Figure 5.11b**). As expected, pre-challenge samples did not show any HAI activity as the only anti-influenza antibody present was R1a-B6 which has previously been shown to be negative for HAI [219, 268]. Post-H1N1 challenge, mice that received AAV encoding cAb1-mIgG2a and PBS, culled on days 4-6, showed similar HAI titers to groups given AAV encoding R1a-B6-mIgG1 and R1a-B6-mIgG2a. HAI titers for mice given R1a-B6 were higher than those of the other 4 groups (**Figure 5.11b**). Unlike groups given R1a-B6-mIgG1 and R1a-B6-mIgG2a, which have cleared the virus completely, mice given R1a-B6 probably needed to mount a stronger immune response because of sustained presence of the virus and R1a-B6 not being present in

concentrations sufficient for protection. Mice from this group also survived for longer than mice given cAb1-mIgG2a and PBS (**Figure 5.10b-c**), producing more antibodies in response to the presence of virus in the process. Two mice given AAV encoding R1a-B6-mIgG1 did not have any HAI titers post-challenge (**Figure 5.11b**). These mice did not show any symptoms of infection during the 14-day study window as well. Coupled with the $TCID_{50}$ data, of which there was no virus recovered in the lungs, it can be gathered that these two mice were probably not infected by influenza at all, and that the virus was already eliminated before the immune response was activated. It can be concluded that after influenza challenge, both viral exposure-induced anti-head HA antibodies and anti-stem R1a-B6 nanobodies were present in mouse sera (**Figure 5.11b**). These results suggest that naïve mice are still able to mount a natural immune response against a CA/09 challenge even after the administration of AAV encoding transgenes, and that this natural immune response acts in parallel with R1a-B6 to protect mice from influenza.

The level of inflammation in terminal lung tissue was compared by Hematoxylin and Eosin (H&E) staining. At the end of the study (14 days post-challenge), mice expressing R1a-B6-mIgG1 and R1a-B6-mIgG2a (*n=16*) showed clear bronchioles and air sacs with no signs of inflammation (**Figure 5.12**) which was consistent with them showing no signs of illness and having no virus recovered from their lungs (**Figure 5.11a**). In contrast, H&E staining revealed marked inflammation in the perivascular and alveolar spaces accompanied by thickening of the alveolar walls (arrows) in lungs of all mice given cAb1-mIgG2a and PBS (untreated), and 6 mice given R1a-B6 (*n=22*) (**Figure 5.12**). These mice showed symptoms of influenza as early as day 4 post-challenge (**Figure 5.10 c,f-g**). Slight lung infiltration can be seen in lung tissue in mice given R1a-B6 that was culled on day 7. Two mice from the group given R1a-B6 (Mouse 3 and Mouse 8) showed no signs of lung inflammation (**Figure 5.12, Table 5.1**) which correlated with the absence of residual virus (**Fig. 5.11a**).

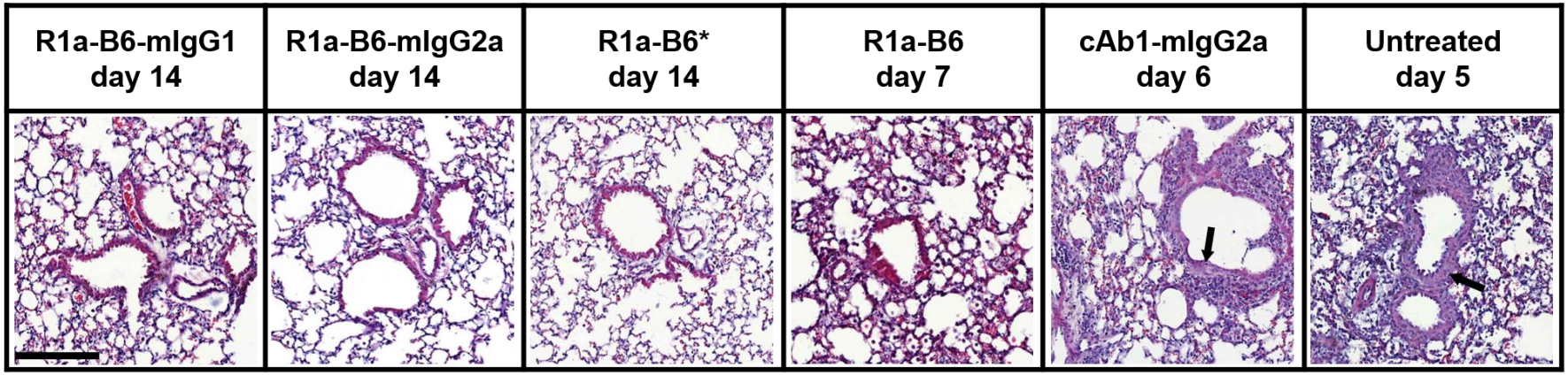

Figure 5.12. Representative histological lung sections from mice post-infection with CA/09. Lungs were harvested from mice as they were culled at the days indicated and stained with H&E. Untreated mice were given PBS. (*) represents mouse 3 (**Figure 5.10f**), the only mouse that survived the CA/09 challenge from the R1a-B6 group. Thickening of alveolar walls are indicated by arrows. Scale bar = 100 µm.

Table 5.1. Summary of relevant values and clinical observations of mice with unusual results that were given R1a-B6 via IM AAV delivery and challenged with CA/09.

Mouse Number	Day of start of symptoms	Clinical Symptoms	Day culled	$TCID_{50}$ /g tissue	HAI TITER (pre-challenge)	HAI TITER (terminal)	Serum Neutralizing Titer	*Degree of Inflammation (0-3)
R1a-B6-mIG2a Mouse 8	N.D.	N.D.	14 (end of study)	$10^{3.06}$	N.D.	80	640	0
R1a-B6 Mouse 3	6	Poorly appearance from day 6, difficulty in breathing from days 7-9, abdominal contractions day 7-8, lost 15% initial body weight by day 7, started gaining weight day 10	14 (end of study)	N.D.	N.D.	320.00	80	0
R1a-B6 Mouse 8	6	Poorly appearance from day 6, difficulty in breathing from days 7-8, abdominal contractions day 7-8, lost 20% initial body weight by day 8 and was culled	8	N.D.	N.D.	320.00	160	0

***** Degree of inflammation is scored from 0-3 (**Section 2.5.5**) with 0 showing no to minimal inflammation and 3 showing the highest degree of inflammation as observed via H&E staining. Lung sections were taken on the day of culling (terminal). N.D. = not detected.

A table was compiled showing mice with unusual results from the CA/09 challenge experiment. In the case of Mouse 8 given R1a-B6-mIgG2a (**Table 5.1**), virus was recovered from its lungs when it was culled on day 14 (**Figure 5.11a**). This mouse did not show any symptoms of influenza throughout the study. However, in comparison to mice given cAb1-mIgG2a and PBS, viral titers obtained from this mouse are still lower (**Figure 5.11a**), showing that even though there is residual virus present, it may not have been enough to produce any disease symptoms. For Mouse 8 given R1a-B6 (**Table 5.1**), there was no recovered virus or any inflammation in lung tissue, despite this, the mouse was still culled on day 6. It is possible that this mouse could have survived if we had let it remain in the study past day 6 (**Figure 5.10f**), which seemed to be the turning point between survival and culling. It is impossible to predict whether this mouse would have gained or lost more weight, as is the case for all mice given R1a-B6. It was observed all mice given R1a-B6 still got sick, but the viral titers were still lower compared to those given PBS (**Figure 5.11a**) and HAI titers showed that mice were fighting off an active infection (**Figure 5.11b**).

Binding and activation of FcγRIV effector cells in mice given nanobody-Fc fusions delivered by AAV was tested to see if there was any observable difference in the prophylactic efficacy of mice given an ADCC(+) (R1a-B6-mIgG2a) or ADCC(-) (R1a-B6-mIgG1) nanobody-Fc fusion. Despite the known *in vitro* differences in ADCC ability as tested in Chapter 3 (**Figure 3.6**), there was no evidence of this altering *in vivo* functionality of nanobody-Fc. All mice that received R1a-B6-mIgG2a and R1a-B6-mIgG1 survived the CA/09 challenge with mice showing no symptoms of influenza (**Figure 5.10b-e**), although it was determined that R1a-B6-mIgG2a produced *in vivo* was capable of mediating ADCC (**Figure 5.13**). This is in contrast to previous reports that broadly neutralizing monoclonal antibodies targeting the hemagglutinin stem requires FcγR interactions to confer protection against a lethal H1N1 challenge [246, 247]. Similar to *in vitro* results from Chapter 3 (**Figure 3.6**), serum from mice given R1a-B6-mIgG2a, but not R1a-B6-mIgG1 and cAb-mIgG2a, demonstrated activation of

FcγRIV pre-challenge (**Figure 5.13a**). This suggested that ADCC was not an essential component of the protective mechanism of action of R1a-B6. However, these observations may also be due to the high concentration of R1a-B6-Fc in circulation that was achieved via AAV delivery (**Figure 5.10a**). These findings agree with previous results that show that at high doses of anti-influenza mAb, *in vivo* protection is FcγR independent [247].

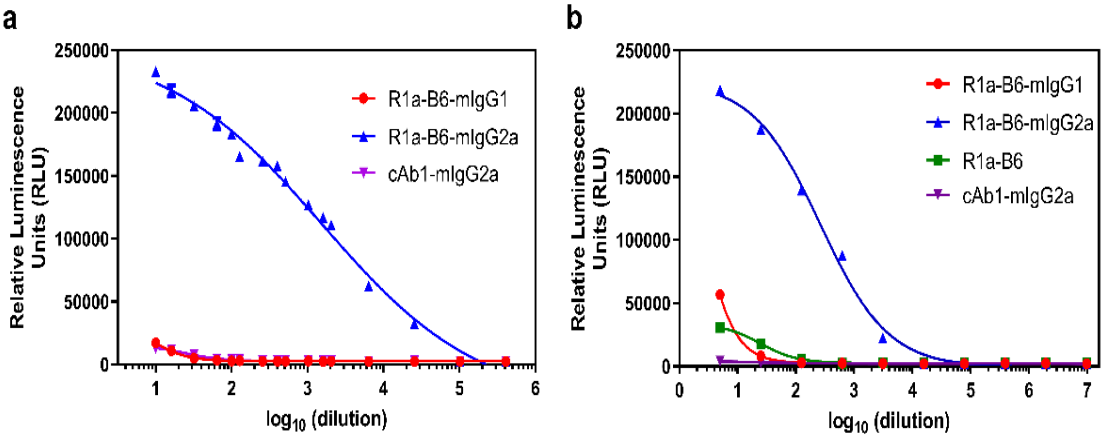

Figure 5.13. Binding and activation of mouse FcγRIV effector cells in mice given nanobody-Fc fusions delivered by AAV. Representative mouse sera were tested for ADCC activity via activation of mFcγRIV **(a)** 39 days post-AAV administration and pre-challenge and **(b)** terminally, after CA/09 challenge. Activity is shown in relative luminescence units (RLU) against dilutions of mouse sera containing nanobody Fc fusions expressed *in vivo*. Each point is shown as the mean and standard error of three replicates. (Error bars that are not visible are shorter than the size of the point symbol and have automatically been removed by the graphing software.)

The ADCC assay was repeated using terminal bleeds post CA/09 challenge and interestingly, a slight activation of FcγRIV effector cells in representative mice from groups given R1a-B6-mIgG1 and R1a-B6 was observed. Both these mice survived until the end of the study (**Figure 5.13b**). R1a-B6-mIgG1, with an ADCC(-) mouse Fc, and monovalent R1a-B6, are both negative for ADCC activity by themselves, suggesting that the slight activation observed may be due to the natural immune response to the virus in mice which we have observed (**Figure 5.11b**). There was no ADCC activity observed for cAb1-mIgG2a, as this representative mouse was culled by day 5 (**Figure 5.13b**). These data demonstrate that protection is not inhibited or

diminished by absence of ADCC activity as we have observed in all mice given R1a-B6-mIgG1 that survived the H1N1 challenge (**Figure 5.10b-d**). This seems to be true in the case of R1a-B6-Fc delivery via AAV with nanobody-Fc persisting in circulation at concentrations greater than 100 µg/mL (**Figure 5.10a**).

It is interesting to speculate how these findings will translate if the nanobodies were equipped with a human-Fc rather than a mouse-Fc, which it would be ideally fused with if this therapy is to advance to the clinic. It has been found that human IgG subclasses bind FcγR with similar relative affinity to the mouse FcγR, and that human IgG binds mouse FcγR with very similar affinities as mouse IgG [172, 292, 412]. This suggests that preclinical testing of human IgG in mouse models may mimic FcγR-mediated effector functions surprisingly well, and these results will possibly be reproducible if the nanobodies were fused to a human instead of a mouse Fc.

5.2.5.2 A/Vietnam/1194/2004(H5N1) NIBRG-14ma (VN/04) challenge

To assess if the prophylactic efficacy of R1a-B6 can extend to a different influenza subtype, an H5N1 influenza challenge model was utilized. The study design is the same as the CA/09 challenge (**Figure 5.9**) with mice receiving 10 MLD_{50} of NIBRG-14ma (VN/04), a mouse-adapted strain of a re-assortant virus derived from A/Vietnam/1194/04(H5N1). Additionally, an extra 3 mice per group were culled 3 days post-challenge for analysis of lung parameters.

Pre-challenge, 39 days post-IM AAV injection, it was found that mice given nanobody-Fc fusions have significantly higher concentration in serum than mice given vectors encoding R1a-B6 or PBS *(*p < 0.05)* (**Figure 5.14a**). Via VN/04 H5N1 ELISA, 80-1000 µg/mL levels of nanobody (**Figure 5.14a**) was detected in groups receiving nanobody-Fc, while there was no substantial level of monovalent R1a-B6 in the sera tested (**Figure 5.14a**). Nanobody levels in all groups are similar to those obtained pre-CA/09 challenge (**Figure 5.10a**).

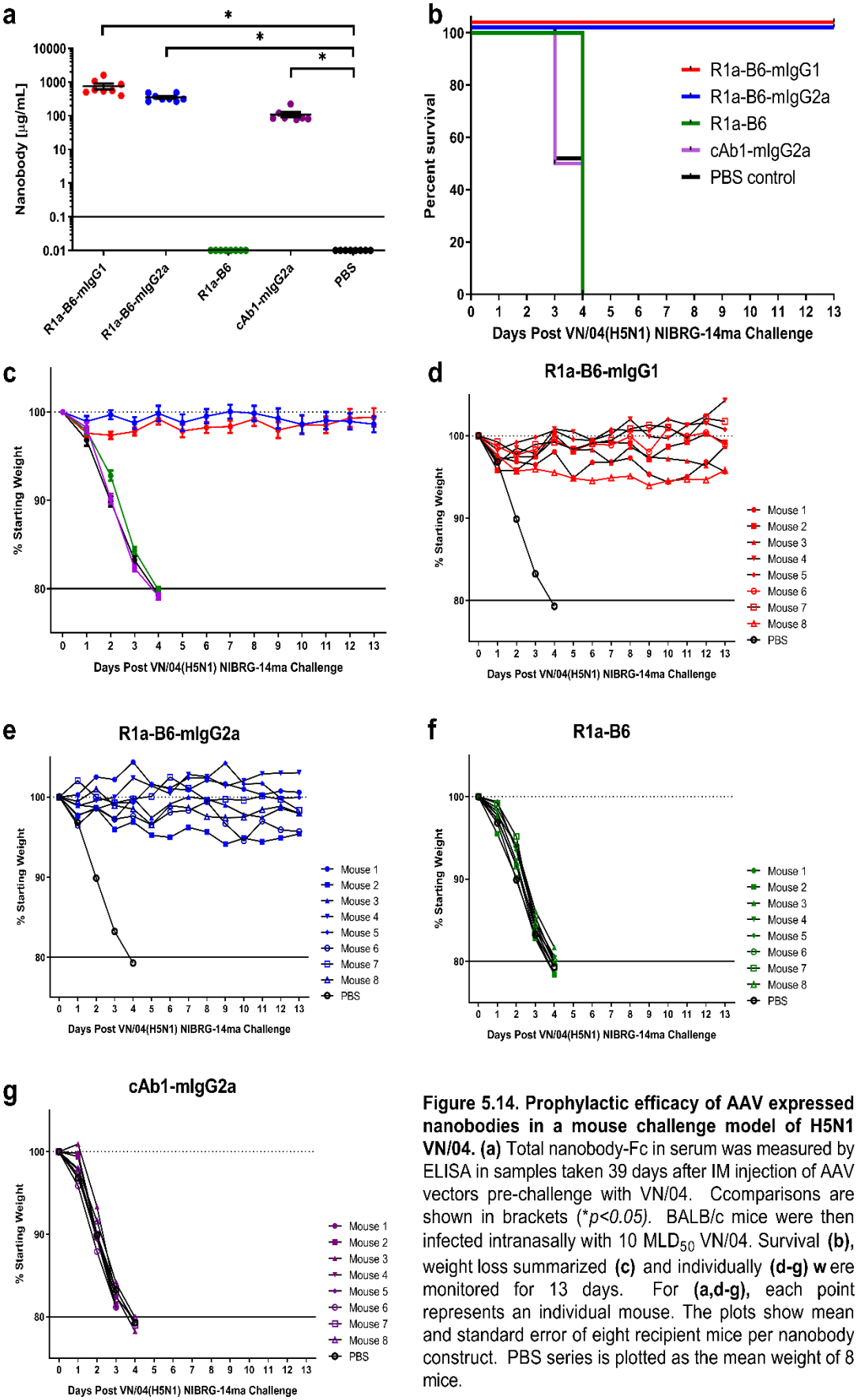

Figure 5.14. Prophylactic efficacy of AAV expressed nanobodies in a mouse challenge model of H5N1 VN/04. (a) Total nanobody-Fc in serum was measured by ELISA in samples taken 39 days after IM injection of AAV vectors pre-challenge with VN/04. Ccomparisons are shown in brackets (*$p<0.05$). BALB/c mice were then infected intranasally with 10 MLD_{50} VN/04. Survival **(b),** weight loss summarized **(c)** and individually **(d-g) w** ere monitored for 13 days. For **(a,d-g),** each point represents an individual mouse. The plots show mean and standard error of eight recipient mice per nanobody construct. PBS series is plotted as the mean weight of 8 mice.

Symptoms of influenza and rapid weight loss were observed 2-days post-challenge in mice given AAV encoding R1a-B6, cAb1-mIgG2a and PBS, which was earlier than those observed after the CA/09 challenge (**Figure 5.14c,f-g**). All mice from these groups (*n=24*) were culled by day 4 (**Figure 5.14b-c**). Similar to the CA/09 challenge, all mice given R1a-B6-mIgG1 and R1a-B6-mIgG2a (*n=16*) did not show any symptoms of influenza or any appreciable weight loss for the 13 day challenge window, demonstrating the cross-subtype prophylactic efficacy of the R1a-B6 Fc fusions. There was also no difference between the two different isotype variants of R1a-B6 as both provided complete protection (**Figure 5.14b-e**). However, unlike the CA/09 challenge, there was no delay in the onset of infection in the group that received monovalent R1a-B6 suggesting that the level of R1a-B6 sustained in mouse sera (**Figure 5.14a**) was not sufficient to protect mice against the H5N1 challenge. This may be due to the higher pathogenicity of wild type H5N1, from which our mouse-adapted strain is derived, compared to CA/09, with the virus having a higher replication rate resulting in more severe clinical outcomes [52, 98], similar to what we have observed (**Figure 14b-c**). It was also previously shown that treatment of H5N1 viruses required higher doses of antiviral to obtain and maintain sufficient systemic drug concentrations [144], something that cannot be achieved with monovalent R1a-B6. This is opposed to what was observed in the CA/09 challenge (**Figure 5.10b-c**).

The extent of protection against NIBRG-14ma (VN/04) conferred by AAV delivery of R1a-B6 was further characterized by determining $TCID_{50}$ and scoring the level of inflammation in lung tissue via H&E staining. To this effect, 3 mice per group 3-days post-challenge were culled in addition to the 8 mice per group as they reached the mandated study endpoint. For both time points, 3 days-post-challenge and when mice were culled during the study, R1a-B6-mIgG1 and R1a-B6-mIgG2a were found to have significantly lower $TCID_{50}$/g of VN/04 than mice given R1a-B6, cAb1-mIgG2a, and PBS *(*$p < 0.05$)* (**Figure 5.15**). Specifically, no virus was detected in the lungs of mice receiving R1a-B6-Fc fusions at either time point (**Figure 5.15**). In contrast, virus

could be detected in groups given R1a-B6, cAb1-mIgG2a, and PBS for both time periods (**Figure 5.15**). These mice (*n=24*) were culled on days 3-4 post-challenge and had average viral titers of $10^{6.7}$ $TCID_{50}$/g of NIBRG-14ma (**Figure 5.15**). In contrast to the CA/09 challenge study, there was no HAI activity against H5N1 either pre- or post-challenge in any of the groups (data not shown). It is speculated that the absence of head specific antibodies, which would be a surrogate indication of a natural immune response to influenza, is due to mice needing to be culled earlier, 3-4 days post-infection, which is insufficient time for mice to mount an immune response. For mice receiving the R1a-B6-Fc fusions, it is hypothesized that the virus was cleared before any immune response could be elicited, which is supported by the complete absence of detectable virus 3 days post challenge (**Figure 5.15a**).

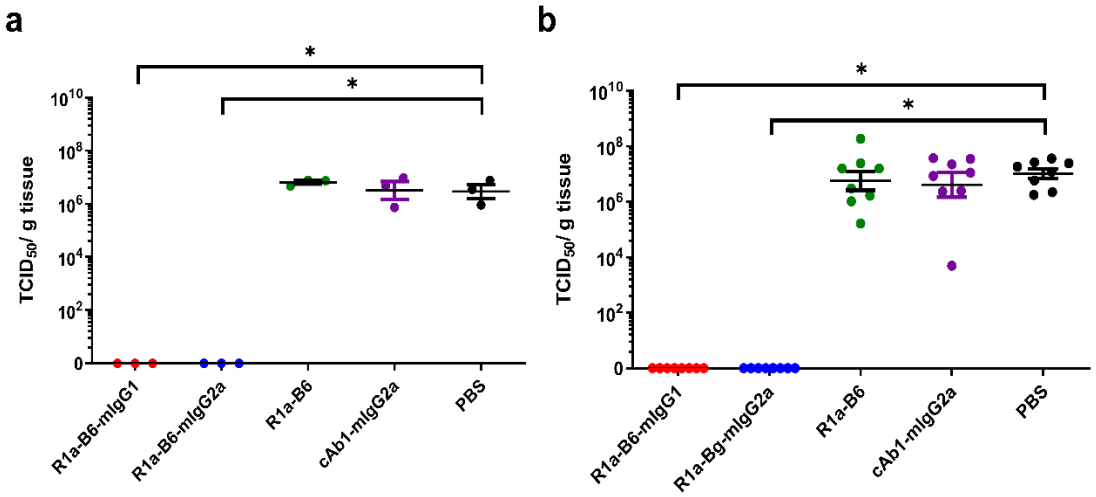

Figure 5.15. $TCID_{50}$ per gram lung tissue obtained from harvested lung samples from mice after VN/04 challenge. Viral titer was determined as indicated by $TCID_{50}$/g tissue from lung homogenates at (**a**) 3 days post-challenge (*n=3* mice/group) and (**b**) as mice were culled during the 13-day challenge window (*n=8* mice/group). For (**b**), lungs were harvested at 13 days for all mice given AAV-R1a-B6-mIgG1 and AAV-R1a-B6-mIgG2a, and on days 3-4 for mice given AAV-R1a-B6, AAV-cAb1-mIgG2a and PBS. Comparisons are shown via brackets (*$p<0.05$) as determined by Student's t-test.

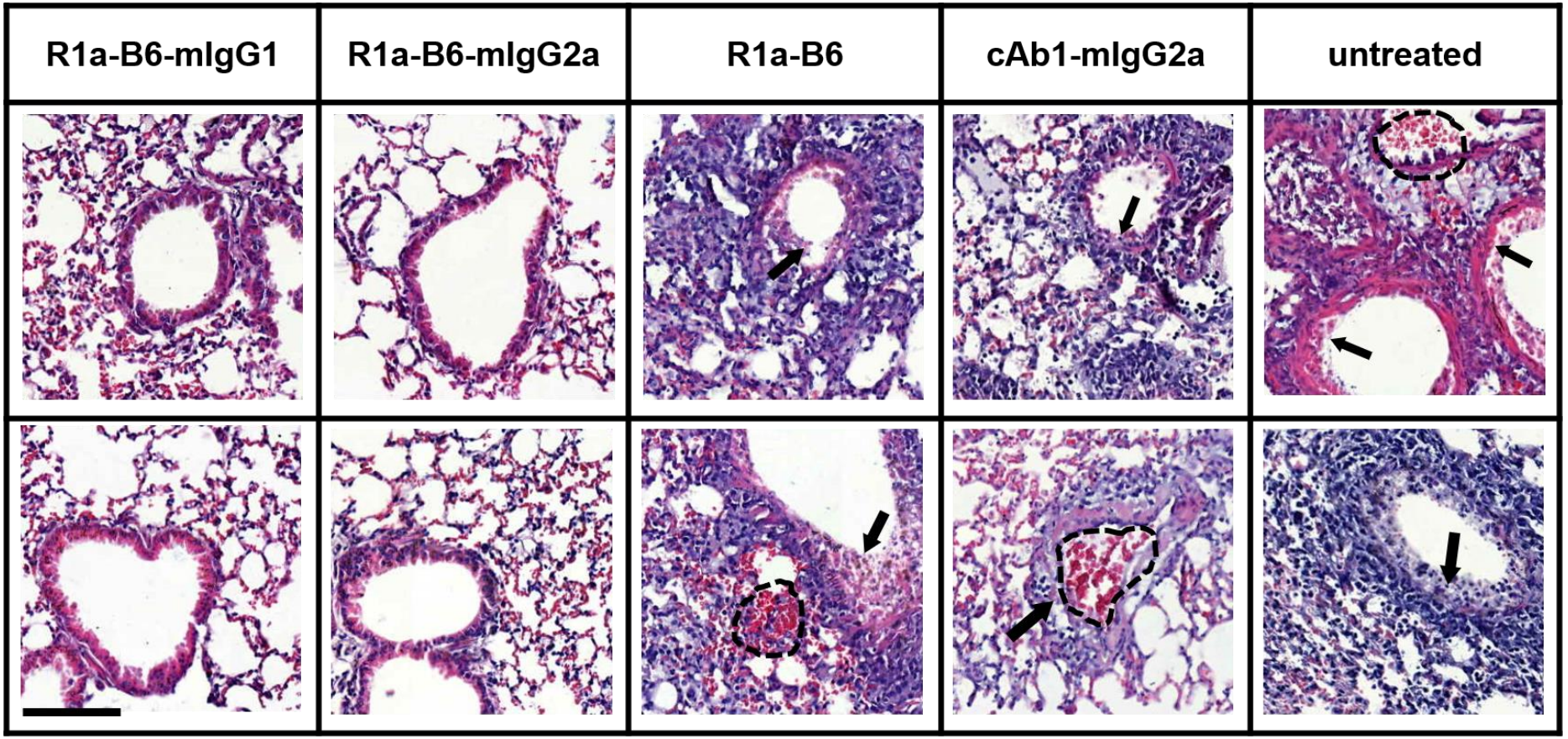

Figure 5.16. Representative histological lung sections from mice post-infection with VN/04 NIBRG-14ma. Lungs harvested 3 days post challenge are shown in the top row and terminal lung harvests on the bottom row. Terminal harvests were carried out on day 13 for mice given R1a-B6-mIgG1 and R1a-B6-mIgG2a, and on day 4 for mice given R1a-B6, cAb1-mIgG2a, and PBS. Lungs were then stained with Hematoxylin and Eosin (H&E). Lung ruptures are indicated by dashed lines and thickening of alveolar walls by arrows. Scale bar = 100 µm

At 3-days post-challenge, lungs taken from mice expressing R1a-B6-mIgG1 and R1a-B6-mIgG2a (*n=6*) showed no signs of inflammation with clear bronchioles and air sacs which is consistent with them having no viral load (**Figure 5.16 top row**), indicating full protection from influenza infection. In contrast, mice expressing R1a-B6, cAb1-mIgG2a, and those given PBS (*n=9*) demonstrated extensive infiltration of the bronchioles and air sacs, thickening of the perivascular wall, and lung ruptures as seen in the accumulation of red blood cells (RBCs) in the alveolar space three days post-infection and terminally (**Figure 5.16 top and bottom rows**). All mice given R1a-B6-mIgG1 and R1a-B6-mIgG2a survived until day 13, and H&E staining showed no inflammation in the lungs (*n=16*).

5.3 Discussion

Vaccination is the main strategy for influenza control, however, high-risk patient groups such as the elderly and immune-compromised, do not always respond well to vaccines. As such, the overall aim of the study was to provide an alternative prophylactic or therapeutic approach against influenza that is independent of the patient's immune system and the prior availability of the matching influenza strain. To accomplish this, gene therapy or vectored prophylaxis to deliver broadly neutralizing nanobody mouse Fc fusions which bind to conserved epitopes on influenza HA was employed.

The choice of Adeno-associated virus (AAV) as gene delivery vector was mainly due to its versatility and excellent safety profile [320, 342, 413]. AAV's flexibility enables it to transduce a wide array of tissues including skeletal muscle, which can serve as a production site for protein products that can act locally or systemically [329, 389]. This figures predominantly in the strategy to deliver the nanobody R1a-B6 [268], reformatted with a mouse Fc region (**Figure 3.1**) intramuscularly to protect mice from influenza.

Intramuscular delivery of AAV was explored instead of intranasal as others have chosen [355, 356, 387] as this has been reported to produce higher and more durable expression levels in systemic circulation [353, 354]. For example, in macaques, AAV expression in the nasal cavity was shown to decrease after 3-4 months likely due to the turnover of nasal epithelial cells and loss of transgene expression [355]. In contrast, the low turnover rate of muscle cells should, in principle, mean that the AAV transgenes can be maintained for much longer [336, 338]. This delivery method is also simpler to implement in a community setting alongside other immunizations.

R1a-B6 was expressed both as a single domain and as an Fc fusion of either mouse IgG1 or IgG2a isotype to evaluate the importance of half-life extension and effector function for *in vivo* efficacy. It was shown that a single IM injection gave robust expression of R1a-B6-Fc fusions (0.3 – 1.1 mg/mL) (**Figures 5.10a, 5.14a**) in the systemic circulation. High levels of nanobody Fc fusions were sustained for a minimum of 6 months with no observable ill effects (**Figure 5.5**). There was no reduction over time which suggests that there was no significant loss of transgenes, transfected cells or immune mediated clearance of R1a-B6 or AAV vector. The level of production is higher than previously reported for conventional human mAbs delivered intramuscularly (50-200 µg/mL) [354] or intranasally (1 µg/mL) [355, 387]. The very high serum concentration seen in this study might reflect the simpler nanobody transgene as compared to a conventional monoclonal antibody which requires the stable assembly of two light chains and two heavy chains inside the cell for successful secretion. It will be interesting to directly compare the impact of route of vector delivery on antibody efficacy because at present, it is unclear if localized AAV gene delivery in the nasal passages will be able to provide long term durable expression.

Complete protection of mice by R1a-B6 Fc fusion in challenge models covering two different influenza subtypes of pandemic potential was demonstrated. A(H1N1)pdm09 is now the existing seasonal influenza strain with vaccines being

manufactured annually to accommodate antigenic drift. A(H5N1) together with A(H7N9), highly pathogenic avian influenza viruses, are emerging pandemic threats [65, 89, 98], with various outbreaks already being documented. The choice of challenge virus was down to which strain is relevant now, in the case of A(H1N1)pdm09, and which strain will pose as an imminent problem in future in the case of A(H5N1).

The mice that survived from both challenges had no residual virus in their lungs and showed normal lung morphology with complete viral clearance (**Figures 5.11a, 5.12, 5.15, 5.16**). An HAI response post challenge with A(H1N1)pdm09 (**Figure 5.11b**) was also seen, suggesting that AAV delivery and expression of R1a-B6, which neutralizes virus after it has attached to host cells, and is itself HAI negative, did not interfere with the natural immune response against the virus. However, two mice given AAV-R1a-B6-mIgG1 survived the CA/09 challenge, did not show any influenza symptoms, and were negative for HAI antibodies post-infection. The same can be said for all mice that survived the VN/04 NIBRG14-ma challenge. Additionally, mice that survived the CA/09 MLD_{50} titration experiment had HAI titers that were less than 40, but still managed to survive. Herein lies the problem of the HAI assay as the main correlate of protection from influenza – as you do not need an HAI titer of ≥40 to be protected. A very efficient and fast-acting antibody as given prophylactically or passively, may be able to clear the virus right away, without the need for the immune system to mount a response. HA stem-binding antibodies are also known to be unable to inhibit hemagglutination, and their discovery was hampered by this bottleneck in previous years. The findings here therefore highlight the need for a better correlate of protection against influenza.

For the CA/09 challenge, monovalent R1a-B6 which was only detectable at very low levels in circulation (**Figure 5.10a**), was able to delay the onset of infection by at least 3 days after a lethal challenge with H1N1 (**Figure 5.10b**), with one mouse surviving until the end of the study. It can be inferred that continuous AAV production

of R1a-B6 partially offsets the rate of clearance by glomerular filtration in the kidneys, providing some protection even in the absence of Fc mediated half-life extension. However, fusion of R1a-B6 to an Fc fragment dramatically improved its pharmacokinetic and pharmacodynamic properties allowing protective levels to be reached over an extended period. The mechanism is expected to be due to FcRn-mediated recycling or Fc-mediated distribution and retention in tissues [368].

All these findings are satisfactory in this context and very encouraging going forward. However, several caveats need be considered if this therapy is to be brought to the clinic against an infectious disease such as influenza. The first is the use of an AAV2/8 vector to deliver broadly neutralizing antibodies. More people will then be exposed to this AAV vector, which would most likely lead to an increased seroprevalence of neutralizing antibodies against this serotype, decreasing its' utility for gene therapy as re-administration of the same serotype might lead to its' ablated function. This has been observed before upon repeated vector administration of the same serotype in immunocompetent mice, with neutralizing antibodies correlating with the amount of vector dose [414]. The second is the unabated high production of these monoclonal antibodies against influenza even without the presence of antigen. Given the serum concentrations of nanobody-Fc observed (**Figures 5.5, 5.10a, 5.14a**), this monoclonal antibody would make up about 10% of accepted serum IgG levels in a healthy adult. This has not been seen in a clinical setting, as usually it is very hard to get transgene levels up [339, 347, 348], nonetheless some form of AAV regulation is required. rAAV has been known to last in circulation for years [349], however, how permanent gene expression can be is yet to be determined.

Monoclonal antibodies which bind to the HA stem have been described as utilizing additional mechanisms to neutralize influenza virus *in vivo* through recruitment of the effector arm of the immune system via Fc-Fcγ receptor interaction [246, 247]. For instance, HA stem-binding antibodies have been reported to inhibit virus propagation by binding HA on virally infected cells and recruiting NK cells to mediate

ADCC [380, 415]. As R1a-B6 is functionally equivalent to other HA stem binding human mAbs [209, 210], it may also have the potential to utilize these additional mechanisms of action. To evaluate the extent ADCC might contribute to the *in vivo* efficacy of R1a-B6, the nanobody was re-formatted as either a mouse IgG2a-Fc fusion (ADCC +) or a mouse IgG1-Fc fusion (ADCC -) to ensure compatibility with mouse FcγRs as confirmed *in vitro* (**Figure 3.6**). As protection was complete with R1a-B6 formatted with either isotype we were not able to see any obvious difference in efficacy between R1a-B6-Fc fusions *in vivo* (**Figure 5.13**). This contrasts with previous studies using passive transfer of the stem binding human mAb FI6 which was similarly tested as a mouse IgG1 and IgG2a in the context of the mouse FcγR system, wherein only mice that received FI6-mouse-IgG2a showed 100% survival from lethal PR8 (H1N1) challenge and mice that received FI6-mouse-IgG1 were all culled [247]. However, further studies by the same group showed that the requirement for FcγR interactions and ADCC was dose dependent with the inference being that efficacy through passive transfer of high doses of FI6 was FcγR interaction independent [246]. It is speculated, as very high stable concentrations in serum of nanobody-Fc were generated using intramuscular AAV delivery of R1a-B6-mIgG2a and R1a-B6-mIgG1, that viral neutralization via inhibition of viral membrane fusion is sufficient to provide protection with no need for FcγR interactions. In addition, the protective effect of monovalent R1a-B6, albeit limited (**Figure 5.10b-c**,**f**), is an unexpected finding and again suggests continual expression *in vivo* may to some extent offset the need for Fc effector functions.

In this study it was shown that the use of adeno-associated virus (AAV) vectors to deliver R1a-B6 through a single IM injection is an attractive approach to confer cross-subtype protection against important influenza subtypes [89] which can enhance preparedness against future potential influenza pandemics. In addition, the data suggest that the potency of R1a-B6 does not depend on the coupling of Fc effector functions for recognition and neutralization of influenza HA. Highly pathogenic avian

influenza H5N1, as well as viruses of subtype H1N1, H2N2, and H9N2, continue to represent pandemic threats and, while pre-pandemic vaccines against these strains have been stockpiled by some governments, there is uncertainty as to exactly what strain could emerge or if these vaccines would be sufficiently effective particularly in at risk patient groups. This alternative approach mitigates these risks and combines the advantages of AAV mediated gene therapy with highly potent cross-neutralizing nanobodies against influenza to provide broad protection independent of the prior availability of the influenza strain and the need for a natural host induced immune response.

CHAPTER 6

CONCLUSION AND FUTURE DIRECTIONS

Influenza infection still contributes to morbidity and mortality in humans and livestock worldwide even with successful vaccination paradigms already in place. There is also the ever-present threat of a pandemic brought about by novel influenza subtypes to which the population has no pre-existing immunity and of which seasonal vaccines may be unable to protect against. Several studies post A(H1N1) 2009 pandemic have shown that seasonal vaccination may have increased the risk of being infected by the pandemic A(H1N1) strain with illness being associated with the receipt of the inactivated influenza seasonal vaccine [132, 133, 416]. These findings warrant further investigation on the utility of seasonal vaccines to alleviate pandemic impact. Lessons from the past have shown us, that despite our efforts, we are still unprepared to mitigate the devastating loss of life and livelihood when the next pandemic comes around.

Current seasonal influenza virus vaccines are hampered by limitations such as annual reformulation to counter antigenic drift, timely production and distribution. Protection provided by these vaccines is partial if any at all against novel strains which arise from antigenic shift or viral gene reassortment in susceptible hosts such as occurs in a pandemic. Ideally, vaccines should be able to protect against both drifted and shifted strains, and this is the goal of a universal influenza vaccine. Efforts towards its development have been encouraged by the discovery of broadly neutralizing antibodies (bnAb) against influenza that target conserved epitopes on the hemagglutinin (HA) stem region. However, antibodies produced via seasonal vaccination are mostly targeted against the immunodominant HA head domain producing a narrow strain-specific response [16, 168, 170]. As such, efforts have been made to produce vaccines that target conserved regions of the influenza virus including the HA stalk domain, the ectodomain of the M2 ion channel or the internal matrix and

nucleoproteins to confer broad protection against all influenza A and B viruses [111]. Harnessing the cross-subtype neutralizing potential of antibodies produced via these targeted vaccinations may be enough to contain seasonal influenza and to prepare against a future pandemic [213].

Moreover, bnAbs can also be utilized as prophylactic or therapeutic tools that may prove useful to patient populations that do not respond well to vaccination. Most of the earliest bnAbs discovered bind to conserved HA stem epitopes using only their heavy chains [210, 238]. In this study, R1a-B6 [268], a novel alpaca-derived nanobody that was previously found to have cross-subtype neutralizing ability against Group I Influenza A strains, was employed as an alternative to conventional mAbs to combat influenza. The nanobody's beneficial biochemical and physical properties such as size, affinity and specificity to antigen, stability, and cheaper production costs and ease of engineering make them attractive tools for research and medicine [254, 260, 417].

In this study, an alternative strategy to vaccination and passive immunotherapy employing bnAbs against influenza that involves the use of gene therapy via AAV delivery of R1a-B6 was presented. This is to provide sufficient long-term protection through antibody production within the patient. R1a-B6 was also reformatted with a mouse Fc of IgG1 and IgG2a isotype to improve its half-life and in the case of mouse IgG2a, to enable it to recruit effector functions such as ADCC *in vivo.* This is in line with our overall goal to design and evaluate an optimal nanobody format that can be employed for immunotherapy against influenza.

R1a-B6-Fc demonstrated cross-subtype binding and neutralization of different Group I influenza A subtypes *in vitro*. The gene therapy approach employed here is also distinct to recent studies that have tried AAV delivery [355, 357, 387] in that intramuscular (IM) delivery via AAV8 of nanobody-Fc genes was explored, instead of AAV9 intranasal (IN) delivery to achieve substantial levels of nanobody-Fc (0.5-1 mg/mL) in circulation for up to 6 months without decline. *In vitro* findings also translated to *in vivo* protection against lethal challenge with pandemic H1N1 and avian

influenza H5N1 in mice. The activation of effector functions did not seem to play a role in protection afforded by R1a-B6-Fc when given via IM AAV delivery, as both R1a-B6-mIgG1 (ADCC-) and R1a-B6-mIgG2a (ADCC+) nanobodies provided complete protection from influenza in our mouse challenge models. Mice did not show any symptoms of influenza during the study window and there was no difference in survival between groups of mice given R1a-B6-mIgG1 and R1a-B6-mIgG2a. It could be that the serum titers at the time of challenge were too high to see any effect in the levels of protection so any patterns related to ADCC function could not be distinguished.

To further develop anti-influenza nanobody-based prophylaxis via AAV towards clinical use, several improvements or probable additions to the nanobody construct and AAV vector in future must be made. This method should also be validated both as a prophylactic via AAV delivery and as a therapeutic treatment option via passive immunotherapy for high risk and vulnerable groups, the targets of the study. Several follow-up experiments to achieve these goals are highlighted below.

Increasing the influenza viral challenge dose to sublethal doses or decreasing the AAV dose in the mouse challenge models can be done next to see if a differentiating response between R1a-B6-mIgG1 and mIgG2a Fc fusion constructs can be found. Moreover, as protection was seen in immunocompetent mice, it would be good to assess if the same strategy would be effective in immunocompromised animals that can represent the primary target population. For these experiments, severe combined immunodeficient (SCID) BALB/c mice will be utilized in place of immunocompetent mice in a lethal A/California/07/2009(H1N1)pdm09 challenge experiment. This is also to demonstrate the ability of R1a-B6-Fc to provide protection in the absence of a functioning natural immune system. Independence from the host immune system is an attractive facet to include when considering the optimal approach for long-term antibody expression *in vivo* against a variable pathogen such as influenza.

Given its anti-influenza *in vitro* potency and *in vivo* efficacy, the use of R1a-B6 as an immunotherapeutic via passive delivery is also another attractive option. The nanobody-Fc format employed in this study is very versatile making it suitable for prophylactic or therapeutic administration, depending on the situation and need. To realize this goal, the nanobody must be modified for human use. Camelid V_HH domains have low immunogenicity [273] and this can be attributed to their high sequence identity with human type 3 V_H domains (V_H3) [250]. However, humanization is still necessary to lessen any possible side effects and to ensure that titers are maintained for the intended duration. Humanization is accomplished by substitution of divergent framework residues to their human heavy chain variable domain equivalents [270]. The challenge in humanizing these nanobodies is making the right choice in mutating framework region residues that would not compromise the specificity or solubility of the nanobody or the heavy chain antibody [284]. Safety and flexibility of mAb based therapeutics are also valuable when treating special populations like children, elderly or pregnant women due to the lower tolerability and higher risks associated with potential side effects in these populations [205].

The development of an alternative half-life extension strategy for nanobodies that does not involve addition of an Fc region should also be looked at. If ADCC is not required for the nanobody to provide a protective effect against influenza as findings in this study suggest, the Fc region can be excluded from the final therapeutic product. It is conceded however that the ADCC assay that was used in the study may not mirror what is actually taking place *in vivo* during infection. The information that can be gleaned from the assay that was employed is that the mouse Fc fused to the nanobody was able to activate mouse FcγRIV in the effector cells provided. If ADCC did or did not take place should still be investigated. The best way to do this is to employ FcγR knockout mice to determine if ADCC does play a role in influenza protection via AAV delivered immunoprophylaxis of R1a-B6.

Eliminating the Fc mitigates some of the concerns of antibody dependent enhancement of influenza [418-420] mediated by interactions with the effector arm of the immune system or pro-inflammatory functions that can lead to cytokine release and other toxic side effects [421]. In addition, this may reduce the risk of transgene immunogenicity through Fc mediated uptake and antigen presentation by immune cells [291, 415]. Thus, a strategy of coupling the nanobody to serum albumin that utilizes mechanisms similar to IgG to stay in circulation longer is being explored.

It should also be pointed out that R1a-B6 is highly potent against Group I Influenza A (IAV) strains but is unable to neutralize viruses from Group II IAV and Influenza B viruses. Discovery of other nanobodies that may be combined with R1a-B6 to protect from both Group I and Group II IAVs and Influenza B is also a possibility. Several nanobodies may be linked together to produce the final therapeutic product. Nonetheless, broadening R1a-B6's cross-reactivity to include Influenza A Group II subtypes and to test whether these molecular changes, when employed, will be effective in influenza neutralization *in vitro* and protection *in vivo* is already underway. Site-directed mutagenesis of R1a-B6's paratope, comprising CDRs and other FR residues that are involved in antigen interaction is now being undertaken at NIBSC. Additionally, these modified nanobodies can also be tested against influenza viruses with mutations in the HA stem region that are likely to escape neutralization by R1a-B6 [219].

It was shown here that intramuscular delivery of AAV8 demonstrated high levels of nanobody-Fc in systemic circulation for up to 6 months with no signs of decrease and no observable side effects in mice. Nonetheless, intranasal delivery of AAV5, AAV6 or AAV9, may also be useful as delivery can be targeted locally at the site of infection in the lungs [357, 387, 422]. However, this also comes with the caveats of quicker cell turnover and recent reports of systemic and sensory neuron toxicity as a direct consequence of transduction in the case of AAV9 [344]. At present,

there is still no best AAV serotype and delivery combination for influenza and further studies comparing these options need to be carried out.

Aside from harnessing the different tropisms of natural AAV serotypes, progress in gene transfer technology has also paved the way for targeted *in vivo* delivery by using specific cell surface markers for cell entry instead of natural AAV receptors [423]. This "receptor targeting" may mitigate particle accumulation in the liver and spleen from systemic AAV administration [423]. Employing promoters that are only active in the relevant cell type may also be utilized [423]. Additionally, engineered AAV mutant strains or chimeras that may be employed for preferential targeting that gives rise to novel tropisms can also be investigated [333, 334].

The sustainability and possible side effects over time of this approach also warrant some consideration. How this strategy will operate side by side with vaccination and how it will affect responses to circulating seasonal influenza is yet to be determined. AAV therapies that are commercially available are very costly but are marketed as "one-shot for a lifetime" regimens [342, 343], potentially making them more cost-effective in the long run. A one-time intramuscular immunization of a broadly neutralizing antibody against influenza seems an attractive option that will ease the difficulties inherently associated with annual vaccinations, and importantly may provide protection against pandemics. AAV vectors persist in tissues primarily as episomes and integration in animal tissues is a rare event [321, 335]. These episomes are not cleared from cells and continuous expression of the transgene by the AAV vector has been observed in human clinical trials [348, 349]. However, several cases of hepatic cell carcinoma in neonatal mice have been reported which have been linked to high AAV vector dose and integration to a specific gene locus [385]. Although uncommon, these murine studies that have documented insertional mutagenesis of AAV vectors leading to genotoxicity have led to a more stringent evaluation of the potential risks and possible solutions associated with AAV-mediated gene therapy. Moreover, issues will remain long into the future of whether production of potent anti-

influenza antibodies over a long period of time would be detrimental to the host or would drive the emergence of viral escape mutants. Resistant viruses selected in the presence of a broadly neutralizing HA stalk-binding antibody have been reported in the past, however, compared to the wild type virus, these viruses release fewer progeny during replication and are also more sensitive to antivirals, suggesting reduced viral fitness [424].

To circumvent the issue of uncontrolled and untargeted AAV expression of transgene that can lead to unwanted immune responses, an “on” or “off” switch can be utilized. microRNAs (miRNA) are thought to sequence-specifically control translation of target mRNAs by binding to sites of antisense complementarity in 3’ untranslated regions (UTRs) suppressing its expression by mRNA destabilization in cells/tissues expressing the cognate miRNA (switch-OFF) [425-428]. Suppression can be fine-tuned by varying the degree of complementarity between miRNA and the binding site. This has also been useful to prevent priming of transgene-specific T cells thereby reducing transgene-directed immunity in mice following intramuscular AAV vector administration [429]. Repression of AAV expression outside target sites has also been done leading to stable and more specific transgene expression [430]. This elegant mechanism can be employed to control expression of broadly neutralizing antibodies against influenza that will be administered via AAV delivery.

In future, for large-scale output, alternative AAV production methods that utilize suspension cell culture systems such as Sf9 insect cells and recombinant baculovirus infection, stable mammalian packaging cell lines, and HSV-1 vectors providing Rep–Cap and rAAV helper functions [332, 391] can be employed. Addition of a reporter gene such as luciferase or GFP would also be helpful for titration experiments. However, it was chosen to not include these reporter genes in the rAAV system to make a lean construct that is well within that of the packaging capacity of AAV. For purification, methods such as combined ion exchange chromatography and affinity purification are now available and can be employed going forward.

The hypothesis that the effector arm of the immune system is not essential for R1a-B6 to provide sufficient protection against influenza in mice opens up new opportunities for designing an optimized transgene using alternative approaches to half-life extension [266, 431]. Further improvements to R1a-B6 may be done to improve specificity, breadth of activity, and to reduce the chance of viral escape mutants. Additionally, nanobodies similar to R1a-B6 with potential neutralizing activity against various influenza strains [268, 367] may be engineered and combined to target different antigenic sites giving rise to neutralizing antibody responses that should pose a daunting challenge for viral escape.

Given these advantages and potential weaknesses, future clinical trials are the only way to demonstrate how realistic this approach against pandemic influenza can be. With these future prospects, our results from gene therapy of a cross-subtype neutralizing nanobody via AAV delivery have been encouraging and have led to new discoveries that would pave the way for enhanced pandemic preparedness and long term durable protection against influenza independent of the immune response in vulnerable patient groups.

CHAPTER 7

REFERENCES

1. Animal Influenza Virus. 2 ed. Methods in Molecular Biology, ed. Walker, J. Vol. 1161. 2014: Humana Press.
2. Bouvier, N.M. and Palese, P. The biology of influenza viruses. *Vaccine,* 2008. **26**: p. D49-D53.
3. Petrova, V.N. and Russell, C.A. The evolution of seasonal influenza viruses. *Nat Rev Microbiol,* 2018. **16**(1): p. 47-60.
4. World Health Organization. Influenza virus infection in humans. 2014; Available from: http://www.who.int/influenza/human_animal_interface/virology_laboratories_and_vaccines/influenza_virus_infections_humans_feb14.pdf?ua=1.
5. World Health Organization. Influenza (Seasonal). 2018; Available from: http://www.who.int/news-room/fact-sheets/detail/influenza-(seasonal).
6. Vemula, S.V., Sayedahmed, E.E., Sambhara, S., and Mittal, S.K. Vaccine approaches conferring cross-protection against influenza viruses. *Expert Rev Vaccines,* 2017. **16**(11): p. 1141-1154.
7. Wiley, D.C. and Skehel, J.J. The Structure and Function of the Hemagglutinin Membrane Glycoprotein of Influenza Virus. *Ann. Rev. Biochem,* 1987. **56**: p. 365-94.
8. de Vries, R.P., de Vries, E., Bosch, B.J., de Groot, R.J., Rottier, P.J., and de Haan, C.A. The influenza A virus hemagglutinin glycosylation state affects receptor-binding specificity. *Virology,* 2010. **403**(1): p. 17-25.
9. Skehel, J.J. and Wiley, D.C. Receptor Binding and Membrane Fusion in Virus Entry: The Influenza Hemagglutinin. *Annu. Rev. Biochem.,* 2000. **69**: p. 531-69.
10. Gottschalk, A. The Influenza Virus Neuraminidase. *Nature,* 1958. **181**.
11. McAuley, J.L., Gilbertson, B.P., Trifkovic, S., Brown, L.E., and McKimm-Breschkin, J.L. Influenza Virus Neuraminidase Structure and Functions. *Front Microbiol,* 2019. **10**: p. 39.
12. Dou, D., Revol, R., Ostbye, H., Wang, H., and Daniels, R. Influenza A Virus Cell Entry, Replication, Virion Assembly and Movement. *Front Immunol,* 2018. **9**: p. 1581.
13. Arranz, R., Coloma, R., Javier, F., Chichón, J., Carrascosa, J., Valpuesta, J., Ortín, J., and Martín-Benito, J. The Structure of Native Influenza Virion Ribonucleoproteins. *Science,* 2012. **338**.
14. Moeller, A., Kirchdoerfer, R., Potter, C., Carragher, B., and Wilson, I. Organization of the Influenza Virus Replication Machinery. *Science,* 2012. **338**(6114): p. 1631-1634.
15. Bizebard, T., Gigant, B., Rigolet, P., Rasmussen, B., Diat, O., Bosecke, P., Wharton, S., Skehel, J.J., and Knossow, M. Structure of influenza virus

haemagglutinin complexed with a neutralizing antibody. *Nature,* 1995. **376**: p. 92-4.

16. Kirkpatrick, E., Qiu, X., Wilson, P.C., Bahl, J., and Krammer, F. The influenza virus hemagglutinin head evolves faster than the stalk domain. *Sci Rep,* 2018. **8**(1): p. 10432.

17. Popova, L., Smith, K., West, A.H., Wilson, P.C., James, J.A., Thompson, L.F., and Air, G.M. Immunodominance of antigenic site B over site A of hemagglutinin of recent H3N2 influenza viruses. *PLoS One,* 2012. **7**(7): p. e41895.

18. Gao, J., Couzens, L., Burke, D.F., Wan, H., Wilson, P., Memoli, M.J., Xu, X., Harvey, R., Wrammert, J., Ahmed, R., Taubenberger, J.K., Smith, D.J., Fouchier, R.A.M., and Eichelberger, M.C. Antigenic Drift of the Influenza A(H1N1)pdm09 Virus Neuraminidase Results in Reduced Effectiveness of A/California/7/2009 (H1N1pdm09)-Specific Antibodies. *MBio,* 2019. **10**(2).

19. Wiley, D.C., Wilson, I.A., and Skehel, J.J. Structural identification of the antibody-binding sites of Hong Kong influenza haemagglutinin and their involvement in antigenic variation. *Nature,* 1981. **289**(5796): p. 373-8.

20. Wilson, J.R., Guo, Z., Tzeng, W.P., Garten, R.J., Xiyan, X., Blanchard, E.G., Blanchfield, K., Stevens, J., Katz, J.M., and York, I.A. Diverse antigenic site targeting of influenza hemagglutinin in the murine antibody recall response to A(H1N1)pdm09 virus. *Virology,* 2015. **485**: p. 252-62.

21. Shih, A.C., Hsiao, T.C., Ho, M.S., and Li, W.H. Simultaneous amino acid substitutions at antigenic sites drive influenza A hemagglutinin evolution. *Proc Natl Acad Sci U S A,* 2007. **104**(15): p. 6283-8.

22. Russell, C.J., Hu, M., and Okda, F.A. Influenza Hemagglutinin Protein Stability, Activation, and Pandemic Risk. *Trends Microbiol,* 2018.

23. Prevention, C.f.D.C.a. 2009 H1N1 Flu ("Swine Flu") and You. 2010; Available from: https://www.cdc.gov/h1n1flu/qa.htm.

24. Cauldwell, A.V., Long, J.S., Moncorge, O., and Barclay, W.S. Viral determinants of influenza A virus host range. *J Gen Virol,* 2014. **95**(Pt 6): p. 1193-1210.

25. Long, J.S., Mistry, B., Haslam, S.M., and Barclay, W.S. Host and viral determinants of influenza A virus species specificity. *Nat Rev Microbiol,* 2019. **17**(2): p. 67-81.

26. Chaisri, U. and Chaicumpa, W. Evolution of Therapeutic Antibodies, Influenza Virus Biology, Influenza, and Influenza Immunotherapy. *Biomed Res Int,* 2018. **2018**: p. 9747549.

27. Russell, R.J., Gamblin, S.J., Haire, L.F., Stevens, D.J., Xiao, B., Ha, Y., and Skehel, J.J. H1 and H7 influenza haemagglutinin structures extend a structural classification of haemagglutinin subtypes. *Virology,* 2004. **325**(2): p. 287-96.

28. Tong, S., Zhu, X., Li, Y., Shi, M., Zhang, J., Bourgeois, M., Yang, H., Chen, X., Recuenco, S., Gomez, J., Chen, L.M., Johnson, A., Tao, Y., Dreyfus, C., Yu, W., McBride, R., Carney, P.J., Gilbert, A.T., Chang, J., Guo, Z., Davis, C.T., Paulson, J.C., Stevens, J., Rupprecht, C.E., Holmes, E.C., Wilson, I.A.,

and Donis, R.O. New world bats harbor diverse influenza A viruses. *PLoS Pathog,* 2013. **9**(10): p. e1003657.

29. Gamblin, S.J. and Skehel, J.J. Influenza hemagglutinin and neuraminidase membrane glycoproteins. *The Journal of biological chemistry,* 2010. **285**(37): p. 28403-28409.

30. Acton, Q.A. H1N1 Virus: New Insights for the Healthcare Professional: 2013 Edition. 2013: ScholarlyEditions.

31. Behrens, G., Gottschalk, R., Gürtler, L., Harder, T.C., Hoffmann, C., Kamps, B.S., Korsman, S., Preiser, W., Reyes-Terán, G., Stoll, M., Werner, O., and van Zyl, G. Influenza Report 2006. 2006, Paris, Cagliari, Wuppertal, Sevilla: Flying Publisher.

32. Cheng, W., Wang, X., Shen, Y., Yu, Z., Liu, S., Cai, J., and Chen, E. Comparison of the three waves of avian influenza A(H7N9) virus circulation since live poultry markets were permanently closed in the main urban areas in Zhejiang Province, July 2014-June 2017. *Influenza Other Respir Viruses,* 2018. **12**(2): p. 259-266.

33. Huo, X., Chen, L., Qi, X., Huang, H., Dai, Q., Yu, H., Xia, Y., Liu, W., Xu, K., Ma, W., Zhang, J., and Bao, C. Significantly elevated number of human infections with H7N9 virus in Jiangsu in eastern China, October 2016 to January 2017. *Euro Surveill,* 2017. **22**(13).

34. Kashyap, A., Steel, J., Oner, A., Dillon, M., Swale, R., Wall, K., Perry, K., Faynboym, A., Ilhan, M., Horowitz, M., Horowitz, L., Palese, P., Bhatt, R., and Lerner, R. Combinatorial antibody libraries from survivors of the Turkish H5N1 avian influenza outbreak reveal virus neutralization strategies. *PNAS,* 2008. **105**(16): p. 5986-5991.

35. Taubenberger, J.K. and Morens, D.M. Influenza: The Once and Future Pandemic. *Public Health Reports,* 2010. **125**.

36. Matsuoka, Y., Matsumae, H., Katoh, M., Eisfeld, A.J., Neumann, G., Hase, T., Ghosh, S., Shoemaker, J.E., Lopes, T.J., Watanabe, T., Watanabe, S., Fukuyama, S., Kitano, H., and Kawaoka, Y. A comprehensive map of the influenza A virus replication cycle. *BMC Systems Biology,* 2013. **7**(97).

37. Wilson, I.A., Skehel, J.J., and Wiley, D.C. Structure of the haemagglutinin membrane glycoprotein of influenza virus at 3 A resolution. *Nature,* 1981. **289**(5796): p. 366-73.

38. Couceiro, J., Paulson, J., and Baum, L. Influenza virus strains selectively recognize sialyloligosaccharides on human respiratory epithelium; the role of the host cell in selection of hemagglutinin receptor specificity. *Virus Research,* 1993. **29**: p. 155-165.

39. Matrosovich, M.N., Matrosovich, T.Y., Gray, T., Roberts, N.A., and Klenk, H.D. Human and avian influenza viruses target different cell types in cultures of human airway epithelium. *Proc Natl Acad Sci U S A,* 2004. **101**(13): p. 4620-4.

40. Imai, M. and Kawaoka, Y. The role of receptor binding specificity in interspecies transmission of influenza viruses. *Curr Opin Virol,* 2012. **2**(2): p. 160-7.

41. Matlin, K., Reggio, H., Helenius, A., and Simons, K. Infectious Entry Pathway of Influenza Virus in a Canine Kidney Cell Line*. The Journal of Cell Biology,* 1981. **91**: p. 601-613.

42. Maeda, T. and Ohnishi, S. Activation of influenza virus by acidic media causes hemolysis and fusion of erythrocytes*. FEBS Letters,* 1980. **122**(2): p. 283-287.

43. Webster, R. and Rott, R. Influenza Virus A Pathogenicity: The Pivotal Role of Hemagglutinin*. Cell,* 1987. **50**: p. 665-666.

44. Martin, K. and Helenius, A. Transport of incoming influenza virus nucleocapsids into the nucleus*. Journal of Virology,* 1991. **65**(1): p. 232-244.

45. Herz, C., Stavnezer, E., Krug, R.M., and Gurney Jr, T. Influenza virus, an RNA virus, synthesizes its messenger RNA in the nucleus of infected cells*. Cell,* 1981. **26**(3): p. 391-400.

46. Engelhardt, O.G. and Fodor, E. Functional association between viral and cellular transcription during influenza virus infection*. Rev Med Virol,* 2006. **16**(5): p. 329-45.

47. Krug, R. Priming of influenza viral RNA transcription by capped heterologous RNAs., in *Current Topics in Microbiology and Immunology*, Shatkin, A.J., Editor. 1981. p. 125-149.

48. Rossman, J.S. and Lamb, R.A. Influenza virus assembly and budding*. Virology,* 2011. **411**(2): p. 229-36.

49. Calder, L.J., Wasilewski, S., Berriman, J.A., and Rosenthal, P.B. Structural organization of a filamentous influenza A virus*. Proc Natl Acad Sci U S A,* 2010. **107**(23): p. 10685-90.

50. Vavricka, C.J., Liu, Y., Kiyota, H., Sriwilaijaroen, N., Qi, J., Tanaka, K., Wu, Y., Li, Q., Li, Y., Yan, J., Suzuki, Y., and Gao, G.F. Influenza neuraminidase operates via a nucleophilic mechanism and can be targeted by covalent inhibitors*. Nat Commun,* 2013. **4**: p. 1491.

51. Gottschalk, A. Neuraminidase: the specific enzyme of influenza virus and Vibrio cholerae*. Biochimica et Biophysica Acta,* 1957. **23**: p. 645-646.

52. Klenk, H.D., Garten, W., and Matrosovich, M. Molecular mechanisms of interspecies transmission and pathogenicity of influenza viruses: Lessons from the 2009 pandemic*. Bioessays,* 2011. **33**(3): p. 180-8.

53. Zambon, M.C. Epidemiology and pathogenesis of influenza*. Journal of Antimicrobial Chemotherapy,* 1999. **44**.

54. Han, S.N. and Meydani, N. Antioxidants, Cytokines, and Influenza Infection in Aged Mice and Elderly Humans*. The Journal of Infectious Diseases,* 2000. **182(Suppl 1)**: p. S74–80.

55. Chen, X., Liu, S., Goraya, M.U., Maarouf, M., Huang, S., and Chen, J.L. Host Immune Response to Influenza A Virus Infection*. Front Immunol,* 2018. **9**: p. 320.

56. Liu, Q., Zhou, Y.H., and Yang, Z.Q. The cytokine storm of severe influenza and development of immunomodulatory therapy*. Cell Mol Immunol,* 2016. **13**(1): p. 3-10.

57. Van Reeth, K. Cytokines in the pathogenesis of in¯uenza. *Veterinary Microbiology,* 2000. **74**: p. 109-16.

58. Yang, M.L., Wang, C.T., Yang, S.J., Leu, C.H., Chen, S.H., Wu, C.L., and Shiau, A.L. IL-6 ameliorates acute lung injury in influenza virus infection. *Sci Rep,* 2017. **7**: p. 43829.

59. Böttcher-Friebertshäuser, E., Garten, W., Matrosovich, M., and Klenk, H.D. The Hemagglutinin: A Determinant of Pathogenicity, in *Influenza Pathogenesis and Control*, Compans, R.W. and Oldstone, M.B.A., Editors. 2014, Springer.

60. Neumann, G. and Kawaoka, Y. Transmission of influenza A viruses. *Virology,* 2015. **479-480**: p. 234-46.

61. Zambon, M.C. The pathogenesis of influenza in humans. *Rev Med Virol,* 2001. **11**(4): p. 227-41.

62. Haga, T. and Horimoto, T. Animal Models to Study Influenza Virus Pathogenesis and Control. *The Open Antimicrobial Agents Journal,* 2010. **2**: p. 15-21.

63. World Health Organization. Influenza (Avian and other zoonotic). 2018; Available from: https://www.who.int/news-room/fact-sheets/detail/influenza-(avian-and-other-zoonotic).

64. Roche, B., Lebarbenchon, C., Gauthier-Clerc, M., Chang, C.M., Thomas, F., Renaud, F., van der Werf, S., and Guegan, J.F. Water-borne transmission drives avian influenza dynamics in wild birds: the case of the 2005-2006 epidemics in the Camargue area. *Infect Genet Evol,* 2009. **9**(5): p. 800-5.

65. World Health Organization, Avian influenza: assessing the pandemic threat. 2005.

66. Bosch, F.X., Garten, W., Klenk, H.D., and Rott, R. Proteolytic Cleavage of Influenza Virus Hemagglutinins: Primary Structure of the Connecting Peptide between HA, and HA2 Determines Proteolytic Cleavability and Pathogenicity of Avian Influenza Viruses. *Virology,* 1981. **113**: p. 725-735.

67. Garten, W. and Klenk, H.D. Understanding Influenza Virus Pathogenicity. *Trends in Microbiology,* 1999. **7**(3).

68. Temperton, N.J., Hoschler, K., Major, D., Nicolson, C., Manvell, R., Hien, V.M., Ha do, Q., de Jong, M., Zambon, M., Takeuchi, Y., and Weiss, R.A. A sensitive retroviral pseudotype assay for influenza H5N1-neutralizing antibodies. *Influenza Other Respir Viruses,* 2007. **1**(3): p. 105-12.

69. Guo, Y., Rumschlag-Booms, E., Wang, J., Xiao, H., Yu, J., Wang, J., Guo, L., Gao, G.F., Cao, Y., Caffrey, M., and Rong, L. Analysis of hemagglutinin-mediated entry tropism of H5N1 avian influenza. *Virol J,* 2009. **6**: p. 39.

70. Qi, W., Jia, W., Liu, D., Li, J., Bi, Y., Xie, S., Li, B., Hu, T., Du, Y., Xing, L., Zhang, J., Zhang, F., Wei, X., Eden, J.S., Li, H., Tian, H., Li, W., Su, G., Lao, G., Xu, C., Xu, B., Liu, W., Zhang, G., Ren, T., Holmes, E.C., Cui, J., Shi, W., Gao, G.F., and Liao, M. Emergence and Adaptation of a Novel Highly Pathogenic H7N9 Influenza Virus in Birds and Humans from a 2013 Human-Infecting Low-Pathogenic Ancestor. *J Virol,* 2018. **92**(2).

71. Su, W., Cheng, K.L., Chu, D.K.W., Zhou, J., Mao, X., Zhong, Z., Song, Y., Peiris, M., Wu, J., and Yen, H.L. Genetic analysis of H7N9 highly pathogenic avian influenza virus in Guangdong, China, 2016-2017. *J Infect,* 2018. **76**(1): p. 93-96.

72. Yang, H., Carney, P.J., Chang, J.C., Guo, Z., and Stevens, J. Structural and Molecular Characterization of the Hemagglutinin from the Fifth-Epidemic-Wave A(H7N9) Influenza Viruses. *J Virol,* 2018. **92**(16).

73. Zhu, W., Zhou, J., Li, Z., Yang, L., Li, X., Huang, W., Zou, S., Chen, W., Wei, H., Tang, J., Liu, L., Dong, J., Wang, D., and Shu, Y. Biological characterisation of the emerged highly pathogenic avian influenza (HPAI) A(H7N9) viruses in humans, in mainland China, 2016 to 2017. *Euro Surveill,* 2017. **22**(19).

74. Taubenberger, J.K. The Origin and Virulence of the 1918 “Spanish” Influenza Virus. *Proc Am Philos Soc,* 2006. **150**(1): p. 86-112.

75. Hanson, A., Imai, M., Hatta, M., McBride, R., Imai, H., Taft, A., Zhong, G., Watanabe, T., Suzuki, Y., Neumann, G., Paulson, J.C., and Kawaoka, Y. Identification of Stabilizing Mutations in an H5 Hemagglutinin Influenza Virus Protein. *J Virol,* 2015. **90**(6): p. 2981-92.

76. Chen, L.M., Blixt, O., Stevens, J., Lipatov, A.S., Davis, C.T., Collins, B.E., Cox, N.J., Paulson, J.C., and Donis, R.O. In vitro evolution of H5N1 avian influenza virus toward human-type receptor specificity. *Virology,* 2012. **422**(1): p. 105-13.

77. de Vries, R.P., Zhu, X., McBride, R., Rigter, A., Hanson, A., Zhong, G., Hatta, M., Xu, R., Yu, W., Kawaoka, Y., de Haan, C.A.M., Wilson, I.A., and Paulson, J.C. Hemagglutinin receptor specificity and structural analyses of respiratory droplet-transmissible H5N1 viruses. *Journal of virology,* 2014. **88**(1): p. 768-773.

78. Neumann, G. and Kawaoka, Y. Host Range Restriction and Pathogenicity in the Context of Influenza Pandemic. *Emerging Infectious Diseases,* 2006. **12**(6): p. 881-886.

79. Taubenberger, J.K. and Kash, J.C. Influenza virus evolution, host adaptation, and pandemic formation. *Cell Host Microbe,* 2010. **7**(6): p. 440-51.

80. Chen, M., Chen, M., and Tan, Y. An avian influenza A (H7N9) virus with polybasic amino acid insertion was found in human infection in southern China, Guangxi, February 2017. *Infect Dis (Lond),* 2018. **50**(1): p. 71-74.

81. Imai, M., Watanabe, T., Kiso, M., Nakajima, N., Yamayoshi, S., Iwatsuki-Horimoto, K., Hatta, M., Yamada, S., Ito, M., Sakai-Tagawa, Y., Shirakura, M., Takashita, E., Fujisaki, S., McBride, R., Thompson, A.J., Takahashi, K., Maemura, T., Mitake, H., Chiba, S., Zhong, G., Fan, S., Oishi, K., Yasuhara, A., Takada, K., Nakao, T., Fukuyama, S., Yamashita, M., Lopes, T.J.S., Neumann, G., Odagiri, T., Watanabe, S., Shu, Y., Paulson, J.C., Hasegawa, H., and Kawaoka, Y. A Highly Pathogenic Avian H7N9 Influenza Virus Isolated from A Human Is Lethal in Some Ferrets Infected via Respiratory Droplets. *Cell Host Microbe,* 2017. **22**(5): p. 615-626 e8.

82. Subbarao, K. Avian influenza H7N9 viruses: a rare second warning. *Cell Res,* 2018. **28**(1): p. 1-2.

83. Heaton, N.S., Moshkina, N., Fenouil, R., Gardner, T.J., Aguirre, S., Shah, P.S., Zhao, N., Manganaro, L., Hultquist, J.F., Noel, J., Sachs, D., Hamilton, J., Leon, P.E., Chawdury, A., Tripathi, S., Melegari, C., Campisi, L., Hai, R., Metreveli, G., Gamarnik, A.V., Garcia-Sastre, A., Greenbaum, B., Simon, V., Fernandez-Sesma, A., Krogan, N.J., Mulder, L.C.F., van Bakel, H., Tortorella, D., Taunton, J., Palese, P., and Marazzi, I. Targeting Viral Proteostasis Limits Influenza Virus, HIV, and Dengue Virus Infection*. Immunity,* 2016. **44**(1): p. 46-58.

84. Ito, T., Kelm, S., Nelson, J., Couceiro, S.S., Castrucci, M.R., Donatelli, I., Baum, L., Kida, H., Webster, R., and Kawaoka, Y. Molecular Basis for the Generation in Pigs of Influenza A Viruses with Pandemic Potential*. Journal of Virology,* 1998. **72**(9): p. 7367-7373.

85. Thangavel, R.R. and Bouvier, N.M. Animal models for influenza virus pathogenesis, transmission, and immunology*. J Immunol Methods,* 2014. **410**: p. 60-79.

86. Iuliano, A.D., Roguski, K.M., Chang, H.H., Muscatello, D.J., Palekar, R., Tempia, S., Cohen, C., Gran, J.M., Schanzer, D., Cowling, B.J., Wu, P., Kyncl, J., Ang, L.W., Park, M., Redlberger-Fritz, M., Yu, H., Espenhain, L., Krishnan, A., Emukule, G., van Asten, L., Pereira da Silva, S., Aungkulanon, S., Buchholz, U., Widdowson, M.-A., Bresee, J.S., Azziz-Baumgartner, E., Cheng, P.-Y., Dawood, F., Foppa, I., Olsen, S., Haber, M., Jeffers, C., MacIntyre, C.R., Newall, A.T., Wood, J.G., Kundi, M., Popow-Kraupp, T., Ahmed, M., Rahman, M., Marinho, F., Sotomayor Proschle, C.V., Vergara Mallegas, N., Luzhao, F., Sa, L., Barbosa-Ramírez, J., Sanchez, D.M., Gomez, L.A., Vargas, X.B., Acosta Herrera, a., Llanés, M.J., Fischer, T.K., Krause, T.G., Mølbak, K., Nielsen, J., Trebbien, R., Bruno, A., Ojeda, J., Ramos, H., an der Heiden, M., del Carmen Castillo Signor, L., Serrano, C.E., Bhardwaj, R., Chadha, M., Narayan, V., Kosen, S., Bromberg, M., Glatman-Freedman, A., Kaufman, Z., Arima, Y., Oishi, K., Chaves, S., Nyawanda, B., Al-Jarallah, R.A., Kuri-Morales, P.A., Matus, C.R., Corona, M.E.J., Burmaa, A., Darmaa, O., Obtel, M., Cherkaoui, I., van den Wijngaard, C.C., van der Hoek, W., Baker, M., Bandaranayake, D., Bissielo, A., Huang, S., Lopez, L., Newbern, C., Flem, E., Grøneng, G.M., Hauge, S., de Cosío, F.G., de Moltó, Y., Castillo, L.M., Cabello, M.A., von Horoch, M., Medina Osis, J., Machado, A., Nunes, B., Rodrigues, A.P., Rodrigues, E., Calomfirescu, C., Lupulescu, E., Popescu, R., Popovici, O., Bogdanovic, D., Kostic, M., Lazarevic, K., Milosevic, Z., Tiodorovic, B., Chen, M., Cutter, J., Lee, V., Lin, R., Ma, S., Cohen, A.L., Treurnicht, F., Kim, W.J., Delgado-Sanz, C., de mateo Ontañón, S., Larrauri, A., León, I.L., Vallejo, F., Born, R., Junker, C., Koch, D., Chuang, J.-H., Huang, W.-T., Kuo, H.-W., Tsai, Y.-C., Bundhamcharoen, K., Chittaganpitch, M., Green, H.K., Pebody, R., Goñi, N., Chiparelli, H., Brammer, L. and Mustaquim, D. Estimates of global seasonal influenza-associated respiratory mortality: a modelling study*. The Lancet,* 2018. **391**(10127): p. 1285-1300.

87. Putri, W., Muscatello, D.J., Stockwell, M.S., and Newall, A.T. Economic burden of seasonal influenza in the United States*. Vaccine,* 2018. **36**(27): p. 3960-3966.

88. Henry, C., Zheng, N.Y., Huang, M., Cabanov, A., Rojas, K.T., Kaur, K., Andrews, S.F., Palm, A.E., Chen, Y.Q., Li, Y., Hoskova, K., Utset, H.A., Vieira, M.C., Wrammert, J., Ahmed, R., Holden-Wiltse, J., Topham, D.J., Treanor, J.J., Ertl, H.C., Schmader, K.E., Cobey, S., Krammer, F., Hensley,

S.E., Greenberg, H., He, X.S., and Wilson, P.C. Influenza Virus Vaccination Elicits Poorly Adapted B Cell Responses in Elderly Individuals. *Cell Host Microbe,* 2019. **25**(3): p. 357-366 e6.

89. Neumann, G. and Kawaoka, Y. Predicting the Next Influenza Pandemics. *J Infect Dis,* 2019. **219**(Supplement_1): p. S14-S20.

90. Palese, P. Influenza: old and new threats. *Nat Med,* 2004. **10**(12 Suppl): p. S82-7.

91. Johnson, N.P. and Mueller, J. Updating the accounts: global mortality of the 1918-1920 "Spanish" influenza pandemic. *Bull Hist Med,* 2002. **76**(1): p. 105-15.

92. Viboud, C., Simonsen, L., Fuentes, R., Flores, J., Miller, M.A., and Chowell, G. Global Mortality Impact of the 1957-1959 Influenza Pandemic. *J Infect Dis,* 2016. **213**(5): p. 738-45.

93. Viboud, C., Grais, R.F., Lafont, B.A.P., Miller, M.A., and Simonsen, L. Multinational Impact of the 1968 Hong Kong Influenza Pandemic: Evidence for a Smoldering Pandemic. *The Journal of Infectious Diseases,* 2005. **192**(2): p. 233-248.

94. Garten, R.J., Davis, C.T., Russell, C.A., Shu, B., Lindstrom, S., Balish, A., Sessions, W.M., Xu, X., Skepner, E., Deyde, V., Okomo-Adhiambo, M., Gubareva, L., Barnes, J., Smith, C.B., Emery, S.L., Hillman, M.J., Rivailler, P., Smagala, J., de Graaf, M., Burke, D.F., Fouchier, R.A., Pappas, C., Alpuche-Aranda, C.M., Lopez-Gatell, H., Olivera, H., Lopez, I., Myers, C.A., Faix, D., Blair, P.J., Yu, C., Keene, K.M., Dotson, P.D., Jr., Boxrud, D., Sambol, A.R., Abid, S.H., St George, K., Bannerman, T., Moore, A.L., Stringer, D.J., Blevins, P., Demmler-Harrison, G.J., Ginsberg, M., Kriner, P., Waterman, S., Smole, S., Guevara, H.F., Belongia, E.A., Clark, P.A., Beatrice, S.T., Donis, R., Katz, J., Finelli, L., Bridges, C.B., Shaw, M., Jernigan, D.B., Uyeki, T.M., Smith, D.J., Klimov, A.I., and Cox, N.J. Antigenic and genetic characteristics of swine-origin 2009 A(H1N1) influenza viruses circulating in humans. *Science,* 2009. **325**(5937): p. 197-201.

95. Neumann, G., Noda, T., and Kawaoka, Y. Emergence and pandemic potential of swine-origin H1N1 influenza virus. *Nature,* 2009. **459**(7249): p. 931-9.

96. Shrestha, S.S., Swerdlow, D.L., Borse, R.H., Prabhu, V.S., Finelli, L., Atkins, C.Y., Owusu-Edusei, K., Bell, B., Mead, P.S., Biggerstaff, M., Brammer, L., Davidson, H., Jernigan, D., Jhung, M.A., Kamimoto, L.A., Merlin, T.L., Nowell, M., Redd, S.C., Reed, C., Schuchat, A., and Meltzer, M.I. Estimating the burden of 2009 pandemic influenza A (H1N1) in the United States (April 2009-April 2010). *Clin Infect Dis,* 2011. **52 Suppl 1**: p. S75-82.

97. Influenza, W.C.o.t.W.C.o.C.A.o.P.H.N. Clinical Aspects of Pandemic 2009 Influenza A (H1N1) Virus Infection. *New England Jornal of Medicine,* 2010. **362**: p. 1708-19.

98. Webster, R.G. and Govorkova, E.A. H5N1 Influenza — Continuing Evolution and Spread. *New England Jornal of Medicine,* 2006. **355**(21): p. 2174-2177.

99. Yu, D., Xiang, G., Zhu, W., Lei, X., Li, B., Meng, Y., Yang, L., Jiao, H., Li, X., Huang, W., Wei, H., Zhang, Y., Hai, Y., Zhang, H., Yue, H., Zou, S., Zhao, X., Li, C., Ao, D., Zhang, Y., Tan, M., Liu, J., Zhang, X., Gao, G.F., Meng, L., and Wang, D. The re-emergence of highly pathogenic avian influenza H7N9

viruses in humans in mainland China, 2019. *Eurosurveillance,* 2019. **24**(21): p. 1900273.

100. Zhou, X. and Muzyczka, N. In vitro Packaging of Adeno-Associated Virus DNA. *Journal of Virology,* 1998. **72**(4): p. 3241-7.

101. Capua, I. and Munoz, O. Emergence of influenza viruses with zoonotic potential: open issues which need to be addressed. A review. *Vet Microbiol,* 2013. **165**(1-2): p. 7-12.

102. Gao, R., Cao, B., Hu, Y., Feng, Z., Wang, D., Hu, W., Chen, J., Jie, Z., Qiu, H., Xu, K., Xu, X., Lu, H., Zhu, W., Gao, Z., Xiang, N., Shen, Y., He, Z., Gu, Y., Zhang, Z., Yang, Y., Zhao, X., Zhou, L., Li, X., Zou, S., Zhang, Y., Li, X., Yang, L., Guo, J., Dong, J., Li, Q., Dong, L., Zhu, Y., Bai, T., Wang, S., Hao, P., Yang, W., Zhang, Y., Han, J., Yu, H., Li, D., Gao, G.F., Wu, G., Wang, Y., Yuan, Z., and Shu, Y. Human infection with a novel avian-origin influenza A (H7N9) virus. *N Engl J Med,* 2013. **368**(20): p. 1888-97.

103. Shi, J., Deng, G., Kong, H., Gu, C., Ma, S., Yin, X., Zeng, X., Cui, P., Chen, Y., Yang, H., Wan, X., Wang, X., Liu, L., Chen, P., Jiang, Y., Liu, J., Guan, Y., Suzuki, Y., Li, M., Qu, Z., Guan, L., Zang, J., Gu, W., Han, S., Song, Y., Hu, Y., Wang, Z., Gu, L., Yang, W., Liang, L., Bao, H., Tian, G., Li, Y., Qiao, C., Jiang, L., Li, C., Bu, Z., and Chen, H. H7N9 virulent mutants detected in chickens in China pose an increased threat to humans. *Cell Res,* 2017. **27**(12): p. 1409-1421.

104. Zhou, L., Chen, E., Bao, C., Xiang, N., Wu, J., Wu, S., Shi, J., Wang, X., Zheng, Y., Zhang, Y., Ren, R., Greene, C.M., Havers, F., Iuliano, A.D., Song, Y., Li, C., Chen, T., Wang, Y., Li, D., Ni, D., Zhang, Y., Feng, Z., Uyeki, T.M., and Li, Q. Clusters of Human Infection and Human-to-Human Transmission of Avian Influenza A(H7N9) Virus, 2013-2017. *Emerg Infect Dis,* 2018. **24**(2).

105. Hu, Y., Lu, S., Song, Z., Wang, W., Hao, P., Li, J., Zhang, X., Yen, H.L., Shi, B., Li, T., Guan, W., Xu, L., Liu, Y., Wang, S., Zhang, X., Tian, D., Zhu, Z., He, J., Huang, K., Chen, H., Zheng, L., Li, X., Ping, J., Kang, B., Xi, X., Zha, L., Li, Y., Zhang, Z., Peiris, M., and Yuan, Z. Association between adverse clinical outcome in human disease caused by novel influenza A H7N9 virus and sustained viral shedding and emergence of antiviral resistance. *Lancet,* 2013. **381**(9885): p. 2273-9.

106. Yang, H., Carney, P.J., Chang, J.C., Villanueva, J.M., and Stevens, J. Structural analysis of the hemagglutinin from the recent 2013 H7N9 influenza virus. *J Virol,* 2013. **87**(22): p. 12433-46.

107. Fineberg, H.V. Pandemic preparedness and response--lessons from the H1N1 influenza of 2009. *N Engl J Med,* 2014. **370**(14): p. 1335-42.

108. World Health Organization Global influenza strategy 2019-2030. 2019.

109. Key Facts about Seasonal Flu Vaccine. 2017; Available from: https://www.cdc.gov/flu/protect/keyfacts.htm.

110. Krammer, F. and Palese, P. Advances in the development of influenza virus vaccines. *Nat Rev Drug Discov,* 2015. **14**(3): p. 167-82.

111. Nachbagauer, R. and Krammer, F. Universal influenza virus vaccines and therapeutic antibodies. *Clin Microbiol Infect,* 2017. **23**(4): p. 222-228.

112. Treanor, J. Influenza vaccine--outmaneuvering antigenic shift and drift. *N Engl J Med,* 2004. **350**(3): p. 218-20.

113. Hsu, A.C. Influenza Virus: A Master Tactician in Innate Immune Evasion and Novel Therapeutic Interventions. *Front Immunol,* 2018. **9**: p. 743.

114. Nieto, K. and Salvetti, A. AAV Vectors Vaccines Against Infectious Diseases. *Front Immunol,* 2014. **5**: p. 5.

115. QGIS-WHO. Influenza Vaccination Zones. 2017 15 September 2017; Available from: https://www.who.int/influenza/vaccines/tropics/vaccination_zone/en/.

116. Mameli, C., Cocchi, I., Fumagalli, M., and Zuccotti, G. Influenza Vaccination: Effectiveness, Indications, and Limits in the Pediatric Population. *Front Pediatr,* 2019. **7**: p. 317.

117. Cox, R.J. Correlates of protection to influenza virus, where do we go from here? *Hum Vaccin Immunother,* 2013. **9**(2): p. 405-8.

118. Cox, R.J., Brokstady, K.A., and Ograz, P. Influenza Virus: Immunity and Vaccination Strategies. Comparison of the Immune Response to Inactivated and Live, Attenuated Influenza Vaccines. *Scandinavian Journal of Immunology,* 2004. **59**: p. 1-15.

119. NHS-England. Who should have the flu vaccine? 2019 15 July 2019; Available from: https://www.nhs.uk/conditions/vaccinations/who-should-have-flu-vaccine/.

120. Hobson, D., Curry, R.L., Beare, A.S., and Ward-Gardner, A. The role of serum haemagglutination-inhibiting antibody in protection against challenge infection with influenza A2 and B viruses. *The Journal of hygiene,* 1972. **70**(4): p. 767-777.

121. Goodwin, K., Viboud, C., and Simonsen, L. Antibody response to influenza vaccination in the elderly: a quantitative review. *Vaccine,* 2006. **24**(8): p. 1159-69.

122. Corti, D., Suguitan, A.L., Jr., Pinna, D., Silacci, C., Fernandez-Rodriguez, B.M., Vanzetta, F., Santos, C., Luke, C.J., Torres-Velez, F.J., Temperton, N.J., Weiss, R.A., Sallusto, F., Subbarao, K., and Lanzavecchia, A. Heterosubtypic neutralizing antibodies are produced by individuals immunized with a seasonal influenza vaccine. *J Clin Invest,* 2010. **120**(5): p. 1663-73.

123. Monto, A.S., Ohmit, S.E., Petrie, J.G., Johnson, E., Truscon, R., Teich, E., Rotthoff, J., Boulton, M., and Victor, J.C. Comparative Efficacy of Inactivated and Live Attenuated Influenza Vaccines. *New England Jornal of Medicine,* 2009. **361**: p. 1260-1267.

124. Osterholm, M.T., Kelley, N.S., Sommer, A., and Belongia, E.A. Efficacy and effectiveness of influenza vaccines: a systematic review and meta-analysis. *The Lancet Infectious Diseases,* 2012. **12**(1): p. 36-44.

125. Hoft, D.F., Babusis, E., Worku, S., Spencer, C.T., Lottenbach, K., Truscott, S.M., Abate, G., Sakala, I.G., Edwards, K.M., Creech, C.B., Gerber, M.A., Bernstein, D.I., Newman, F., Graham, I., Anderson, E.L., and Belshe, R.B. Live and inactivated influenza vaccines induce similar humoral responses, but

only live vaccines induce diverse T-cell responses in young children. *J Infect Dis,* 2011. **204**(6): p. 845-53.

126. Hoft, D.F., Lottenbach, K.R., Blazevic, A., Turan, A., Blevins, T.P., Pacatte, T.P., Yu, Y., Mitchell, M.C., Hoft, S.G., and Belshe, R.B. Comparisons of the Humoral and Cellular Immune Responses Induced by Live Attenuated Influenza Vaccine and Inactivated Influenza Vaccine in Adults. *Clin Vaccine Immunol,* 2017. **24**(1).

127. Sasaki, S., Sullivan, M., Narvaez, C.F., Holmes, T.H., Furman, D., Zheng, N.Y., Nishtala, M., Wrammert, J., Smith, K., James, J.A., Dekker, C.L., Davis, M.M., Wilson, P.C., Greenberg, H.B., and He, X.S. Limited efficacy of inactivated influenza vaccine in elderly individuals is associated with decreased production of vaccine-specific antibodies. *J Clin Invest,* 2011. **121**(8): p. 3109-19.

128. Vanderven, H.A., Jegaskanda, S., Wines, B.D., Hogarth, P.M., Carmuglia, S., Rockman, S., Chung, A.W., and Kent, S.J. Antibody-Dependent Cellular Cytotoxicity Responses to Seasonal Influenza Vaccination in Older Adults. *J Infect Dis,* 2017. **217**(1): p. 12-23.

129. Lewnard, J.A. and Cobey, S. Immune History and Influenza Vaccine Effectiveness. *Vaccines (Basel),* 2018. **6**(2).

130. Restivo, V., Costantino, C., Bono, S., Maniglia, M., Marchese, V., Ventura, G., Casuccio, A., Tramuto, F., and Vitale, F. Influenza vaccine effectiveness among high-risk groups: A systematic literature review and meta-analysis of case-control and cohort studies. *Hum Vaccin Immunother,* 2018. **14**(3): p. 724-735.

131. Treanor, J. Weathering the influenza vaccine crisis. *N Engl J Med,* 2004. **351**(20): p. 2037-40.

132. Zhang, X.-S., Pebody, R., De Angelis, D., White, P.J., Charlett, A., and McCauley, J.W. The Possible Impact of Vaccination for Seasonal Influenza on Emergence of Pandemic Influenza via Reassortment. *PloS one,* 2014. **9**(12): p. e114637-e114637.

133. Cowling, B.J., Ng, S., Ma, E.S., Cheng, C.K., Wai, W., Fang, V.J., Chan, K.H., Ip, D.K., Chiu, S.S., Peiris, J.S., and Leung, G.M. Protective efficacy of seasonal influenza vaccination against seasonal and pandemic influenza virus infection during 2009 in Hong Kong. *Clin Infect Dis,* 2010. **51**(12): p. 1370-9.

134. Fedson, D.S. Pandemic Influenza and the Global Vaccine Supply. *Clinical Infectious Diseases,* 2003. **36**(12): p. 1552-1561.

135. Raymond, D.D., Stewart, S.M., Lee, J., Ferdman, J., Bajic, G., Do, K.T., Ernandes, M.J., Suphaphiphat, P., Settembre, E.C., Dormitzer, P.R., Del Giudice, G., Finco, O., Kang, T.H., Ippolito, G.C., Georgiou, G., Kepler, T.B., Haynes, B.F., Moody, M.A., Liao, H.X., Schmidt, A.G., and Harrison, S.C. Influenza immunization elicits antibodies specific for an egg-adapted vaccine strain. *Nat Med,* 2016. **22**(12): p. 1465-1469.

136. Viboud, C. and Epstein, S. First Flu is Forever. *Science,* 2016. **354**(6313).

137. Jefferson, T., Demicheli, V., Rivetti, D., Jones, M., Di Pietrantonj, C., and Rivetti, A. Antivirals for influenza in healthy adults: systematic review. *The Lancet,* 2006. **367**(9507): p. 303-313.

138. Uyeki, T.M., Bernstein, H.H., Bradley, J.S., Englund, J.A., File, T.M., Fry, A.M., Gravenstein, S., Hayden, F.G., Harper, S.A., Hirshon, J.M., Ison, M.G., Johnston, B.L., Knight, S.L., McGeer, A., Riley, L.E., Wolfe, C.R., Alexander, P.E., and Pavia, A.T. Clinical Practice Guidelines by the Infectious Diseases Society of America: 2018 Update on Diagnosis, Treatment, Chemoprophylaxis, and Institutional Outbreak Management of Seasonal Influenzaa. *Clin Infect Dis,* 2019. **68**(6): p. e1-e47.

139. De Clercq, E. Antiviral agents active against influenza A viruses. *Nat Rev Drug Discov,* 2006. **5**(12): p. 1015-25.

140. Smith, S.M. and Gums, J.G. Antivirals for Influenza: Strategies for Use in Pediatrics. *Pediatric Drugs,* 2010. **12**(5): p. 285-299.

141. Centers for Disease Control and Prevention. Influenza Antiviral Drug Resistance. 2017; Available from: https://www.cdc.gov/flu/about/qa/antiviralresistance.htm.

142. Hussain, M., Galvin, H.D., Haw, T.Y., Nutsford, A.N., and Husain, M. Drug resistance in influenza A virus: the epidemiology and management. *Infect Drug Resist,* 2017. **10**: p. 121-134.

143. Hayden, F.G. Antiviral Resistance in Influenza Viruses — Implications for Management and Pandemic Response. *New England Journal of Medicine,* 2006. **354**(8).

144. de Jong, M.D., Tran, T.T., Truong, H.K., Vo, M.H., Smith, G.J., Nguyen, V.C., Bach, V.C., Phan, T.Q., Do, Q.H., Guan, Y., Peiris, J.S., Tran, T.H., and Farrar, J. Oseltamivir resistance during treatment of influenza A (H5N1) infection. *New England Jornal of Medicine,* 2005. **353**(25): p. 2667-72.

145. O'Hanlon, R. and Shaw, M.L. Baloxavir marboxil: the new influenza drug on the market. *Curr Opin Virol,* 2019. **35**: p. 14-18.

146. Damjanovic, D., Divangahi, M., Kugathasan, K., Small, C.L., Zganiacz, A., Brown, E.G., Hogaboam, C.M., Gauldie, J., and Xing, Z. Negative regulation of lung inflammation and immunopathology by TNF-alpha during acute influenza infection. *Am J Pathol,* 2011. **179**(6): p. 2963-76.

147. Dienz, O., Rud, J.G., Eaton, S.M., Lanthier, P.A., Burg, E., Drew, A., Bunn, J., Suratt, B.T., Haynes, L., and Rincon, M. Essential role of IL-6 in protection against H1N1 influenza virus by promoting neutrophil survival in the lung. *Mucosal Immunol,* 2012. **5**(3): p. 258-66.

148. Ivanov, S., Renneson, J., Fontaine, J., Barthelemy, A., Paget, C., Fernandez, E.M., Blanc, F., De Trez, C., Van Maele, L., Dumoutier, L., Huerre, M.R., Eberl, G., Si-Tahar, M., Gosset, P., Renauld, J.C., Sirard, J.C., Faveeuw, C., and Trottein, F. Interleukin-22 reduces lung inflammation during influenza A virus infection and protects against secondary bacterial infection. *J Virol,* 2013. **87**(12): p. 6911-24.

149. Ichiyama, T., Isumi, H., Ozawa, H., Matsubara, T., Morishima, T., and Furukawa, S. Cerebrospinal Fluid and Serum Levels of Cytokines and Soluble Tumor Necrosis Factor Receptor in Influenza Virus-associated

Encephalopathy. *Scandinavian Journal of Infectious Diseases,* 2003. **35**(1): p. 59-61.

150. Luo, C., Liu, J., Qi, W., Ren, X., Lu, R., Liao, M., and Ning, Z. Dynamic analysis of expression of chemokine and cytokine gene responses to H5N1 and H9N2 avian influenza viruses in DF-1 cells. *Microbiol Immunol,* 2018. **62**(5): p. 327-340.

151. Hufford, M.M., Kim, T.S., Sun, J., and Braciale, T.J. The Effector T Cell Response to Influenza Infection. 2014. **386**: p. 423-455.

152. Lukacher, A.E., Braciale, V.L., and Braciale, T.J. In vivo effector function of influenza virus-specific cytotoxic T lymphocyte clones is highly specific. *Journal of Experimental Medicine,* 1984. **160**(3): p. 814-826.

153. Topham, D.J., Tripp, R.A., Sarawar, S.R., Sangster, M.Y., and Doherty, P.C. Immune CD4+ T cells promote the clearance of influenza virus from major histocompatibility complex class II -/- respiratory epithelium. *Journal of Virology,* 1996. **70**: p. 1288-1291.

154. Topham, D.J. and Doherty, P.C. Clearance of an influenza A virus by CD4+ T cells is inefficient in the absence of B cells. *Journal of virology,* 1998. **72**(1): p. 882-885.

155. Bahadoran, A., Lee, S.H., Wang, S.M., Manikam, R., Rajarajeswaran, J., Raju, C.S., and Sekaran, S.D. Immune Responses to Influenza Virus and Its Correlation to Age and Inherited Factors. *Front Microbiol,* 2016. **7**: p. 1841.

156. Kreijtz, J.H., Fouchier, R.A., and Rimmelzwaan, G.F. Immune responses to influenza virus infection. *Virus Res,* 2011. **162**(1-2): p. 19-30.

157. Koskinen, P., Vuorinen, T., and Meurman, O. Influenza A and B virus IgG and IgM serology by enzyme immunoassays. *Epidemiology and infection,* 1987. **99**(1): p. 55-64.

158. Li, Z.-N., Lin, S.-C., Carney, P.J., Li, J., Liu, F., Lu, X., Liu, M., Stevens, J., Levine, M., Katz, J.M., and Hancock, K. IgM, IgG, and IgA Antibody Responses to Influenza A(H1N1)pdm09 Hemagglutinin in Infected Persons during the First Wave of the 2009 Pandemic in the United States. *Clinical and Vaccine Immunology,* 2014. **21**: p. 1054-1060.

159. Baumgarth, N., Herman, O.C., Jager, G.C., Brown, L., Herzenberg, L.A., and Herzenberg, L.A. Innate and acquired humoral immunities to influenza virus are mediated by distinct arms of the immune system. *Proceedings of the National Academy of Sciences,* 1999. **96**: p. 2250-2255.

160. Meade, P., Kuan, G., Strohmeier, S., Maier, H.E., Amanat, F., Balmaseda, A., Ito, K., Kirkpatrick, E., Javier, A., Gresh, L., Nachbagauer, R., Gordon, A., and Krammer, F. Influenza Virus Infection Induces a Narrow Antibody Response in Children but a Broad Recall Response in Adults. *mBio Clinical Science and Epidemiology,* 2020. **11**(1).

161. Kopf, M., Brombacher, F., and Bachmann, M.F. Role of IgM antibodies versus B cells in influenza virus-specific immunity. *European Journal of Immunology,* 2002. **32**(8): p. 2229-2236.

162. Qiu, C., Tian, D., Wan, Y., Zhang, W., Qiu, C., Zhu, Z., Ye, R., Song, Z., Zhou, M., Yuan, S., Shi, B., Wu, M., Liu, Y., Gu, S., Wei, J., Zhou, Z., Zhang,

X., Zhang, Z., Hu, Y., Yuan, Z., and Xu, J. Early adaptive humoral immune responses and virus clearance in humans recently infected with pandemic 2009 H1N1 influenza virus. *PLoS One,* 2011. **6**(8): p. e22603.

163. Ruddick, J.H. and Leslie, G.A. Structure and biologic functions of human IgD. XI. Identification and ontogeny of a rat lymphocyte immunoglobulin having antigenic cross-reactivity with human IgD. *Journal of immunology (Baltimore, Md. : 1950),* 1977. **118**(3): p. 1025-1031.

164. Chen, K. and Cerutti, A. The function and regulation of immunoglobulin D. *Curr Opin Immunol,* 2011. **23**(3): p. 345-52.

165. Skountzou, I., Satyabhama, L., Stavropoulou, A., Ashraf, Z., Esser, E.S., Vassilieva, E., Koutsonanos, D., Compans, R., and Jacob, J. Influenza virus-specific neutralizing IgM antibodies persist for a lifetime. *Clin Vaccine Immunol,* 2014. **21**(11): p. 1481-9.

166. Actor, J.K. Humoral Immunity. 2012: p. 17-24.

167. Stavnezer, J. and Schrader, C.E. IgH chain class switch recombination: mechanism and regulation. *Journal of immunology (Baltimore, Md. : 1950),* 2014. **193**(11): p. 5370-5378.

168. Krammer, F. The human antibody response to influenza A virus infection and vaccination. *Nature Reviews Immunology,* 2019. **19**(6): p. 383-397.

169. Abreu, R.B., Clutter, E.F., Attari, S., Sautto, G.A., and Ross, T.M. IgA Responses Following Recurrent Influenza Virus Vaccination. *Front Immunol,* 2020. **11**: p. 902.

170. Andrews, S.F., Huang, Y., Kaur, K., Popova, L.I., Ho, I.Y., Pauli, N.T., Dunand, C.J.H., Taylor, W.M., Lim, S., Huang, M., Qu, X., Lee, J.-H., Salgado-Ferrer, M., Krammer, F., Palese, P., Wrammert, J., Ahmed, R., and Wilson, P.C. Immune history profoundly affects broadly protective B cell responses to influenza. *Science Translational Medicine,* 2015. **7**(316).

171. Vidarsson, G., Dekkers, G., and Rispens, T. IgG subclasses and allotypes: from structure to effector functions. *Front Immunol,* 2014. **5**: p. 520.

172. Bruhns, P. Properties of mouse and human IgG receptors and their contribution to disease models. *Blood,* 2012. **119**(24): p. 5640-9.

173. Balkovic, E., Florack, J., and Six, H. Immunoglobulin G subclass antibody responses of mice to influenza virus antigens given in different forms. *Antiviral Research,* 1987. **8**: p. 151-160.

174. Hocart, M., Mackenzie, J., and Stewart, G. The Immunoglobulin G Subclass Responses of Mice to Influenza A Virus: the Effect of Mouse Strain, and the Neutralizing Abilities of Individual Protein A-Purified Subclass Antibodies. *Journal of General Virology,* 1989. **70**: p. 2439-48.

175. Zhang, Y., Xu, C., Zhang, H., Liu, G.D., Xue, C., and Cao, Y. Targeting Hemagglutinin: Approaches for Broad Protection against the Influenza A Virus. *Viruses,* 2019. **11**(5).

176. Tan, H.X., Jegaskanda, S., Juno, J.A., Esterbauer, R., Wong, J., Kelly, H.G., Liu, Y., Tilmanis, D., Hurt, A.C., Yewdell, J.W., Kent, S.J., and Wheatley, A.K. Subdominance and poor intrinsic immunogenicity limit humoral immunity targeting influenza HA stem. *J Clin Invest,* 2019. **129**(2): p. 850-862.

177. Yu, X., Tsibane, T., McGraw, P.A., House, F.S., Keefer, C.J., Hicar, M.D., Tumpey, T.M., Pappas, C., Perrone, L.A., Martinez, O., Stevens, J., Wilson, I.A., Aguilar, P.V., Altschuler, E.L., Basler, C.F., and Crowe, J.E., Jr. Neutralizing antibodies derived from the B cells of 1918 influenza pandemic survivors. *Nature,* 2008. **455**(7212): p. 532-6.

178. Reber, A. and Katz, J. Immunological assessment of influenza vaccines and immune correlates of protection. *Expert Review of Vaccines,* 2013. **12**(5): p. 519-536.

179. WHO Global Influenza Surveillance Network. Manual for the Laboratory Diagnosis and Virological Surveillance of Influenza. 2011; Available from: http://www.who.int/influenza/gisrs_laboratory/manual_diagnosis_surveillance_influenza/en/index.html.

180. Alladi, C.S.H., Jagadesh, A., Prabhu, S.G., and Arunkumar, G. Hemagglutination Inhibition Antibody Response Following Influenza A(H1N1)pdm09 Virus Natural Infection: A Cross-Sectional Study from Thirthahalli, Karnataka, India. *Viral Immunol,* 2019. **32**(5): p. 230-233.

181. Coudeville, L., Bailleux, F., Riche, B., Megas, F., Andre, P., and Ecochard, R. Relationship between haemagglutination-inhibiting antibody titres and clinical protection against influenza: development and application of a bayesian random-effects model. *BMC medical research methodology,* 2010. **10**: p. 18-18.

182. Huijskens, E.G.W., Reimerink, J., Mulder, P.G.H., van Beek, J., Meijer, A., de Bruin, E., Friesema, I., de Jong, M.D., Rimmelzwaan, G.F., Peeters, M.F., Rossen, J.W.A., and Koopmans, M. Profiling of Humoral Response to Influenza A(H1N1)pdm09 Infection and Vaccination Measured by a Protein Microarray in Persons with and without History of Seasonal Vaccination. *PLOS ONE,* 2013. **8**(1): p. e54890.

183. Huber, V.C., McKeon, R.M., Brackin, M.N., Miller, L.A., Keating, R., Brown, S.A., Makarova, N., Perez, D.R., Macdonald, G.H., and McCullers, J.A. Distinct contributions of vaccine-induced immunoglobulin G1 (IgG1) and IgG2a antibodies to protective immunity against influenza. *Clin Vaccine Immunol,* 2006. **13**(9): p. 981-90.

184. Burlington, D.B., Clements, M.L., Meiklejohn, G., Phelan, M., and Murphy, B.R. Hemagglutinin-specific antibody responses in immunoglobulin G, A, and M isotypes as measured by enzyme-linked immunosorbent assay after primary or secondary infection of humans with influenza A virus. *Infection and Immunity,* 1983. **41**(2): p. 540.

185. Gould, V.M.W., Francis, J.N., Anderson, K.J., Georges, B., Cope, A.V., and Tregoning, J.S. Nasal IgA Provides Protection against Human Influenza Challenge in Volunteers with Low Serum Influenza Antibody Titre. *Front Microbiol,* 2017. **8**: p. 900.

186. Jackson, K.J., Liu, Y., Roskin, K.M., Glanville, J., Hoh, R.A., Seo, K., Marshall, E.L., Gurley, T.C., Moody, M.A., Haynes, B.F., Walter, E.B., Liao, H.X., Albrecht, R.A., Garcia-Sastre, A., Chaparro-Riggers, J., Rajpal, A., Pons, J., Simen, B.B., Hanczaruk, B., Dekker, C.L., Laserson, J., Koller, D., Davis, M.M., Fire, A.Z., and Boyd, S.D. Human responses to influenza vaccination show seroconversion signatures and convergent antibody rearrangements. *Cell Host Microbe,* 2014. **16**(1): p. 105-14.

187. Hsu, J.P., Zhao, X., Chen, M.I.C., Cook, A.R., Lee, V., Lim, W.Y., Tan, L., Barr, I.G., Jiang, L., Tan, C.L., Phoon, M.C., Cui, L., Lin, R., Leo, Y.S., and Chow, V.T. Rate of decline of antibody titers to pandemic influenza A (H1N1-2009) by hemagglutination inhibition and virus microneutralization assays in a cohort of seroconverting adults in Singapore. *BMC Infectious Diseases,* 2014. **14**(1): p. 414.

188. Deal, C.E. and Balazs, A.B. Engineering humoral immunity as prophylaxis or therapy. *Curr Opin Immunol,* 2015. **35**: p. 113-22.

189. Casadevall, A., Dadachova, E., and Pirofski, L.A. Passive antibody therapy for infectious diseases. *Nat Rev Microbiol,* 2004. **2**(9): p. 695-703.

190. Keller, M. and Stiehm, R. Passive Immunity in Prevention and Treatment of Infectious Diseases. *Clinical Microbiology Reviews,* 2000. **13**(4): p. 602-14.

191. Marasco, W.A. and Sui, J. The growth and potential of human antiviral monoclonal antibody therapeutics. *Nat Biotechnol,* 2007. **25**(12): p. 1421-34.

192. Berry, C.M. Antibody immunoprophylaxis and immunotherapy for influenza virus infection: Utilization of monoclonal or polyclonal antibodies? *Hum Vaccin Immunother,* 2018. **14**(3): p. 796-799.

193. Shriver, Z., Trevejo, J.M., and Sasisekharan, R. Antibody-Based Strategies to Prevent and Treat Influenza. *Front Immunol,* 2015. **6**: p. 315.

194. Stevens, N.E., Hatjopolous, A., Fraser, C.K., Alsharifi, M., Diener, K.R., and Hayball, J.D. Preserved antiviral adaptive immunity following polyclonal antibody immunotherapy for severe murine influenza infection. *Sci Rep,* 2016. **6**: p. 29154.

195. Luke, T.C., Kilbane, E.M., Jackson, J.L., and Hoffman, S.L. Meta-analysis: convalescent blood products for Spanish influenza pneumonia: a future H5N1 treatment? *Ann Intern Med,* 2006. **145**(8): p. 599-609.

196. Zhou, B., Zhong, N., and Guan, Y. Treatment with convalescent plasma for influenza A (H5N1) infection. *N Engl J Med,* 2007. **357**(14): p. 1450-1.

197. Kumar, A., Meldgaard, T.S., and Bertholet, S. Novel Platforms for the Development of a Universal Influenza Vaccine. *Front Immunol,* 2018. **9**: p. 600.

198. Basu, A., Antanasijevic, A., Wang, M., Li, B., Mills, D.M., Ames, J.A., Nash, P.J., Williams, J.D., Peet, N.P., Moir, D.T., Prichard, M.N., Keith, K.A., Barnard, D.L., Caffrey, M., Rong, L., and Bowlin, T.L. New small molecule entry inhibitors targeting hemagglutinin-mediated influenza a virus fusion. *J Virol,* 2014. **88**(3): p. 1447-60.

199. Makau, J.N., Watanabe, K., Ishikawa, T., Mizuta, S., Hamada, T., Kobayashi, N., and Nishida, N. Identification of small molecule inhibitors for influenza a virus using in silico and in vitro approaches. *PLoS One,* 2017. **12**(3): p. e0173582.

200. Wu, X., Wu, X., Sun, Q., Zhang, C., Yang, S., Li, L., and Jia, Z. Progress of small molecular inhibitors in the development of anti-influenza virus agents. *Theranostics,* 2017. **7**(4): p. 826-845.

201. Sparrow, E., Friede, M., Sheikh, M., Torvaldsen, S., and Newall, A.T. Passive immunization for influenza through antibody therapies, a review of the

pipeline, challenges and potential applications. *Vaccine,* 2016. **34**(45): p. 5442-5448.

202. Wong, H.K., Lee, C.K., Hung, I.F.N., Leung, J.N.S., Hong, J., Yuen, K.Y., and Lin, C.K. Practical limitations of convalescent plasma collection: a case scenario in pandemic preparation for influenza A (H1N1) infection. *Transfusion,* 2010. **50**(9): p. 1967-1971.

203. Czajkowsky, D.M., Hu, J., Shao, Z., and Pleass, R.J. Fc-fusion proteins: new developments and future perspectives. *EMBO Mol Med,* 2012. **4**(10): p. 1015-28.

204. Rath, T., Baker, K., Dumont, J.A., Peters, R.T., Jiang, H., Qiao, S.W., Lencer, W.I., Pierce, G.F., and Blumberg, R.S. Fc-fusion proteins and FcRn: structural insights for longer-lasting and more effective therapeutics. *Crit Rev Biotechnol,* 2015. **35**(2): p. 235-54.

205. Hey, A.S. Safety and General Considerations for the Use of Antibodies in Infectious Diseases, in *Recombinant Antibodies for Infectious Diseases*, Lim, T.S., Editor. 2017, Springer International Publishing: Cham. p. 265-294.

206. Schwartzberg, L.S., Stepanski, E.J., Fortner, B.V., and Houts, A.C. Retrospective chart review of severe infusion reactions with rituximab, cetuximab, and bevacizumab in community oncology practices: assessment of clinical consequences. *Support Care Cancer,* 2008. **16**(4): p. 393-8.

207. Stebbings, R., Findlay, L., Edwards, C., Eastwood, D., Bird, C., North, D., Mistry, Y., Dilger, P., Liefooghe, E., Cludts, I., Fox, B., Tarrant, G., Robinson, J., Meager, T., Dolman, C., Thorpe, S.J., Bristow, A., Wadhwa, M., Thorpe, R., and Poole, S. "Cytokine Storm" in the Phase I Trial of Monoclonal Antibody TGN1412: Better Understanding the Causes to Improve PreClinical Testing of Immunotherapeutics. *The Journal of Immunology,* 2007. **179**(5): p. 3325.

208. Corti, D., Voss, J., Gamblin, S.J., Codoni, G., Macagno, A., Jarrossay, D., Vachieri, S.G., Pinna, D., Minola, A., Vanzetta, F., Silacci, C., Fernandez-Rodriguez, B.M., Agatic, G., Bianchi, S., Giacchetto-Sasselli, I., Calder, L., Sallusto, F., Collins, P., Haire, L.F., Temperton, N., Langedijk, J.P., Skehel, J.J., and Lanzavecchia, A. A Neutralizing Antibody Selected from Plasma Cells That Binds to Group 1 and Group 2 Influenza A Hemagglutinins. *Science,* 2011. **333**(6044): p. 850-6.

209. Ekiert, D., Bhabha, G., Elsliger, M.A., Friesen, R.H., Jongeneelen, M., Throsby, M., Goudsmit, J., and Wilson, I. Antibody Recognition of a Highly Conserved Influenza Virus Epitope. *Science,* 2009. **324**(5924): p. 246-51.

210. Sui, J., Hwang, W.C., Perez, S., Wei, G., Aird, D., Chen, L.M., Santelli, E., Stec, B., Cadwell, G., Ali, M., Wan, H., Murakami, A., Yammanuru, A., Han, T., Cox, N.J., Bankston, L.A., Donis, R.O., Liddington, R.C., and Marasco, W.A. Structural and functional bases for broad-spectrum neutralization of avian and human influenza A viruses. *Nat Struct Mol Biol,* 2009. **16**(3): p. 265-73.

211. Padilla-Quirarte, H.O., Lopez-Guerrero, D.V., Gutierrez-Xicotencatl, L., and Esquivel-Guadarrama, F. Protective Antibodies Against Influenza Proteins. *Front Immunol,* 2019. **10**: p. 1677.

212. Watanabe, A., McCarthy, K.R., Kuraoka, M., Schmidt, A.G., Adachi, Y., Onodera, T., Tonouchi, K., Caradonna, T.M., Bajic, G., Song, S., McGee, C.E., Sempowski, G.D., Feng, F., Urick, P., Kepler, T.B., Takahashi, Y., Harrison, S.C., and Kelsoe, G. Antibodies to a Conserved Influenza Head Interface Epitope Protect by an IgG Subtype-Dependent Mechanism. *Cell,* 2019. **177**(5): p. 1124-1135 e16.

213. Neu, K.E., Henry Dunand, C.J., and Wilson, P.C. Heads, stalks and everything else: how can antibodies eradicate influenza as a human disease? *Curr Opin Immunol,* 2016. **42**: p. 48-55.

214. Li, Y., Myers, J.L., Bostick, D.L., Sullivan, C.B., Madara, J., Linderman, S.L., Liu, Q., Carter, D.M., Wrammert, J., Esposito, S., Principi, N., Plotkin, J.B., Ross, T.M., Ahmed, R., Wilson, P.C., and Hensley, S.E. Immune history shapes specificity of pandemic H1N1 influenza antibody responses. *J Exp Med,* 2013. **210**(8): p. 1493-500.

215. Magadan, J.G., Altman, M.O., Ince, W.L., Hickman, H.D., Stevens, J., Chevalier, A., Baker, D., Wilson, P.C., Ahmed, R., Bennink, J.R., and Yewdell, J.W. Biogenesis of influenza a virus hemagglutinin cross-protective stem epitopes. *PLoS Pathog,* 2014. **10**(6): p. e1004204.

216. Schneemann, A., Speir, J.A., Tan, G.S., Khayat, R., Ekiert, D.C., Matsuoka, Y., and Wilson, I.A. A virus-like particle that elicits cross-reactive antibodies to the conserved stem of influenza virus hemagglutinin. *J Virol,* 2012. **86**(21): p. 11686-97.

217. Avnir, Y., Tallarico, A.S., Zhu, Q., Bennett, A.S., Connelly, G., Sheehan, J., Sui, J., Fahmy, A., Huang, C.Y., Cadwell, G., Bankston, L.A., McGuire, A.T., Stamatatos, L., Wagner, G., Liddington, R.C., and Marasco, W.A. Molecular signatures of hemagglutinin stem-directed heterosubtypic human neutralizing antibodies against influenza A viruses. *PLoS Pathog,* 2014. **10**(5): p. e1004103.

218. Dreyfus, C., Ekiert, D.C., and Wilson, I.A. Structure of a classical broadly neutralizing stem antibody in complex with a pandemic H2 influenza virus hemagglutinin. *J Virol,* 2013. **87**(12): p. 7149-54.

219. Gaiotto, T. and Hufton, S.E. Cross-Neutralising Nanobodies Bind to a Conserved Pocket in the Hemagglutinin Stem Region Identified Using Yeast Display and Deep Mutational Scanning. *PLoS One,* 2016. **11**(10): p. e0164296.

220. Wyrzucki, A., Dreyfus, C., Kohler, I., Steck, M., Wilson, I.A., and Hangartner, L. Alternative recognition of the conserved stem epitope in influenza A virus hemagglutinin by a VH3-30-encoded heterosubtypic antibody. *J Virol,* 2014. **88**(12): p. 7083-92.

221. Zhu, X., Guo, Y.H., Jiang, T., Wang, Y.D., Chan, K.H., Li, X.F., Yu, W., McBride, R., Paulson, J.C., Yuen, K.Y., Qin, C.F., Che, X.Y., and Wilson, I.A. A unique and conserved neutralization epitope in H5N1 influenza viruses identified by an antibody against the A/Goose/Guangdong/1/96 hemagglutinin. *J Virol,* 2013. **87**(23): p. 12619-35.

222. Corti, D., Cameroni, E., Guarino, B., Kallewaard, N.L., Zhu, Q., and Lanzavecchia, A. Tackling influenza with broadly neutralizing antibodies. *Curr Opin Virol,* 2017. **24**: p. 60-69.

223. O'Donnell, C.D., Vogel, L., Wright, A., Das, S.R., Wrammert, J., Li, G.M., McCausland, M., Zheng, N.Y., Yewdell, J.W., Ahmed, R., Wilson, P.C., and Subbarao, K. Antibody pressure by a human monoclonal antibody targeting the 2009 pandemic H1N1 virus hemagglutinin drives the emergence of a virus with increased virulence in mice*. MBio,* 2012. **3**(3).

224. Schmeisser, F., Vasudevan, A., Verma, S., Wang, W., Alvarado, E., Weiss, C., Atukorale, V., Meseda, C., and Weir, J.P. Antibodies to antigenic site A of influenza H7 hemagglutinin provide protection against H7N9 challenge*. PLoS One,* 2015. **10**(1): p. e0117108.

225. Shen, C., Chen, J., Li, R., Zhang, M., Wang, G., Stegalkina, S., Zhang, L., Chen, J., Cao, J., Bi, X., Anderson, S., Alefantis, T., Zhang, M., Cai, X., Yang, K., Zheng, Q., Fang, M., Yu, H., Luo, W., Zheng, Z., Yuan, Q., Zhang, J., Wai-Kuo Shih, J., Kleanthous, H., Chen, H., Chen, Y., and Xia, N. A multimechanistic antibody targeting the receptor binding site potently cross-protects against influenza B viruses*. Science Translational Medicine,* 2017. **9**.

226. Bangaru, S., Lang, S., Schotsaert, M., Vanderven, H.A., Zhu, X., Kose, N., Bombardi, R., Finn, J.A., Kent, S.J., Gilchuk, P., Gilchuk, I., Turner, H.L., Garcia-Sastre, A., Li, S., Ward, A.B., Wilson, I.A., and Crowe, J.E., Jr. A Site of Vulnerability on the Influenza Virus Hemagglutinin Head Domain Trimer Interface*. Cell,* 2019. **177**(5): p. 1136-1152 e18.

227. Brandenburg, B., Koudstaal, W., Goudsmit, J., Klaren, V., Tang, C., Bujny, M.V., Korse, H.J., Kwaks, T., Otterstrom, J.J., Juraszek, J., van Oijen, A.M., Vogels, R., and Friesen, R.H. Mechanisms of hemagglutinin targeted influenza virus neutralization*. PLoS One,* 2013. **8**(12): p. e80034.

228. Lee, P.S., Yoshida, R., Ekiert, D.C., Sakai, N., Suzuki, Y., Takada, A., and Wilson, I.A. Heterosubtypic antibody recognition of the influenza virus hemagglutinin receptor binding site enhanced by avidity*. Proc Natl Acad Sci U S A,* 2012. **109**(42): p. 17040-5.

229. Kanyavuz, A., Marey-Jarossay, A., Lacroix-Desmazes, S., and Dimitrov, J.D. Breaking the law: unconventional strategies for antibody diversification*. Nature Reviews Immunology,* 2019. **19**(6): p. 355-368.

230. Wilson, I.A., Niman, H.L., Houghten, R.A., Cherenson, A.R., Connolly, M.L., and Lerner, R.A. The structure of an antigenic determinant in a protein*. Cell,* 1984. **37**(3): p. 767-78.

231. van den Beucken, T., Pieters, H., Steukers, M., van der Vaart, M., Ladner, R.C., Hoogenboom, H.R., and Hufton, S.E. Affinity maturation of Fab antibody fragments by fluorescent-activated cell sorting of yeast-displayed libraries*. FEBS Lett,* 2003. **546**(2-3): p. 288-94.

232. Tonegawa, S. Somatic generation of antibody diversity*. Nature,* 1983. **302**(5909): p. 575-581.

233. Murin, C.D., Wilson, I.A., and Ward, A.B. Antibody responses to viral infections: a structural perspective across three different enveloped viruses*. Nat Microbiol,* 2019. **4**(5): p. 734-747.

234. Lerner, R.A. Rare antibodies from combinatorial libraries suggests an S.O.S. component of the human immunological repertoire*. Mol Biosyst,* 2011. **7**(4): p. 1004-12.

235. Lerner, R.A. Combinatorial antibody libraries: new advances, new immunological insights. *Nat Rev Immunol,* 2016. **16**(8): p. 498-508.

236. Lang, S., Xie, J., Zhu, X., Wu, N., Lerner, R., and Wilson, I. Antibody 27F3 Broadly Targets Influenza A Group 1 and 2 Hemagglutinins through a Further Variation in VH1-69 Antibody Orientation on the HA Stem. *Cell Rep,* 2017. **20**(12): p. 2935-2943.

237. Rajpal, A., Beyaz, N., Haber, L., Cappuccilli, G., Yee, H., Bhatt, R.R., Takeuchi, T., Lerner, R.A., and Crea, R. A general method for greatly improving the affinity of antibodies by using combinatorial libraries. *Proc Natl Acad Sci U S A,* 2005. **102**(24): p. 8466-71.

238. Throsby, M., van den Brink, E., Jongeneelen, M., Poon, L.L., Alard, P., Cornelissen, L., Bakker, A., Cox, F., van Deventer, E., Guan, Y., Cinatl, J., ter Meulen, J., Lasters, I., Carsetti, R., Peiris, M., de Kruif, J., and Goudsmit, J. Heterosubtypic neutralizing monoclonal antibodies cross-protective against H5N1 and H1N1 recovered from human IgM+ memory B cells. *PLoS One,* 2008. **3**(12): p. e3942.

239. Hoogenboom, H.R., de Bruine, A.P., Hufton, S.E., Hoet, R.M., Arends, J.W., and Roovers, R.C. Antibody phage display technology and its applications. *Immunotechnology,* 1998. **4**(1): p. 1-20.

240. Sheehan, J. and Marasco, W.A. Phage and Yeast Display. *Microbiology Spectrum,* 2015. **3**(1).

241. Li, G.M., Chiu, C., Wrammert, J., McCausland, M., Andrews, S.F., Zheng, N.Y., Lee, J.H., Huang, M., Qu, X., Edupuganti, S., Mulligan, M., Das, S.R., Yewdell, J.W., Mehta, A.K., Wilson, P.C., and Ahmed, R. Pandemic H1N1 influenza vaccine induces a recall response in humans that favors broadly cross-reactive memory B cells. *Proc Natl Acad Sci U S A,* 2012. **109**(23): p. 9047-52.

242. Ekiert, D.C., Friesen, R.H., Bhabha, G., Kwaks, T., Jongeneelen, M., Yu, W., Ophorst, C., Cox, F., Korse, H.J., Brandenburg, B., Vogels, R., Brakenhoff, J.P., Kompier, R., Koldijk, M.H., Cornelissen, L.A., Poon, L.L., Peiris, M., Koudstaal, W., Wilson, I.A., and Goudsmit, J. A highly conserved neutralizing epitope on group 2 influenza A viruses. *Science,* 2011. **333**(6044): p. 843-50.

243. Friesen, R.H., Lee, P.S., Stoop, E.J., Hoffman, R.M., Ekiert, D.C., Bhabha, G., Yu, W., Juraszek, J., Koudstaal, W., Jongeneelen, M., Korse, H.J., Ophorst, C., Brinkman-van der Linden, E.C., Throsby, M., Kwakkenbos, M.J., Bakker, A.Q., Beaumont, T., Spits, H., Kwaks, T., Vogels, R., Ward, A.B., Goudsmit, J., and Wilson, I.A. A common solution to group 2 influenza virus neutralization. *Proc Natl Acad Sci U S A,* 2014. **111**(1): p. 445-50.

244. Fu, Y., Zhang, Z., Sheehan, J., Avnir, Y., Ridenour, C., Sachnik, T., Sun, J., Hossain, M.J., Chen, L.M., Zhu, Q., Donis, R.O., and Marasco, W.A. A broadly neutralizing anti-influenza antibody reveals ongoing capacity of haemagglutinin-specific memory B cells to evolve. *Nat Commun,* 2016. **7**: p. 12780.

245. Wrammert, J., Koutsonanos, D., Li, G.M., Edupuganti, S., Sui, J., Morrissey, M., McCausland, M., Skountzou, I., Hornig, M., Lipkin, W.I., Mehta, A., Razavi, B., Del Rio, C., Zheng, N.Y., Lee, J.H., Huang, M., Ali, Z., Kaur, K., Andrews, S., Amara, R.R., Wang, Y., Das, S.R., O'Donnell, C.D., Yewdell, J.W., Subbarao, K., Marasco, W.A., Mulligan, M.J., Compans, R., Ahmed, R.,

and Wilson, P.C. Broadly cross-reactive antibodies dominate the human B cell response against 2009 pandemic H1N1 influenza virus infection. *J Exp Med,* 2011. **208**(1): p. 181-93.

246. DiLillo, D.J., Palese, P., Wilson, P.C., and Ravetch, J.V. Broadly neutralizing anti-influenza antibodies require Fc receptor engagement for in vivo protection. *J Clin Invest,* 2016. **126**(2): p. 605-10.

247. DiLillo, D.J., Tan, G.S., Palese, P., and Ravetch, J.V. Broadly neutralizing hemagglutinin stalk-specific antibodies require FcgammaR interactions for protection against influenza virus in vivo. *Nat Med,* 2014. **20**(2): p. 143-51.

248. Simhadri, V.R., Dimitrova, M., Mariano, J.L., Zenarruzabeitia, O., Zhong, W., Ozawa, T., Muraguchi, A., Kishi, H., Eichelberger, M.C., and Borrego, F. A Human Anti-M2 Antibody Mediates Antibody-Dependent Cell-Mediated Cytotoxicity (ADCC) and Cytokine Secretion by Resting and Cytokine-Preactivated Natural Killer (NK) Cells. *PLoS One,* 2015. **10**(4): p. e0124677.

249. Hamers-Casterman, C., Atarhouch, T., Muyldermans, S., Robinson, G., Hamers, C., Bajyana Songa, E., Bendahman, N., and Hammers, R. Naturally-occurring antibodies devoid of light chains. *Nature,* 1993. **363**: p. 446-8.

250. Muyldermans, S., Atarhouch, T., Saldanha, J., Barbosa, J.A.R.G., and Hamers, R. Sequence and structure of VH domain from naturally occurring camel heavy chain immunoglobulins lacking light chains. *Protein Engineering,* 1994. **7**(9): p. 1129-35.

251. Muyldermans, S. Single domain camel antibodies: current status. *Reviews in Molecular Biotechnology,* 2001. **74**: p. 277-302.

252. Arbabi Ghahroudi, M., Desmyter, A., Wyns, L., Hamers, R., and Muyldermans, S. Selection and identification of single domain antibody fragments from camel heavy-chain antibodies. *FEBS Letters,* 1997. **414**(3): p. 521-526.

253. Muyldermans, S., Baral, T.N., Retamozzo, V.C., De Baetselier, P., De Genst, E., Kinne, J., Leonhardt, H., Magez, S., Nguyen, V.K., Revets, H., Rothbauer, U., Stijlemans, B., Tillib, S., Wernery, U., Wyns, L., Hassanzadeh-Ghassabeh, G., and Saerens, D. Camelid immunoglobulins and nanobody technology. *Vet Immunol Immunopathol,* 2009. **128**(1-3): p. 178-83.

254. Harmsen, M.M. and De Haard, H.J. Properties, production, and applications of camelid single-domain antibody fragments. *Applied microbiology and biotechnology,* 2007. **77**(1): p. 13-22.

255. De Genst, E., Silence, K., Decanniere, K., Conrath, K., Loris, R., Kinne, J., Muyldermans, S., and Wyns, L. Molecular basis for the preferential cleft recognition by dromedary heavy-chain antibodies. *Proc Natl Acad Sci U S A,* 2006. **103**(12): p. 4586-91.

256. De Genst, E., Saerens, D., Muyldermans, S., and Conrath, K. Antibody repertoire development in camelids. *Dev Comp Immunol,* 2006. **30**(1-2): p. 187-98.

257. Desmyter, A., Transue, T.R., Ghahroudi, M.A., Dao Thi, M.-H., Poortmans, F., Hamers, R., Muyldermans, S., and Wyns, L. Crystal structure of a camel single-domain VH antibody fragment in complex with lysozyme. *Nature Structural Biology,* 1996. **3**(9): p. 803-811.

258. Bannas, P., Hambach, J., and Koch-Nolte, F. Nanobodies and Nanobody-Based Human Heavy Chain Antibodies As Antitumor Therapeutics. *Frontiers in immunology,* 2017. **8**: p. 1603-1603.

259. Harmsen, M.M., Ruuls, R.C., Nijman, I.J., Niewold, T.A., Frenken, L.G., and de Geus, B. Llama heavy-chain V regions consist of at least four distinct subfamilies revealing novel sequence features. *Mol Immunol,* 2000. **37**(10): p. 579-90.

260. Muyldermans, S. Nanobodies: natural single-domain antibodies. *Annu Rev Biochem,* 2013. **82**: p. 775-97.

261. Abderrazek, R.B., Hmila, I., Vincke, C., Benlasfar, Z., Pellis, M., Dabbek, H., Saerens, D., El Ayeb, M., Muyldermans, S., and Bouhaouala-Zahar, B. Identification of potent nanobodies to neutralize the most poisonous polypeptide from scorpion venom. *Biochem J,* 2009. **424**(2): p. 263-72.

262. Linden, R.H.J.v.d., Frenken, L.G.J., Geus, B.d., Harmsen, M.M., Ruuls, R.C., Stok, W., Ron, L.d., Wilson, S., Davis, P., and Verrips, C.T. Comparison of physical chemical properties of llama VHH antibody fragments and mouse monoclonal antibodies. *Biochimica et Biophysica Acta* 1999. **1431**: p. 37-46.

263. Dumoulin, M., Conrath, K., Van Meirhaeghe, A., Meersman, F., Heremans, K., Frenken, L.G., Muyldermans, S., Wyns, L., and Matagne, A. Single-domain antibody fragments with high conformational stability. *Protein Sci,* 2002. **11**(3): p. 500-15.

264. Wu, Y., Jiang, S., and Ying, T. Single-Domain Antibodies As Therapeutics against Human Viral Diseases. *Front Immunol,* 2017. **8**: p. 1802.

265. Conrath, K., Vincke, C., Stijlemans, B., Schymkowitz, J., Decanniere, K., Wyns, L., Muyldermans, S., and Loris, R. Antigen binding and solubility effects upon the veneering of a camel VHH in framework-2 to mimic a VH. *J Mol Biol,* 2005. **350**(1): p. 112-25.

266. De Vlieger, D., Ballegeer, M., Rossey, I., Schepens, B., and Saelens, X. Single-Domain Antibodies and Their Formatting to Combat Viral Infections. *Antibodies,* 2018. **8**(1): p. 1.

267. Harmsen, M., Blokker, J., Pritz-Verschuren, S., Bartelink, W., van der Burg, H., and Koch, G. Isolation of Panels of Llama Single-Domain Antibody Fragments Binding All Nine Neuraminidase Subtypes of Influenza A Virus. *Antibodies,* 2013. **2**(4): p. 168-192.

268. Hufton, S.E., Risley, P., Ball, C.R., Major, D., Engelhardt, O.G., and Poole, S. The breadth of cross sub-type neutralisation activity of a single domain antibody to influenza hemagglutinin can be increased by antibody valency. *PLoS One,* 2014. **9**(8): p. e103294.

269. Romão, E., Poignavent, V., Vincke, C., Ritzenthaler, C., Muyldermans, S., and B., M. Construction of High-Quality Camel Immune Antibody Libraries., in *Phage Display. Methods in Molecular Biology*, Hust, M. and Lim, T., Editors. 2018, Humana Press: New York, NY.

270. Vincke, C., Loris, R., Saerens, D., Martinez-Rodriguez, S., Muyldermans, S., and Conrath, K. General strategy to humanize a camelid single-domain antibody and identification of a universal humanized nanobody scaffold. *J Biol Chem,* 2009. **284**(5): p. 3273-84.

271. Batra, S., Jain, M., Wittel, U., Chauhan, S., and Colcher, D. Pharmacokinetics and biodistribution of genetically engineered antibodies. *Current Opinion in Biotechnology,* 2002. **13**: p. 603-608.

272. Keizer, R.J., Huitema, A.D.R., Schellens, J.H.M., and Beijnen, J.H. Clinical Pharmacokinetics of Therapeutic Monoclonal Antibodies. *Clinical Pharmacokinetics,* 2010. **49**(8): p. 493-507.

273. Cortez-Retamozo, V., Lauwereys, M., Hassanzadeh Gh, G., Gobert, M., Conrath, K., Muyldermans, S., De Baetselier, P., and Revets, H. Efficient tumor targeting by single-domain antibody fragments of camels. *Int J Cancer,* 2002. **98**(3): p. 456-62.

274. Junghans, R.P. and Anderson, C.L. The protection receptor for IgG catabolism is the beta2-microglobulin-containing neonatal intestinal transport receptor. *Proceedings of the National Academy of Sciences,* 1996. **93**: p. 5512-5516.

275. Els Conrath, K., Lauwereys, M., Wyns, L., and Muyldermans, S. Camel single-domain antibodies as modular building units in bispecific and bivalent antibody constructs. *J Biol Chem,* 2001. **276**(10): p. 7346-50.

276. Fan, K., Jiang, B., Guan, Z., He, J., Yang, D., Xie, N., Nie, G., Xie, C., and Yan, X. Fenobody: A Ferritin-Displayed Nanobody with High Apparent Affinity and Half-Life Extension. *Analytical Chemistry,* 2018. **90**(9): p. 5671-5677.

277. Yamaoka, T., Tabata, Y., and Ikada, Y. Distribution and tissue uptake of poly(ethylene glycol) with different molecular weights after intravenous administration to mice. *J Pharm Sci,* 1994. **83**(4): p. 601-6.

278. Harmsen, M.M., van Solt, C.B., Fijten, H.P., van Keulen, L., Rosalia, R.A., Weerdmeester, K., Cornelissen, A.H., De Bruin, M.G., Eble, P.L., and Dekker, A. Passive immunization of guinea pigs with llama single-domain antibody fragments against foot-and-mouth disease. *Vet Microbiol,* 2007. **120**(3-4): p. 193-206.

279. Kratz, F. Albumin as a drug carrier: design of prodrugs, drug conjugates and nanoparticles. *J Control Release,* 2008. **132**(3): p. 171-83.

280. Chaudhury, C., Mehnaz, S., Robinson, J.M., Hayton, W.L., Pearl, D.K., Roopenian, D.C., and Anderson, C.L. The Major Histocompatibility Complex–related Fc Receptor for IgG (FcRn) Binds Albumin and Prolongs Its Lifespan. *Journal of Experimental Medicine,* 2003. **197**(3): p. 315-322.

281. Hoefman, S., Ottevaere, I., Baumeister, J., and Sargentini-Maier, M.L. Pre-Clinical Intravenous Serum Pharmacokinetics of Albumin Binding and Non-Half-Life Extended Nanobodies (R). *Antibodies,* 2015. **4**(3): p. 141-156.

282. Terryn, S., Francart, A., Lamoral, S., Hultberg, A., Rommelaere, H., Wittelsberger, A., Callewaert, F., Stohr, T., Meerschaert, K., Ottevaere, I., Stortelers, C., Vanlandschoot, P., Kalai, M., and Van Gucht, S. Protective effect of different anti-rabies virus VHH constructs against rabies disease in mice. *PLoS One,* 2014. **9**(10): p. e109367.

283. Van Roy, M., Ververken, C., Beirnaert, E., Hoefman, S., Kolkman, J., Vierboom, M., Breedveld, E., t Hart, B., Poelmans, S., Bontinck, L., Hemeryck, A., Jacobs, S., Baumeister, J., and Ulrichts, H. The preclinical pharmacology of the high affinity anti-IL-6R Nanobody(R) ALX-0061 supports

its clinical development in rheumatoid arthritis. *Arthritis Res Ther,* 2015. **17**: p. 135.

284. Hultberg, A., Temperton, N.J., Rosseels, V., Koenders, M., Gonzalez-Pajuelo, M., Schepens, B., Ibanez, L.I., Vanlandschoot, P., Schillemans, J., Saunders, M., Weiss, R.A., Saelens, X., Melero, J.A., Verrips, C.T., Van Gucht, S., and de Haard, H.J. Llama-derived single domain antibodies to build multivalent, superpotent and broadened neutralizing anti-viral molecules. *PLoS One,* 2011. **6**(4): p. e17665.

285. Palomo, C., Mas, V., Detalle, L., Depla, E., Cano, O., Vazquez, M., Stortelers, C., and Melero, J.A. Trivalency of a Nanobody Specific for the Human Respiratory Syncytial Virus Fusion Glycoprotein Drastically Enhances Virus Neutralization and Impacts Escape Mutant Selection. *Antimicrob Agents Chemother,* 2016. **60**(11): p. 6498-6509.

286. Lutje Hulsik, D., Liu, Y.Y., Strokappe, N.M., Battella, S., El Khattabi, M., McCoy, L.E., Sabin, C., Hinz, A., Hock, M., Macheboeuf, P., Bonvin, A.M., Langedijk, J.P., Davis, D., Forsman Quigley, A., Aasa-Chapman, M.M., Seaman, M.S., Ramos, A., Poignard, P., Favier, A., Simorre, J.P., Weiss, R.A., Verrips, C.T., Weissenhorn, W., and Rutten, L. A gp41 MPER-specific llama VHH requires a hydrophobic CDR3 for neutralization but not for antigen recognition. *PLoS Pathog,* 2013. **9**(3): p. e1003202.

287. Matz, J., Kessler, P., Bouchet, J., Combes, O., Ramos, O.H.P., Barin, F., Baty, D., Martin, L., Benichou, S., and Chames, P. Straightforward Selection of Broadly Neutralizing Single-Domain Antibodies Targeting the Conserved CD4 and Coreceptor Binding Sites of HIV-1 gp120. *Journal of Virology,* 2013. **87**: p. 1137-1149.

288. Harmsen, M.M., Van Solt, C.B., Fijten, H.P., and Van Setten, M.C. Prolonged in vivo residence times of llama single-domain antibody fragments in pigs by binding to porcine immunoglobulins. *Vaccine,* 2005. **23**(41): p. 4926-34.

289. Stalin Raj, V., Okba, N.M.A., Gutierrez-Alvarez, J., Drabek, D., van Dieren, B., Widagdo, W., Lamers, M.M., Widjaja, I., Fernandez-Delgado, R., Sola, I., Bensaid, A., Koopmans, M.P., Segalés, J., Osterhaus, A.D.M.E., Bosch, B.J., Enjuanes, L., and Haagmans, B.L. Chimeric camel/human heavy-chain antibodies protect against MERS-CoV infection. *Science advances,* 2018. **4**(8): p. eaas9667-eaas9667.

290. Bobkov, V., Zarca, A.M., Van Hout, A., Arimont, M., Doijen, J., Bialkowska, M., Toffoli, E., Klarenbeek, A., van der Woning, B., van der Vliet, H.J., Van Loy, T., de Haard, H., Schols, D., Heukers, R., and Smit, M.J. Nanobody-Fc constructs targeting chemokine receptor CXCR4 potently inhibit signaling and CXCR4-mediated HIV-entry and induce antibody effector functions. *Biochem Pharmacol,* 2018. **158**: p. 413-424.

291. DiLillo, D.J. and Ravetch, J.V. Fc-Receptor Interactions Regulate Both Cytotoxic and Immunomodulatory Therapeutic Antibody Effector Functions. *Cancer Immunol Res,* 2015. **3**(7): p. 704-13.

292. Nimmerjahn, F. and Ravetch, J.V. Fcgamma receptors: old friends and new family members. *Immunity,* 2006. **24**(1): p. 19-28.

293. van der Vaart, J.M., Pant, N., Wolvers, D., Bezemer, S., Hermans, P.W., Bellamy, K., Sarker, S.A., van der Logt, C.P., Svensson, L., Verrips, C.T., Hammarstrom, L., and van Klinken, B.J. Reduction in morbidity of rotavirus

induced diarrhoea in mice by yeast produced monovalent llama-derived antibody fragments. *Vaccine,* 2006. **24**(19): p. 4130-7.

294. Gunaydin, G., Yu, S., Graslund, T., Hammarstrom, L., and Marcotte, H. Fusion of the mouse IgG1 Fc domain to the VHH fragment (ARP1) enhances protection in a mouse model of rotavirus. *Sci Rep,* 2016. **6**: p. 30171.

295. McEwan, W.A., Tam, J.C.H., Watkinson, R.E., Bidgood, S.R., Mallery, D.L., and James, L.C. Intracellular antibody-bound pathogens stimulate immune signaling via the Fc receptor TRIM21. *Nature immunology,* 2013. **14**(4): p. 327-336.

296. Geoghegan, E.M., Zhang, H., Desai, P.J., Biragyn, A., and Markham, R.B. Antiviral activity of a single-domain antibody immunotoxin binding to glycoprotein D of herpes simplex virus 2. *Antimicrob Agents Chemother,* 2015. **59**(1): p. 527-35.

297. Wang, S.X., Michiels, J., Arien, K.K., New, R., Vanham, G., and Roitt, I. Inhibition of HIV Virus by Neutralizing Vhh Attached to Dual Functional Liposomes Encapsulating Dapivirine. *Nanoscale Res Lett,* 2016. **11**(1): p. 350.

298. Wei, G., Meng, W., Guo, H., Pan, W., Liu, J., Peng, T., Chen, L., and Chen, C.-Y. Potent Neutralization of Influenza A Virus by a Single-Domain Antibody Blocking M2 Ion Channel Protein. *PLOS ONE,* 2011. **6**(12): p. e28309.

299. Ibanez, L.I., De Filette, M., Hultberg, A., Verrips, T., Temperton, N., Weiss, R.A., Vandevelde, W., Schepens, B., Vanlandschoot, P., and Saelens, X. Nanobodies with in vitro neutralizing activity protect mice against H5N1 influenza virus infection. *J Infect Dis,* 2011. **203**(8): p. 1063-72.

300. Tillib, S.V., Ivanova, T.I., Vasilev, L.A., Rutovskaya, M.V., Saakyan, S.A., Gribova, I.Y., Tutykhina, I.L., Sedova, E.S., Lysenko, A.A., Shmarov, M.M., Logunov, D.Y., Naroditsky, B.S., and Gintsburg, A.L. Formatted single-domain antibodies can protect mice against infection with influenza virus (H5N2). *Antiviral Res,* 2013. **97**(3): p. 245-54.

301. Cardoso, F.M., Ibañez, L.I., Van den Hoecke, S., De Baets, S., Smet, A., Roose, K., Schepens, B., Descamps, F.J., Fiers, W., Muyldermans, S., Depicker, A., and Saelens, X. Single-Domain Antibodies Targeting Neuraminidase Protect against an H5N1 Influenza Virus Challenge. *Journal of Virology,* 2014. **88**: p. 8278-8296.

302. Del Rosario, J.M.M., Smith, M., Zaki, K., Risley, P., Temperton, N., Engelhardt, O.G., Collins, M., Takeuchi, Y., and Hufton, S.E. Protection From Influenza by Intramuscular Gene Vector Delivery of a Broadly Neutralizing Nanobody Does Not Depend on Antibody Dependent Cellular Cytotoxicity. *Front Immunol,* 2020. **11**: p. 627.

303. Scully, M., Cataland, S.R., Peyvandi, F., Coppo, P., Knobl, P., Kremer Hovinga, J.A., Metjian, A., de la Rubia, J., Pavenski, K., Callewaert, F., Biswas, D., De Winter, H., Zeldin, R.K., and Investigators, H. Caplacizumab Treatment for Acquired Thrombotic Thrombocytopenic Purpura. *N Engl J Med,* 2019. **380**(4): p. 335-346.

304. Friedmann, T. A brief history of gene therapy. *Nature Genetics,* 1992. **2**(2): p. 93-98.

305. Keeler, A.M., ElMallah, M.K., and Flotte, T.R. Gene Therapy 2017: Progress and Future Directions. *Clin Transl Sci,* 2017. **10**(4): p. 242-248.

306. Collins, M. and Thrasher, A. Gene therapy: progress and predictions. *Proc Biol Sci,* 2015. **282**(1821): p. 20143003.

307. Kotterman, M.A., Chalberg, T.W., and Schaffer, D.V. Viral Vectors for Gene Therapy: Translational and Clinical Outlook. *Annu Rev Biomed Eng,* 2015. **17**: p. 63-89.

308. Warnock, J., Daigre, C., and Al-Rubeai, M. Viral Vectors for Gene Therapy, in *Methods in Molecular Biology*, Walker, J., Editor. 2011, Humana Press.

309. Thomas, C.E., Ehrhardt, A., and Kay, M.A. Progress and problems with the use of viral vectors for gene therapy. *Nature Reviews Genetics,* 2003. **4**(5): p. 346-358.

310. Kay, M.A., Glorioso, J.C., and Naldini, L. Viral vectors for gene therapy: the art of turning infectious agents into vehicles of therapeutics. *Nature Medicine,* 2001. **7**(1): p. 33-40.

311. Zufferey, R., Nagy, D., Mendel, R.J., Naldini, L., and Trono, D. Multiply attenuated lentiviral vector achieves efficient gene delivery in vivo. *Nature Biotechnology,* 1997. **15**.

312. Naldini, L., Blomer, U., Gallay, P., Ory, D., Mulligan, R., Gage, F., Verma, I., and Trono, D. In Vivo Gene Delivery and Stable Transduction of Nondividing Cells by a Lentiviral Vector. *Science,* 1996. **272**(5259): p. 363-267.

313. Douglas, J.T. Adenoviral vectors for gene therapy. *Molecular Biotechnology,* 2007. **36**(1): p. 71-80.

314. Duffy, A.M., O'Doherty, A.M., O'Brien, T., and Strappe, P.M. Purification of adenovirus and adeno-associated virus: comparison of novel membrane-based technology to conventional techniques. *Gene Ther,* 2005. **12 Suppl 1**: p. S62-72.

315. Medicine, T.J.o.G., Gene Therapy Clinical Trials Worldwide. 2019, John Wiley and Sons Ltd.

316. Joseph, A., Zheng, J.H., Chen, K., Dutta, M., Chen, C., Stiegler, G., Kunert, R., Follenzi, A., and Goldstein, H. Inhibition of in vivo HIV infection in humanized mice by gene therapy of human hematopoietic stem cells with a lentiviral vector encoding a broadly neutralizing anti-HIV antibody. *J Virol,* 2010. **84**(13): p. 6645-53.

317. Skaricic, D., Traube, C., De, B., Joh, J., Boyer, J., Crystal, R.G., and Worgall, S. Genetic delivery of an anti-RSV antibody to protect against pulmonary infection with RSV. *Virology,* 2008. **378**(1): p. 79-85.

318. Tutykhina, I.L., Sedova, E.S., Gribova, I.Y., Ivanova, T.I., Vasilev, L.A., Rutovskaya, M.V., Lysenko, A.A., Shmarov, M.M., Logunov, D.Y., Naroditsky, B.S., Tillib, S.V., and Gintsburg, A.L. Passive immunization with a recombinant adenovirus expressing an HA (H5)-specific single-domain antibody protects mice from lethal influenza infection. *Antiviral Res,* 2013. **97**(3): p. 318-28.

319. Daya, S. and Berns, K.I. Gene therapy using adeno-associated virus vectors. *Clin Microbiol Rev,* 2008. **21**(4): p. 583-93.

320. Naso, M.F., Tomkowicz, B., Perry, W.L., and Strohl, W.R. Adeno-Associated Virus (AAV) as a Vector for Gene Therapy. *BioDrugs,* 2017. **31**(4): p. 317-334.

321. Weitzman, M.D. and Linden, R.M. Adeno-associated virus biology. *Methods Mol Biol,* 2011. **807**: p. 1-23.

322. Deyle, D.R. and Russell, D.W. Adeno-associated virus vector integration. *Current Opinion in Molecular Therapeutics,* 2009. **11**(4): p. 442-7.

323. Goncalves, M.A. Adeno-associated virus: from defective virus to effective vector. *Virol J,* 2005. **2**: p. 43.

324. Grieger, J.C. and Samulski, R.J. Adeno-associated virus vectorology, manufacturing, and clinical applications. *Methods Enzymol,* 2012. **507**: p. 229-54.

325. Adeno-Associated Virus: Methods and Protocols. Methods in Molecular Biology, ed. Walker, J. Vol. 807. 2011: Humana Press.

326. Xie, Q., Bu, W., Bhatia, S., Hare, J., Somasundaram, T., Azzi, A., and Chapman, M. The atomic structure of adeno-associated virus (AAV-2), a vector for human gene therapy. *Proc Natl Acad Sci USA,* 2002. **99**: p. 10405-10.

327. Johnson, F., Ozer, H., and Hoggan, M. Structural proteins of adeno-associated virus type 3. *Journal of Virology,* 1971. **8**: p. 860-3.

328. Pillay, S., Meyer, N.L., Puschnik, A.S., Davulcu, O., Diep, J., Ishikawa, Y., Jae, L.T., Wosen, J.E., Nagamine, C.M., Chapman, M.S., and Carette, J.E. An essential receptor for adeno-associated virus infection. *Nature,* 2016. **530**(7588): p. 108-112.

329. Zincarelli, C., Soltys, S., Rengo, G., and Rabinowitz, J.E. Analysis of AAV serotypes 1-9 mediated gene expression and tropism in mice after systemic injection. *Mol Ther,* 2008. **16**(6): p. 1073-80.

330. Tenenbaum, L., Lehtonen, E., and Monahan, P.E. Evaluation of Risks Related to the Use of Adeno-Associated Virus-Based Vectors. *Current Gene Therapy,* 2003. **3**: p. 545-65.

331. Valdmanis, P.N. and Kay, M.A. Future of rAAV Gene Therapy: Platform for RNAi, Gene Editing, and Beyond. *Hum Gene Ther,* 2017. **28**(4): p. 361-372.

332. Nass, S.A., Mattingly, M.A., Woodcock, D.A., Burnham, B.L., Ardinger, J.A., Osmond, S.E., Frederick, A.M., Scaria, A., Cheng, S.H., and O'Riordan, C.R. Universal Method for the Purification of Recombinant AAV Vectors of Differing Serotypes. *Mol Ther Methods Clin Dev,* 2018. **9**: p. 33-46.

333. Asokan, A., Schaffer, D.V., and Samulski, R.J. The AAV vector toolkit: poised at the clinical crossroads. *Mol Ther,* 2012. **20**(4): p. 699-708.

334. Lisowski, L., Tay, S.S., and Alexander, I.E. Adeno-associated virus serotypes for gene therapeutics. *Curr Opin Pharmacol,* 2015. **24**: p. 59-67.

335. Berns, K.I. and Muzyczka, N. AAV: An Overview of Unanswered Questions. *Hum Gene Ther,* 2017. **28**(4): p. 308-313.

336. Mingozzi, F. and High, K.A. Immune responses to AAV vectors: overcoming barriers to successful gene therapy*. Blood,* 2013. **122**(1): p. 23-36.

337. Calcedo, R., Vandenberghe, L.H., Gao, G., Lin, J., and Wilson, J.M. Worldwide epidemiology of neutralizing antibodies to adeno-associated viruses*. J Infect Dis,* 2009. **199**(3): p. 381-90.

338. Greig, J.A., Calcedo, R., Grant, R.L., Peng, H., Medina-Jaszek, C.A., Ahonkhai, O., Qin, Q., Roy, S., Tretiakova, A.P., and Wilson, J.M. Intramuscular administration of AAV overcomes pre-existing neutralizing antibodies in rhesus macaques*. Vaccine,* 2016. **34**(50): p. 6323-6329.

339. Ertl, H.C.J. and High, K.A. Impact of AAV Capsid-Specific T-Cell Responses on Design and Outcome of Clinical Gene Transfer Trials with Recombinant Adeno-Associated Viral Vectors: An Evolving Controversy*. Hum Gene Ther,* 2017. **28**(4): p. 328-337.

340. Burnett, J.R. and Hooper, A.J. Alipogene tiparvovec, an adeno-associated virus encoding the Ser(447)X variant of the human lipoprotein lipase gene for the treatment of patients with lipoprotein lipase deficiency. *Current Opinion in Molecular Therapeutics,* 2009. **11**(6): p. 681-91.

341. Bryant, L.M., Christopher, D.M., Giles, A.R., Hinderer, C., Rodriguez, J.L., Smith, J.B., Traxler, E.A., Tycko, J., Wojno, A.P., and Wilson, J.M. Lessons learned from the clinical development and market authorization of Glybera*. Hum Gene Ther Clin Dev,* 2013. **24**(2): p. 55-64.

342. Russell, S., Bennett, J., Wellman, J.A., Chung, D.C., Yu, Z.-F., Tillman, A., Wittes, J., Pappas, J., Elci, O., McCague, S., Cross, D., Marshall, K.A., Walshire, J., Kehoe, T.L., Reichert, H., Davis, M., Raffini, L., George, L.A., Hudson, F.P., Dingfield, L., Zhu, X., Haller, J.A., Sohn, E.H., Mahajan, V.B., Pfeifer, W., Weckmann, M., Johnson, C., Gewaily, D., Drack, A., Stone, E., Wachtel, K., Simonelli, F., Leroy, B.P., Wright, J.F., High, K.A., and Maguire, A.M. Efficacy and safety of voretigene neparvovec (AAV2-hRPE65v2) in patients with RPE65 -mediated inherited retinal dystrophy: a randomised, controlled, open-label, phase 3 trial*. The Lancet,* 2017. **390**(10097): p. 849-860.

343. Mahajan, R. Onasemnogene Abeparvovec for Spinal Muscular Atrophy: The Costlier Drug Ever*. International journal of applied & basic medical research,* 2019. **9**(3): p. 127-128.

344. Hinderer, C., Katz, N., Buza, E.L., Dyer, C., Goode, T., Bell, P., Richman, L.K., and Wilson, J.M. Severe Toxicity in Nonhuman Primates and Piglets Following High-Dose Intravenous Administration of an Adeno-Associated Virus Vector Expressing Human SMN*. Human Gene Therapy,* 2018. **29**(3): p. 285-298.

345. Sumner, C.J. and Crawford, T.O. Two breakthrough gene-targeted treatments for spinal muscular atrophy: challenges remain*. The Journal of Clinical Investigation,* 2018. **128**(8): p. 3219-3227.

346. Castaman, G. and Matino, D. Hemophilia A and B: molecular and clinical similarities and differences*. Haematologica,* 2019. **104**(9): p. 1702-1709.

347. Manno, C.S., Pierce, G.F., Arruda, V.R., Glader, B., Ragni, M., Rasko, J.J.E., Ozelo, M.C., Hoots, K., Blatt, P., Konkle, B., Dake, M., Kaye, R., Razavi, M., Zajko, A., Zehnder, J., Rustagi, P., Nakai, H., Chew, A., Leonard, D., Wright,

J.F., Lessard, R.R., Sommer, J.M., Tigges, M., Sabatino, D., Luk, A., Jiang, H., Mingozzi, F., Couto, L., Ertl, H.C., High, K.A., and Kay, M.A. Successful transduction of liver in hemophilia by AAV-Factor IX and limitations imposed by the host immune response. *Nature Medicine,* 2006. **12**(3): p. 342-347.

348. Nathwani, A.C., Tuddenham, E.G.D., Rangarajan, S., Rosales, C., McIntosh, J., Linch, D.C., Chowdary, P., Riddell, A., Pie, A.J., Harrington, C., O'Beirne, J., Smith, K., Pasi, J., Glader, B., Rustagi, P., Ng, C.Y.C., Kay, M.A., Zhou, J., Spence, Y., Morton, C.L., Allay, J., Coleman, J., Sleep, S., Cunningham, J.M., Srivastava, D., Basner-Tschakarjan, E., Mingozzi, F., High, K.A., Gray, J.T., Reiss, U.M., Nienhuis, A.W., and Davidoff, A.M. Adenovirus-Associated Virus Vector–Mediated Gene Transfer in Hemophilia B. *New England Journal of Medicine,* 2011. **365**(25): p. 2357-2365.

349. Nathwani, A.C., Reiss, U.M., Tuddenham, E.G., Rosales, C., Chowdary, P., McIntosh, J., Della Peruta, M., Lheriteau, E., Patel, N., Raj, D., Riddell, A., Pie, J., Rangarajan, S., Bevan, D., Recht, M., Shen, Y.M., Halka, K.G., Basner-Tschakarjan, E., Mingozzi, F., High, K.A., Allay, J., Kay, M.A., Ng, C.Y., Zhou, J., Cancio, M., Morton, C.L., Gray, J.T., Srivastava, D., Nienhuis, A.W., and Davidoff, A.M. Long-term safety and efficacy of factor IX gene therapy in hemophilia B. *N Engl J Med,* 2014. **371**(21): p. 1994-2004.

350. Chamberlain, K., Riyad, J.M., and Weber, T. Cardiac gene therapy with adeno-associated virus-based vectors. *Current Opinion in Cardiology,* 2017. **32**(3): p. 275-282.

351. Santiago-Ortiz, J.L. and Schaffer, D.V. Adeno-associated virus (AAV) vectors in cancer gene therapy. *Journal of controlled release : official journal of the Controlled Release Society,* 2016. **240**: p. 287-301.

352. Sipo, I., Knauf, M., Fechner, H., Poller, W., Planz, O., Kurth, R., and Norley, S. Vaccine protection against lethal homologous and heterologous challenge using recombinant AAV vectors expressing codon-optimized genes from pandemic swine origin influenza virus (SOIV). *Vaccine,* 2011. **29**(8): p. 1690-9.

353. Balazs, A.B., Chen, J., Hong, C.M., Rao, D.S., Yang, L., and Baltimore, D. Antibody-based protection against HIV infection by vectored immunoprophylaxis. *Nature,* 2011. **481**(7379): p. 81-4.

354. Balazs, A.B., Bloom, J.D., Hong, C.M., Rao, D.S., and Baltimore, D. Broad protection against influenza infection by vectored immunoprophylaxis in mice. *Nat Biotechnol,* 2013. **31**(7): p. 647-52.

355. Limberis, M.P., Adam, V.S., Wong, G., Gren, J., Kobasa, D., Ross, T.M., Kobinger, G.P., Tretiakova, A., and Wilson, J.M. Intranasal antibody gene transfer in mice and ferrets elicits broad protection against pandemic influenza. *Sci Transl Med,* 2013. **5**(187): p. 187ra72.

356. Adam, V.S., Crosariol, M., Kumar, S., Ge, M.Q., Czack, S.E., Roy, S., Haczku, A., Tretiakova, A., Wilson, J.M., and Limberis, M.P. Adeno-associated virus 9-mediated airway expression of antibody protects old and immunodeficient mice against influenza virus. *Clin Vaccine Immunol,* 2014. **21**(11): p. 1528-33.

357. Laursen, N., Friesen, R.H., Zhu, X., Jongeneelen, M., Blokland, S., Vermond, J., van Eijgen, A., Tang, C., van Diepen, H., Straetemans, R., Hoffman, R., Nieusma, T., Pallesen, J., Turner, H., Bernard, S., Ward, A., Luo, J., Poon,

L.L., Tretiakova, A., Wilson, J.M., Limberis, M.P., Vogels, R., Brandenburg, B., Kolkman, J., and Wilson, I.A. Universal protection against influenza infection by a multidomain antibody to influenza hemagglutinin. *Science,* 2018. **362**: p. 598-602.

358. Paules, C.I., Marston, H.D., Eisinger, R.W., Baltimore, D., and Fauci, A.S. The Pathway to a Universal Influenza Vaccine. *Immunity,* 2017. **47**(4): p. 599-603.

359. Nabel, G.J. and Fauci, A.S. Induction of unnatural immunity: prospects for a broadly protective universal influenza vaccine. *Nature Medicine,* 2010. **16**(12): p. 1389-1391.

360. Paules, C.I., Sullivan, S.G., Subbarao, K., and Fauci, A.S. Chasing Seasonal Influenza — The Need for a Universal Influenza Vaccine. *New England Journal of Medicine,* 2017. **378**(1): p. 7-9.

361. Mathew, N.R. and Angeletti, D. Recombinant Influenza Vaccines: Saviors to Overcome Immunodominance. *Front Immunol,* 2019. **10**: p. 2997.

362. Neu, K.E., Guthmiller, J.J., Huang, M., La, J., Vieira, M.C., Kim, K., Zheng, N.Y., Cortese, M., Tepora, M.E., Hamel, N.J., Rojas, K.T., Henry, C., Shaw, D., Dulberger, C.L., Pulendran, B., Cobey, S., Khan, A.A., and Wilson, P.C. Spec-seq unveils transcriptional subpopulations of antibody-secreting cells following influenza vaccination. *J Clin Invest,* 2019. **129**(1): p. 93-105.

363. Reed, L.J. and Muench, H. A Simple Method of Estimating Fifty Per Cent Endpoints. *The American Journal of Hygiene,* 1938. **27**(3): p. 493-7.

364. Carnell, G.W., Ferrara, F., Grehan, K., Thompson, C.P., and Temperton, N.J. Pseudotype-based neutralization assays for influenza: a systematic analysis. *Front Immunol,* 2015. **6**: p. 161.

365. Grieger, J.C., Choi, V.W., and Samulski, R.J. Production and characterization of adeno-associated viral vectors. *Nat Protoc,* 2006. **1**(3): p. 1412-28.

366. Werling, N.J., Satkunanathan, S., Thorpe, R., and Zhao, Y. Systematic Comparison and Validation of Quantitative Real-Time PCR Methods for the Quantitation of Adeno-Associated Viral Products. *Hum Gene Ther Methods,* 2015. **26**(3): p. 82-92.

367. Ramage, W., Gaiotto, T., Ball, C., Risley, P., Carnell, G.W., Temperton, N., Cheung, C.Y., Engelhardt, O.G., and Hufton, S.E. Cross-Reactive and Lineage-Specific Single Domain Antibodies against Influenza B Hemagglutinin. *Antibodies,* 2019. **8**(1).

368. Wu, B. and Sun, Y.N. Pharmacokinetics of Peptide-Fc fusion proteins. *J Pharm Sci,* 2014. **103**(1): p. 53-64.

369. Corti, D. and Lanzavecchia, A. Broadly neutralizing antiviral antibodies. *Annu Rev Immunol,* 2013. **31**: p. 705-42.

370. Expert Committe on Biological Standardization, W.H.O., Generic protocol for the calibration of seasonal/pandemic influenza antigen working reagents by WHO Essential Regulatory Laboratories. 2012.

371. Morrison, B.J., Roman, J.A., Luke, T.C., Nagabhushana, N., Raviprakash, K., Williams, M., and Sun, P. Antibody-dependent NK cell degranulation as a marker for assessing antibody-dependent cytotoxicity against pandemic 2009

influenza A(H1N1) infection in human plasma and influenza-vaccinated transchromosomic bovine intravenous immunoglobulin therapy. *J Virol Methods,* 2017. **248**: p. 7-18.

372. Jegaskanda, S., Job, E.R., Kramski, M., Laurie, K., Isitman, G., de Rose, R., Winnall, W.R., Stratov, I., Brooks, A.G., Reading, P.C., and Kent, S.J. Cross-reactive influenza-specific antibody-dependent cellular cytotoxicity antibodies in the absence of neutralizing antibodies. *J Immunol,* 2013. **190**(4): p. 1837-48.

373. Leon, P.E., He, W., Mullarkey, C.E., Bailey, M.J., Miller, M.S., Krammer, F., Palese, P., and Tan, G.S. Optimal activation of Fc-mediated effector functions by influenza virus hemagglutinin antibodies requires two points of contact. *Proc Natl Acad Sci U S A,* 2016. **113**(40): p. E5944-E5951.

374. Kuipers, H., Use of ADCC reporter bioassays in influenza vaccine development. 2016, Janssen Pharmaceutical, Infectious Diseases and Vaccines.

375. Garcia, J.M., Lagarde, N., Ma, E.S., de Jong, M.D., and Peiris, J.S. Optimization and evaluation of an influenza A (H5) pseudotyped lentiviral particle-based serological assay. *J Clin Virol,* 2010. **47**(1): p. 29-33.

376. Martinez-Sobrido, L., Cadagan, R., Steel, J., Basler, C.F., Palese, P., Moran, T.M., and Garcia-Sastre, A. Hemagglutinin-pseudotyped green fluorescent protein-expressing influenza viruses for the detection of influenza virus neutralizing antibodies. *J Virol,* 2010. **84**(4): p. 2157-63.

377. Oh, S., Selleck, P., Temperton, N.J., Chan, P.K., Capecchi, B., Manavis, J., Higgins, G., Burrell, C.J., and Kok, T. Neutralizing monoclonal antibodies to different clades of Influenza A H5N1 viruses. *J Virol Methods,* 2009. **157**(2): p. 161-7.

378. Alberini, I., Del Tordello, E., Fasolo, A., Temperton, N.J., Galli, G., Gentile, C., Montomoli, E., Hilbert, A.K., Banzhoff, A., Del Giudice, G., Donnelly, J.J., Rappuoli, R., and Capecchi, B. Pseudoparticle neutralization is a reliable assay to measure immunity and cross-reactivity to H5N1 influenza viruses. *Vaccine,* 2009. **27**(43): p. 5998-6003.

379. de Vries, R.D., Nieuwkoop, N.J., Pronk, M., de Bruin, E., Leroux-Roels, G., Huijskens, E.G.W., van Binnendijk, R.S., Krammer, F., Koopmans, M.P.G., and Rimmelzwaan, G.F. Influenza virus-specific antibody dependent cellular cytoxicity induced by vaccination or natural infection. *Vaccine,* 2017. **35**(2): p. 238-247.

380. Jegaskanda, S. The Potential Role of Fc-Receptor Functions in the Development of a Universal Influenza Vaccine. *Vaccines (Basel),* 2018. **6**(2).

381. Jegaskanda, S., Reading, P.C., and Kent, S.J. Influenza-specific antibody-dependent cellular cytotoxicity: toward a universal influenza vaccine. *J Immunol,* 2014. **193**(2): p. 469-75.

382. Vanderven, H.A., Jegaskanda, S., Wheatley, A.K., and Kent, S.J. Antibody-dependent cellular cytotoxicity and influenza virus. *Curr Opin Virol,* 2017. **22**: p. 89-96.

383. Dreyfus, C., Laursen, N.S., Kwaks, T., Zuijdgeest, D., Khayat, R., Ekiert, D.C., Lee, J.H., Metlagel, Z., Bujny, M.V., Jongeneelen, M., van der Vlugt, R.,

Lamrani, M., Korse, H.J., Geelen, E., Sahin, O., Sieuwerts, M., Brakenhoff, J.P., Vogels, R., Li, O.T., Poon, L.L., Peiris, M., Koudstaal, W., Ward, A.B., Wilson, I.A., Goudsmit, J., and Friesen, R.H. Highly conserved protective epitopes on influenza B viruses. *Science,* 2012. **337**(6100): p. 1343-8.

384. Miller, M.S., Gardner, T.J., Krammer, F., Aguado, L.C., Tortorella, D., Basler, C.F., and Palese, P. Neutralizing Antibodies Against Previously Encountered Influenza Virus Strains Increase over Time: A Longitudinal Analysis. *Science Translational Medicine,* 2013. **5**(198): p. 198ra107.

385. Chandler, R.J., Sands, M.S., and Venditti, C.P. Recombinant Adeno-Associated Viral Integration and Genotoxicity: Insights from Animal Models. *Hum Gene Ther,* 2017. **28**(4): p. 314-322.

386. Grieger, J.C. and Samulski, R.J. Packaging capacity of adeno-associated virus serotypes: impact of larger genomes on infectivity and postentry steps. *J Virol,* 2005. **79**(15): p. 9933-44.

387. Limberis, M.P., Racine, T., Kobasa, D., Li, Y., Gao, G.F., Kobinger, G., and Wilson, J.M. Vectored expression of the broadly neutralizing antibody FI6 in mouse airway provides partial protection against a new avian influenza A virus, H7N9. *Clin Vaccine Immunol,* 2013. **20**(12): p. 1836-7.

388. Wang, D., Zhong, L., Nahid, M.A., and Gao, G. The potential of adeno-associated viral vectors for gene delivery to muscle tissue. *Expert Opin Drug Deliv,* 2014. **11**(3): p. 345-364.

389. Wang, Z., Zhu, T., Qiao, C., Zhou, L., Wang, B., Zhang, J., Chen, C., Li, J., and Xiao, X. Adeno-associated virus serotype 8 efficiently delivers genes to muscle and heart. *Nat Biotechnol,* 2005. **23**(3): p. 321-8.

390. Mingozzi, F. and High, K.A. Immune Responses to AAV in Clinical Trials. *Current Gene Therapy,* 2011. **11**: p. 321-330.

391. Shin, J.H., Yue, Y., and Duan, D. Recombinant adeno-associated viral vector production and purification. *Methods Mol Biol,* 2012. **798**: p. 267-84.

392. William W. Hauswirth, Alfred S. Lewin, Sergei Zolotukhin, and Muzyczka, N. Chapter: [48] Production and purification of recombinant adeno-associated virus, in *Methods in Enzymology*. 2000, Elsevier.

393. Nakai, H., Fuess, S., Storm, T.A., Muramatsu, S., Nara, Y., and Kay, M.A. Unrestricted hepatocyte transduction with adeno-associated virus serotype 8 vectors in mice. *J Virol,* 2005. **79**(1): p. 214-24.

394. Matsushita, T., Elliger, S., Elliger, C., Podsakoff, G., Villarreal, L., Kurtzman, J., Iwaki, Y., and Colosi, P. Adeno-associated virus vectors can be efficiently produced without helper virus. *Gene Therapy,* 1998. **5**: p. 938-45.

395. Dobnik, D., Kogovsek, P., Jakomin, T., Kosir, N., Tusek Znidaric, M., Leskovec, M., Kaminsky, S.M., Mostrom, J., Lee, H., and Ravnikar, M. Accurate Quantification and Characterization of Adeno-Associated Viral Vectors. *Front Microbiol,* 2019. **10**: p. 1570.

396. Kohlbrenner, E., Henckaerts, E., Rapti, K., Gordon, R.E., Linden, R.M., Hajjar, R.J., and Weber, T. Quantification of AAV particle titers by infrared fluorescence scanning of coomassie-stained sodium dodecyl sulfate-polyacrylamide gels. *Hum Gene Ther Methods,* 2012. **23**(3): p. 198-203.

397. Nam, H.J., Lane, M.D., Padron, E., Gurda, B., McKenna, R., Kohlbrenner, E., Aslanidi, G., Byrne, B., Muzyczka, N., Zolotukhin, S., and Agbandje-McKenna, M. Structure of adeno-associated virus serotype 8, a gene therapy vector. *J Virol,* 2007. **81**(22): p. 12260-71.

398. Mori, S., Wang, L., Takeuchi, T., and Kanda, T. Two novel adeno-associated viruses from cynomolgus monkey: pseudotyping characterization of capsid protein. *Virology,* 2004. **330**(2): p. 375-83.

399. Hirata, R.K. and Russell, D.W. Design and Packaging of Adeno-Associated Virus Gene Targeting Vectors. *Journal of Virology,* 2000. **74**(10): p. 4612-20.

400. Aurnhammer, C., Haase, M., Muether, N., Hausl, M., Rauschhuber, C., Huber, I., Nitschko, H., Busch, U., Sing, A., Ehrhardt, A., and Baiker, A. Universal Real-Time PCR for the Detection and Quantification of Adeno-Associated Virus Serotype 2-Derived Inverted Terminal Repeat Sequences. *Human Gene Therapy,* 2011. **23**.

401. Rohr, U., Wulf, M.A., Stahn, S., Steidl, U., Haas, R., and Kronenwett, R. Fast and reliable titration of recombinant adeno-associated virus type-2 using quantitative real-time PCR. *Journal of Virological Methods,* 2002. **106**(2002): p. 81-88.

402. Luke, C.J. and Subbarao, K. The Role of Animal Models In Influenza Vaccine Research. *Influenza Vaccines for the Future,* 2010: p. 223-272.

403. Sidwell, R.W. and Smee, D.F. In vitro and in vivo assay systems for the study of influenza virus inhibitors. *Antiviral Research,* 2000. **48**: p. 1-16.

404. Cochran, K.W., Maassab, H.F., Tsunoda, A., and Berlin, B.S. Studies On The Antiviral Activity of Amantadine Hydrochloride. *Annals of the New York Academy of Sciences,* 1965. **130**(1): p. 432-439.

405. Herlocher, M.L., Truscon, R., Fenton, R., Klimov, A., Elias, S., Ohmit, S.E., and Monto, A.S. Assessment of Development of Resistance to Antivirals in the Ferret Model of Influenza Virus Infection. *The Journal of Infectious Diseases,* 2003. **188**(9): p. 1355-1361.

406. Hoffman, C.E. Amantadine HCl and related compounds., in *Inhibitors of Viral Functions.*, Carter, W.A., Editor. 1973, CRC Press: Boca Raton, Florida. p. 199-212.

407. Blick, T., Sahasrabudhe, A., McDonald, M., Owens, I., Morley, P., Fenton, R., and McKimm-Breschkin, J. The Interaction of Neuraminidase and Hemagglutinin Mutations in Influenza Virus in Resistance to 4-Guanidino-Neu5Ac2en. *Journal of Virology,* 1998. **246**.

408. Bouvier, N.M. and Lowen, A.C. Animal Models for Influenza Virus Pathogenesis and Transmission. *Viruses,* 2010. **2**(8): p. 1530-1563.

409. Dati, F., Johnson, A.M., and Whicher, J.T. The existing interim consensus reference ranges and the future approach. *Clin Chem Lab Med,* 2001. **39**(11): p. 1134-6.

410. Guo, Y., Tian, X., Wang, X., and Xiao, Z. Adverse Effects of Immunoglobulin Therapy. *Front Immunol,* 2018. **9**: p. 1299.

411. Rojas, R. and Apodaca, G. Immunoglobulin transport across polarized epithelial cells. *Nature Reviews Molecular Cell Biology,* 2002. **3**(12): p. 944-956.

412. Dekkers, G., Bentlage, A.E.H., Stegmann, T.C., Howie, H.L., Lissenberg-Thunnissen, S., Zimring, J., Rispens, T., and Vidarsson, G. Affinity of human IgG subclasses to mouse Fc gamma receptors. *MAbs,* 2017. **9**(5): p. 767-773.

413. Rajapaksha, I., Angus, P., and Herath, C. Adeno-Associated Virus (AAV)-Mediated Gene Therapy for Disorders of Inherited and Non-Inherited Origin. 2019.

414. Rivière, C., Danos, O., and Douar, A.M. Long-term expression and repeated administration of AAV type 1, 2 and 5 vectors in skeletal muscle of immunocompetent adult mice. *Gene Therapy,* 2006. **13**(17): p. 1300-1308.

415. Jegaskanda, S., Vanderven, H.A., Wheatley, A.K., and Kent, S.J. Fc or not Fc; that is the question: Antibody Fc-receptor interactions are key to universal influenza vaccine design. *Hum Vaccin Immunother,* 2017. **13**(6): p. 1-9.

416. Janjua, N.Z., Skowronski, D.M., Hottes, T.S., Osei, W., Adams, E., Petric, M., Sabaiduc, S., Chan, T., Mak, A., Lem, M., Tang, P., Patrick, D.M., De Serres, G., and Bowering, D. Seasonal influenza vaccine and increased risk of pandemic A/H1N1-related illness: first detection of the association in British Columbia, Canada. *Clin Infect Dis,* 2010. **51**(9): p. 1017-27.

417. Ewert, S., Cambillau, C., Conrath, K., and Plückthun, A. Biophysical Properties of Camelid VHH Domains Compared to Those of Human VH3 Domains. *Biochemistry,* 2002. **41**(11): p. 3628-3636.

418. Khurana, S., Loving, C., Manischewitz, J., King, L., Gauger, P., Henningson, J., Vincent, A., and Golding, H. Vaccine-Induced Anti-HA2 Antibodies Promote Virus Fusion and Enhance Influenza Virus Respiratory Disease. *Science Translational Medicine,* 2013. **5**(200).

419. Ramakrishnan, B., Viswanathan, K., Tharakaraman, K., Dancik, V., Raman, R., Babcock, G.J., Shriver, Z., and Sasisekharan, R. A Structural and Mathematical Modeling Analysis of the Likelihood of Antibody-Dependent Enhancement in Influenza. *Trends Microbiol,* 2016. **24**(12): p. 933-943.

420. Skowronski, D.M., De Serres, G., Crowcroft, N.S., Janjua, N.Z., Boulianne, N., Hottes, T.S., Rosella, L.C., Dickinson, J.A., Gilca, R., Sethi, P., Ouhoummane, N., Willison, D.J., Rouleau, I., Petric, M., Fonseca, K., Drews, S.J., Rebbapragada, A., Charest, H., Hamelin, M.E., Boivin, G., Gardy, J.L., Li, Y., Kwindt, T.L., Patrick, D.M., Brunham, R.C., and Canadian, S.T. Association between the 2008-09 seasonal influenza vaccine and pandemic H1N1 illness during Spring-Summer 2009: four observational studies from Canada. *PLoS Med,* 2010. **7**(4): p. e1000258.

421. Brennan, F.R., Morton, L.D., Spindeldreher, S., Kiessling, A., Allenspach, R., Hey, A., Muller, P.Y., Frings, W., and Sims, J. Safety and immunotoxicity assessment of immunomodulatory monoclonal antibodies. *MAbs,* 2010. **2**(3): p. 233-55.

422. Halbert, C. and Miller, D. AAV-Mediated Gene Transfer to Mouse Lungs, in *Gene Delivery to Mammalian Cells: Viral Gene Transfer Techniques*, Heiser, W.C., Editor. 2004, Humana Press.

423. Buchholz, C.J., Friedel, T., and Buning, H. Surface-Engineered Viral Vectors for Selective and Cell Type-Specific Gene Delivery*. Trends Biotechnol,* 2015. **33**(12): p. 777-790.

424. Chai, N., Swem, L.R., Reichelt, M., Chen-Harris, H., Luis, E., Park, S., Fouts, A., Lupardus, P., Wu, T.D., Li, O., McBride, J., Lawrence, M., Xu, M., and Tan, M.-W. Two Escape Mechanisms of Influenza A Virus to a Broadly Neutralizing Stalk-Binding Antibody*. PLOS Pathogens,* 2016. **12**(6): p. e1005702.

425. Lagos-Quintana, M., Rauhut, R., Yalcin, A., Meyer, J., Lendeckel, W., and Tuschl, T. Identification of Tissue-Specific MicroRNAs from Mouse*. Current Biology,* 2002. **12**(9): p. 735-739.

426. Domenger, C. and Grimm, D. Next-generation AAV vectors-do not judge a virus (only) by its cover*. Hum Mol Genet,* 2019. **28**(R1): p. R3-R14.

427. Hoffmann, M.D., Aschenbrenner, S., Grosse, S., Rapti, K., Domenger, C., Fakhiri, J., Mastel, M., Borner, K., Eils, R., Grimm, D., and Niopek, D. Cell-specific CRISPR-Cas9 activation by microRNA-dependent expression of anti-CRISPR proteins*. Nucleic Acids Res,* 2019. **47**(13): p. e75.

428. Mou, H., Zhong, G., Gardner, M.R., Wang, H., Wang, Y.W., Cheng, D., and Farzan, M. Conditional Regulation of Gene Expression by Ligand-Induced Occlusion of a MicroRNA Target Sequence*. Mol Ther,* 2018. **26**(5): p. 1277-1286.

429. Boisgerault, F., Gross, D.-A., Ferrand, M., Poupiot, J., Darocha, S., Richard, I., and Galy, A. Prolonged Gene Expression in Muscle Is Achieved Without Active Immune Tolerance Using MicrorRNA 142.3p-Regulated rAAV Gene Transfer*. Human Gene Therapy,* 2013. **24**(4): p. 393-405.

430. Xie, J., Xie, Q., Zhang, H., Ameres, S.L., Hung, J.H., Su, Q., He, R., Mu, X., Seher Ahmed, S., Park, S., Kato, H., Li, C., Mueller, C., Mello, C.C., Weng, Z., Flotte, T.R., Zamore, P.D., and Gao, G. MicroRNA-regulated, systemically delivered rAAV9: a step closer to CNS-restricted transgene expression*. Mol Ther,* 2011. **19**(3): p. 526-35.

431. Kontermann, R.E. Half-life extended biotherapeutics*. Expert Opin Biol Ther,* 2016. **16**(7): p. 903-15.